Morphological and behavioural characterisation of fibroblast sub-types found in human skin dermis

A thesis submitted by

Helena Topouzi

For the degree of

Doctor of Philosophy

Department of Bioengineering

Imperial College London

February 2018

Declaration of originality

I hereby declare that this thesis is entirely the result of my own work.

Helena Topouzi
February 2018

Copyright declaration

The copyright of this thesis rests with the author and is made available under a Creative Commons Attribution Non-Commercial No Derivatives licence. Researchers are free to copy, distribute or transmit the thesis on the condition that they attribute it, that they do not use it for commercial purposes and that they do not alter, transform or build upon it. For any reuse or redistribution, researchers must make clear to others the licence terms of this work.

Acknowledgments

After four years, it seems appropriate that I finally thank all the people that have been supporting me throughout this long journey. First and foremost, I would like to express my gratitude to my supervisor Dr Claire A. Higgins for her support, guidance and patience throughout all these years. She gave me the opportunity to work with her and taught me so much and for that I am truly grateful.

I would also like to thank my colleagues in Higgins lab for not only the academic support but for all the meals, jokes and bowling games we shared that made my time more enjoyable. I would specifically like to thank Dr Niall J. Logan who has supported me from the beginning and has always advised me when I needed help. I would also like to thank Dr Martina Ghetti for all her support even in the short time she spent with us in the lab.

I would like to acknowledge Dr Greg Williams, Dr Paul Farrant, Mr Paul Hitchen and Dr David Chambers for providing practical support during my PhD. I would also like to thank the Department of Bioengineering for funding my studies, without which the work could not have been carried out.

My deepest appreciation goes to my friends and family, especially my parents for encouraging me and believing in me even when I was doubting myself. Words cannot describe how grateful I am for everything you have done for me. I am deeply grateful to my partner Michalis for all his support and encouragement. Thank you for being there for me, believing in me and pushing me to be the best I can be.

I hope I have made you all proud.

Abstract

There are multiple fibroblast populations found in adult skin dermis. Within this thesis I will discuss three of these; papillary fibroblasts, reticular fibroblasts and dermal papilla fibroblasts, which were recently shown to arise from a common cellular progenitor during development. These three fibroblasts populations are defined by their spatial location and are under the influence of the surrounding macroenvironment. One of the first questions in this thesis was whether these three populations would maintain their distinct identities *in vitro*, once surrounding influential factors were removed. I used knowledge of the different spatial locations in human skin to isolate and establish cell cultures from each fibroblast subtype. Then immunofluorescence with a panel of antibodies was used to assess expression in the different populations. I found that Vimentin and Collagen I are expressed in all of the three populations. Podoplanin and Dipeptidyl-peptidase IV were specific for papillary fibroblasts, while Alpha smooth muscle actin and Calponin 1 was highly expressed in dermal papilla and reticular fibroblasts in contrast with the papillary fibroblasts. I was able to establish an expression map that can serve as a platform for identifying and characterising different fibroblast populations *in vitro*. Next, I evaluated the protein composition of the extracellular matrix synthesized by each population. I found that these three fibroblast populations deposit unique extracellular matrix *in vitro*. Then, I wanted to determine how these fibroblast populations influence behaviour in juxtaposed cell populations, such as epithelial keratinocytes. In skin homeostasis, dermal fibroblasts are responsible for coordinating the migration and differentiation of keratinocytes in the overlying epithelium. From the initial experiments I knew that dermal papilla fibroblasts, papillary fibroblasts and reticular fibroblasts have a unique

identity in culture. Therefore, I hypothesised that these sub-populations of fibroblasts would be able to influence reepithelialisation differently after wounding. Using a scratch assay, I identified that conditioned media from the dermal papilla and reticular fibroblasts is able to promote significantly faster keratinocyte migration than normal growth media. In an attempt to understand what cytokine(s) are responsible for this enhanced migration, I analysed the cytokines released in the conditioned media and I identified three cytokines that appear to be key players in this enhanced wound healing; AXL, CCL19 and BMP6. I then tested the effects of these cytokines on keratinocytes in a scratch assay *in vitro* and found that they significantly enhance wound closure in comparison to the untreated cells. An *ex vivo* wound healing assay was then used so as to determine whether the *in vitro* scratch assay studies could be replicated in an *ex vivo* model. The results show that AXL is able to promote reepithelialisation significantly faster than the control. CCL19 and BMP6 have been correlated with wound closure before but there is no mention in the literature on AXL during wound healing. Therefore, using microarray analysis, I identified a list of genes that are activated in a 'wounded' environment in the keratinocytes, with the addition of dermal papilla conditioned media and AXL, in an effort to find the gene(s) responsible for this enhanced healing. Using Genespring, a commercialised software, I identified a list of genes that are significantly expressed in the keratinocytes and identified a potential pathway of action of AXL. Further testing should be carried out as AXL could potentially be used as a therapy for faster wound closure.

Table of Contents

Declaration of originality 1
Copyright declaration 1
Acknowledgments 2
Abstract 3
Table of Contents 5
List of figures 11
List of tables 15
List of abbreviations 16
List of reagents 20
Chapter 1. General introduction 23
1.1. Skin structure and function 24
1.1.1. Epidermis 25
1.1.2. Dermis 25
1.1.3. Hypodermis 26
1.1.4. Hair follicle 28
1.2. Skin and hair morphogenesis 29
1.2.1. Reciprocal interactions in skin morphogenesis 30
1.2.2. Postnatal skin 34
1.2.3. WNT signaling in skin development 34
1.3. Dermal fibroblast populations in adult skin and their function *in vivo* 37
1.3.1. The role of follicular fibroblasts, DPFi, in skin 37
1.3.1.1. Hair cycle 37
1.3.1.2. Importance of the dermal condensate and dermal papilla 39
1.3.1.3. Inductivity 40
1.3.2. The role of interfollicular fibroblasts, PFi and RFi in skin 42

1.3.2.1. What is the role of PFi? 43

1.3.2.2. What is the role of RFi? 43

1.4. Anatomic diversity of fibroblasts 46

1.5. Human skin as a model system 47

1.6. Aims 49

Chapter 2. Defining fibroblast subtypes in the skin. 50

2.1. Introduction 51

2.1.1. Dermal fibroblast heterogeneity in murine skin 51

2.1.2. Human dermal fibroblasts and extracellular environment 53

2.1.3. Fibroblasts from sub-anatomical locations have different expression profiles 54

2.2. Specific aims in Chapter 2 58

2.3. Materials and Methods 59

2.3.1. Human skin biopsies 59

2.3.2. Isolation and culture of site-matched fibroblasts 60

2.3.3. KC isolation and culture 63

2.3.4. Immunofluorescence 64

2.3.5. Osteogenic differentiation 67

2.3.5.1. Alizarin red staining 67

2.3.5.2. Calcium assay 67

2.3.6. Adipogenic differentiation 68

2.3.6.1. Oil Red O staining 68

2.3.7. Alamar blue cell viability assay 69

2.3.8. Morphology analysis 69

2.3.9. mRNA extraction, reverse transcription and RT-PCR 70

2.3.10. Matrix deposition 71

2.3.11. ECM samples analysed by mass spectrometry 72

2.3.12. Statistical analysis of data 74

2.4. Results 75

2.4.1. Distinguishing between the different dermal compartments of scalp skin 75

2.4.2. Fibroblasts have distinct expression profiles and behavioural characteristics *in vitro* at P4 78

2.4.3. Alamar blue assay shows differences in the proliferation rate of the sub populations 84

2.4.4. Occipital scalp populations exhibit morphological differences at an early passage 86

2.4.5. Prolonged passage alters morphology and protein expression pattern 90

2.4.6. Osteogenic and adipogenic differentiation 96

2.4.7. Osteogenic differentiation on frontal vs occipital scalp 99

2.4.8. Mass spectrometry analysis on the ECM of all three fibroblast subtypes 102

2.5. Discussion 105

2.5.1. Isolation and characterisation of fibroblast in research 105

2.5.2. Fibroblasts have distinct expression characteristics at P4 106

2.5.3. CD26- A PFi marker or a fibrotic marker? 107

2.5.4. PFi are the dominant fibroblast subtype in the blended Fi cultures 107

2.5.5. Are the cells reverting to a homogenous state with increasing passage? 109

2.5.6. Differentiation using osteogenic and adipogenic cues shows different differentiation potential of the three fibroblast subtypes 112

2.5.7. Frontal versus occipital scalp fibroblasts 113

2.5.8. Mass spectrometry reveals unique deposition of ECM from each fibroblast population 114

2.5.9. Concluding remarks 115

Chapter 3. Assessing fibroblast sub-type function with respect to wound healing. 116

3.1. Introduction 117

3.1.1. Skin homeostasis 117

3.1.2. The role of the dermis in epithelial homeostasis 117

3.1.3. Wound healing 118

3.1.4. Wound healing and scar formation 120

3.1.5. The role of the dermis in wound healing 123

3.1.6. Other dermal subtypes in wound repair 125

3.1.7. Growth factors and cytokines: What is their role in wound healing? 126

3.1.8. Current strategies to advance our understanding in wound healing 131

3.2. Specific aims in Chapter 3 133

3.3. Materials and Methods 134

3.3.1. Human skin biopsies 134

3.3.2. Isolation and cell culture of fibroblasts and KC 135

3.3.3. Conditioned media collection 135

3.3.4. KC wound healing assays using fibroblast conditioned media 135

3.3.5. Mitomycin C treated KC scratch assay using fibroblast conditioned media 137

3.3.6. Scratch assay analysis 138

3.3.7. Human cytokine antibody array 139

3.3.8. Human cytokine array analysis..... 141

3.3.9. Optimisation of cytokine concentrations and cytokine scratch assay..... 142

3.3.10. Microarray to determine the effect of AXL and DPFi CM on KC gene expression ……..143

3.3.11. Microarray computational analysis..... 144

3.3.12. Human *ex vivo* wound model..... 145

3.3.13. Statistical analysis of data..... 146

3.4. Results..... 147

3.4.1. Scratch assay shows faster wound closure in KC with DPFi CM..... 147

3.4.2. Mitomycin C treatment of KC reveals faster 'wound' closure..... 156

3.4.3. Cytokine array reveals CCL19, AXL and BMP6 to be significantly expressed in the DPFi compared to PFi or RFi..... 162

3.4.4. Scratch assay with overexpressed cytokines *in vitro*..... 167

3.4.5. Scratch assay with combinations of overexpressed cytokines *in vitro*..... 172

3.4.6. Scratch assay with PDGF-BB..... 175

3.4.7. *Ex vivo* wound healing assay..... 177

3.4.8. Microarray reveals unique gene expression in response to AXL..... 179

3.4.9. Potential pathways activated by AXL..... 189

3.5. Discussion..... 191

3.5.1. Ibidi versus scratch assay: Which method best mimics the wounding effect?..... 191

3.5.2. DPFi CM promotes KC migration in a paracrine manner..... 195

3.5.3. MITC induces enhanced migration..... 196

3.5.4. IL6- an important cytokine for reepithelialisation..... 197

3.5.5. A novel cytokine in wound healing: AXL 198
3.5.6. AXL and regulation of reepithelialisation 199
3.5.7. AXL receptor could be stimulated by EGFR activation 202
3.5.8. AXL: An attractive alternative to PDGF-BB in chronic wound healing 202
3.5.9. Concluding remarks 203
Chapter 4. Final discussions and future directions 204
4.1. General Discussion 205
4.1.1. Fibroblast heterogeneity and anatomic diversity 205
4.1.2. How plastic are dermal fibroblast subpopulations? 206
4.1.3. DPFi and RFi: a potential source of myofibroblasts? 206
4.1.4. AXL: A novel therapeutic for wound closure 207
4.2. Future directions 210
4.2.1. Plasticity of DPFi, PFi and RFi in culture 210
4.2.2. Livecyte: alternative to current scratch assay method 210
4.2.3. *Ex vivo* wound healing assay 210
4.2.4. Mode of action of AXL 211
4.2.5. Is AXL necessary? 211
References 212
Appendix 229

List of figures

Figure 1.1.1. Skin structure. 27

Figure 1.1.2. Components of the hair follicle. 29

Figure 1.2.1. Skin morphogenesis. 32

Figure 1.2 2. Common fibroblast progenitor. 33

Figure 1.2.3. WNT signalling reporter activity in embryonic skin during hair development. 36

Figure 1.2.4. WNT knockdown in the placode and dermal condensate. 36

Figure 1.3.1. Hair cycle. 38

Figure 1.3.2. Ablation experiments in adult mice dermal papilla. 40

Figure 1.3.3. Human dermal papilla spheroid inductivity. 42

Figure 1.3.4. Reticular and papillary fibroblasts in wound healing. 45

Figure 1.6.1. Macroscopic image of occipital scalp skin biopsy. 49

Figure 2.1.1. Summary of literature assessing fibroblast expression in development, neonate and adult skin. 57

Figure 2.3.2. Human dermal papilla micro-dissection method using a stereomicroscope. 61

Figure 2.3.3. Papillary and reticular fibroblast micro-dissection method using a stereomicroscope. 63

Figure 2.4.1. Immunofluorescence staining of human scalp skin *in vivo*. 76

Figure 2.4.2. Statistical analysis of cells per mm^2. 77

Figure 2.4.3. Isolation technique ensures bonafide fibroblasts. 79

Figure 2.4.4. Fibroblast identities at P4. 83

Figure 2.4.5. Alamar blue assay. 85

Figure 2.4.6. Morphological differences of DPFi, PFi and RFi at P4. 89

Figure 2.4.7. Morphological differences of DPFi, PFi and RFi with increasing passage number. 92

Figure 2.4.8. Expression profile of DPFi, PFi and RFi at P10 compared to P4. .. 95

Figure 2.4 9. Fibroblasts in osteogenic and growth media. 97

Figure 2.4.10. Fibroblasts in adipogenic and growth media. 98

Figure 2.4.11. Occipital and frontal scalp fibroblasts cultured in osteogenic and growth media. 101

Figure 2.5.1. Fibroblast expression map in development, neonate and adult. 111

Figure 3.1.1. Stages of wound repair. 120

Figure 3.1.2. Wound healing stages in adult, embryo and chronic wounds. .. 122

Figure 3.1.3. Reepithelialisation phase of wound repair. 123

Figure 3.1.4. RFi in wound healing. 124

Figure 3.3.1. Two methods of performing a KC wound healing assay. 137

Figure 3.3.2. Schematic of experimental procedure to prepare skin for the human ex vivo wound assay. 146

Figure 3.4.1. Ibidi insert wound healing assay. 148

Figure 3.4.2. KC scratch assay using the Ibidi inserts. 150

Figure 3.4.3. Scratch assay using a p200 pipette tip. 152

Figure 3.4.4. KC scratch assay analysis of the p200 experiment. 155

Figure 3.4.5. KC proliferation assay. 157

Figure 3.4.6. Distance covered by KC cells treated with MITC. 160

Figure 3.4.7. Cell front velocity of KC cells treated with MITC. 161

Figure 3.4.8. Normalised human cytokine antibody arrays. 163

Figure 3.4.9. Correlation analysis between DPFi, PFi and RFi CM. 166

Figure 3.4.10. Cytokine optimisation. 168

Figure 3.4.11. Cytokine overexpression. 171

Figure 3.4.12. Cell front velocity with overexpression of cytokine combinations. 174

Figure 3.4.13. Scratch assay using Livecyte by Phasefocus. 176

Figure 3.4.14. Ex vivo wound healing assay. 178

Figure 3.4.15. PCA plot and normalised signal intensity. 181

Figure 3.4.16. Volcano plots and Venn diagrams to compare up regulated and down regulated genes. 184

Figure 3.4.17. Up regulated and down regulated genes in AXL. 186

Figure 3.4.18. Four-way Venn diagrams. 188

Figure 3.4.19. Pathways activated/inhibited by AXL and DPFi CM. 190

Figure 3.5.1. Chapter 3 methods and outcomes. 194

Figure 3.5.2. Proposed mechanism of IL6 in wound healing. 198

Figure 3.5.3. AXL receptor structure. 200

Figure 3.5.4. Amino acid sequence of Human AXL...... 201

Figure A.1. Alamar blue standard curve graph...... 229

Figure A.2. Analysis of the KC wound healing assay of the second patient using the Ibidi inserts...... 230

List of tables

Table 2.3.1. Human skin biopsies in Chapter 2. 59

Table 2.3.2. Primary antibodies and secondary antibodies used. 66

Table 2.3.3 Primers used for RT-PCR analysis...... 71

Table 2.4.1. Mass Spectrometry data of ECM matrices for each fibroblast sub-type...... 104

Table 3.1.1. Summary of section 3.1.6...... 130

Table 3.3.1. Human skin biopsies in Chapter 2. 134

Table 3.4.1. Up regulated and down regulated genes specific for AXL...... 189

Table A.1. Fold change of 2577 genes in the KC differentially regulated across all conditions...... 231

List of abbreviations

ABAM	Antibiotics- Antimycotics
ACTA2	Alpha smooth muscle actin
AM	Adipogenic media
AXL	AXL receptor tyrosine kinase
Bmlip1	PR domain zinc finger protein 1
BMP	Bone morphogenic protein
BMP6	Bone morphogenic protein 6
CC-	Chemokines
CCL19	Chemokine ligand 19
Ccl2	Chemokine ligand 2
CD26	Dipeptidyl peptidase 4
CM	Conditioned medium
CNN1	Calponin 1
COL1	Collagen 1
COL1A1	Alpha 1 chain collagen I
COL1A2	Alpha 2 chain collagen I
COL6A1	Alpha 1 chain collagen VI
COL6A2	Alpha 2 chain collagen VI
COL6A3	Alpha 3 chain collagen VI
DHT	Dihydrotestosterone
Dkk1	Dickkopf related protein 1
Dlk1	Delta like homologue 1

dMEM	Dulbecco’s minimal essential medium
DPFi	Dermal papilla fibroblasts
Dpp4	Dipeptidyl peptidase 4
DTI	Defined trypsin inhibitor
DTT	Dithiothreitol
ECM	Extracellular Matrix
EDGS	Epilife derived growth supplement
EGF	Epidermal growth factor
EGFR	Epidermal growth factor receptor
EMIL1	Emilin 1
EtOH	Ethanol
FBLN2	Fibulin 2
FBN1	Fibrillin 1
FBS	Fetal bovine serum
FDA	Food and drug administration
FGF	Fibroblast growth factor
Fgf2	Fibroblast growth factor 2
Fgf7	Keratinocyte growth factor
Fi	Fibroblasts (blended)
FN1	Fibronectin
GM	Growth media
H&E	Haematoxylin and eosin
HCl	Hydrogen chloride
IAM	Iodoacetadime

IBMX	3-Isobutyl-1-methylxanthine
IF	Immunofluorescence
IL-	Interleukins
IL22	Interleukin 22
IL22R	Interleukin 22 receptor
IL6	Interleukin 6
K14	Keratin 14
KC	Keratinocytes
Kgf	Keratinocyte growth factor
Lef1	Lymphoid enhancer binding factor 1
Lrig1	Leucine repeats and immunoglobulin like domain 1
MITC	Mitomycin C
N	Number of biological replicates
n	Number of technical replicates
NFH	Neurofilament heavy chain
OM	Osteogenic media
P10	Passage 10
P4	Passage 4
PBS	Phosphate buffered saline
PDGF	Platelet derived growth factor
Pdgfrα	Alpha type platelet derived growth factor receptor
PDPN	Podoplanin
PFA	Paraformaldehyde
PFi	Papillary fibroblasts

PGE2	Prostaglandin E2
PLGS	Protein Lynx Global Server
RFi	Reticular fibroblasts
rhEGF	Recombinant human epidermal growth factor
rhIGF1	Recombinant human insulin-like growth factor 1
RT-PCR	Reverse transcription polymerase chain reaction
Sox2	Sex determining region box 2
THBS1	Thrombospondin
TNC	Tenascin
VIM	Vimentin
VTN	Vitronectin
α-SMA	Alpha smooth muscle actin

List of reagents

ABAM	Gibco life technologies
dMEM	Gibco life technologies
FBS	Gibco life technologies
PBS	Gibco life technologies
Trypsin-EDTA	Gibco life technologies
DTI	Gibco life technologies
Dispase	Gibco life technologies
Epilife	Gibco life technologies
EDGS	Gibco life technologies
Coating matrix kit	Gibco life technologies
Formalin	Sigma
EtOH	Sigma
DPX mounting media	Merck
Trichrome blue kit	Abcam
PFA	Agar scientific
Triton X	Sigma
Goat Serum	Vector laboratories
Dexamethasone	Sigma
Ascorbate-2-phosphate	Sigma
B-glycerophosphate	Sigma
Alizarin red	Millipore
HCl	Sigma

Calcium assay kit	BioAssay systems
Insulin	Sigma
IBMX	Sigma
Indomethacin	Sigma
Oil red O	Abcam
Isopropanol	Sigma
alamarBlue®	Invitrogen
Qiagen RNeasy kit	Qiagen
OligoDT	Life technologies
dNTP mix	Life technologies
5x first strand buffer	Life technologies
DTT	Life technologies
RNAseOUT	Life technologies
Superscript III RT	Life technologies
SYBR Green Master Mix	Life technologies
Primers	Invitrogen
Gelatin	Sigma
Glutaraldehyde	Sigma
Glucine	Sigma
Ascorbic acid	Sigma
NH4OH	Sigma
DnaseI	Roche
Trypsin	Sigma
DTT	Sigma

Iodoacetadime	Sigma
Trifluoroacetic acid	Sigma
2 well inserts	Ibidi
Mitomycin C	Sigma
Human cytokine array	RayBiotech
AXL	R&D systems
CCL19	Biolegend
IL6	Gibco life technologies
BMP6	Biolegend
PDGF-BB	Biolegend

Chapter 1. General introduction

1.1. Skin structure and function

The integument system is the largest organ in the body and is composed by skin and its appendages. Skin mainly acts as a first mechanism of defence, to protect the organism from pathogens and minimise water loss from the body. It has a built in mechanism to restore its structure and function in case of damage, in order to protect the body from external factors. Skin is a stratified structure composed of epidermal, dermal and hypodermal layers (Figure 1.1.1.). However, this is an oversimplified way of describing the integument as each segment has its own complexity that contributes to the maintenance of organ homeostasis. Multi-layered, stratified Keratinocytes (KC) comprise the majority of cells within the epidermis, while the underlying dermis is predominantly composed of connective tissue with fibroblasts, blood vessels, nerves and immune cells (Driskell and Watt, 2015, Sriram et al., 2015). Even further beneath the surface is the hypodermis, also known as dermal white adipose tissue; a layer of adipocytes that acts as an energy reserve and has a role in metabolic homeostasis (Driskell et al., 2014, Alexander et al., 2015).

There are two types of skin in humans and other primates; hairy skin and non-hairy skin. Hairy skin covers the majority of the body and is characterised by the presence of hair follicles and sebaceous glands. The skin on the body has vellus hair while the one on the scalp has terminal hair. Non-hairy skin is present on the soles and palms (also known as palmoplantar), does not contain any hair follicles and has a thicker epidermal layer. It is important to mention that for the purposes of this thesis I will only focus on hairy skin and specifically that found on the scalp as I am studying the fibroblast populations in the follicular and interfollicular dermis.

1.1.1. Epidermis

The outer most layer of skin is comprised mostly of epithelial cells, known as KCs. The epidermis is divided into four layers on body skin or five layers on palmoplantar skin. From the outer most to the inner most, these layers or stratums are: the stratum corneum, the stratum lucidum (only in palmoplantar skin), the stratum granulosum, the stratum spinosum and the stratum basale (Figure 1.1.1.). The stratum basale is generally referred to as the basal layer and contains proliferative KCs whilst the other layers contain differentiated KCs which move from the basal layer through to the stratum corneum. Stem cells within the basal layer maintain epidermal homeostasis by continuous regeneration of the KCs which will later on differentiate to replace the cells in the stratum corneum. The basal layer sits on the basement membrane which anchors the epidermis with the dermis (Hsu et al., 2014).

1.1.2. Dermis

The dermis sits between the epidermis and the hypodermis (Figure 1.1.1.). It mainly acts as a supportive tissue to the epidermis (Werner and Smola, 2001). Evidence suggest that the dermis is responsible for the production of several components of the basement membrane which sits between the dermis and the epidermis and offers support to the epithelium (Lee and Cho, 2005).

Fibroblasts within the dermis are responsible for the extracellular matrix (ECM) deposition which provides structural support to the tissue (Tracy et al., 2016). The ECM is composed of fibrillar matrix proteins and non-fibrillar forming proteins (Tracy et al., 2016). The fibrillar matrix protein Collagen, constitutes the bulk of the ECM while

other fibrous forming proteins include Fibronectin and Fibrillin all of which give the tissue its integrity and flexibility.

The dermis is divided into two regions, the papillary dermis which sits adjacent to the epidermis and the reticular dermis which is deeper in the dermis and closer to the hypodermis. Within these regions, it also contains hair follicles, nerve endings, sweat glands, sebaceous glands and blood vessels that contribute to the functionality of the tissue by enhancing sensation and regulating the body temperature.

1.1.3. Hypodermis

This is the lowermost layer of the integument system which is also known as the dermal white adipose tissue. This region has mainly adipocytes that are grouped together in lobules and are separated by connective tissue. Its function is to act as an energy reserve and is an important thermal regulator of the body. Even though the hypodermis does not contain any fibroblast populations, the end bulb of the hair follicle which is surrounded by dermal sheath fibroblasts sits in the hypodermal compartment of the skin and engulfed in it are the dermal papilla fibroblasts (DPFi) (Figure 1.1.1.).

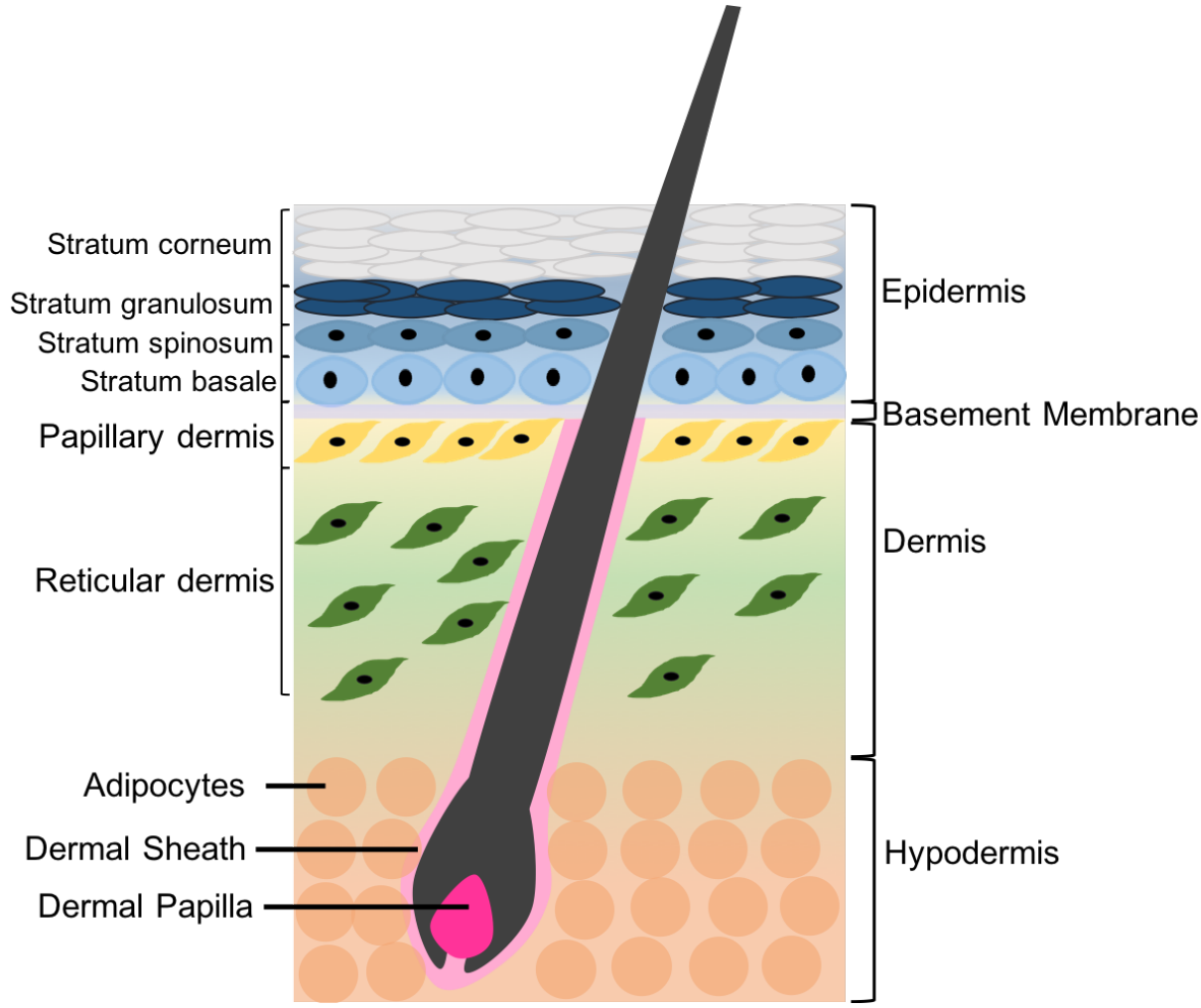


Figure 1.1.1. Skin structure.

The outermost layer of skin is the epidermis that contains the KC. The epidermis is divided into; stratum corneum, stratum granulosum, stratum spinosum and stratum basale. The basement membrane is located under the epidermis. The dermis sits in between the epidermis and the hypodermis and is divided into two compartments; the papillary dermis and the reticular dermis. The hypodermis contains adipocytes and the dermal papilla, which is the base of the hair follicle. The hair follicle is surrounded by the dermal sheath or else known as the connective tissue sheath.

1.1.4. Hair follicle

The epidermis produces numerous appendages that differ from species to species. In humans, these appendages include the hair follicle and sweat glands (Figure 1.1.2.)(Gonzales and Fuchs, 2017). The role of the hair follicle is to protect the surface and regulate the temperature of the body but nowadays is also important for aesthetic purposes. It is composed of sebaceous glands, an inner root sheath and an outer root sheath which are epidermal in origin, and a dermal sheath and dermal papilla which are mesenchymal in origin. Humans have two types of hair; vellus hair and terminal hair. Terminal hair is restricted to a few body sites including the scalp. In this thesis, I will only be focusing on the fibroblasts within the terminal hair follicle also known as the DPFi which are found on the base of the hair follicle engulfed within the hair matrix. I will not be including the dermal sheath fibroblast in my observations. Despite them having a key role in supplying cells to the dermal papilla at the initiation of anagen, the original aims for this thesis were established after publication of a manuscript analysing establishment of cell identity in three skin fibroblast populations; those of the upper and lower skin dermis, and those within the dermal papilla (Driskell et al., 2013). This paper did not refer to the dermal sheath, and thus when I started my thesis project, I established matched cell populations from cells in the upper dermis, lower dermis, and dermal papilla dermis only.

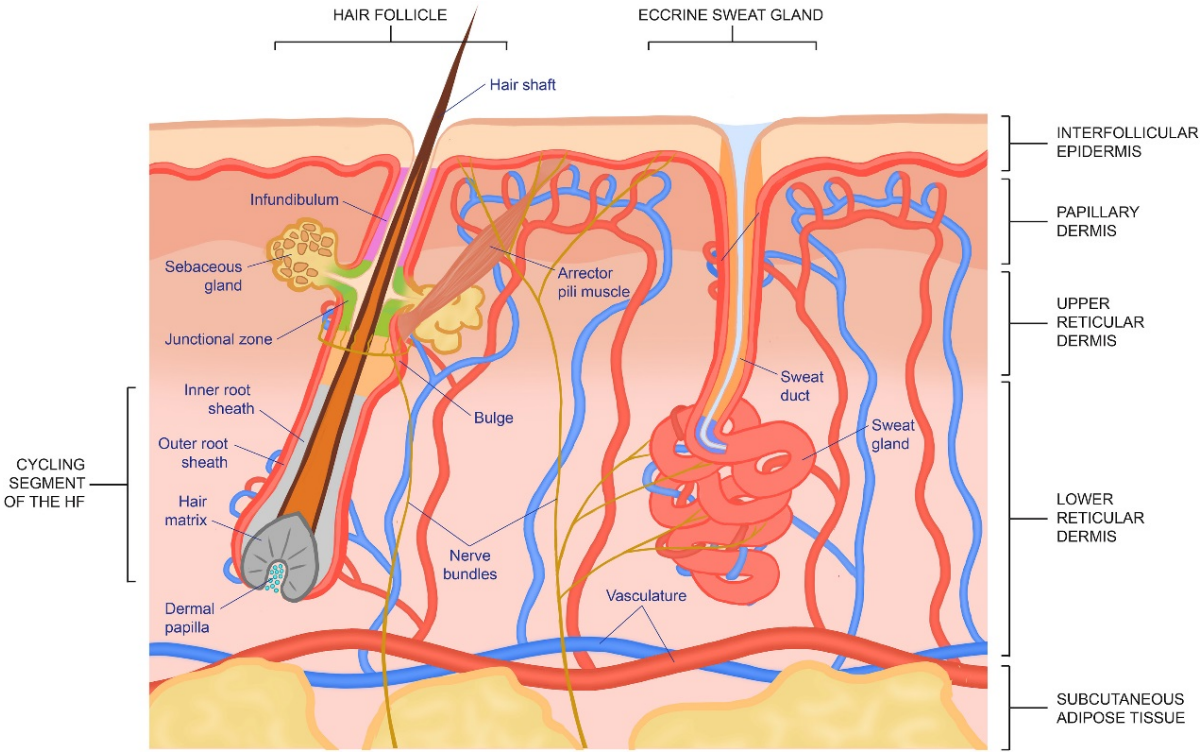


Figure 1.1.2. Components of the hair follicle.

Appendages of the skin include the hair follicle and sweat gland. The dermal papilla is engulfed on the base of the hair follicle within the hair matrix (Gonzales and Fuchs, 2017).

1.2. Skin and hair morphogenesis

From the knowledge we have acquired from murine and chick embryo experiments in the 1970s, we know that skin and hair follicle morphogenesis is driven by reciprocal epithelial-mesenchymal interactions, with the initiating signal for these interactions arising in the mesenchymal dermis (Dhouailly and Sengel, 1972, Dhouailly, 1973, Millar, 2002). The hair follicle is composed of two tissue types; the mesenchyme and the epithelium. The dermal papilla and dermal sheath make up the mesenchyme and the remainder of the follicle is epithelial in nature.

1.2.1. Reciprocal interactions in skin morphogenesis

During mouse embryogenesis, the formation of the hair follicle is described as a cascade of reciprocal signals between the juxtaposed epithelial and mesenchyme compartments. Early in development, a unipotent dermis and epidermis are observed (Figure 1.2.1A). At this point of their embryonic life, all of the fibroblasts in the dermis express Delta-like homologue 1 (Dlk1), Leucine-rich repeats and immunoglobulin-like domains 1 (Lrig1) and Alpha-type platelet-derived growth factor receptor (Pdgfrα) (Driskell et al., 2013). The first step of hair development is characterised by epidermal thickenings uniformly spread across the epidermis which are known as placodes (Figure 1.2.1B). Placode development occurs as a result of an unknown signal (known as the first dermal signal) from the dermis that acts on the epidermis. We do not know what this signal is but there is evidence that it is associated with the WNT signalling pathway which will be discussed further in section 1.2.3. WNT signalling molecules are expressed in both dermal and epidermal compartments during hair follicle morphogenesis (van Amerongen and Nusse, 2009, Andl et al., 2002).

In response to this first dermal signal, a signal from the placode, signals to the dermal fibroblasts resulting in the formation of a dermal condensate (Figure 1.2.1C). One contender for this placodal signal in mouse skin is FGF20 (Huh et al., 2013) although this is not conclusive. The fibroblasts in the condensate are double the density of surrounding fibroblasts, however, there is no evidence of proliferation occurring resulting in condensation. Therefore, the condensate is believed to arise as a result of fibroblast migration towards the placode signal (Michon et al. 2007). Fibroblasts that accumulate in the dermal condensate start expressing hair specific markers, such as

Sex determining region-Box 2 (Sox2) (Driskell et al. 2009) that signify a change from a fibroblast to a condensate and hair follicle fate.

A second dermal signal, initiating from the newly formed dermal condensate, signals to the placode causing proliferation and invasion of these epithelial cells into the dermis, resulting in the formation of the hair germ (Figure 1.2.1D). At the same time as hair follicles are developing, the epidermis is stratifying, and the dermis is getting thicker. In the dermis we see a divergence of the remaining fibroblasts, resulting in the formation of two cell types in distinct spatial locations that have arisen from a common fibroblast progenitor (Driskell et al. 2013). We know there is divergence since the fibroblasts in murine skin start to express different markers in their respective locations. The upper dermis, adjacent to the basement membrane (which separates the epidermis and dermis), is now referred to as the papillary dermis, and expresses PR domain zinc finger protein 1 (Blimp1), Pdgfrα and Lrig (Figure 1.2.1E). The lower dermis is now known as the reticular dermis and fibroblasts here express Pdgfrα, and Dlk1 (Driskell et al. 2013).

The hair germ continues to grow down and becomes the hair peg (Figure 1.2.1F) and then the bulbous peg (Figure 1.2.1G). The bulbous peg is the last stage of follicle morphogenesis observed during embryogenesis in mouse skin. By postnatal day 2, the hair follicle has formed from the bulbous peg. The dermal condensate, which was observed during morphogenesis, becomes the dermal papilla and is engulfed inside the epithelial portion of the hair follicle (Figure 1.2.1H). The dermal papilla is a small cluster of mesenchymal cells that reside at the base of the hair follicle.

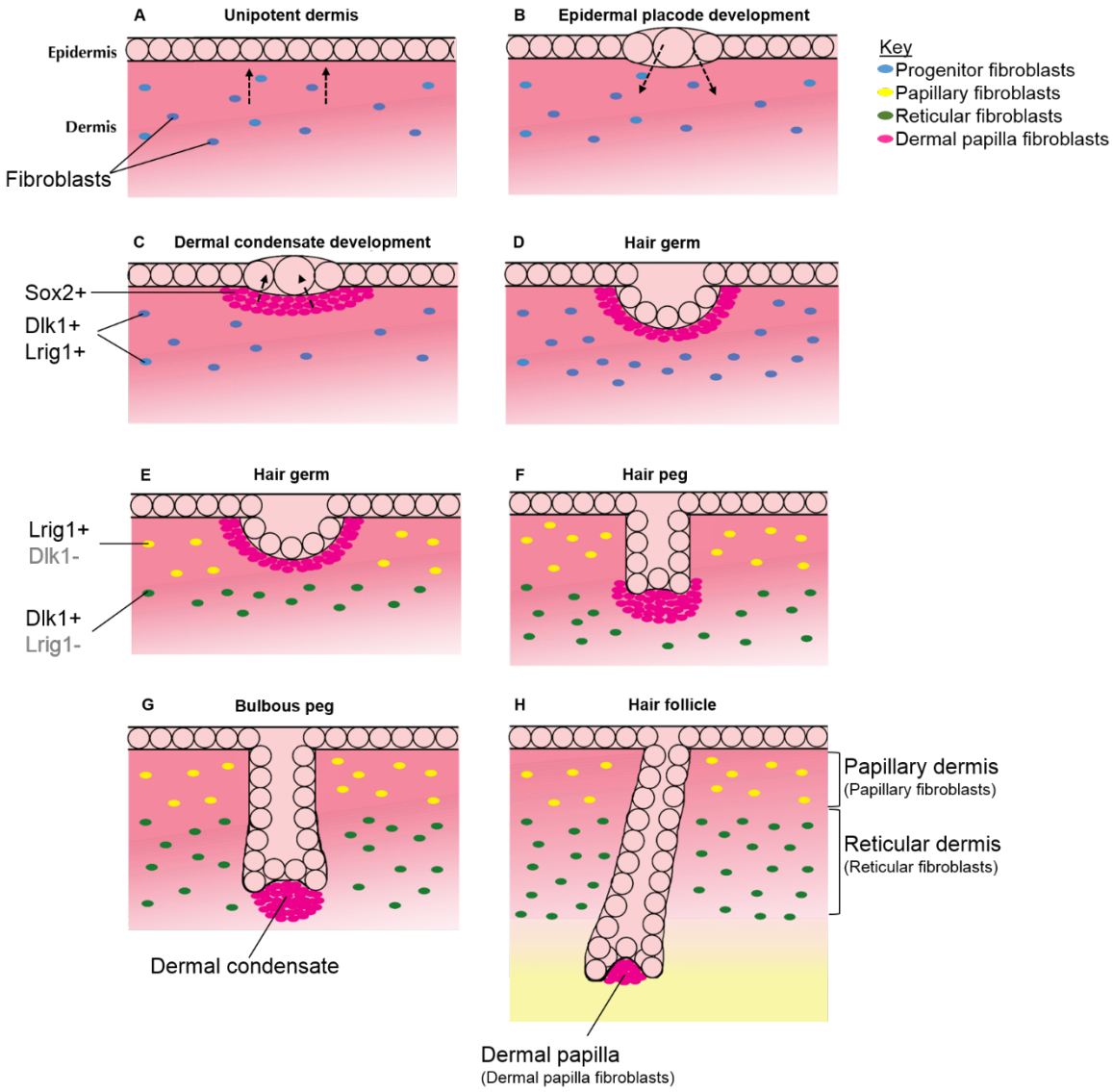


Figure 1.2.1. Skin morphogenesis.

(A) At the start of embryogenesis there is a unipotent dermis and epidermis. (B) An unknown signal (black arrows) from the dermal fibroblasts (blue) acts on the epidermis and promotes placode development. (C) In response to that signal a reciprocal signal (black arrows) from the epidermis promotes condensate formation and attracts fibroblasts that switch on condensate markers such as Sox2. (D) After condensate formation, the cells in the placode proliferate to form the hair germ. (E) As the hair germ forms there is a divergence of fibroblasts that causes formation of two layers in the dermis; the papillary dermis (yellow) and the reticular dermis (green). The hair germ continues to grow down and becomes the hair peg (F) then the bulbous peg (G) and eventually the hair follicle (H). The dermal condensate is now engulfed by the epithelium of the hair follicle and is now known as the dermal papilla.

At the start of development, Dlk1 and Lrig1 are expressed in all fibroblasts, but upon divergence Dlk1 is expressed in the fibroblasts in the lower reticular dermis and Lrig1 is expressed in the fibroblasts in the upper papillary dermis. These are known retrospectively as reticular fibroblasts (RFi) and papillary fibroblasts (PFi). Transplantation assays in mice showed that the fibroblasts become committed to a particular lineage (either papillary or reticular) by postnatal day 2 and after this time point cannot transdifferentiate into one another (Figure 1.2.2.) (Driskell et al. 2013). However before P2 a PFi can become a DPFi and vice versa.

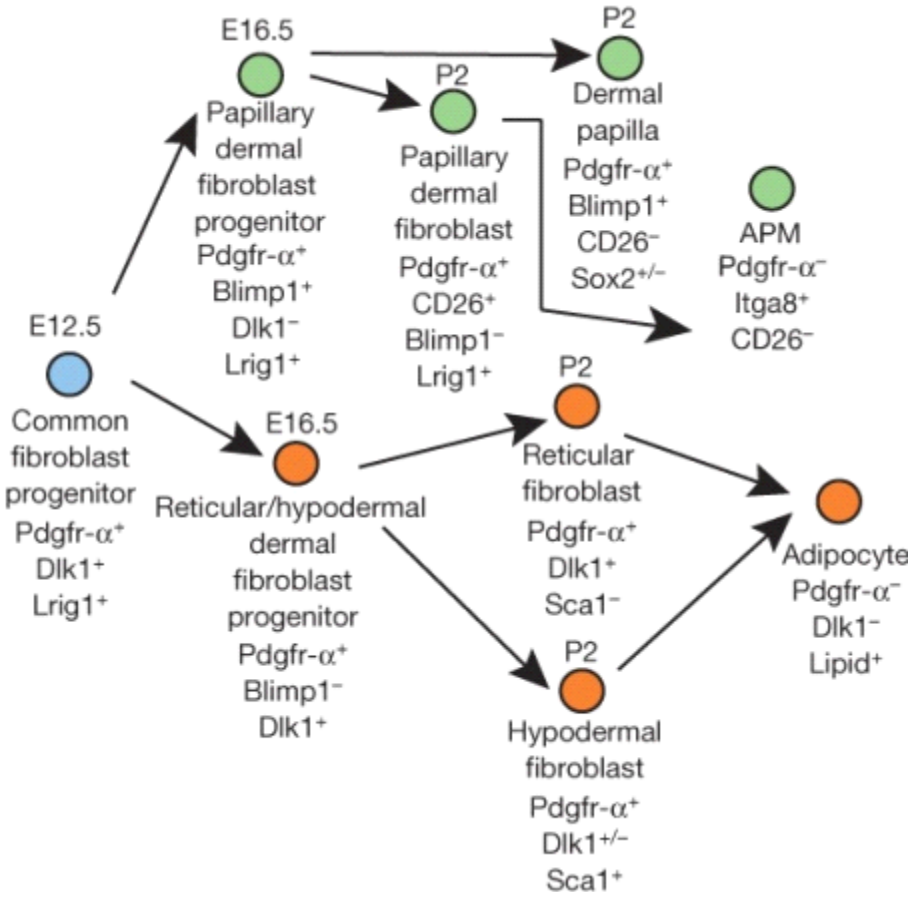


Figure 1.2 2. Common fibroblast progenitor.

At E16.5 there is a divergence of fibroblasts. The DPFi, PFi and RFi all arise from a common dermal fibroblast progenitor (Driskell et al., 2013).

1.2.2. Postnatal skin

In postnatal skin there are therefore multiple fibroblast populations three of which have been defined by their spatial location; DPFi of the hair follicle, PFi and RFi (Driskell et al., 2013). Although these three populations now have distinct expression profiles and locations, they all originally arose from a common fibroblast progenitor (Figure 1.2.2.). Alongside acquiring divergent expression profiles, these three fibroblast populations have distinct functions in skin and hair development and homeostasis. It is important to note that dermal sheath fibroblasts can also be defined by their spatial location, even though they are not included in the aforementioned study. Other subpopulations of dermal fibroblasts are also present which can be characterised by their function (eg. Fibrotic fibroblast) (Rinkevich et al., 2015) but for the purposes of this thesis I will focus on these three populations defined by spatial location.

1.2.3. WNT signaling in skin development

The Wnt/β catenin signalling pathway is thought to have an important role in hair follicle development (van Amerongen and Nusse, 2009). *In vivo*, DPFi express the Wnt ligand WNT10b which is proposed to be associated with their ability to promote hair follicle formation (Li et al., 2011). In the chick and mouse embryos, it has been found that Wnt ligands are expressed throughout the epithelium leading to the formation of feather/hair placodes (Chang et al., 2004). These ligands are expressed in the epithelium and promote Wnt signalling activity throughout the dermis. Wnt signalling in the dermis later becomes refined as Dickkopf-related protein 1 (Dkk1), a Wnt inhibitor, is expressed in between Wnt positive dermal condensates. Dkk1 acts as an inhibitor and is normally expressed in the dermis. Andl and colleagues generated

a transgenic mouse that ectopically expressed Dkk1. Lymphoid enhancer-binding factor 1 (Lef1) is normally expressed in the epidermis during embryonic development and later on becomes up regulated in the placode and dermal condensate. When Dkk1 was overexpressed in the epidermis, Lef1 was absent in the epithelial cells and subsequently hair development was blocked. Through these experiments they have brought to light that Wnt/β-catenin signaling is necessary for the initial steps in hair follicle development (Andl et al., 2002).

Early in embryonic life (E12.5), Wnt ligands are expressed in the epidermis which activate broad Wnt signaling across the dermis (Figure 1.2.3A). This dermal activity leads to activation of Wnt signaling in the placode at E13.5 (Figure 1.2.3B), and then strong activity is observed in the condensate at E14.5 (Figure 1.2.3C) (Chen et al., 2012). Recently, Chen and colleagues showed the importance of Wnt activity for placode formation by a series of elegant transgenic knock out experiments. When β catenin was ablated in the dermis using a conditional knockout mouse, it resulted in an inability of the dermis to respond to the Wnt ligands in the epidermis. Subsequently, dermal Wnt signalling and Lef1 expression is disrupted (Figure 1.2.4.) (Chen et al., 2012). That led to the loss of dermal condensate formation and consequently the loss of the hair follicle development. The authors demonstrate that Wnt signaling is essential for the initiation of hair follicle development.

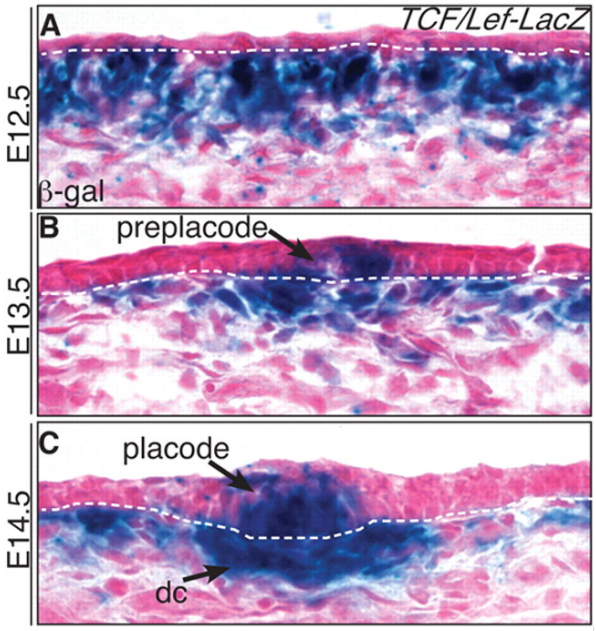


Figure 1.2.3. WNT signalling reporter activity in embryonic skin during hair development.

(A) At E12.5, broad Wnt activity is sustained across the skin dermis. (B/C) By E14.5 Wnt signalling is up regulated in the hair follicle placode and becomes refined with the dermal condensate (Chen et al., 2012).

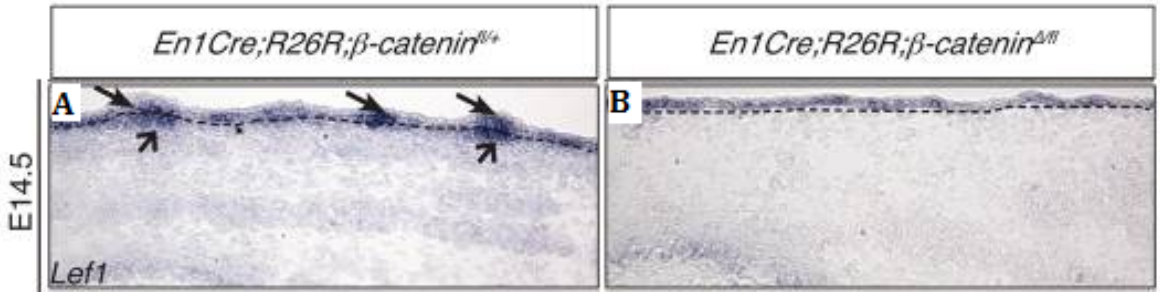


Figure 1.2.4. WNT knockdown in the placode and dermal condensate.

(A) Lef1 is expressed in a patterned manner in the placode and dermal condensate in control mice, (B) Ablation of β catenin in the dermis, using a conditional knockout, leads to loss of both placode and condensate formation. Lef1 expression is no longer patterned in the epidermis and is absent in the dermis (Chen et al., 2012).

1.3. Dermal fibroblast populations in adult skin and their function *in vivo*

1.3.1. The role of follicular fibroblasts, DPFi, in skin

The base of the hair follicle is located in the hypodermis, and within is engulfed the dermal papilla. From murine embryo studies it has become well accepted that the dermal condensate regulates hair development. In the adult, the dermal papilla is responsible for hair growth by regulating the hair cycle.

1.3.1.1. Hair cycle

Epithelial-mesenchymal interactions observed in development that are important for follicle morphogenesis are also observed in the adult during follicle cycling. Hair follicles go through continuous cycles of growth (anagen), regression (catagen), and resting phases (telogen) during their lifetime (Figure 1.3.1), during which time the dermal papilla cell number fluctuates (Greco et al., 2009, Plikus et al., 2011, Rahmani et al., 2014). Anagen is the growth phase of the hair follicle cycle. The epithelial matrix cells in the base of the hair follicle proliferate in response to signalling from the dermal papilla and differentiate into the hair shaft and concentric layers that support the fibre (Higgins et al., 2009). After the growth phase (anagen), cells in the lower follicle regress and this phase is known as catagen. At this point the number of cells in the dermal papilla starts decreasing, due to migration of the cells towards the dermal sheath which will later apoptose (Rahmani et al., 2014). The hair fibre which was actively growing becomes a club fibre which will later be shed from the follicle. Also, apoptosis in the epithelial strand that separates the dermal papilla from the club fibre

brings the papilla so it rests just underneath the club fibre. The club fibre is surrounded by an outer layer of epithelial cells known as the old bulge (Greco et al., 2009). The bulge is the epithelial stem cell compartment of the hair follicle. At the end of telogen, signals from the dermal papilla activate the bulge cells leading to the initiation of anagen (Greco et al., 2009). The dermal papilla increases in size because of an influx of dermal sheath stem cells which differentiate into dermal papilla cells, thus exiting telogen and re-entering anagen (Rahmani et al., 2014). These interactions between the dermal papilla and the bulge are similar to those observed between the condensate and the placode in development.

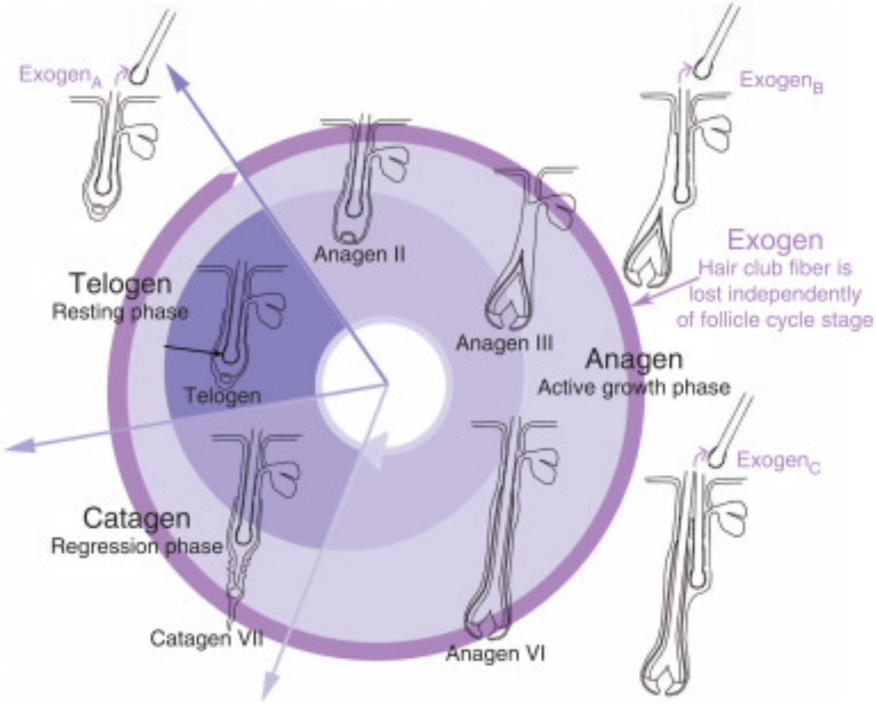


Figure 1.3.1. Hair cycle.

Anagen is the growth phase, catagen the regression phase and telogen the rest phase of the hair follicle (Higgins et al., 2009).

It has been shown that certain signalling pathways, including the Wnt, Bone morphogenic proteins (BMP) and Fibroblast growth factors (FGF) pathways (Plikus,

2012), are important for this continuous cycle. BMP signalling is also of great importance as it maintains the bulge stem cells in a quiescent state during the resting phase telogen. Inhibition of BMP induces proliferation of bulge cells and the follicle enters anagen from telogen (Greco et al., 2009).

1.3.1.2. Importance of the dermal condensate and dermal papilla

The presence of the condensate is necessary for hair follicle development as the irradiation experiments performed by Jacobson in the 1960s showed an arrest to hair follicle development after embryonic irradiation (Jacobson, 1966). In these experiments, irradiation of the embryo disrupted the epithelial-mesenchymal junction of developing hair follicles. Disruption of this junction leads to a loss of reciprocal interactions and dispersal of the condensate. When the condensate is dispersed, hair follicle development cannot proceed.

More recently, the importance of the dermal papilla for hair follicle cycling was demonstrated by Rompolas and colleagues. They showed in mice, that when an adult dermal papilla in telogen is ablated with a laser, the hair follicle remains at rest (quiescent) and cannot reenter anagen. Comparatively, surrounding hair follicles that still have dermal papillae are not affected and continue their growth normally (Figure 1.3.2.) (Rompolas et al., 2012). These findings, together with Jacobson's experiments support that a condensed mesenchyme is vital for hair development and growth. Clustered dermal cells signal to, and act on KCs resulting in non-autonomous activation of the KCs and promotion of hair growth.

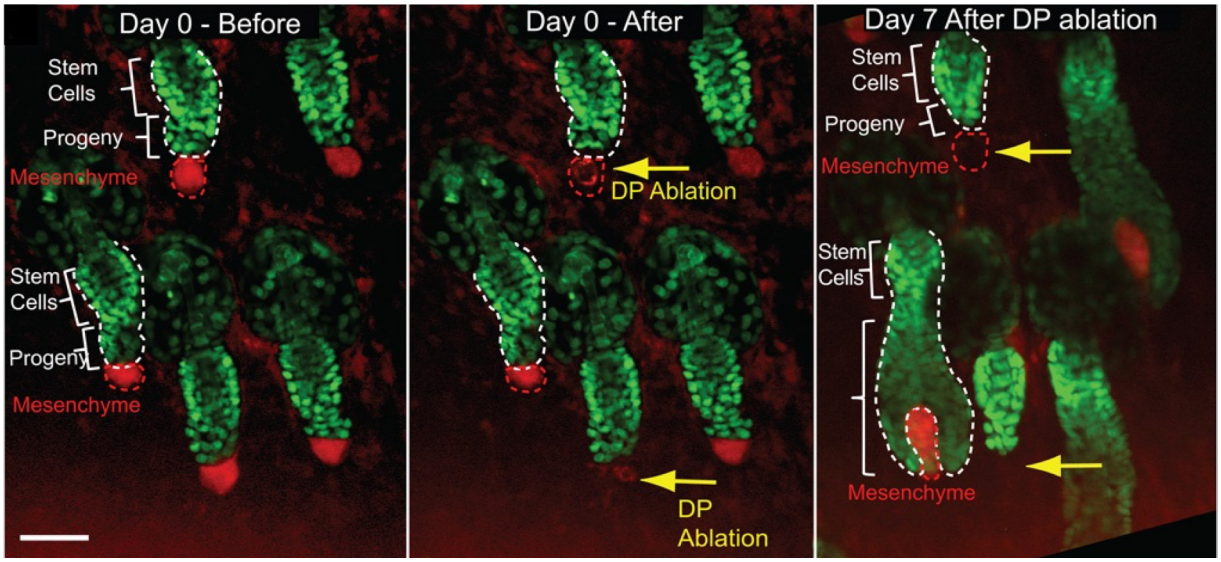


Figure 1.3.2. Ablation experiments in adult mice dermal papilla.

Before and after the dermal papilla (red) is ablated in relation to the epithelium (green) and the surrounding hair follicles. The ablated follicle remains quiescent while other follicles re-enter anagen (Rompolas et al., 2012).

1.3.1.3. Inductivity

Not only are dermal papilla cells required to promote follicle cycling, but they are also inductive. When removed from the hair follicle and placed in direct contact with a non-hairy epidermis they have the capacity to induce formation of a hair follicle in the reciprocal epidermis, thus reprogramming the epidermis to a follicle fate. If the dermal papilla is close to the epidermis but not in direct contact, it does not induce hair follicle formation showing the importance of cell contact in hair follicle formation (Jahoda et al. 1993). Intact dermal sheath has also been shown to be inductive, but when it is cultured, it loses its inductivity (Reynolds et al., 1999).

Approximately 30 years ago, Jahoda and colleagues demonstrated that rodent dermal papillae are highly inductive (Jahoda et al., 1984). They have also established a

method of isolation and expansion of the dermal papilla cells from their non-proliferative state at the bottom of the hair follicle, to a proliferative state *in vitro* (Jahoda & Oliver 1984). Interestingly, rat whisker papilla cells retain their inductive capacity during early passages in culture although they lose it at higher passages (Jahoda et al. 1993).

When human dermal papilla are placed in culture their transcriptional profile is dramatically altered (Higgins et al. 2013). When they are *in vivo*, other dermal papilla cells surround them and suddenly when moved to a culture petri dish they have minimal physical contact with other cells. In addition, our laboratory has shown that perturbation of dermal papilla cells by growth in culture results in disruption of Wnt signalling (Higgins et al. 2013). Therefore, they lose their capacity to instruct hair growth immediately upon placement into tissue culture in contrast to the rat dermal papilla that remains inductive at early passages in culture (Jahoda et al., 1993).

Dermal papilla removed from rat whiskers will spontaneously form aggregations or clumps in culture (Jahoda & Oliver 1984). On the other hand, human DPFi do not spontaneously clump in culture, although in their natural environment *in vivo* the cells are aggregated just as they are in rat follicles. More recently, our lab demonstrated that it is possible to force human dermal papilla cells (Figure 1.3.3A) into spheroids by culturing cells in hanging drops (Figure 1.3.3B) (Higgins 2010). This spheroid structure morphologically resembles the *in vivo* dermal papilla (Figure 1.3.3C and D). We went on to show that human dermal papilla cells grown in a 3D structure in the form of spheroids, partially regain their inductive capacity and can instruct hair growth in recipient human epidermis (Higgins et al. 2013).

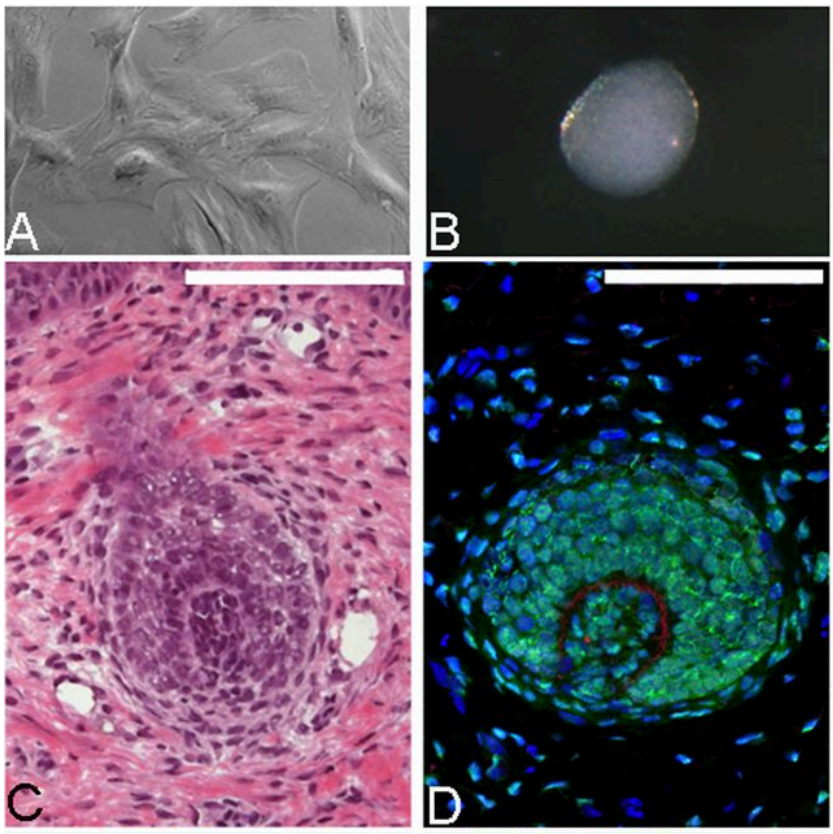


Figure 1.3.3. Human dermal papilla spheroid inductivity.

(A) Dermal papilla cells in 2D culture. (B) Dermal papilla cells in spheroid form after 2 days in a hanging drop. (C) Hematoxylin and Eosin staining of a de novo hair follicle induced by a dermal papilla spheroid. (D) Human specific antibody in green indicates the new hair follicle formation, laminin-5 is shown in red and indicates the basement membrane, the boundary between the dermal papilla and the matrix and DAPI in blue stained the nucleus of the cells (Higgins et al., 2013).

1.3.2. The role of interfollicular fibroblasts, PFi and RFi in skin

As mentioned previously, there are different dermal fibroblast populations in postnatal skin. We know already that the function of the DPFi is to control hair follicle cycling. However, the function of PFi and RFi in the dermis remains to be elucidated, although it is generally accepted that the PFi acts as a support to the overlying epidermis.

1.3.2.1. What is the role of PFi?

PFi populate the upper dermal compartment which is located adjacent to the epidermis. They are generally thought to have a supportive role in epidermal function (Werner and Smola, 2001) but their exact role in the dermis is not fully understood. Research using dermal equivalents have shown that in young skin the papillary dermis is able to promote epidermal morphogenesis in comparison to the reticular dermis (Mine et al., 2008). In these experiments, KCs seeded on dermal equivalents containing PFi, were able to fully differentiate and stratify to form a functioning epidermis, whilst KCs seeded on RFi generated a thinner and undifferentiated epidermis. This evidence further reinforces the idea that the PFi play a supportive role in skin.

1.3.2.2. What is the role of RFi?

The RFi lie below the PFi and it has been suggested that they become activated during wound healing. Previous studies from the Watt laboratory have aimed to identify how different fibroblast populations contribute to wound healing (Driskell et al., 2013). Transgenic mice that enabled conditional tracing of either RFi or PFi were used and the response of the different fibroblast populations to a repairing wound was evaluated. This was performed using lineage tracing where the Dlk1 positive RFi were tagged with tdTomato (Figure 1.3.4A) and Blimp1 positive PFi with eGFP (Figure 1.3.4D). The mice were injected with tamoxifen to activate the reporter and injured with a full thickness wound.

These wound healing lineage tracing studies elegantly showed the Dlk1 positive RFi to be the first population of fibroblasts to contribute to the process of dermal

regeneration as they migrated first to repopulate the wound 7 days post injury (Figure 1.3.4B). When the same experiment was done with the Blimp1 positive PFi, no positive cells were found in the wound site wither 7 or 17 days after injury (Figure 1.3.4E,F).

These experiments show that RFi are the first to proliferate and repopulate the skin dermis after full thickness wounding. It is thought that RFi proliferate and repopulate the wound, where they contribute to dermal remodelling that is observed during wound closure. Given the nature and importance of mesenchymal epithelial interactions in all other aspects of skin development, I hypothesised that the presence of RFi in a wound might also promote epithelial migration and elicit a wound healing response in overlying KC. This hypothesis is tested in Chapter 3 of this thesis.

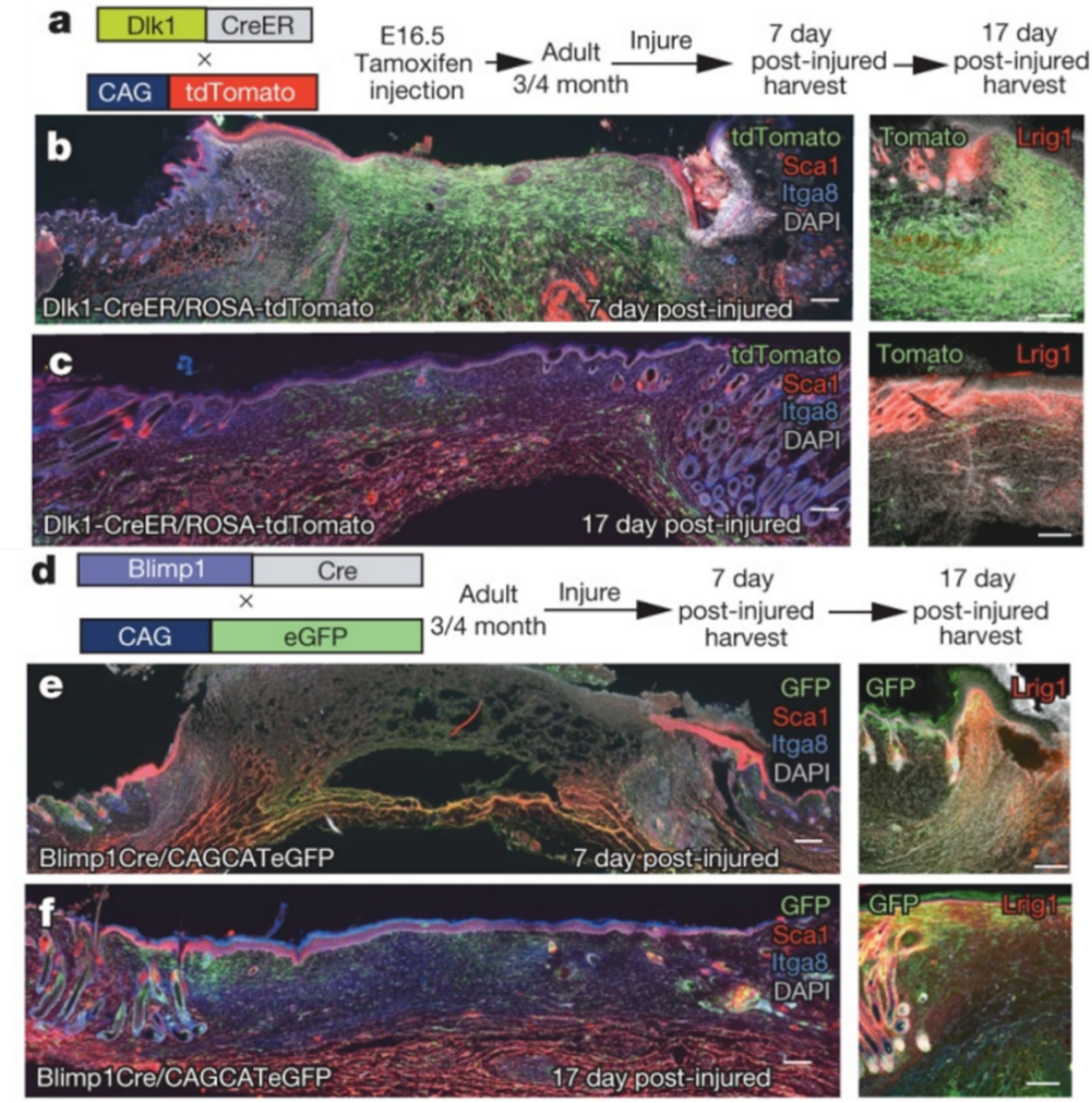


Figure 1.3.4. Reticular and papillary fibroblasts in wound healing.

(A) Dlk1+ RFi were tagged with tdTomato and activated using tamoxifen. (B) A biopsy was taken 7 days post injury that showed Dlk1+ cells in the dermal wound. (C) 17 days post injury the wound is closed and the DLK1+ cells are not present. (D) Blimp1+ PFi were tagged with eGFP and activated using tamoxifen. (E-F) No Blimp1+ cells were found in the wound bed 7 or 17 days post injury. (Driskell et al., 2013).

1.4. Anatomic diversity of fibroblasts

Fibroblasts are cells that are defined by their ability to deposit ECM and they are considered a part of the class of connective tissue cells. Even though they are the most abundant cell in the skin dermis, and a key player in wound healing, this cell type is still ill defined. The word fibroblast is a very general one that covers a broad population of cells that in fact are very dissimilar. In fact, fibroblasts from different body sites such as heart and tendons, differ in their in their orientation and ECM deposition (Doane and Birk, 1991).

Even within a single tissue the fibroblasts are highly heterogenous as it is the case with the dermal fibroblast populations (Philippeos et al., 2018). In skin, fibroblasts arise from three developmental origins; dorsal dermis is from the dermomyotome, ventral dermis is from the lateral plate mesoderm, while craniofacial dermis is derived from neural crest ectoderm (Thulabandu et al., 2017). This is reflected by the different HOX genes expressed in the fibroblasts of the head and the trunk of the body, which control the body plan of an embryo from head to tail (Chang et al., 2002). Recent work on the intrinsic function of fibroblasts showed that dermal fibroblasts retain their ability to contribute to scar formation even when they are transfected to oral cavity fibroblasts that usually do not scar (Rinkevich et al., 2015). These differences in the origin as well as the expression and behaviour of dermal fibroblasts, highlight how diverse a population they are. It also indicates that if we are to begin to understand them we, as scientists, should treat fibroblasts from different body sites and even those in different sub-anatomical locations as separate entities.

1.5. Human skin as a model system

Cross talk between the epithelium and mesenchyme is crucial for hair follicle, skin development and homeostasis and therefore the signalling mechanisms behind these processes are very important. Most studies in this area are carried out in rodents and although a great wealth of information has surfaced from these experiments, translating these findings to understand human development has proven difficult. Our laboratory works solely with human skin biopsies obtained from the occipital scalp of patients (Figure 1.6.1.). From the epidermis we can isolate KC while in the dermis there are the three dermal populations previously described that can be isolated and analysed *in vitro*.

Rodents are the most widely used model to help researchers identify molecular and cellular processes. Mouse skin is morphologically similar to human skin, having an epidermis, dermis and a hypodermis. In addition, both human and mouse hair undergo continuous cycles of anagen, catagen and telogen throughout their lifetime. Although mouse and human skin/hair resemble each other in these aspects, they have some important differences. They differ in anagen length (mouse lasting just a few weeks, while human's lasting several years), in epithelial architecture (mouse epidermis does not have rete ridges while they are present in human skin which is much thicker than mouse skin) and in wound healing mechanisms (mice heal by contraction while humans heal by inflammation and reepithelialisation) (Wong et al., 2011). Mouse hair also grows in a wave pattern with one follicle influencing the next while human follicles grow in a mosaic pattern and are independent of their neighbour. Mouse models have contributed significantly to our understanding of skin and hair development and regeneration. Being able to translate the findings from a mouse model to an *in vitro*

culture using human cells would give us an even better understanding of hair regeneration and wound healing processes in humans.

1.6. Aims

There are two main aims in this thesis that have been divided into two results chapters. The first aim was to isolate DPFi, PFi and RFi from a single piece of scalp skin (Figure 1.6.1.), using a microdisection approach. Then I assessed cell morphology, expression, behavioural and ECM deposition differences in order to identify defining characteristics which can be used to distinguish DPFi, PFi and RFi derived from human scalp skin dermis, from one another. This work in discussed in Chapter 2. Given the involvement of the dermal fibroblasts populations in wound healing, the second aim was to assess how DPFi, PFi and RFi from human skin affect KC migration and wound closure *in vitro*. This work is discussed in Chapter 3.

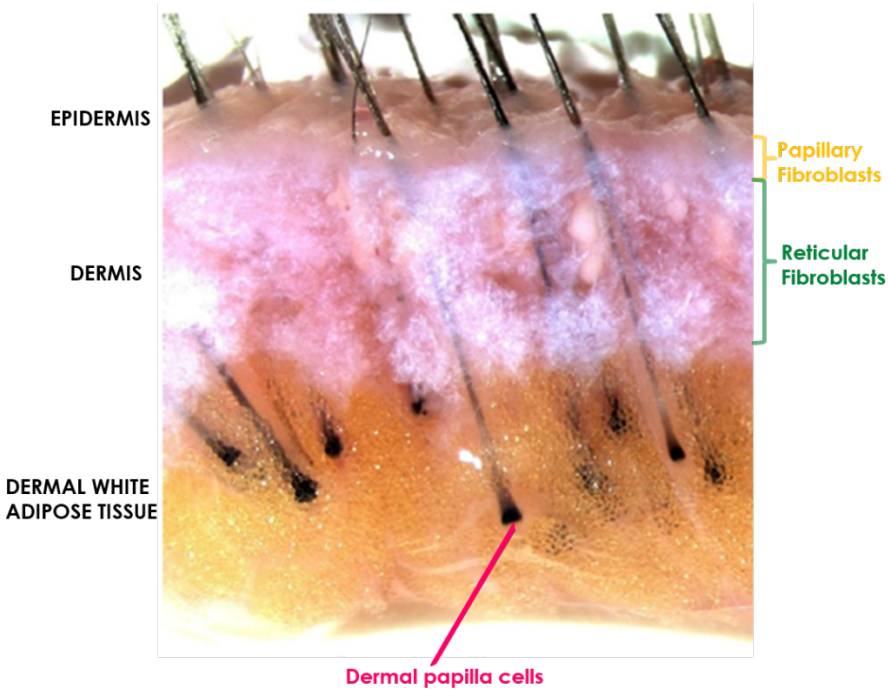


Figure 1.6.1. Macroscopic image of occipital scalp skin biopsy.

The biopsy outlines the position of the epidermis (skin barrier), the dermis and the white adipose tissue. In the dermis there are four dermal populations defined by their location; the PFi, RFi, DPFi and dermal sheath fibroblasts, while in the epidermis there are KC, melanocytes and Langerhans cells.

Chapter 2. Defining fibroblast subtypes in the skin.

2.1. Introduction

Within the skin dermis, dermal fibroblasts are responsible for ECM deposition and organisation (Pflieger et al., 2006, Theocharidis et al., 2016, Tracy et al., 2016). Despite there being clear differences in fibroblasts in different tissues (Castor et al., 1962), across anatomical locations within a single tissue such as the skin (Chang et al., 2002), and even within a single location of a given tissue (Harper and Grove, 1979, Janson et al., 2012), the term fibroblast collectively refers to any cell within connective tissue that produces ECM. This nomenclature means researchers may be studying a cell type termed as a fibroblast, but in reality, fibroblasts used in one laboratory may be very different from those used in another.

In this chapter, I will focus on characterising fibroblast sub-types in a single anatomical location; occipital scalp skin. All the work here was performed by me, and the majority of the results are being written up as a research publication in which I am first author. The mass spectrometry analysis of dermal matrices was performed by me and has been incorporated into a publication (Ghetti et al., 2017) in which I am second author. A part of the microdisection figure was taken from a methods review in which I am also first author (Topouzi et al., 2017).

2.1.1. Dermal fibroblast heterogeneity in murine skin

Early work focusing on fibroblast heterogeneity suggests that we should consider fibroblasts from different body sites as different cell sub-types (Chang et al., 2002, Rinn et al., 2006), while in recent years there has been an effort to refine this nomenclature, and various groups have categorised fibroblasts in the skin dermis with

regard to their lineage, positional identity, expression profiles or functional heterogeneity (Sorrell et al., 2004, Sorrell et al., 2008, Janson et al., 2012, Driskell and Watt, 2015). For example, mouse dorsal skin dermis has been described as originating from a multipotent progenitor via an upper and lower fibroblast lineage during development (Figure 1.2.2.) (Driskell and Watt, 2015). While the lower lineage is believed to contribute RFi of the lower reticular dermis, the upper lineage contributes PFi to the upper papillary dermis, and DPFi to the dermal papilla of the hair follicle dermis. Within the dermal papilla, which is a flame shaped mesenchyme at the base of the hair follicle, DPFi become irreversibly committed to a papilla identity shortly after birth (Driskell et al., 2013, Driskell and Watt, 2015).

RNA-Seq of embryonic and neonate murine skin has successfully identified differences between the interfollicular dermal fibroblasts (PFi and RFi combined), compared to the DPFi (Sennett et al., 2015, Rezza et al., 2016) while a recent single cell RNA-Seq paper highlighted fibroblast heterogeneity in the skin even further describing the dermal papilla as having four microniches containing DPFi with different expression profiles (Yang et al., 2017). Another example of this heterogenic identity that different populations of fibroblasts exhibit, which contributes to the difficulties in defining fibroblasts, comes from the observation that the fibrogenic capacity of these populations is not limited to defined sub-anatomical locations such as the papillary, reticular or hair follicle dermis (Rinkevich et al., 2015, Hu and Longaker, 2016). Suffice to say, fibrogenic tendency of fibroblasts cannot be defined simply by using spatial location. Instead, fibroblasts with fibrogenic capacity are believed to reside throughout the papillary and reticular dermis in a scattered pattern. Fibrogenic fibroblasts are fibroblasts promote the development of fibers, thus ECM. These fibrogenic fibroblasts

in adult skin are marked by Dipeptidyl peptidase-4 (Dpp4 otherwise known as Cd26) (Hu and Longaker, 2016), which is intriguing as in skin development Cd26 expression is restricted to the upper lineage fibroblasts that contribute to the papillary dermis (Driskell et al., 2013).

2.1.2. Human dermal fibroblasts and extracellular environment

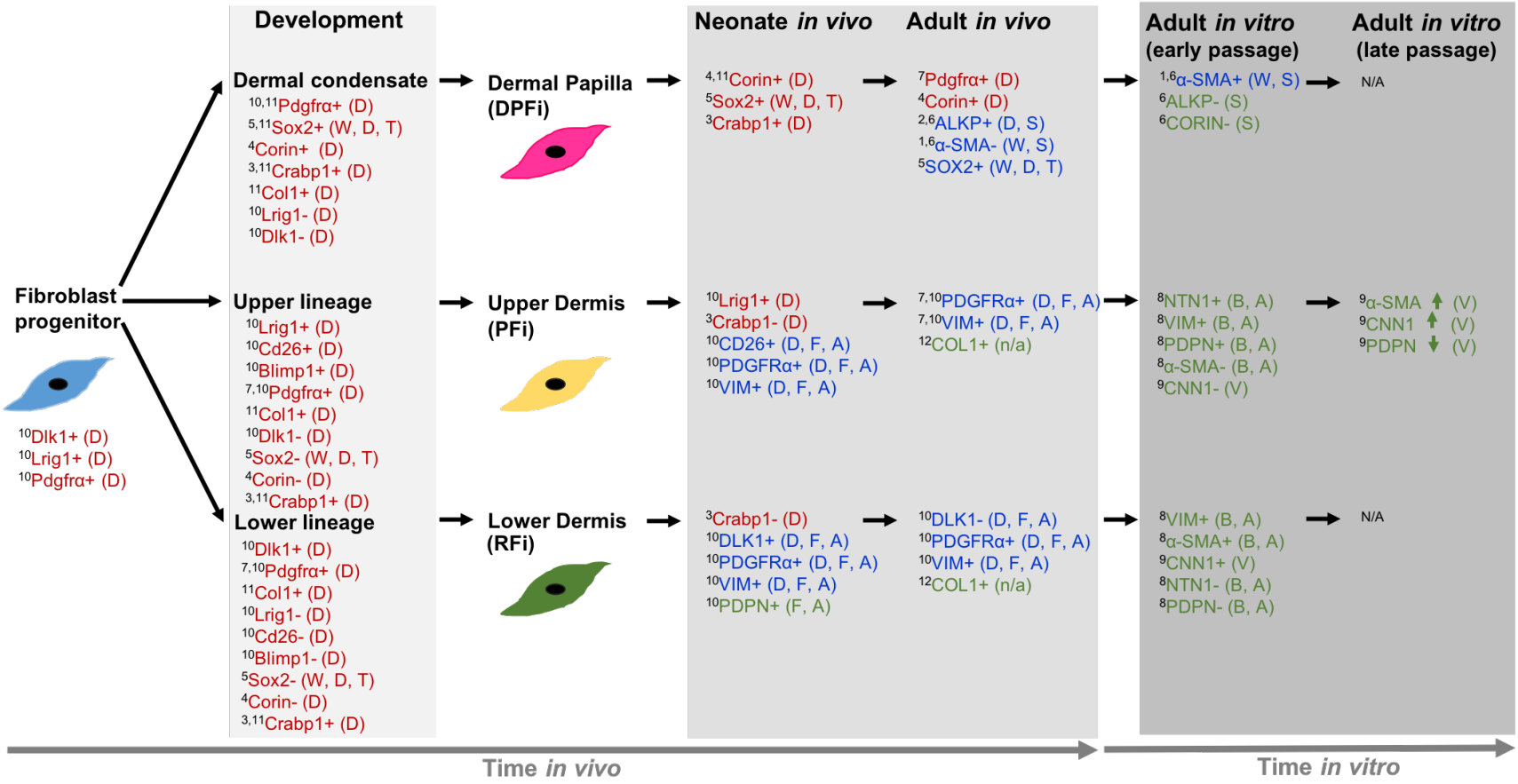
In human skin, there are clear morphological differences between the papillary, reticular and hair follicle (dermal papilla) dermis, however, fibroblast heterogeneity within the human skin dermis is not well understood. Lineage tracing of human skin is not possible, and so fibroblasts can either be defined by their spatial location, their expression profiles or their function. The spatial location of fibroblasts can be directly related to their function, as early heterotopic recombination experiments elegantly demonstrated that fibroblasts can instruct differentiation of epithelia, which is important for skin development and repair (Dhouailly, 1973, Yamaguchi et al., 1999, Pearton et al., 2005). As mentioned before, fibroblasts secrete ECM which in turn characterises their surrounding microenvironment and thus spatial location *in vivo* (Tracy et al., 2016). The human dermal papilla has been shown to be rich in fibrillar matrix proteins such as fibronectin (FN1), interstitial collagens type I and type III, glycoproteins such as thrombospondin (THBS1) and proteoglycans such as versican (Messenger et al., 1991, Pablos et al., 1998, Jahoda et al., 1992, Werner et al., 2007b, Soma et al., 2005). The ECM secreted by PFi and RFi between the dermal papillae, in the interfollicular space also has a distinct phenotype and composition. The PFi fibres are known to be thin and not well organised, whereas RFi fibres are thick and well aligned (Schafer et al., 1985a, Schonherr et al., 1993, Sorrell and Caplan, 2004). These

differences in ECM composition in the different dermal compartments, highlight the existence of different fibroblast subtypes in the human skin dermis.

2.1.3. Fibroblasts from sub-anatomical locations have different expression profiles

A number of analyses have been performed on fibroblasts from human skin dermis, usually on cells grown *in vitro* after they have been removed from their microenvironment with surrounding spatial cues. To our knowledge there have been no studies evaluating differences between DPFi, PFi and RFi, isolated from human skin taken from the same anatomical location. The majority of studies usually assess just one or two of the different populations, or group all fibroblasts together as a single population. However, these studies have shown that fibroblasts *in vitro* taken from different sub-anatomical locations such as the upper and lower dermis have different expression profiles and behavioural traits. Figure 2.1.1. summarises the results from these studies in mouse and human fibroblast sub-populations. For example, gene expression analysis performed on fibroblasts isolated from ventral skin tissue (mammary reduction or abdominal correction) and grown *in vitro* identified PODOPLANIN (PDPN) as a PFi cell marker (Janson et al., 2012), while CALPONIN 1 (CNN1) and ALPHA SMOOTH MUSCLE ACTIN (α-SMA) were highly expressed in ventral tissue RFi but not in site matched PFi (Janson et al., 2012, Janson et al., 2013). These observations were made on cells at a low passage (passage 3-6) *in vitro*, however, if cells are grown for an extended number of passages (passage 15-20), PFi are believed to differentiate into RFi as they start expressing RFi markers such as α-SMA (Janson et al., 2013). It is important to note here, that dermal fibroblasts do not actively proliferate *in vivo*, but when these cells are *in vitro* they are driven into

proliferation in the presence of serum. Nevertheless, human PFi exhibit an increased rate of growth in comparison to RFi, showing that even though they share a similar morphology, these cells have different proliferative capacities in culture (Harper and Grove, 1979, Schafer et al., 1985b, Sorrell et al., 2004). When assessing other functional characteristics of human fibroblasts, DPFi have been previously described as being multipotent *in vitro*, capable of differentiating into osteoblasts and adipocytes (Richardson et al., 2005, Jahoda et al., 2003). In addition, a sub-population of BmprIB+ RFi were recently shown to also be osteogenic *in vitro* (Wang et al., 2016), while Bmpr1B- RFi are not osteogenic (He et al., 2011). These findings further highlight that there is fibroblast heterogeneity even within specific sub-anatomical locations.



KEY

Genes/ proteins expressed/ not expressed in fibroblasts, identified in Murine studies

Genes/proteins expressed/ not expressed in fibroblasts, identified in Human and Mouse studies

Genes/ proteins expressed/ not expressed in fibroblasts, identified in Human studies

Figure 2.1.1. Summary of literature assessing fibroblast expression in development, neonate and adult skin.

At the beginning of development there is a fibroblast progenitor from which the DPFi, PFi and RFi arise. This figure reviews the genes identified in mouse and human studies during development and in postnatal fibroblasts *in vivo* and *in vitro*. The genes identified in mouse studies are shown in red, the genes identified in human and mouse studies are shown in blue and the genes identified in human studies are shown in green. The body site from which the fibroblast populations were isolated are in brackets next to each gene name where D= dorsal, V= ventral, W= whiskers, T= tail, B=breast, F= foreskin, A= abdomen and S= scalp. The arrows in the late passage stage display the relative expression difference from the early passage stage. This illustration was made from the following references put in chronological order: 1. (Jahoda et al., 1991), 2. (Handjiski et al., 1994), 3. (Watt and Collins, 2008), 4. (Enshell-Seijffers et al., 2008), 5. (Driskell et al., 2009), 6. (Higgins et al., 2010), 7. (Collins et al., 2011), 8. (Janson et al., 2012), 9. (Janson et al., 2013), 10. (Driskell et al., 2013), 11. (Sennett et al., 2015), 12. (Hasebe et al., 2017).

2.2. Specific aims in Chapter 2

Given the recent work indicating that DPFi, PFi and RFi in mouse skin are derived from a multipotent progenitor, in this chapter of my thesis the expression pattern, behavioural properties and ECM deposition of DPFi, PFi and RFi cell populations isolated from human occipital scalp skin are compared against one another, *in vitro*.

I have isolated fibroblasts defined by their spatial location, rather than using a cell surface marker or functional characteristic. Therefore, my first aim was to isolate all three fibroblasts populations from a single piece of scalp skin, using a microdissection approach. My second aim was to assess cell morphology, expression, behavioural and ECM deposition differences in order to identify defining characteristics which can be used to distinguish DPFi, PFi and RFi derived from human scalp skin dermis, from one another.

2.3. Materials and Methods

2.3.1. Human skin biopsies

All human scalp skin biopsies were taken from the occipital scalp of patients (unless otherwise stated) undergoing surgical proceedings after receiving informed consent, and using IC-REC approved consent forms. Tissue is held under ICHTB HTA license 12275, and used in the ICHTB approved project R15055. During my PhD project, I received frontal scalp skin from Dr. Paul Farrant from the Brighton's General Hospital Dermatology Department, and occipital scalp skin from Dr. Greg Williams from the Farjo Hair Institute in London.

Table 2.3.1 provides full information on the patients used in this chapter. Biopsies used in Chapter 2 are from different patients than biopsies used in chapter 3, apart from P2D that has been used in both chapters.

Table 2.3.1. Human skin biopsies in Chapter 2.

Patient	Gender	Age	Site of isolation	Matched cell populations available
P2A	Male	20	Occipital scalp	DPFi, PFi, RFi
P2B	Male	52	Occipital scalp	DPFi, PFi, RFi
P2C	Male	38	Occipital scalp	DPFi, PFi, RFi
P2D	Male	64	Occipital scalp	DPFi, PFi, RFi
P2D	Male	72	Frontal scalp	DPFi, PFi, RFi

2.3.2. Isolation and culture of site-matched fibroblasts

Scalp skin (Figure 2.3.1A) was washed in Dulbecco's minimal essential medium (dMEM; Gibco Life Technologies) with 2% Antibiotics-Antimycotics (2% ABAM; Gibco Life Technologies) for 20 minutes for cleaning prior to dissection. Using a sterile Pasteur pipette, 8 small drops, and 1 larger drop of dMEM supplemented with 1xABAM were placed onto an inverted lid of a petri dish (Figure 2.3.1B). Each small drop was used to hold a single end-bulb for inversion in. The drops were covered by placing the base of the petri dish inside the lid. The fat and connective tissue around the lower follicle was removed using scissors. Under a stereo microscope the end bulb of the hair follicle was visible; this was carefully cut off using sterile scissors and placed into dMEM with 1% ABAM (Figure 2.3.1C). With a fine needle (27Gx3/4") the end of the hair follicle was fixed in place, while another needle was used to invert the end bulb structure and expose the dermal papilla containing DPFi (Figure 2.3.1D-F). The dermal papilla was then separated from the inverted end bulb and transferred into a 35 mm tissue culture dish covered in dMEM with 1% ABAM and 20% Fetal Bovine Serum (FBS; Gibco Life Technologies; Figure 2.3.1G). A needle was used to scratch through the papilla and adhere it to the base of the plate (Figure 2.3.1H). The plates were then placed in the incubator at 37°C, 5% CO_2 and left undisturbed for 10 days during which time the papillae collapsed and cells grew from the papilla in an explant (Figure 2.3.1I).

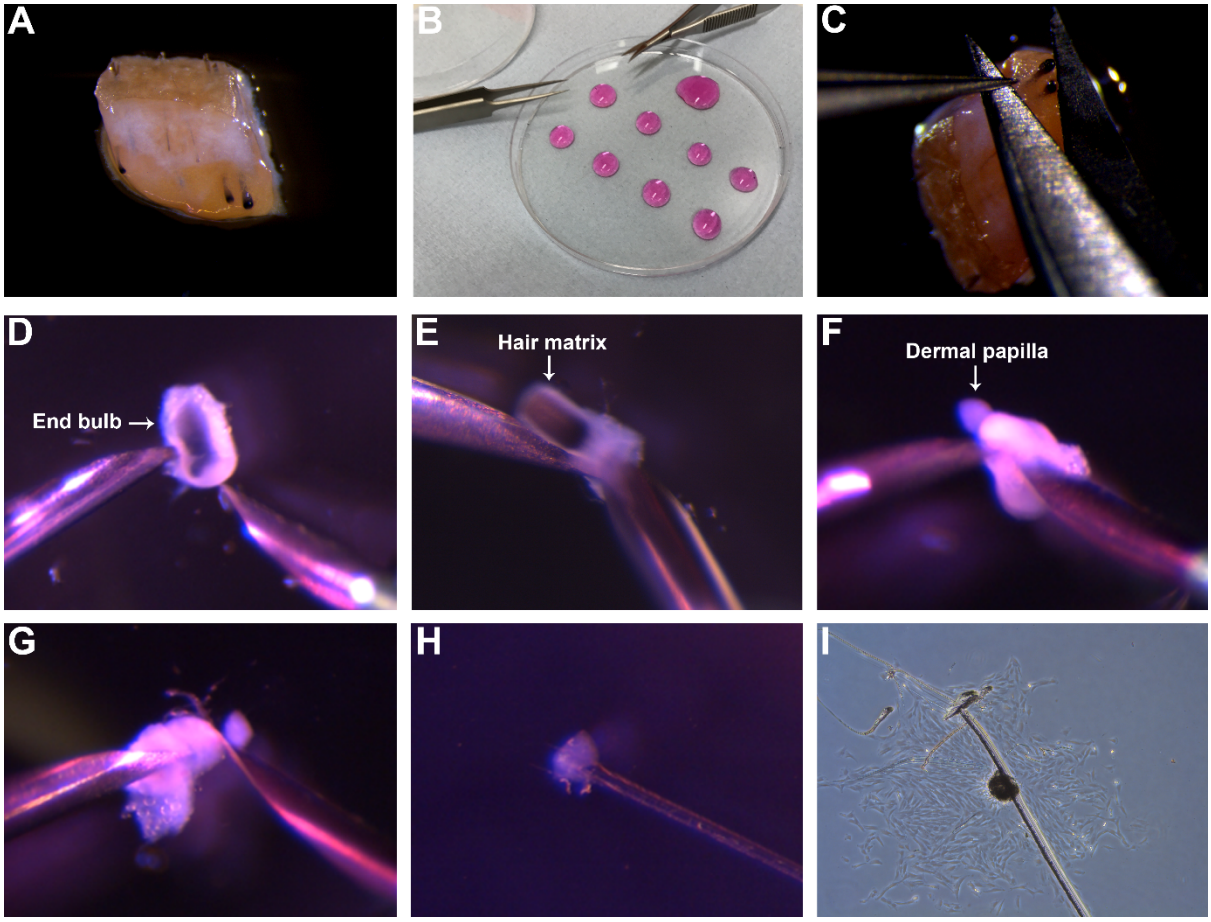


Figure 2.3.1. Human dermal papilla micro-dissection method using a stereomicroscope.

(A) Skin biopsy prior to papilla isolation. (B) Petri dish lid with drops of dMEM for dissection. (C) Transection of the hair follicle with scissors. (D) A transected hair follicle end bulb. (E) Inversion of the end bulb. (F) Inverted end bulb and exposed dermal papilla. (G) Transection of the dermal papilla. (H) Dermal papilla adhered to a 35mm dish with a scratch. (I) Growth of cells in a starburst formation around a single dermal papilla (Topouzi et al., 2017).

With the remaining piece of skin (Figure 2.3.2A) the hypodermis was cut off to clean up the tissue (Figure 2.3.2B). Using a scalpel blade to cut very close to the epidermis, the papillary and reticular dermis were separated into two pieces (Figure 2.3.2C-D). Any remaining hair fibres in either piece of skin were then removed with watchmaker's forceps. The pieces of skin were then placed into separate 35 mm dishes and chopped

into small pieces using scissors, and equally distributed around the dry dish. Once the tissue pieces have adhered to the base of the dish (usually 5 minutes later), dMEM containing 20% FBS and 1% ABAM was added to each dish to cover the tissue pieces and the dish was transferred to an incubator. After 10 days, cells had migrated out of the adhered skin in an explant culture.

For the blended dermal fibroblasts, occipital scalp skin (Figure 2.3.1A) was washed in dMEM with 2% ABAM for 20 minutes for cleaning prior to dissection. The hypodermis was cut off to clean up the tissue making sure that the end bulbs were still intact. The piece of skin was then placed into a 35 mm dish and chopped into small pieces using scissors, and equally distributed around the dry dish. Once the tissue pieces have adhered to the base of the dish (usually 5 minutes later), dMEM containing 20% FBS and 1% ABAM was added to each dish to cover the tissue pieces and the dish was transferred to an incubator. After 10 days, cells had migrated out of the adhered skin in an explant culture.

To passage the DPFi, PFi, RFi and blended fibroblasts, the plate/flask was washed two times with Phosphate Buffered Saline (PBS; Gibco life technologies). Then, 1% Trypsin-EDTA (Gibco life technologies) was added to the cells for approximately 5 minutes at 37º C. The cells were checked under a microscope to ensure they have detached, and then dMEM 10% FBS was added to stop the reaction with Trypsin. The cells were counted and then centrifuged at 1400 rpm for 4 minutes. The supernatant was removed and the pellet was reconstituted in dMEM 10% FBS. The cells were seeded at a density of 6000 cells per cm^2.

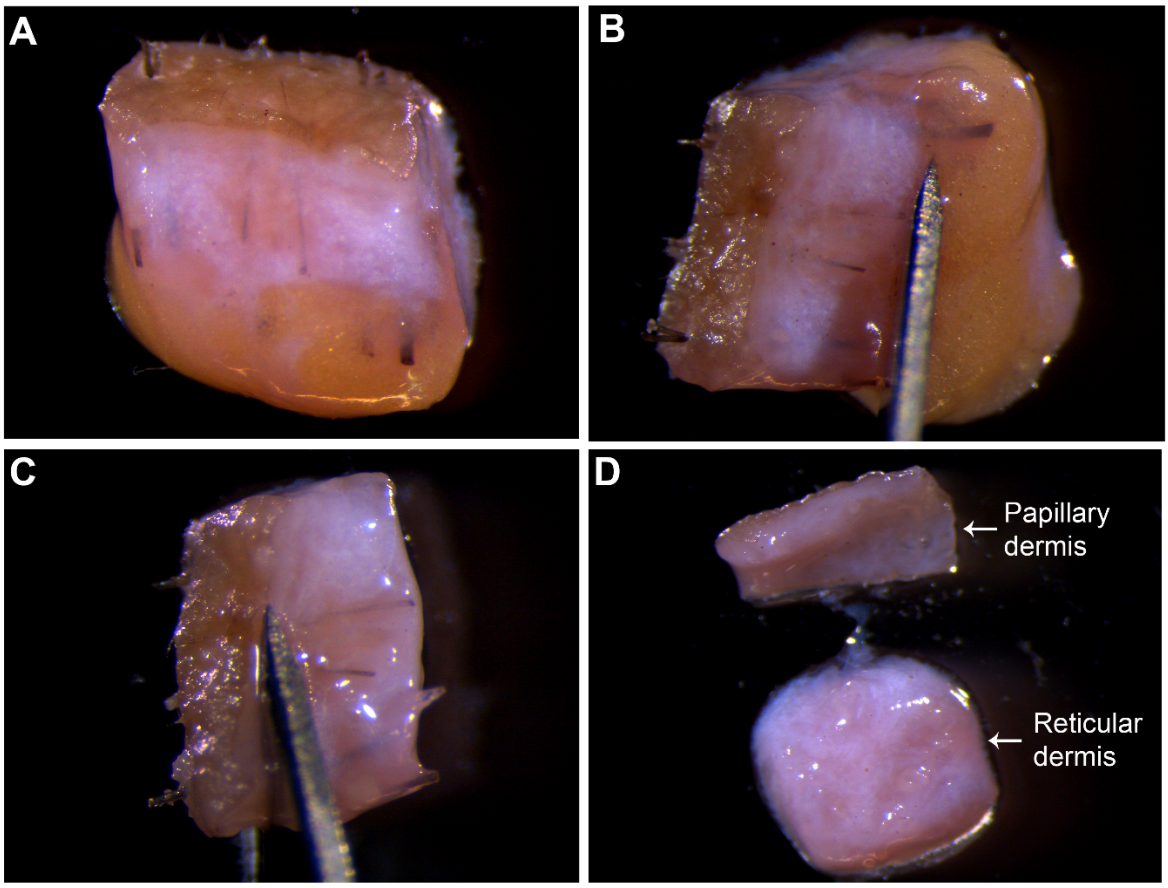


Figure 2.3.2. Papillary and reticular fibroblast micro-dissection method using a stereomicroscope.

(A) Skin biopsy after papilla isolation. (B) Adipose tissue removal. (C) Transection of the dermis in two layers. (D) Clear separation of the papillary and reticular dermal layers.

2.3.3. KC isolation and culture

Scalp skin was washed in dMEM with 2% ABAM for 20 minutes for cleaning prior to dissection. The adipose tissue was cut off the skin, and the rest of the tissue was placed in Dispase (Gibco Life Technologies) solution overnight at 4ºC. After the overnight incubation, using sterile forceps, the epidermis was peeled off the dermis and was placed in 5 mL 1% Trypsin in a waterbath, at 37ºC. The solution was shaken

every 5 minutes to ensure that the cells are freed from the epidermis. The reaction was quenched using 5 mL Defined Trypsin Inhibitor (DTI; Gibco Life Technologies). A cell strainer with 40 µm pore sized was used to remove any pieces of tissue. The cells were then centrifuged into a pellet at 1400 rpm for 8 minutes. The supernatant was removed and Epilife (Gibco Life Technologies) with Epilife Defined Growth Supplement (EDGS; Gibco Life Technologies) and 1% ABAM was added to the cells. EDGS contains purified bovine serum albumin, purified bovine transferrin, hydrocortisone, recombinant human insulin-like growth factor type-1 (rhIGF-1), prostaglandin E2 (PGE2) and recombinant human epidermal growth factor (rhEGF). The cells were then plated at a density of 5000 cells per cm^2 in flasks that had been pre-coated using the coating matrix kit (Gibco Life Technologies), which contains collagen I.

2.3.4. Immunofluorescence

Cells grown on coverslips or 7 µm frozen skin sections cut on a cryostat were fixed with 4% paraformaldehyde (PFA) for 10 minutes then washed with PBS three times in 5 minute washes. They were then permeabilised and blocked using 5% Goat Serum with 0.3% Triton X (Sigma) in PBS for 20 minutes and then incubated with the primary antibody overnight at 4ºC. All of the antibodies are summarized in table 2.3.2. Phalloidin-488 (1:40, Thermo Fisher) was also used to detect F-actin. The following day, antibodies were washed off using three washes of PBS, each for 5 minutes and then the samples were incubated with the secondary antibodies summarized in table 2.3.2. They were then washed three times with PBS for 5 minutes and mounted onto glass slides using prolong gold antifade reagent with DAPI (Life Technologies) for visualization. The slides were imaged on a Leica confocal microscope. All analysis

was performed with at least two biological replicates, and the relative expression differences were consistent in cells isolated from both patients. To assess nucleolin number, I counted 40 nuclei, in cells from 2 patients, and found the differences in nucleolin number to be consistently significant between cell sub-types and patient samples.

Table 2.3.2. Primary antibodies and secondary antibodies used.

Name	Host species	Company	Catalogue number	Dilution
Vimentin	Chicken	Abcam	ab24525	1:200
PDPN	Mouse	Abcam	ab10288	1:1000
CD26	Mouse	Biorad	MCA1317T	1:100
Collagen I	Rabbit	Abcam	ab34710	1:200
α-SMA	Mouse	Abcam	ab7817	1:200
Nucleolin	Mouse	Abcam	ab136649	1:200
K14	Chicken	Abcam	ab7800	1:400
NFH	Chicken	Chemicon international	AB5539	1:400
488 anti-mouse	Goat	Molecular probes	A-11001	1:200
546 anti-rabbit	Goat	Molecular probes	A-11010	1:200
633 anti-chicken	Goat	Molecular probes	A-21103	1:200

2.3.5. Osteogenic differentiation

Cells were seeded at a density of 6000 cells per cm^2 in 6 well plates. After 24 hours the media was changed to osteogenic or growth media were appropriate. Osteogenic media was composed of dMEM with 10% FBS, supplemented with 100 nM Dexamethasone (Sigma), 50 µM ascorbate-2-phosphate (Sigma), 10 mM β-glycerophosphate (Sigma) and 1% ABAM, modified from (Zuk et al., 2001). Growth media was composed of dMEM with 10% FBS and 1% ABAM. Cells were cultured for a period of 14 days in their respective media and then analysed using alizarin red staining and a calcium assay which are described below.

2.3.5.1. Alizarin red staining

Cells were washed with deionized water and fixed with 4% PFA for 10 minutes. After fixation, they were washed with deionized water and incubated in 40 mM Alizarin red (Millipore) stock solution for 10 minutes at room temperature, with gentle rocking. They were then washed 3-5 times with water and were left to dry at room temperature before imaging.

2.3.5.2. Calcium assay

Cells were washed with PBS and were then incubated in 500 µl Hydrogen chloride (HCl; Sigma) for 1 hour at room temperature, with gentle rocking. From this 500 µl, three technical repeats of 5 µl were removed and added to separate wells of a 96 well plate. Next, 100 µl of reagents A and B from the Calcium assay kit (BioAssay systems) were added in each well. Absorbance was measured in a plate reader at a wavelength of 612 nm.

2.3.6. Adipogenic differentiation

Cells were seeded at a density of 6000 cells per cm^2 in 6 well plates. After 24 hours the media was changed to adipogenic or growth media were appropriate. Adipogenic media was composed of dMEM with 15% FBS, supplemented with 100 nM Dexamethasone (Sigma), 2.07 µM Insulin (Sigma), 0.5 mM IBMX (Sigma), 200 µM Indomethacin (Sigma) and 1% ABAM, modified from (Zuk et al., 2001). Growth media was composed of dMEM with 10% FBS and 1% ABAM. Cells were cultured for a period of 21 days in their respective media and then analysed using Oil Red O staining.

2.3.6.1. Oil Red O staining

After 21 days in adipogenic media or growth media, the cells were fixed using 10% Formalin for 45 minutes. In the meantime, Oil red O stock solution was prepared by adding 60 mg Oil Red O (Abcam) to 20 mL 100% isopropanol and left undisturbed for 20 min. Then, 3 parts of Oil red O stock solution were added to 2 parts of water and left undisturbed for 10 min. This solution was then filtered through a Whatman No.1 filter paper to make the Oil red O working solution. After the fixation step, the cells were washed two times using distilled water. 2 mL of 60% Isopropanol (Sigma) was then placed on the cells to wash them for 15 minutes. The wash in isopropanol was then discarded, and the cells were evenly covered with Oil red O working solution. They were incubated with the working solution for 15 minutes on a rotating plate. They were then washed three times with distilled water, until no excess stain could be seen. Then, Haematoxylin was added to the cells for 1 minute. After this incubation, the cells were washed three times with distilled water. The cells were then covered with water

and imaged under the phase-contrast microscope. Lipid droplets appeared red whilst nuclei appeared blue.

To quantify the oil red o staining, the cells were dried overnight at room temperature. The next day, 300 µl of 100% isopropanol was added to each well of the 6 well plate which dissolved the Oil Red O on the cells into the solution. Then, 100 µl aliquots were taken in triplicate and the absorbance of Oil red O in isopropanol was measured at 510 nm using a plate reader.

2.3.7. Alamar blue cell viability assay

Cells were seeded in a 6 well plate at a density of 6000 cells per cm^2. After 24, 72 and 168 hours, 100 µl of alamarBlue® reagent (Invitrogen) was added directly to cells in 1 ml culture medium. The cells were incubated for 3 hours at 37ºC, protected from direct sunlight. After 3 hours, 100 µl aliquots were taken in duplicate and their absorbance was measured at 570 nm, using 600 nm as a reference wavelength.

2.3.8. Morphology analysis

Phase-contrast cell culture images were analysed using the ImageJ software to obtain the cell size, cell shape and nuclear area of the fibroblast subpopulations. Cell and nuclear area was determined by measuring around each shape, and determining the total covered area. Cell shape was determined as a ratio of the width to length of each cell. For each cell type, and at each passage, at least 40 cells were imaged. Statistical analysis was performed in Graphpad prism 6 using two-way Anova tests.

2.3.9. mRNA extraction, reverse transcription and RT-PCR

RNA extraction was performed using a QiaShredder for homogenization and Qiagen RNeasy Mini kit (Qiagen, Germany) for extraction, to obtain RNA from fresh tissue, DPFi, PFi and RFi. Once the RNA was extracted, the following components (all from Life Technologies) were added to a nuclease free micro centrifuge tube to reverse transcribe cDNA; 1 µl of oligoDT, 100 ng of total RNA added up to 11 µl with RNAse free water and 1 µl of dNTP mix 10 mM. The mixture was then heated to 65°C for 5 min and incubated on ice for 1 min. The following components were then added to the tube; 4 µl of 5x First strand buffer, 1 µl of DTT 0.1 M, 1 µl of RNAseOUT, and 1 µl of Superscript III RT. The micro centrifuge tubes were then incubated at 50°C for 60 min followed by inactivation of the reaction by heating it at 70°C for 15 min. The reaction was then cooled down at 4°C and cDNA was stored at -20°C.

For the RT-PCR, a 20 µl reaction was used. The following reagents were added together; 10 µl PowerUP™ SYBR Green Master Mix (2X; Life Technologies), 1 µl Forward and Reverse primer (Table 2.3.2.), which I designed using DNA sequences on the UCSC genome database (build GRCh38/hg38) unless otherwise stated, 1 µl diluted cDNA template and 8 µl RNase free water. RT-PCRs were run on an ABI 7500Fast RealTime PCR with the cycles as follows: 2 minutes at 50°C and 2 minutes at 95°C followed by 35 cycles of 15 seconds at 95°C and 1 minute at 60°C. Expression analysis was performed relative to GAPDH using the ddCT algorithm, with expression in fresh tissue used as a baseline comparison (value=1). RT-PCR was performed using cDNA from two biological replicates, and the relative expressions were consistent in both patients. Statistical analysis was performed using two-way Anova test.

Table 2.3.3 Primers used for RT-PCR analysis.

*Primer was taken from Janson et al. (2013)

Gene	Sequence (5' to 3')	Product size
GAPDH	F- GGTCACCAGGGCTGCTTTTA	216
	R- TCGCCCCACTTGATTTTGGA	
PDPN*	F- GCCACCAGTCACTCCACGGAGAA	164
	R- TTGGCAGCAGGGCGTAACCC	
CD26	F- TAC TCT GCT CTG TGG TGG TG	126
	R- GTT GGA TTC ACA GCT CCT GC	
α-SMA	F- GGT GAC GAA GCA CAG AGC AA	91
	R- GGG CAA CAC GAA GCT CAT TG	
CNN1	F- CCA GAA GTA TGA CCA CCA GC	263
	R- TGG ACT GCA CCT GTG TAT GG	

2.3.10. Matrix deposition

T25 flasks or sterile 13 mm glass coverslips placed in each well of a 24 well plate were incubated with 0.2% sterile Gelatin (Sigma) in PBS for 60 minutes at 37º C. They were then washed three times with PBS, crosslinked with 1% sterile Glutaraldehyde (Sigma) in PBS for 30 minutes at room temperature, followed by three times washing with PBS. Crosslinking was quenched with 1M sterile glycine in PBS for 20 minutes at room

temperature, followed by three times PBS washing. The coverslips were stored at 4ºC until used, or for maximum one month.

After the surface of the T25 or coverslip was prepared for matrix deposition, fibroblasts were seeded at a density of 6000 cells per cm^2 and cultured overnight at 37º C, 5% CO_2 to adhere to the T25 or coverslips. Growth medium supplemented with 50µg ml^{-1} ascorbic acid (Sigma) was added and subsequently changed every 2 days. Cells were cultured for 10 days after the addition of ascorbic acid. This promoted the deposition of ECM proteins.

To remove the cells from the ECM, medium was aspirated and cells were washed in PBS. Pre-warmed extraction buffer containing 10mM NH_4OH (Sigma), 0.25% Triton X-100 in PBS was added for 4 minutes at room temperature to allow cell lysis. Half of the buffer was carefully removed and PBS was added to substitute it. The same step was repeated until no cells were visible on the ECM. The DNA residue was then digested with 10µg ml^{-1} DNAse I (Roche) in PBS for 30 minutes at 37ºC, followed by two washes with PBS. Matrices were stored at 4ºC until used, or for maximum one month.

2.3.11. ECM samples analysed by mass spectrometry

After cell elimination, ECM proteins were proteolyzed in each well using 2.5 µg Trypsin (Gibco, Invitrogen) in 250 µl of 30mM Tris (pH 8.0) at 37°C overnight. Pre-digested matrix proteins were scraped off from the wells using a cell scraper and collected into 1.5 ml microfuge tubes. With assistance from Mr Paul Hitchen in the Mass Spec Facility at Imperial College, the samples were reduced by the addition of Dithiothreitol

(DTT; final concentration 10mM) and incubated for 30 minutes at 56°C. After reduction, Iodoacetadime (IAM; final concentration 55mM) was added to keep the disulfide bonds separate and unfolded, and samples were incubated for 30 minutes at room temperature protected from direct sunlight. Finally, the samples were further digested by Trypsin at 37°C overnight before terminating the digest with the addition of 10% trifluoroacetic acid (final concentration 0.5%).

Samples were analysed by LC–MS using a nanoAcquity UPLC™ system (Waters MS Technologies, Manchester, UK) by Mr Paul G Hitchen in the Mass Spectrometry facility of Imperial College. 1 µl (1-3 µg protein digest) of sample was injected onto each trapping column (Waters, C18, 180µm×20mm) using partial loop injection, for 1 min at a flow rate of 15µL/min with 0.1% (v/v) formic acid. Samples were resolved on an analytical column (Waters, nanoAcquity UPLC™ M-class HSS T3 75µm×150mm 1.8µm column) using a gradient of 97% A (0.1% (v/v) formic acid) 3% B (99.9% acetonitrile 0.1% (v/v) formic acid) to 60% A 40% B over 36 min at a flow rate of 300 nl min^{-1}. The nanoAcquity UPLC™ was coupled to a Synapt™ G2 mass spectrometer (Waters) and data acquired using a MS^E program with 1s scan times and a collision energy ramp of 15–40eV for elevated energy scans. The mass spectrometer was calibrated before use and throughout the analytical run at 1 minute intervals using the NanoLockSpray™ source with glufibrinopeptide.

To quantitatively analyse the mass spectrometry results I performed peptide identification using the ProteinLynx Global SERVER™ (PLGS) v3.1 (Waters). The data was processed using a low energy threshold of 150 and an elevated energy threshold of 30. A fixed carbamidomethyl modification for cysteine was specified. The search thresholds used were: minimum fragment ion matches per peptide 3; minimum

fragment ion matches per protein 7; minimum peptides per protein 2 and a false positive value of 4. Data was searched against the most recent UniProtKB/Swiss-Prot human database entry (Boutet et al., 2016). For normalisation, each sample had a known Trypsin concentration, which was used as an internal standard. All protein hits were identified with a confidence of above 95%. The PLGS protein score was based on the probability that the observed match between the experimental data and the PLGS database was not a random event, thus minimising potential random hits. Furthermore, if two or more proteins shared an identical peptide but the peptide in question was regulated differently, then the peptide was not included in the analysis. Peptide intensity was determined as the sum of the peptide ions for all unique peptides for each protein. A total peptide score was taken as the integrated total of all normalised peptide intensities, for all identified ECM proteins.

2.3.12. Statistical analysis of data

The data collected in this chapter, were analysed using Graphpad prism 6 and statistical analysis of each experiment is outlined in the corresponding method or figure legend. Number of biological replicates (N) and number of technical replicates (n) are also indicated in the figure legends.

2.4. Results

2.4.1. Distinguishing between the different dermal compartments of scalp skin

To get a better understanding of the different layers in human scalp skin, immunofluorescence (IF) staining was used with VIMENTIN (VIM) and COLLAGEN 1 (COL1), both fibroblast markers, PDPN which has been shown to mark PFi (Janson et al., 2013), CD26 which has been shown to mark PFi cells during development (Driskell et al., 2013) and DAPI to mark cell nuclei (Figure 2.4.1). Statistical analysis of DAPI staining on the IF tissue sections showed that the papillary dermis is significantly denser with cells than the reticular dermis. When comparing both to the dermal papilla, the dermal papilla contains significantly more cells per area than both (Figure 2.4.2.). These stainings highlighted the existence of different dermal regions, justifying the subsequent experiment in the chapter which seek to analyse differences between these cells in culture.

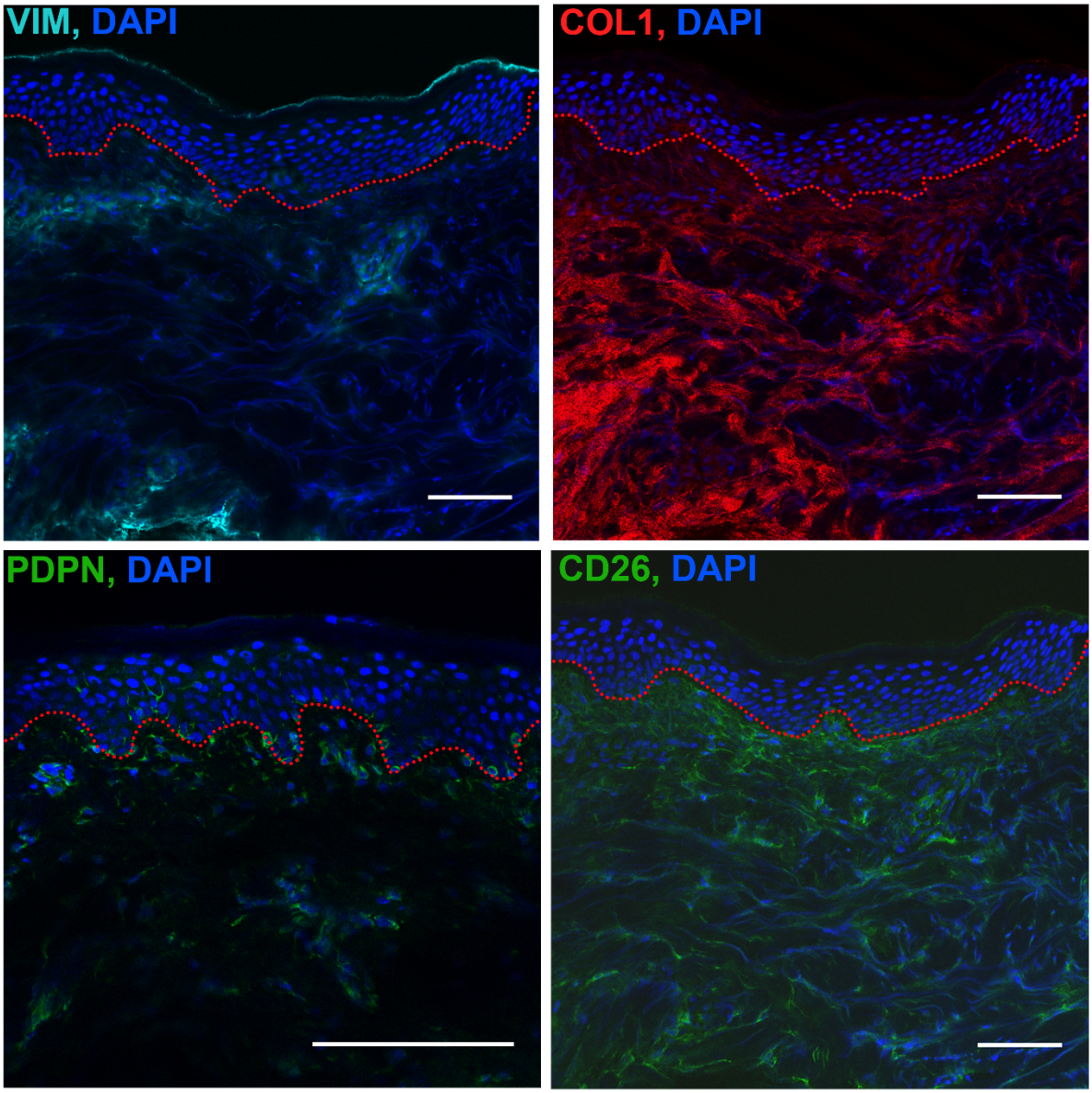


Figure 2.4.1. Immunofluorescence staining of human scalp skin *in vivo*.

IF staining of human skin showing VIM in cyan, COL1 in red, PDPN and CD26 in green and DAPI in blue. Red dotted line indicates the basement membrane. This figure shows a representative result from N=1. N=2 was used; P2A and P2B. Scale bars: 120 µm.

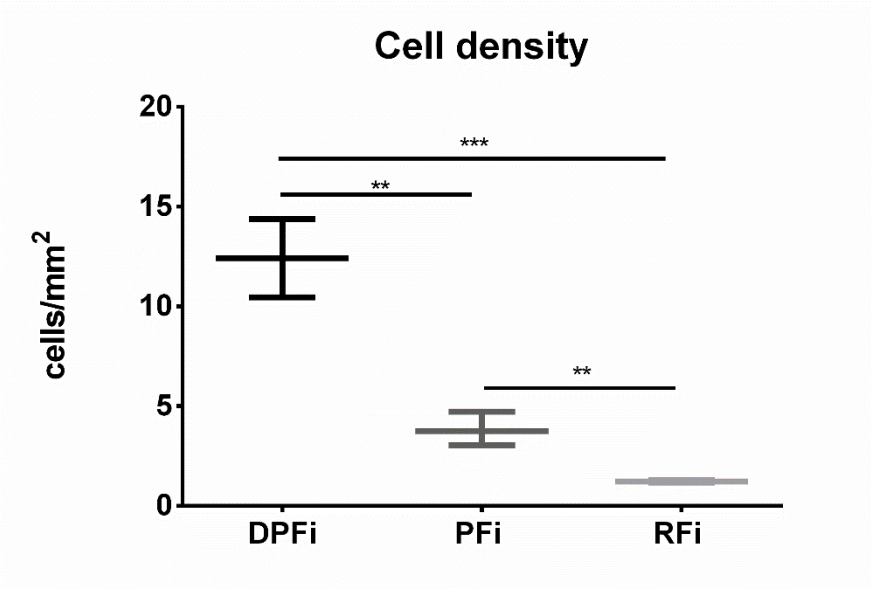


Figure 2.4.2. Statistical analysis of cells per mm^2.

The graph shows the number of nuclei count per mm^2 based on the DAPI staining of human scalp skin *in vivo* from Figure 2.4.1B. N=1 (P2A) and n=3 were used to calculate the cell density. Values were analysed by an unpaired t-test. Error bars show the minimum and maximum values. Significance is displayed in the graph (P ≤ 0.05 = *, P ≤ 0.01 = **, P ≤ 0.001 =***, P ≤ 0.0001 =****).

2.4.2. Fibroblasts have distinct expression profiles and behavioural characteristics *in vitro* at P4

After identifying the different regions where DPFi, PFi and RFi lie in the skin cell cultures were established for each cell type using a microdissection technique (Topouzi et al., 2017), as described in the methods (Figure 2.3.1. and 2.3.2.). The first question I asked, was whether the cell cultures were bonafide fibroblasts or whether the isolation technique was contaminated with neighboring KC or perhaps neuronal cells which reside in the dermis. Using indirect IF on DPFi, PFi and RFi at passage 4 (P4), I found that the cells did not express Keratin 14 (K14), an epithelial marker, or Neurofilament heavy chain (NFH), a neurofilament marker, despite the skin from which they were isolated expressing both of these markers (Figure 2.4.3.). In the case of NFH, some background staining was observed in the DPFi although this was not specific. However, the cells were found to uniformly express VIM and COL1, both markers of fibroblasts (Figure 2.4.4A), which were also expressed throughout the skin dermis *in vivo* (Figure 2.4.1B). Thus, I concluded that my isolation approach enabled me to isolate fibroblasts rather than other cell types.

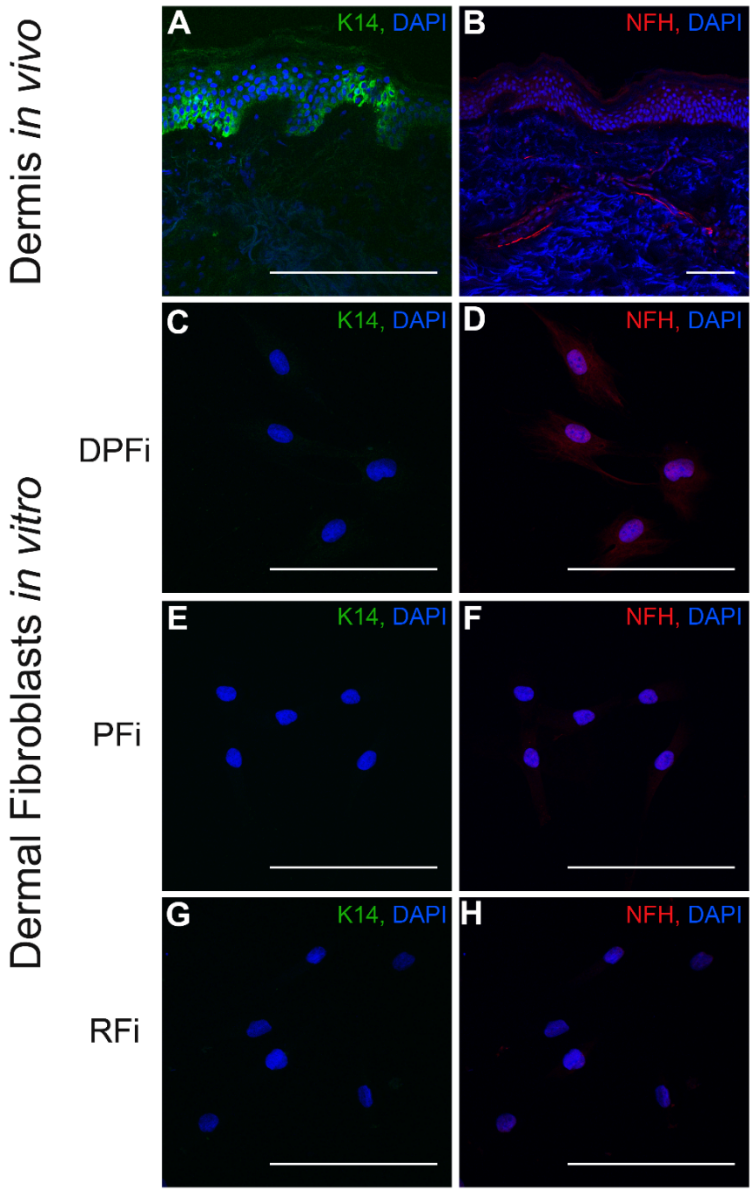


Figure 2.4.3. Isolation technique ensures bonafide fibroblasts.

IF analysis of K14 (green) and NFH (red), with DAPI (blue) marking cell nuclei. While K14 is expressed in KC *in vivo* (A), and NFH is expressed in neuronal cells within the skin dermis (B), expression is not observed in DPFi (C, D), PFi (E, F), or RFi (G, H), isolated from the skin dermis. This figure shows a representative result from N=1. N=2 was used; P2A and P2B. Scale bars A-H: 130 μm.

To determine whether these fibroblast populations differentially express other markers that were previously identified as present in mouse and human fibroblasts, IF staining was performed, followed by confocal microscopy to image cells. While *in vivo*, PDPN is expressed in the papillary dermis, and CD26 is found within both the papillary and reticular dermis (Figure 2.4.1B), *in vitro* I found that PDPN and CD26 are both expressed in the PFi but not the RFi nor DPFi (Figure 2.4.4A). In comparison, while F-Actin was expressed in all fibroblasts in all sub-types, α-SMA was found to be heterogeneously expressed (Figure 2.4.4A). Specifically, 70% of DPFi expressed α-SMA, while just 15% of RFi, and 1% of PFi expressed α-SMA. While α-SMA is a well described marker of DPFi *in vitro*, it is not usually expressed by DPFi *in vivo* (Jahoda et al., 1991).

To further assess relative expression between populations of fibroblasts in culture, RT-PCR analysis was performed on mRNA isolated from the three fibroblasts populations at P4. Complementing the initial IF analysis, I found that both *PDPN* and *CD26* were expressed at significantly higher levels in the PFi compared to the DPFi and the RFi, while *α-SMA* and *CNN1* were significantly expressed in the DPFi compared to the PFi (Figure 2.4.8B). Expression of *α-SMA* and *CNN1* was also observed in RFi, but at much lower levels than the DPFi. This initial analysis shows that dermal fibroblasts have distinct expression characteristics from one another, despite having no spatial orientation cues *in vitro*. However, based on expression alone it is difficult to distinguish between the DPFi and RFi.

Investigations focusing on the dermis often consider dermal fibroblasts as a single cell sub-type, and isolate cells from the entire dermis together. With this in mind, I wondered if any of the fibroblast populations might be preferentially selected if a whole

piece of skin containing hair follicles was explanted for culture. Using IF, I found that this blended fibroblast (Fi) population expressed both VIM and COL1 (Figure 2.4.4B) as expected as these are markers of fibroblasts. When PDPN and CD26 were analysed, strong expression of both these markers was found, whilst α-SMA was only present in 2% of the blended Fi culture. This suggests that the majority of the cells in the blended Fi culture are actually PFi. It is important to note here that the experiment in Figure 2.4.4B was performed at a different time, with different patients than 2.4.4A which could explain the CD26 intensity differences.

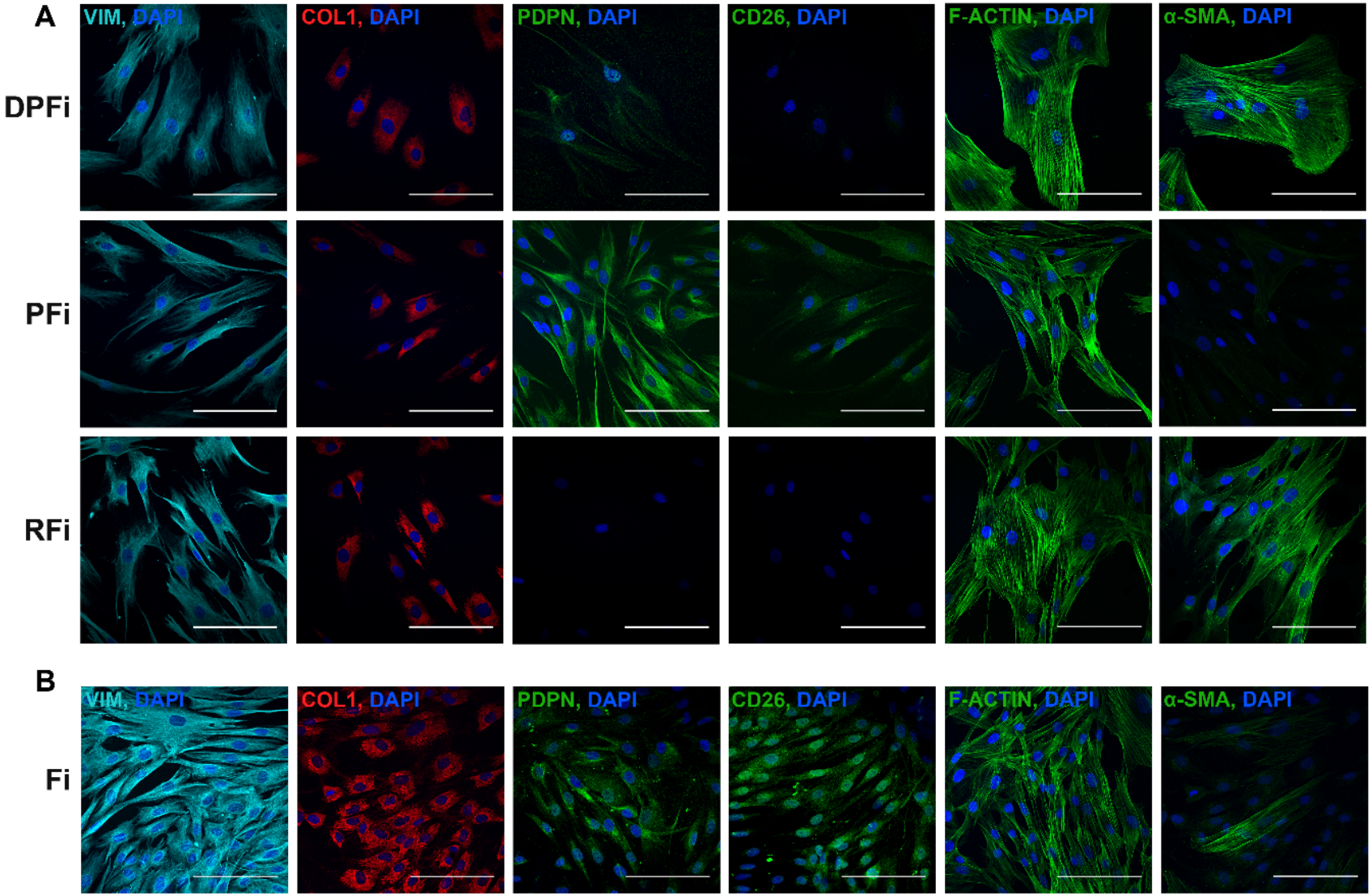

A
VIM, DAPI
COL1, DAPI
PDPN, DAPI
CD26, DAPI
F-ACTIN, DAPI
α-SMA, DAPI
DPFi
PFi
RFi
B
VIM, DAPI
COL1, DAPI
PDPN, DAPI
CD26, DAPI
F-ACTIN, DAPI
α-SMA, DAPI
Fi

Figure 2.4.4. Fibroblast identities at P4.

(A-B) IF analysis of (A) DPFi, PFi, RFi and (B) blended Fi population at P4 using VIM (cyan), COL1 (red), PDPN (green), CD26 (green), F-ACTIN (green), α-SMA (green) and DAPI (blue). This figure shows a representative result from N=1. N=2 (P2A and P2B) was used in (A) and N=1 (P2C) in (B). Scale bars in A, B: 130 μm.

2.4.3. Alamar blue assay shows differences in the proliferation rate of the sub populations

It has been previously reported that human PFi proliferate faster than the RFi at an early passage, *in vitro* (Azzarone and Macieira-Coelho, 1982). In an attempt to include the DPFi in these observations, the alamar blue assay was performed in DPFi, PFi and RFi cultures. A standard curve was made for each population using 5000, 10000, 15000 and 20000 cells (Appendix Figure A.1.). It was found that the slope of the standard curve was 4.82E-06, 1.97E-06 and 2.29E-06 for the DPFi, PFi and RFi respectively. Using these values, the number of cells per well was calculated and plotted in a bar graph (Figure 2.4.5). Even though all the populations were seeded at the same density, it was found that the PFi cells have a significantly higher number of cells after 7 days in culture when compared to the RFi and DPFi. Thus, I was able to conclude that the PFi cells are proliferating significantly faster than the other two populations being analysed in my study.

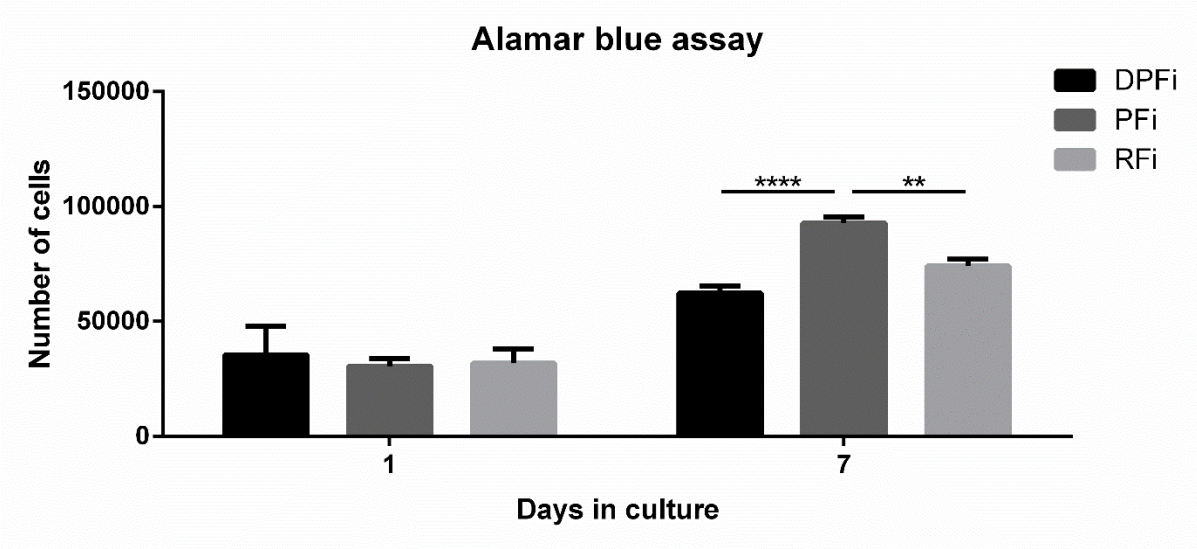


Figure 2.4.5. Alamar blue assay.

The graph shows the number of cells of DPFi, PFi and RFi after 1 and 7 days in culture. The number of cells was calculated according to a standard curve for each population. This figure shows a representative result from N=1. N=2 (P2A and P2B) and n=4 were used in this experiment. Results were analysed using two-way Anova and the error bars represent standard deviation. Significance is displayed in the graph (P ≤ 0.05 = *, P ≤ 0.01 = **, P ≤ 0.001 =***, P ≤ 0.0001 =****).

2.4.4. Occipital scalp populations exhibit morphological differences at an early passage

After observing differences in expression and proliferation rate between the fibroblast sub-types, I also wanted to assess whether there were morphological differences between the fibroblast sub-types which may be useful for characterisation (Figure 2.4.6.). On first observation, the DPFi appeared rounder whilst the PFi and RFi were more elongated and spindle shaped. This has also been reported within the literature (Messenger et al. 1986) however, quantitative image analysis revealed no significant differences in cell shape between the three fibroblast sub-types (Figure 2.4.6C). On the contrary, cell area measurements revealed that DPFi cells at P4 were significantly larger than the PFi and RFi. DPFi have an average cell size of 15000 μm^2, while PFi and RFi have an average size of 3500 μm^2 and 6500 μm^2 respectively (Figure 2.4.6B). After assessing total cell area, nuclear size was also assessed and I found that the DPFi nuclei are also significantly larger than both the PFi and RFi nuclei at P4 (Figure 2.4.6D). A data spread can be observed in the DPFi (Figure 2.4.6B & D). Even though I excluded the presence of KC and neuronal cells from my DPFi cultures (Figure 2.4.3.), future tests should aim to identify if endothelial cells are also absent from the cultures, in order to identify if this data spread is due to the heterogeneity of the population or if there a small number of endothelial cells present.

To investigate if differences in nuclear area resulted in differences in nuclear architecture I used an antibody against nucleolin, which marks regions of euchromatin in the nucleus (Tajrishi et al., 2011), and has also been correlated with enhanced proliferation and migration of dermal fibroblasts (Jiang et al., 2015). Intriguingly, I observed that the DPFi had on average 3 nucleolin spots per nuclei, compared to PFi

and RFi, which each had 5 nucleolin spots per nuclei (Figure 2.4.6E, F). Thus, when the IF analysis is combined together with nucleolin count, the three fibroblast populations can be distinguished from one another. Lastly, the nucleolin spots in the blended Fi population were analysed, and it was found that these cells had on average 5 nucleolin spots per nuclei supporting the initial IF data suggesting these cells are PFi (Figure 2.4.6F).

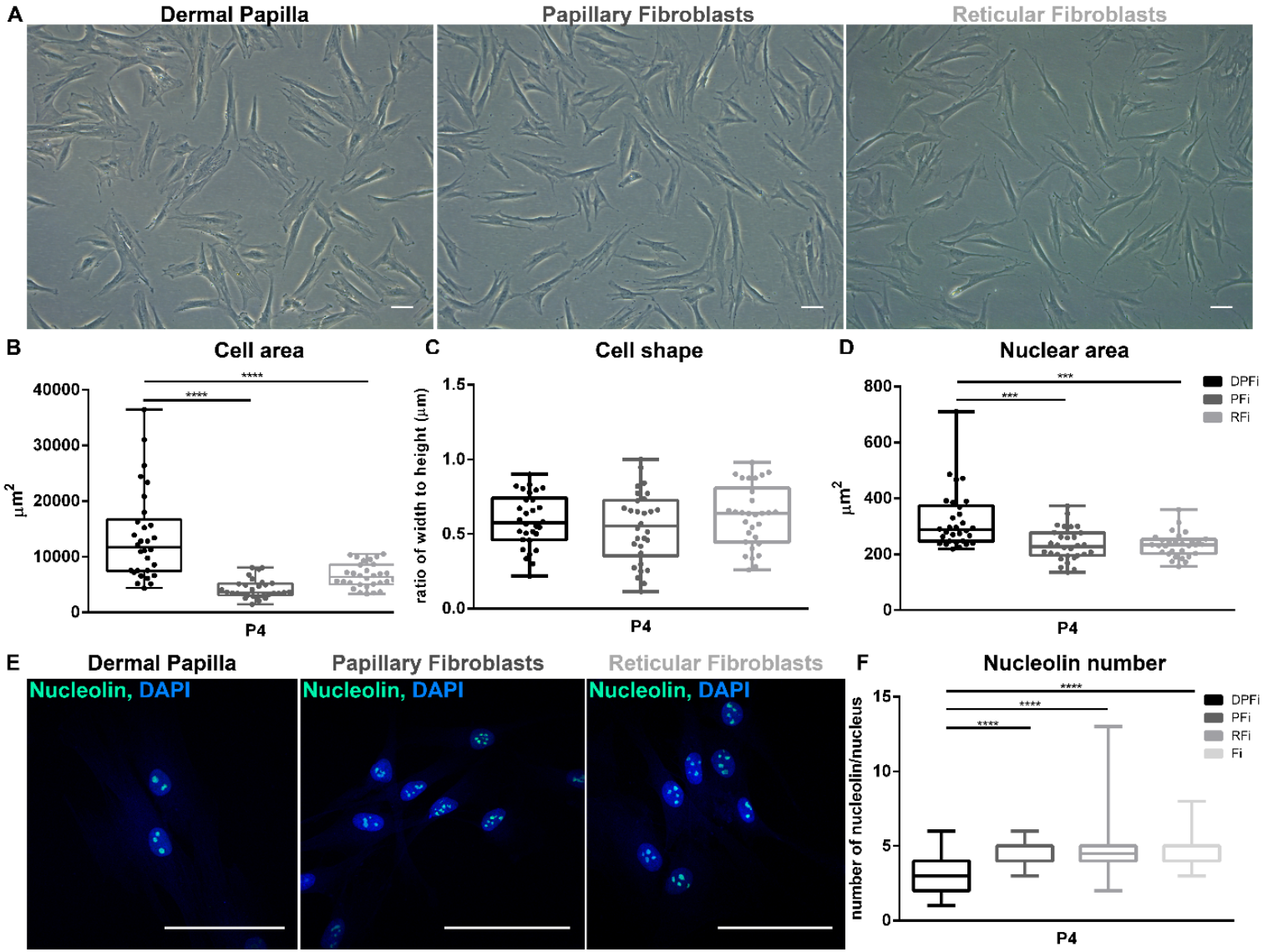

A
Dermal Papilla
Papillary Fibroblasts
Reticular Fibroblasts
B
Cell area
μm²
40000
30000
20000
10000
0
****
****
P4
C
Cell shape
ratio of width to height (μm)
1.5
1.0
0.5
0.0
P4
D
Nuclear area
μm²
800
600
400
200
0
***
***
DPFi
PFi
RFi
P4
E
Dermal Papilla
Papillary Fibroblasts
Reticular Fibroblasts
Nucleolin, DAPI
Nucleolin, DAPI
Nucleolin, DAPI
F
Nucleolin number
number of nucleolin/nucleus
15
10
5
0
****
****
****
DPFi
PFi
RFi
Fi
P4

Figure 2.4.6. Morphological differences of DPFi, PFi and RFi at P4.

(A) Phase-contrast images of the three fibroblast sub-types *in vitro*. Box plots analysing the (B) cell area (µm2), (C) cell shape (µm) and (D) nuclear area (µm2). (E) IF analysis of Nucleolin (green) and DAPI (blue). (F) Box plot analysing the number of nucleolin spots per nucleus in the DPFi, PFi, RFi and Fi. This figure shows a representative result from N=1. N=2 (P2A and P2B) and n=40 were used in this experiment. Results were analysed using two-way Anova (B-D) and an unpaired t-test (F). The error bars represent minimum and maximum values of the 40 cells included in this study. Significance is displayed in the graphs in B-D, F ($P \leq 0.05$ = *, $P \leq 0.01$ = **, $P \leq 0.001$ =***, $P \leq 0.0001$ =****). Scale bars in A: 50 µm, C: 60 µm.

2.4.5. Prolonged passage alters morphology and protein expression pattern

While the initial analysis was performed in cells at P4 I noticed I was not getting the same results at other passages I therefore decided to look at the effect of increasing passage on cell size and shape. To address this, the fibroblast sub-types where studied to observe any changes with prolonged passage. First, the cell morphology was addressed and it was observed that the cell area of the DPFi decreases gradually with increasing passage to the point that there is no longer a significant difference between the size of the DPFi cells with the size of the PFi or RFi by passage 10 (P10) (Figure 2.4.7A). While no significant difference between the cell shape from P1-P10 (Figure 2.4.7B) was found, it was found that the nuclear area of the DPFi cells is also decreased at P10 with a significant difference between the DPFi and the other two populations (Figure 2.4.7C). I then looked at other features specifically at P10. Whilst assessing changes in the nuclear architecture, the analysis showed that at P10 the DPFi had on average 2 nucleolin spots per nuclei, compared to PFi and RFi, which each had 4 spots (Figure 2.4.7D). Even though the average number of nucleolin spots decreased across the populations from P4 to P10, this was not a significant change (Figure 2.4.7E).

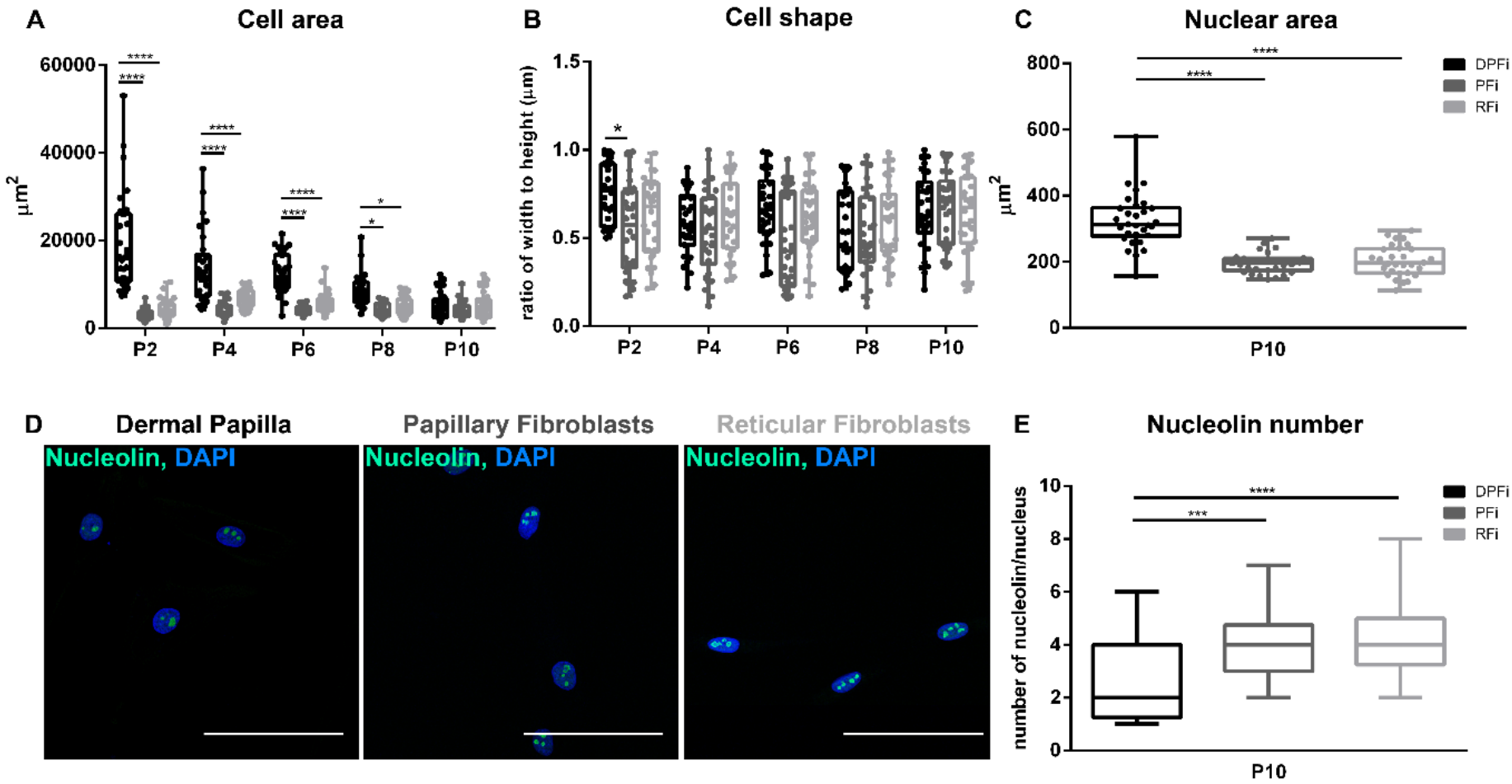

A
Cell area
60000
40000
20000
0
µm2
****
****
****
****
****
****
*
*
P2
P4
P6
P8
P10
B
Cell shape
1.5
1.0
0.5
0.0
ratio of width to height (µm)
*
P2
P4
P6
P8
P10
C
Nuclear area
800
600
400
200
0
µm2
****
****
P10
DPFi
PFi
RFi
D
Dermal Papilla
Papillary Fibroblasts
Reticular Fibroblasts
Nucleolin, DAPI
Nucleolin, DAPI
Nucleolin, DAPI
E
Nucleolin number
10
8
6
4
2
0
number of nucleolin/nucleus
****
***
P10
DPFi
PFi
RFi

Figure 2.4.7. Morphological differences of DPFi, PFi and RFi with increasing passage number. Box plots analysing the (A) cell area (μm^2), (B) cell shape (µm) and (C) nuclear area (μm^2) in cells from P2 through P10. (D) IF analysis of Nucleolin (green) and DAPI (blue) in cells at P10. (E) Box plot analysing the number of nucleolin spots per nucleus in the DPFi, PFi and RFi of cells at P10. This figure shows a representative result from N=1. N=2 (P2A and P2B) and n=40 were used in this experiment. Results were analysed using two-way Anova (A-C) and an unpaired t-test (F). The error bars represent minimum and maximum values of the 40 cells included in this study. Significance is displayed in the graphs in A, C ($P \leq 0.05$ = *, $P \leq 0.01$ = **, $P \leq 0.001$ =***, $P \leq 0.0001$ =****). Scale bars in B: 60 µm.

Given the morphological changes observed with prolonged passage, and the apparent transition to a homogenous morphology with relation to cell size, the study was refocused to assess expression differences between the fibroblast sub-types in cells at P10. To assess this, IF was performed using antibodies against CD26, PDPN, and α-SMA, and RT-PCR against the aforementioned genes and *CNN1*, which had been previously studied at P4 (Figure 2.4.8A, B). As observed at P4, *PDPN* and *CD26* were still expressed within PFi. However, at P10 expression was also observed at low levels in DPFi, and in the RFi expression was at comparable levels to the PFi. Looking at *α-SMA* and *CNN1*, I found that while expression decreased across cell types, there was still significantly more expression within DPFi at P10 compared to the RFi and PFi. Thus, it appears at P10 the three cell types are more similar to each other than they were at P4, when differences were more striking.

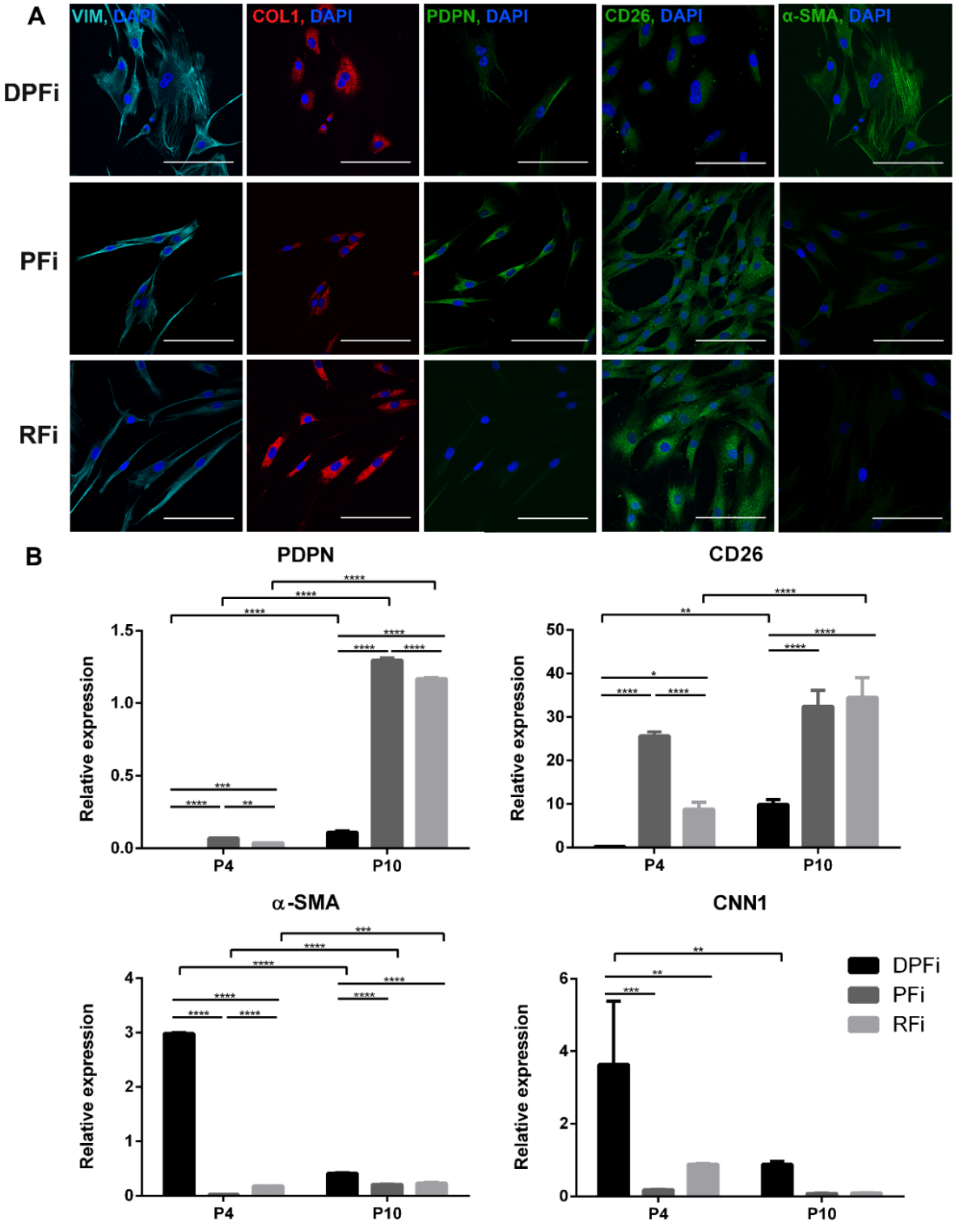

A
VIM, DAPI
COL1, DAPI
PDPN, DAPI
CD26, DAPI
α-SMA, DAPI
DPFi
PFi
RFi
B
PDPN
CD26
α-SMA
CNN1
Relative expression
P4
P10
DPFi
PFi
RFi

Figure 2.4.8. Expression profile of DPFi, PFi and RFi at P10 compared to P4.

(A) IF analysis of DPFi, PFi, RFi at P10 using VIM (cyan), COL1 (red), PDPN (green), CD26 (green), α-SMA (green) and DAPI (blue). (B) RT-PCR analysis showing the relative expression of *PDPN, CD26, α-SMA*, and *CNN1* in DPFi, PFi and RFi at P4 and P10, with expression relative to expression in *ex vivo* skin. This figure shows a representative result from N=1. N=2 (P2A and P2B) and n=3 were used in this experiment. Results were analysed using one-way Anova (B) and the error bars represent standard deviation. Significance is displayed in the graphs ($P \leq 0.05$ = *, $P \leq 0.01$ = **, $P \leq 0.001$ =***, $P \leq 0.0001$ =****). Scale bars in A: 130 μm.

2.4.6. Osteogenic and adipogenic differentiation

Looking into the behavioural characteristic of the fibroblasts, it has been previously demonstrated that human DPFi are able to differentiate into osteoblasts and adipocytes when the appropriate differentiation cues are added to the culture medium (Jahoda et al., 2003, Richardson et al., 2005). Here, I cultured all three populations in osteogenic and adipogenic media, in two separate experiments, to ask whether the PFi and RFi have the same differentiation potential as the DPFi.

In the case of the osteogenic differentiation experiment, I found that within the 14 day time frame of the study, only the DPFi differentiate into mineral producing osteoblasts, which also deposit significantly more calcium than both the PFi and RFi (Figure 2.4.9.).

In the adipogenic differentiation experiment, all three fibroblast populations differentiated into fat producing adipocyte-like cells in the 21 day time frame of the experiment, as it can be seen in the Oil red O staining (Figure 2.4.10A). Quantification of the Oil red O staining showed that all three populations release significantly more lipid droplets when compared to their matching growth media. When comparing across populations, RFi has been shown to release significantly more lipid droplets that DPFi and PFi in the adipogenic media (Figure 2.4.10B).

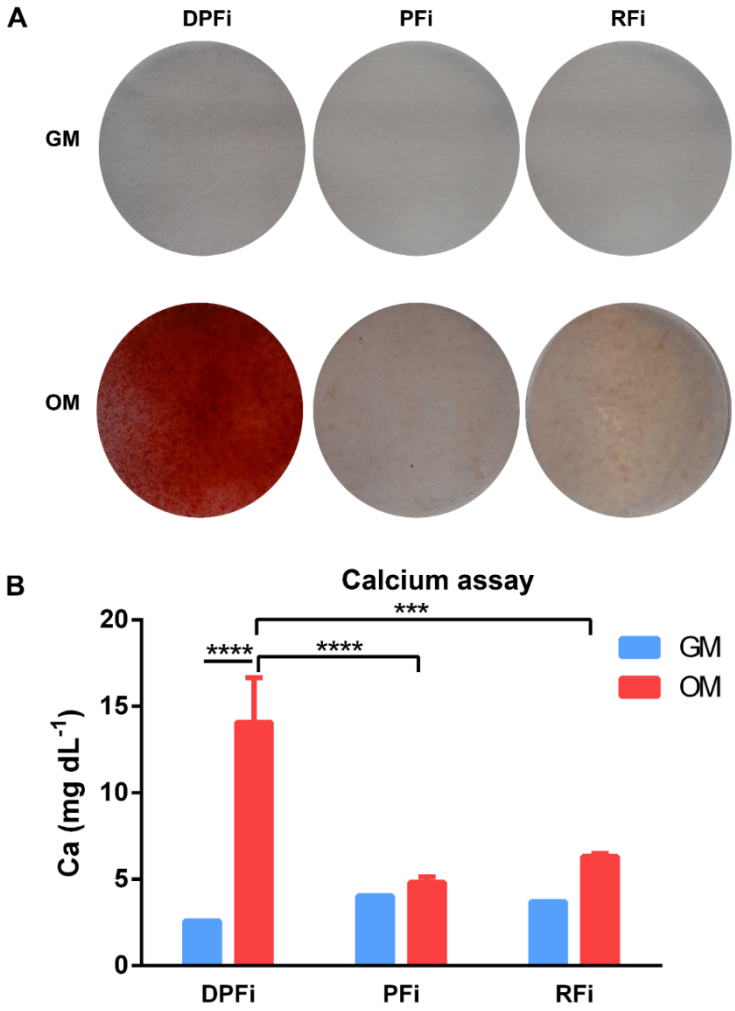


Figure 2.4 9. Fibroblasts in osteogenic and growth media.

(A) Analysis using Alizarin Red to detect mineralisation in DPFi, PFi and RFi in growth media (GM) and osteogenic media (OM) after 14 days in culture. (B) Bar graph representing the calcium released (mg dL^{-1}) in DPFi, PFi and RFi on GM versus OM after 14 days in culture. This figure shows a representative result from N=1. N=2 (P2A and P2D) and n=3 were used in this experiment. Results were analysed using two-way Anova (B) and the error bars represent standard error. Significance is displayed in the graph ($P \leq 0.05$ = *, $P \leq 0.01$ = **, $P \leq 0.001$ =***, $P \leq 0.0001$ =****).

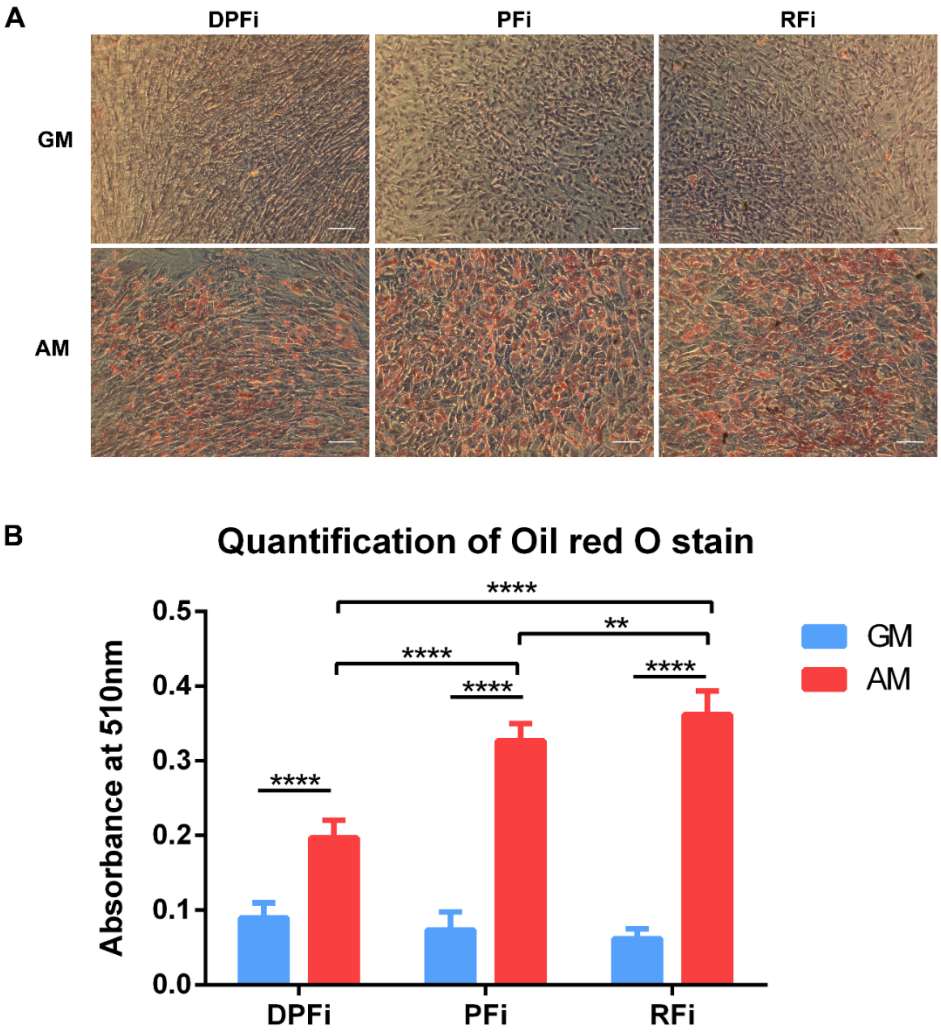


Figure 2.4.10. Fibroblasts in adipogenic and growth media.

(A) Analysis using oil red o staining to detect fat droplets in growth media (GM) and adipogenic media (AM). (B) Quantification of Oil red o stain by measuring the absorbance at 510 nm. This figure shows a representative result from N=1. N=2 (P2A and P2D) and n=3 were used in this experiment. Results were analysed using two-way Anova (B) and the error bars represent standard error. Significance is displayed in the graph (P ≤ 0.05 = *, P ≤ 0.01 = **, P ≤ 0.001 =***, P ≤ 0.0001 =****).

2.4.7. Osteogenic differentiation on frontal vs occipital scalp

Following the analysis on the occipital scalp above, and bearing in mind the heterogeneity that these fibroblasts populations have, not only on a single body site but across the body, I wondered whether or not these cells differentiate with the same potential across different body sites. Frontal scalp is neural crest derived while occipital scalp is mesoderm derived, and so it might be a greater challenge for frontal DPFi to differentiate into osteoblasts compared to occipital scalp. The osteogenic capacity of these cells was tested across all three populations isolated from occipital and frontal scalp. Interestingly, using alizarin red I found that during the 14 day period in culture, only the occipital scalp DPFi, and not the frontal scalp DPFi, differentiated into calcium releasing osteoblasts (Figure 2.4.11A,B). The calcium assay has confirmed this result by showing a significantly higher calcium release in the occipital scalp DPFi when compared to the frontal DPFi cultured in OM (Figure 2.4.11C). Caution needs to be taken when comparing the results as only one patient was used for the frontal scalp experiment due to limited access to follicles. The occipital biopsies were from a 20 year old and a 64 year old patient while the frontal biopsies were from a 72 year old patient.

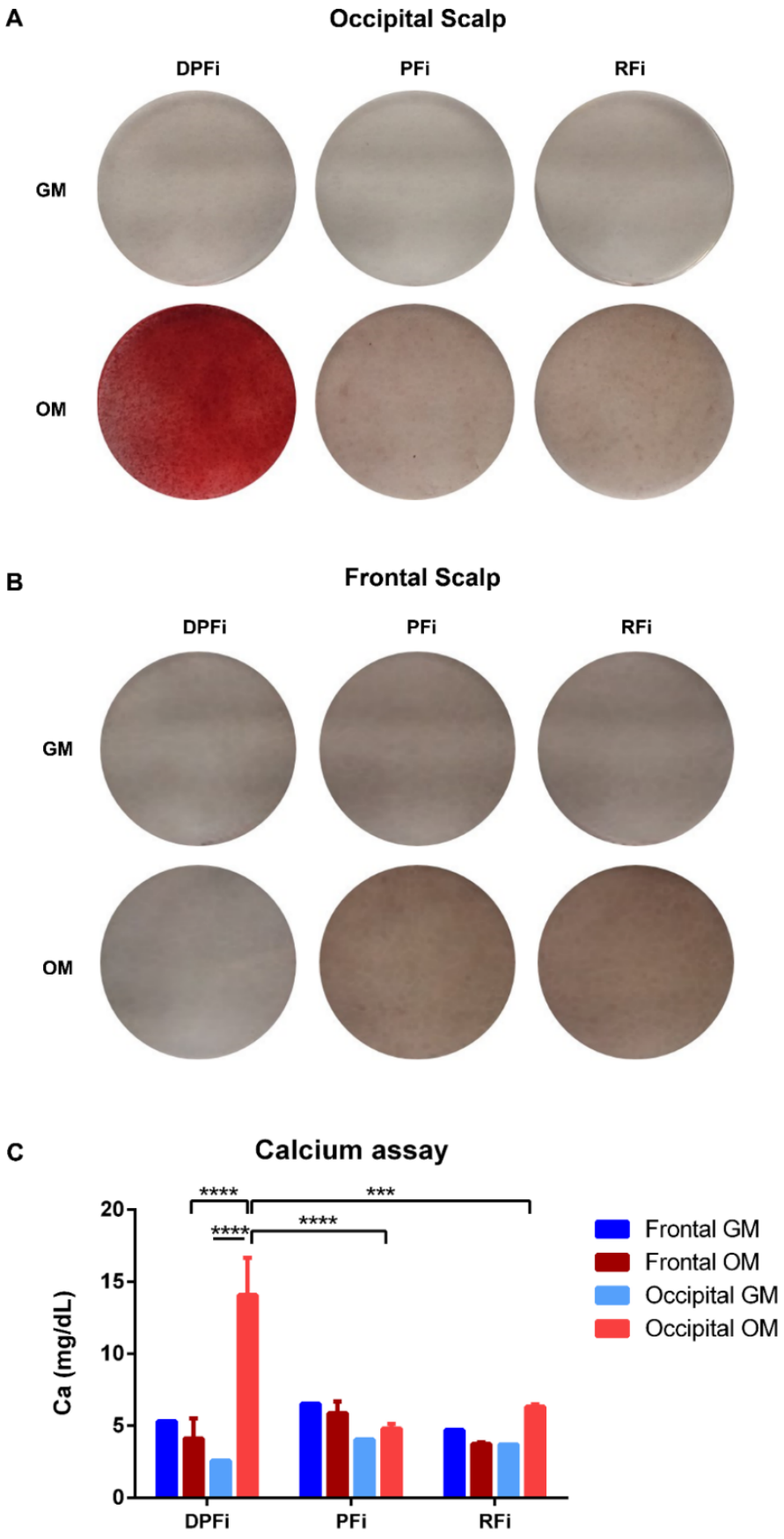

A
Occipital Scalp
DPFi
PFi
RFi
GM
OM
B
Frontal Scalp
DPFi
PFi
RFi
GM
OM
C
Calcium assay
****
***
****
****
20
15
10
5
0
Ca (mg/dL)
DPFi
PFi
RFi
Frontal GM
Frontal OM
Occipital GM
Occipital OM

Figure 2.4.11. Occipital and frontal scalp fibroblasts cultured in osteogenic and growth media. Analysis using Alizarin Red to detect mineralisation in DPFi, PFi and RFi from the (A) occipital scalp and from the (B) frontal scalp in growth media (GM) and osteogenic media (OM) after 14 days in culture. (C) Bar graph representing the calcium released (mg dL^{-1}) in DPFi, PFi and RFi of occipital and frontal scalp, on GM versus OM after 14 days in culture. This figure shows a representative result from N=1. N=2 (P2A and P2D) was used in (A) and N=1 (P2E) in (B). N=3 was used in (A) and (B). Results were analysed using two-way Anova and the error bars represent standard error. Significance is displayed in the graph ($P \leq 0.05$ = *, $P \leq 0.01$ = **, $P \leq 0.001$ =***, $P \leq 0.0001$ =****).

2.4.8. Mass spectrometry analysis on the ECM of all three fibroblast subtypes

Given the different expression, morphological and behavioral characteristics I have hereby reported, I pondered whether these three populations of fibroblasts secrete unique ECMs to one another. The three cell types were seeded on gelatin coating which has been found to critically improve the final yield of proteins (Franco-Barraza et al., 2016) and by the addition of ascorbic acid they deposited ECM onto the pre-coated surface (see method 2.3.10). Ascorbic acid was added as it has been found to enhance the deposition of collagens in culture (Guo et al., 2007). Staining and image analysis of matrices was performed by Dr. Martina Ghetti and has already been published (Ghetti et al., 2017), revealing distinct matrices are deposited by the three fibroblast subtypes. As Martina identified differences in the morphological composition of matrices using immunofluorescence, I used mass spectrometry to detect the chemical composition of DPFi, PFi and RFi cell assembled ECMs.

The analysis identified 12 ECM proteins which passed the significance cutoff threshold within the DPFi, PFi and RFi cell assembled ECMs (Table 2.4.1.). DPFi had the highest peptide intensity over a 10 day time frame, which led to the conclusion that it produced the most ECM of the three populations. All identified proteins were interstitial ECM rather than basement membrane ECM. As shown in table 2.4.1, FN1 was equally produced by all three different fibroblasts subpopulations. Surprisingly, alpha 1 chain COLLAGEN 1 (COL1A1), which is generally thought to be expressed throughout the dermis, was not found in the PFi ECM, even when peptides that didn't pass the significance cutoff threshold were considered.

Interstitial ECM is usually classified into fibrous ECMs (collagens and elastin), proteoglycans, or 'other'. The mass spectrometry analysis identified different collagens, one proteoglycan, and proteins which fell into the 'other' category, nearly all of which were adhesive glycoproteins (Table 2.4.1). Specifically, adhesive glycoproteins are the linker proteins, which connect cells with fibrous ECM. Of the fibrous ECMs, the analysis showed that while alpha 1 chain COLLAGEN VI (COL6A1) and alpha 3 chain COLLAGEN V1 (COL6A3) were present in all three ECMs, alpha 2 chain COLLAGEN VI (COL6A2) and alpha 2 chain COLLAGEN 1 (COL1A2) were only found in the DPFi ECM. TENASCIN (TNC) and FIBULIN 2 (FBLN2) were present in all ECMs. On the other hand, THBS1 was present at high levels in the DPFi, at low levels in the RFi but was not present in the PFi ECM. VITRONECTIN (VTN) was present in the DPFi ECM AND PFi ECM, while FIBRILIN 1 (FBN1) and EMILIN 1 (EMIL1) were unique to the RFi ECM (Table 2.4.1.).

Table 2.4.1. Mass Spectrometry data of ECM matrices for each fibroblast sub-type.

Listed in the table are the protein symbol and accession number (ID) from Swiss-prot, for all the ECM proteins detected. PLGS Score: A statistical measure of peptide assignment accuracy. Coverage: Percentage of protein sequence covered by identified peptides for each protein. Peptide intensity sum: Sum of the peptide ion intensities for each protein, normalized against a trypsin internal control. Total Peptide Intensity: Sum of the peptide ions for all peptides identified, for each ECM protein. Values are the average of matrices from N=2 (Ghetti et al., 2017).

Protein Symbol	Protein ID	DPFi ECM			PFi ECM			RFi ECM			ECM type
		PLGS Score	Coverage (%)	Peptide Intensity Sum	PLGS Score	Coverage (%)	Peptide Intensity Sum	PLGS Score	Coverage (%)	Peptide Intensity Sum	
FINC	P02751	13937	49	9138740	4245	44	4349942	4511	47	6198948	Adhesive glycoprotein
CO1A1	P02452	241	25	319566	--	--	--	--	--	--	Fibrous
CO1A2	P08123	1018	15	398538	--	--	--	89	14	26986	Fibrous
CO6A1	P12109	5787	42	1399723	208	18	79824	259	26	142226	Fibrous
CO6A2	P12110	2448	28	721444	--	--	--	--	--	--	Fibrous
CO6A3	P12111	2561	34	3888636	169	22	218064	268	25	683339	Fibrous
TNC	P24821	1931	30	1579325	549	27	647935	681	30	885657	Adhesive glycoprotein
THBS1	P07996	1014	31	575557	--	--	--	129	21	106958	Adhesive glycoprotein
FBLN2	P98095	431	23	171414	129	17	61035	238	24	217243	Ca2+ binding glycoprotein
VTN	P04004	403	16	44674	95	18	12991	--	--	--	Adhesive glycoprotein
FBN1	P35555	--	--	--	--	--	--	118	17	136846	Adhesive glycoprotein
EMIL1	Q9Y6C2	--	--	--	--	--	--	95	9	21431	Adhesive glycoprotein
Total Peptide Intensity		**18246137**			**5414781**			**8392648**			

2.5. Discussion

2.5.1. Isolation and characterisation of fibroblast in research

In vitro models, and in particular those using fibroblasts, are widely used in research and are the focus of several studies regarding wound healing and skin tissue homeostasis (Werner and Grose, 2003, Werner et al., 2007a, Higgins et al., 2010). However, fibroblasts are often grouped into a cell category together, while in reality even those from a single anatomical location are quite heterogeneous, with different expression profiles, function, lineage and even clonal characteristics (Sorrell et al., 2007). In mouse skin, DPFi, PFi and RFi were recently shown to arise from a multipotent common progenitor. In human skin it is not possible to do lineage tracing, however DPFi, PFi and RFi are located in distinct sub-anatomical locations within the adult dermis. For this reason we used a microdissection approach to isolate bonafide DPFi (Topouzi et al., 2017), PFi and RFi from human scalp skin for further assessment. Microdissection has both benefits and disadvantages. For example, isolation based on spatial location definitively yields fibroblasts from the papillary, reticular or hair follicle dermis; however these are still heterogeneous populations as indicated by the variable percentages of α-SMA we observed in cultures of these cells. An alternative way to isolate fibroblasts for characterization would be enzymatic digestion followed by single cell RNA-Seq, as has been performed on the skin epidermis (Joost et al., 2017, Yang et al., 2017). In comparison to microdissection this would identify fibroblasts based on their transcriptional signatures, and would likely identify several unknown new populations. However, at the same time spatial information is lost with single cell RNA-Sequencing. Another alternative approach where spatial information

is retained is spatial transcriptomics (Ståhl et al., 2016). However, while there are advantages to every approach there are also caveats and with spatial transcriptomics the whole skin dermis with multiple cell types such as fibroblasts, immune, vascular and neuronal cells would be profiled. While scientifically this is interesting it moves me away from my original research question, which was to characterize fibroblast sub-types within human skin.

2.5.2. Fibroblasts have distinct expression characteristics at P4

One of the principal goals of my study, was to determine the behavioral and expression characteristics of DPFi, PFi and RFi isolated from human scalp skin. Based on previous studies looking at the expression patterns within skin fibroblasts, I chose a panel of markers that I believed would be differentially expressed in at least two of the three fibroblast populations under analysis. I found that using a combination of expression analysis, and counting of nucleolin marks within nuclei, I could accurately distinguish between scalp skin fibroblast sub-types at P4. For example, DPFi nuclei contain 3 nucleolin spots and express α-SMA and CNN1, while RFi contain 5 nucleolin spots and express α-SMA and CNN1. Comparatively, PFi contain 5 nucleolin spots and express PDPN and CD26, but not α-SMA and CNN1. This expression study was informative, as it told us that fibroblast sub-types maintain distinct identities at an early passage in culture, even though they have been removed from their surrounding environmental cues, present *in vivo.*

2.5.3. CD26- A PFi marker or a fibrotic marker?

Cd26 expression in murine skin has resulted in some interesting dichotomies, and thus also warrants discussion here. Cd26 was originally described as a marker of the upper dermal fibroblast lineage which gives rise to the PFi, distinguishing these cells from those of the lower dermis (Driskell et al., 2013). Subsequently, Cd26 was said to mark cells derived from an En1+ lineage which have fibrogenic capacity, and are distributed in a spattered pattern throughout both the reticular and papillary dermis in adult mice (Rinkevich et al., 2015). In our staining of adult human skin we find CD26 expressed on cells in both the reticular and papillary dermis. However, in our cells in culture CD26 was only found in the PFi isolated from the papillary dermis. There are two possible explanations for this result. Firstly, it may be that despite us trying to isolate cells from the whole reticular dermis to have representative RFi, culture conditions are selecting for fibroblasts which are CD26 negative from a highly heterogeneous reticular dermis. Alternatively, a perhaps more intriguing suggestion is that growth of cells in culture reverts cells to a more embryonic state. This correlates with the observation that CD26 is only expressed in the PFi *in vitro*, in the same manner that only upper lineage fibroblasts express Cd26 during development. Raising further questions is our observation that RFi also start to express CD26 by P10 *in vitro*, perhaps indicating that *in vitro* cell aging sometimes recapitulates *in vivo* aging.

2.5.4. PFi are the dominant fibroblast subtype in the blended Fi cultures

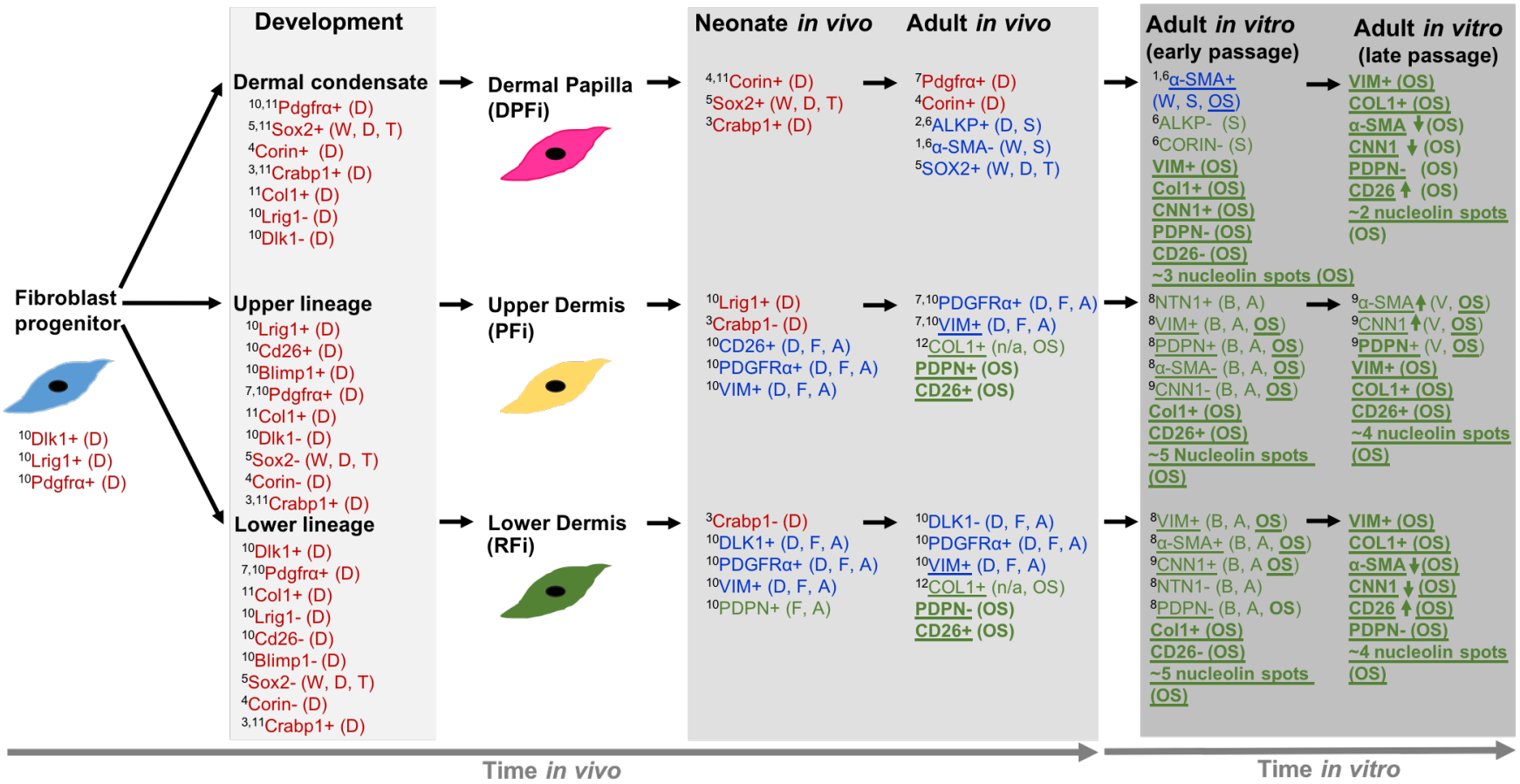
Human skin PFi have been described as being highly proliferative in culture in contrast with the RFi, even though the reticular dermis is much thicker than the papillary dermis. This has also been shown in this study, taking into account the DPFi in these

comparisons. The PFi are highly proliferative in comparison to both the RFi and the DPFi. Most studies assessing skin fibroblasts isolate cells from both the papillary and reticular dermis, and class all derived cells as dermal fibroblasts, which I refer to as blended Fi. Here, in an effort to determine what populations of dermal fibroblasts are present in a blended Fi culture, I performed IF with the panel of antibodies that I had used to distinguish between DPFi, PFi and RFi. Remarkably, I found that the cells present in a blended Fi population contain on average 5 nucleolin spots per nuclei, and express both CD26 and PDPN. This leads to the conclusion that the dominant fibroblast sub-type in the blended Fi cultures is indeed PFi, from the papillary dermis.

The ages of the patients from whom cells were isolated in our study range from 20 to 55 years old. It is well described that the papillary dermis of mammary skin becomes thinner with increasing age (Mine et al., 2008), and thus one would assume there are also less PFi present in aged skin. It would therefore be interesting to determine whether the observation that PFi are dominant in blended Fi cultures still holds true when cells from even older individuals are used, or cells from a different body site which has a differential rate of extrinsic aging compared to scalp skin (Tobin, 2017). Extrinsic ageing can be defined as changes caused due to UV radiation as well as other external environmental factors (Tobin, 2017). Therefore, biopsies obtained from aged patients from tummy tucks or from other body sites which are less exposed to UV radiation could result in a different dominant population than skin obtained from scalp biopsies which are more probable to be exposed to environmental cues. It is very important to acknowledge these differences in our studies in order to be able to objectively define the effect of ageing on the fibroblast populations in the dermis.

2.5.5. Are the cells reverting to a homogenous state with increasing passage?

Previous work assessing RFi and PFi from human skin *in vitro* has suggested that with prolonged passage PFi cells differentiate into RFi (Janson et al., 2013), however no reference has been made to the DPFi or RFi at prolonged passage. Our analysis suggests that PFi markers used in our study increase in expression in the DPFi and RFi, while DPFi and RFi markers such as α-SMA decrease by P10. One possible interpretation is that with increasing passage, and further distance from environmental cues which help to determine cell identity, fibroblasts are reverting to a unique homogenous state rather than turning into one another. It is important to note however, that the genes and proteins we chose to profile are only markers, and do not inform us of fibroblast behaviour or lineage, which contribute collectively to determining cell identity.



KEY

Genes/ proteins expressed/ not expressed in fibroblasts, identified in Murine studies

Genes/ proteins expressed/ not expressed in fibroblasts, identified in Human and Mouse studies

Genes/ proteins expressed/ not expressed in fibroblasts, identified in Human studies

My findings in Human cells

Figure 2.5.1. Fibroblast expression map in development, neonate and adult.

At the beginning of development there is a fibroblast progenitor from which the DPFi, PFi and RFi arise. This figure reviews the genes identified in mouse and human studies during development and in postnatal fibroblasts *in vivo* and *in vitro*. The genes identified in mouse studies are shown in red, the genes identified in human and mouse studies are shown in blue, the genes identified in human studies are shown in green, the genes I have tested are underlined in green and the findings I contributed which are novel are in green, underlined and bold. The body site from which the fibroblast populations were isolated are in brackets next to each gene name where D= dorsal, V= ventral, W= whiskers, T= tail, B=breast, F= foreskin, A= abdomen, S= scalp and OS= occipital scalp. The arrows in the late passage stage display the relative expression difference from the early passage stage. This illustration was made from the following references put in chronological order: 1. (Jahoda et al., 1991), 2. (Handjiski et al., 1994), 3. (Watt and Collins, 2008), 4. (Enshell-Seijffers et al., 2008), 5. (Driskell et al., 2009), 6. (Higgins et al., 2010), 7. (Collins et al., 2011), 8. (Janson et al., 2012), 9. (Janson et al., 2013), 10. (Driskell et al., 2013), 11. (Sennett et al., 2015), 12. (Hasebe et al., 2017).

2.5.6. Differentiation using osteogenic and adipogenic cues shows different differentiation potential of the three fibroblast subtypes

It was previously demonstrated that DPFi have the capacity to differentiate into osteoblasts and adipocytes when the relevant cues are introduced into the culture (Richardson et al., 2005). When the cells were cultured in osteogenic differentiation media, the PFi and the RFi did not share this differentiation capacity. This shows that the cells are truly different in culture not only in expression but they also have different behavioural traits. Interestingly, when the three populations were cultured in adipogenic media, all three produced fat droplets, with the RFi releasing significantly more than the other two populations. This may be due to the fact that during development the dermal adipocytes have been proposed to arise from the same developmental origin as the RFi (Figure 2.1.1.). The mechanisms by which these cells differentiate into osteoblasts and adipocytes are not currently known.

The timing of the differentiation could play a major part in this differentiation process, as a fellow lab member has shown that when the PFi and RFi are left in osteogenic media for longer they eventually turn into calcium releasing osteoblasts (data unpublished). This observation, suggests that DPFi are more plastic than PFi or RFi and have a greater potency to differentiation into osteoblasts. The same cannot be said for the adipogenic differentiation, as all three cell populations differentiate into adipocytes within the same time frame. This could also be explained in terms of the differentiation path the cells have to follow. Since adipocytes are also present in skin, this path is more direct than differentiating the fibroblasts into bone. These differences in potency, highlight the distinctive behavior of the cells and further reinforces the statement that we have to treat them as separate entities.

2.5.7. Frontal versus occipital scalp fibroblasts

While the skin epidermis is derived from a single ectodermal origin, the skin dermis arises from three developmental origins; dorsal dermis is from the dermomyotome, ventral dermis is from the lateral plate mesoderm, while craniofacial dermis is derived from neural crest ectoderm (Driskell and Watt, 2015). These different origins are believed to influence the behaviours and characteristics of hair follicles in each location (Topouzi and Higgins, 2016). For example, frontal scalp follicles are regarded as hormonally sensitive, and in response to elevated dihydrotestosterone (DHT) will undergo miniaturisation leading to androgenetic alopecia. On the other hand, occipital scalp follicles are unresponsive to DHT, meaning balding patterns on the scalp often reflect the developmental origin of the fibroblasts in each location (Price, 2003).

In an attempt to investigate the differenced in hair follicles in each location, the osteogenic differentiation capacity of DPFi, PFi and RFi isolated from frontal scalp, was compared to that of the occipital scalp. Within the 14 day time frame, the frontal scalp DPFi, PFi and RFi failed to differentiate into osteoblasts, while only the DPFi from the occipital scalp culture turned into calcium releasing osteoblasts. This was a very interesting result, as it not only highlights the differences in the DPFi across anatomical locations but also raises the question of whether the DPFi used in research should be chosen from specific locations of the body.

2.5.8. Mass spectrometry reveals unique deposition of ECM from each fibroblast population

Fibroblasts are considered to deposit the bulk of the ECM in the dermis. As mentioned before, during development there is common progenitor of fibroblasts that later on becomes the DPFi, PFi and RFi. It is currently unknown whether the fibroblasts have predetermined identities that enable them to become a specific population or whether the environment guides them towards their identity. To start answering this question, I wanted to study the ECM deposited by DPFi, PFi and RFi. First, I had to determine if there are any differences in ECM deposition in culture, therefore I performed mass spectrometry.

From my results, it was observed that the composition of the ECM deposited by the fibroblasts in *vitro* is very unique for each population as the peptide intensity sums of each protein identified were different across populations. Specifically, the adhesive glycoprotein THBS1 was highly abundant in the DPFi ECM which correlates with the information we have from the in *vivo* mouse experiments (Pablos et al., 1998). This further reinforced my results above that these populations are distinct even when their environmental cues are no longer present in culture.

In order to study the question of whether the ECM can guide fibroblast identity I went on to seed PFi and RFi on DPFi ECM and observe whether these populations are able to transdifferentiate in to DPFi if seeded on DPFi ECM. Unfortunately, due to a lot of optimization that needed to be done this experiment, it was not completed in time and I further discuss this in my future directions in Chapter 4.

2.5.9. Concluding remarks

In summary, in this chapter I demonstrated that fibroblasts from a single anatomical location, human occipital scalp dermis, have distinct expression profiles and behavioural characteristics when grown *in vitro*. Therefore, fibroblasts in the skin should be referred to as distinct fibroblast sub-types, as they possess different characteristics both *in vivo* and *in vitro*. Clearly defining fibroblasts will help us to study the fundamental processes involved in homeostasis and tissue repair, and take a first step towards elucidating the contribution of different fibroblast sub-types to these processes.

Chapter 3. Assessing fibroblast sub-type function with respect to wound healing.

3.1. Introduction

3.1.1. Skin homeostasis

As discussed in Chapter 2, the dermal layer is comprised of two compartments; the upper dermis, which is the papillary dermis and contains the PFi and the lower dermis, known as the reticular dermis that the RFi reside in (Harper and Grove, 1979). During murine development, DPFi of the hair follicle originate from the same development origin as the aforementioned fibroblast types in the dermis (Driskell and Watt, 2015). Unlike the epidermis which regenerates continually, DPFi reside on the base of the hair follicle which transitions through cycles of anagen (growth), catagen (regression) and telogen (arrest) through its lifetime (Alonso and Fuchs, 2006). We know from recombination experiments that cross talk between the dermis and epidermis is critical for hair cycling and skin homeostasis.

In this chapter, I will assess the contribution of the dermal fibroblasts mentioned above, when homeostasis is perturbed, specifically with regard to wound closure. All the work performed in this chapter was performed by me and is being used to write a patent application, which will be followed up with a manuscript after patent submission.

3.1.2. The role of the dermis in epithelial homeostasis

Epithelial-mesenchymal interactions are very important during skin and hair development as well as skin homeostasis (Jahoda and Reynolds, 1993, Driskell et al., 2013). During skin homeostasis, fibroblasts in the skin dermis release signals that help maintain the basal KC in a self-renewing state. Evidence of this cutaneous mesenchymal-epithelial interaction came in the 1970s when it was observed that

primary KC are supported for many passages when they were seeded on fibroblast feeders (Rheinwald and Green, 1975). In these experiments, the presence of the fibroblasts as well as growth factors such as Epidermal Growth Factor (EGF) that were added to the media, supported stem cell renewal and epithelial proliferation, while preventing differentiation. This shows that fibroblasts as well as growth factors released by fibroblasts and neighbouring cells are very important in maintaining homeostasis of the overlying epidermal cells.

Experiments on murine embryo experiments gave us the insight that hair follicle morphogenesis is driven by reciprocal epithelial-mesenchymal interactions (Millar, 2002). This is described as a cascade of reciprocal signals between the juxtaposed epithelial and mesenchyme compartments. This exchange in signals enables the formation of the dermal condensate in the embryo and this cascade of events is thought to be orchestrated by a different cytokines and growth factors released by the dermal compartment. FGFs are one of the families of growth factors that have been implicated in the formation of the dermal condensate (Andl et al., 2002). The dermal condensate then gives rise to the dermal papilla in the hair follicle of the adult. The dermal papilla plays a vital role in the growth and homeostasis of the hair follicle in the adult where it has a role directing differentiation and growth of epithelial cells in the hair follicle matrix.

3.1.3. Wound healing

According to statistics, chronic wounds affect 1-2 % of the world's population at any given time (Gottrup et al., 2010). In the UK, NHS spends 5.3 billion pounds per year to treat chronic wounds and associated comorbidities (Guest et al., 2015). Not only these conditions are a huge burden in the healthcare system of the country, but more

importantly it affects negatively the quality of life of the patients (Evans and Pinzur, 2005).

In wounding, loss of integrity of the epidermal layer may lead to serious disability and infections. When cutaneous wounding occurs, human skin has evolved the capability of repairing the wound in a series of four overlapping stages: haemostasis, inflammation, reepithelialisation and remodelling (Shaw and Martin, 2009). Other groups have characterised this as a three step process by combining haemostasis and inflammation in one step (Figure 3.1.1.) (Gurtner et al., 2008). Most wounds are characterised by an initial leakage of blood. The first step towards wound healing, is haemostasis, which involves fibrin clot formation in order to stop haemorrhage. This fibrin clot then aids fibroblasts and other cells to migrate into the clot in order to form the granulation tissue (Laurens et al., 2006). Then parallel to haemostasis, inflammation, occurs in order to protect the organism from pathogenic infections. Reepithelialisation, involves a combination of proliferation, migration and differentiation of the KCs to cover the wounded area. During this stage fibroblasts deposit ECM to replace the fibrin clot (Xue and Jackson, 2015). The last stage of wound repairing is the remodelling stage which, depending on the species and type of wound, can take years to be completed. During this stage, all of the processes from the previous stages cease and there is major remodelling of the ECM in the wounded area (Shaw and Martin, 2009, Guo and Dipietro, 2010). These steps aid the epidermis to alter its proliferative and migratory dynamics in order to re-establish a functional epithelium (Park et al., 2017).

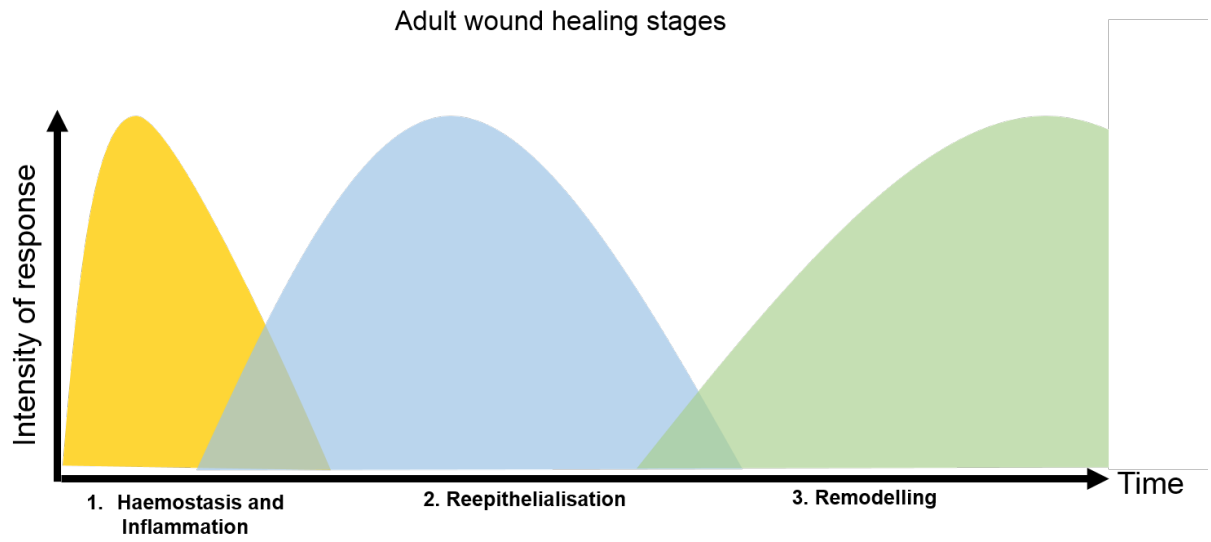


Figure 3.1.1. Stages of wound repair.

1. Haemostasis and inflammation involve the formation of a fibrin clot. 2. The reepithelialisation stage involves migration, proliferation and differentiation of the KC. 3. The remodelling stage involves the remodelling of the ECM in the wounded area.

3.1.4. Wound healing and scar formation

Scar formation is a physiological result of wound healing in mammalian adults (Figure 3.1.2A). That is, except from the case of African spiny mouse that can regenerate scarlessly (Seifert et al., 2012). This mouse has little inflammation during wound healing and an up regulation of metalloproteinases that break down the ECM (Brant et al., 2015). As this mouse has the ability to heal scarlessly during its lifetime it can be hypothesized that promoting a faster inflammatory phase as well as promoting ECM degradation could be the key to scarless healing.

Interestingly, embryonic wounds exhibit scarless healing and complete restoration of the skin architecture (Figure 3.1.2B). During foetal wound healing, there is almost no inflammation stage which has been proposed to be the reason in this scarless phenotype. Research has demonstrated, using a genetically modified neonatal mouse

that is incapable of having an inflammatory response, that it has the ability to heal scarlessly (Redd et al., 2004). On the contrary, chronic wounds which do not heal are described to have a much longer inflammatory phase than healthy wounds (Figure 3.1.2C). Perhaps this means, that accelerating wound reepithelialisation will in turn shorten the inflammatory phase. This raises the possibility that accelerating reepithelialisation could be a therapy for chronic wounds which could also reduce scar formation.

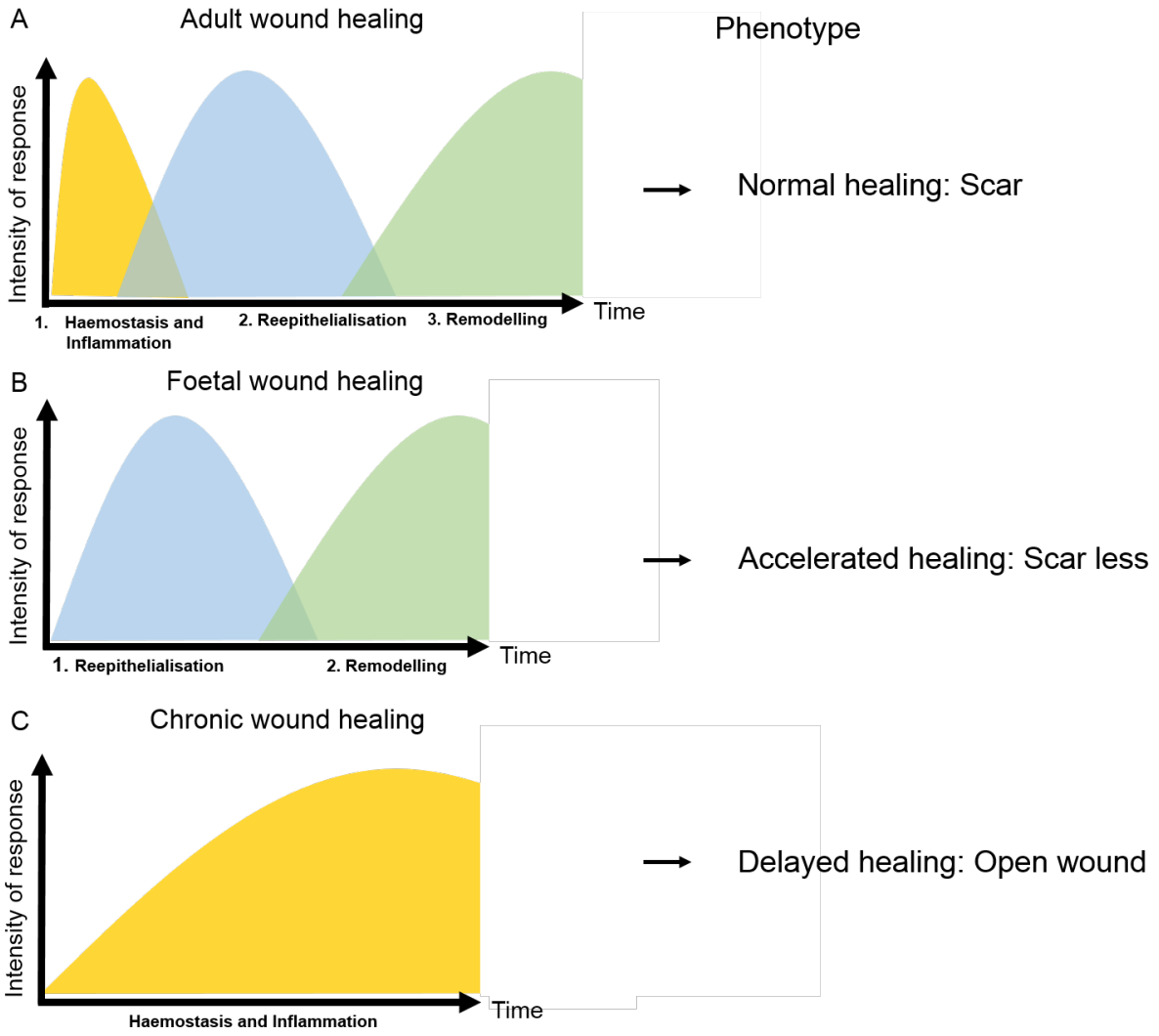


Figure 3.1.2. Wound healing stages in adult, embryo and chronic wounds.

(A) Adult wound healing has three overlapping phases; 1. Haemostasis and inflammation, 2. Reepithelialisation and 3. Remodelling. When the remodelling stage is completed there is a scar. (B) Foetal wound healing only has the reepithelialisation and remodelling stages and results in a scar less phenotype. (C) Chronic wounds are permanently in the inflammation stage thus no reepithelialisation occurs and remains an open wound.

3.1.5. The role of the dermis in wound healing

Fibroblasts are critical during the reepithelialisation stage of wound healing as they deposit ECM into the wound bed (Xue and Jackson, 2015). This provides a scaffold for the KC to migrate on (Figure 3.1.3). Recent evidence, showed that the ECM is not only able to act as a matrix for KC migration but it also functions as a storage and delivery system for cytokines and growth factors produced during the healing process (Schultz and Wysocki, 2009).

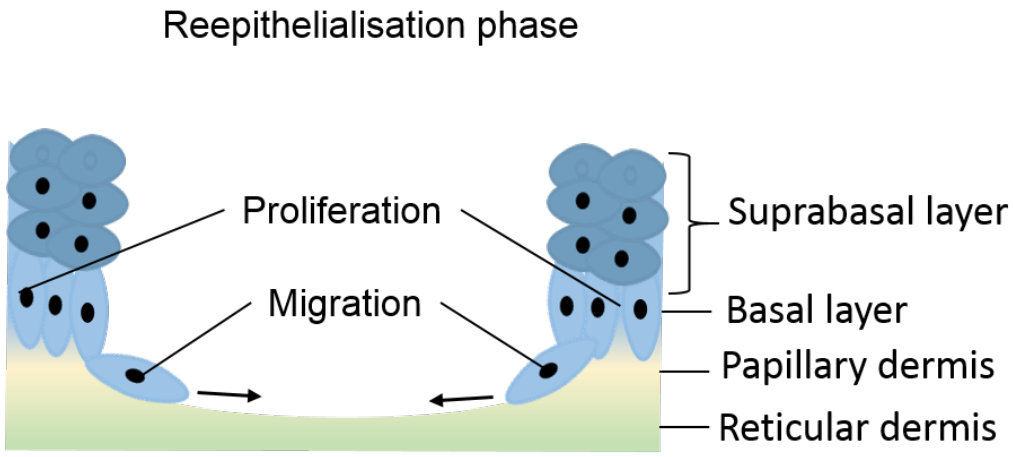


Figure 3.1.3. Reepithelialisation phase of wound repair.

The KC migrate onto the ECM scaffold that has been deposited by the fibroblasts. Proliferation of the KC occurs in the basal layer to compensate for the KC migrating into the wound bed.

Recently, it has been demonstrated in an *in vivo* experiment using a full thickness wound in adult mice, that the RFi are the first population to migrate into the dermal wound and repopulate the repairing dermis (Figure 3.1.4.) (Driskell et al., 2013). After the initial dermal repair, the epithelium migrates in to close the epidermal wound (Driskell et al., 2013). From this evidence, I hypothesized that the RFi are releasing

growth factors/cytokines to enable the KC to start migrating and reepithelialise the wound.

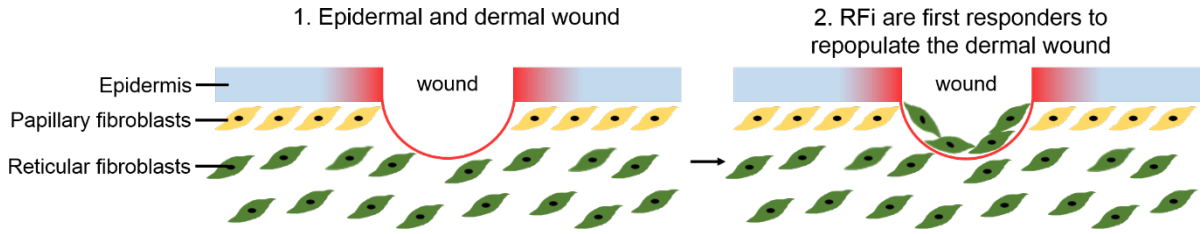


Figure 3.1.4. RFi in wound healing.

Cartoon to summarise research which showed that RFi migrate into the wound bed to repopulate the dermal wound after injury.

Hair follicles have also been shown to be important during reepithelialisation. A clinical study has recently shown that individuals with venous leg ulcers had a significant wound reduction when skin grafts containing hair follicles were grafted to the site of the wound in comparison to skin grafts from a non-hairy site (Jimenez et al., 2012). The proposed mechanism for the hair follicle role in wound healing is the contribution of bulge stem cells enabling reepithelialisation (Jimenez et al., 2015). Following this, another laboratory has studied the addition of human DPFi along with hair follicle stem cells in an acellular porcine dermal scaffold. They reported that in a full thickness wound in mice, addition of this graft favoured neovascularization, remodelling and reduced inflammation in the wound and also resulted in less scarring compared to the scaffold without hair follicles (Leiros et al., 2014). These findings suggest that the DPFi may be able to modulate proper dermal remodelling during cutaneous wound healing.

3.1.6. Other dermal subtypes in wound repair

Myofibroblasts are also present during wound healing and are responsible for wound contraction (Gabbiani et al., 1971). The origin of these wound myofibroblasts has been hypothesized to be the dermal fibroblasts in the wound edge. In general, these dermal fibroblasts are known to be activated after injury (Li and Wang, 2011). This activated form has been reported to express ACTA2 or else known as α-SMA (Li and Wang, 2011, Rockey et al., 2013). Based on *in vitro* studies, there is also a hypothesis supporting that myofibroblasts could originate from the DPFi because of the expression of α-SMA in culture as well as the differentiating capability of the cells (Jahoda and Reynolds, 2001), which has raised questions of whether the DPFi can also differentiate into a myofibroblast in a cutaneous wound. The reason behind this differentiation of fibroblasts into myofibroblasts could be explained by mechanical force stimulation (Hinz, 2010). The stiffness of a wounded ECM is higher than the soft ECM that an unwounded dermis usually has. This difference in stiffness could be one of the triggers behind the differentiation of the fibroblasts as a stiffer ECM changes the behaviour of a cell.

Myofibroblasts are present during the first stages of wound repair but were known to be degraded during the remodelling stage. Their role during the initial stages of repair is to migrate into the wound and deposit ECM to enhance wound contraction (Li and Wang, 2011). Interestingly, a research group has recently found in a mouse study that in wounded sites where the hair follicles have regenerated, there is formation of new adipocytes predominantly around the hair follicles (Plikus et al., 2017). Using lineage tracing, they found that myofibroblasts from the wound edge were converting into adipocytes in response to signalling from hair follicles. This interesting finding shows

the important of the hair follicle and the dermal papilla for the complete regeneration of skin during healing.

3.1.7. Growth factors and cytokines: What is their role in wound healing?

Recent advances have introduced the use of autologous skin grafts as well as growth factors and cytokines as a potential solution to the chronic wound problem. After wounding, a cascade of events occurs in order to repair the damage to the tissue. This process starts immediately after injury and is completed in four stages with the help of cytokines and growth factors that have to be present to instruct the cells during wound closure. Several growth factor families have been reportedly shown to be involved in wound healing such as platelet derived growth factor family (PDGF), FGF, EGF as well as bone morphogenic proteins (BMPs). In addition, cytokines have been showed to play an important role during wound healing such as chemokines (CC-) and interleukins (IL-). I will discuss some of the major players in wound healing here (summarised in Table 3.1.1.) although it is a complex process and there are several growth factors and cytokines that play lesser roles which I may not mention.

PDGF and its isomers, have been described to be involved in stimulation of cell growth and mobility of fibroblasts during wound healing. It has also been correlated with the contraction of fibroblasts that could explain their differentiation into myofibroblasts (Heldin and Westermark, 1999). Interestingly, the isomer BB of PDGF was the first growth factor to be approved by the Food and Drug Administration (FDA) for the treatment of human diabetic foot ulcers which will be discussed more in section 3.1.8. (Nagai and Embil, 2002). Apart from its therapeutic potential, research has shown there is a decrease of PDGF levels in back skin wounds on diabetic mice compared to wild type (Beer et al., 1997). Diabetic mice also have impaired wound healing

suggesting there is a correlation between PDGF expression and wound healing. To support this correlation, another study showed that in aged mice where the wound healing process is slowed down, there was a delay in the appearance of PDGF and EGF into the wound bed (Ashcroft et al., 1997).

FGFs and EGFs are two other families of growth factors that have been shown to have a role in wound healing. Specifically, expression of Fibroblast growth factor 7 (Fgf7; otherwise known as Keratinocyte growth factor; Kgf) was found in normal and wounded skin dermis of mice, with significant up regulation after wounding at the wound edge (Werner et al., 1992) supporting a role for Fgf7 during wound healing. Fibroblast growth factor 2 (Fgf2) expression has been observed in the epithelium surface of the wound and in the dermis adjacent of the wound site in adult mouse skin (Werner & Grose 2003). FGFs have also been associated with hyper proliferation in the epithelium during wound healing. Fgf7 is normally found at low levels in the dermis and its receptor Fgfr2IIb is found in the epidermis. After skin injury they are both up regulated in their respective compartments. Werner and colleagues have also generated transgenic mice where Fgfr2IIb was conditionally knocked out in the epidermis. When the mice were injured with a full thickness wound Fgf7 increased in the dermis. However, very slow reepithelialisation was observed in the epidermis. That could suggest that interaction between Fgf7 and its receptor Fgfr2IIb is required for normal wound healing to promote reepithelialisation of the epithelium (Werner & Grose 2003). Interestingly, *in vitro*, RFi release more Fgf7 that PFi, which further supports my hypothesis that RFi are controlling wound reepithelialisation (JM et al. 2004).

EGF is one of the growth factors added to the media when culturing KC to offer support to the cells. It is secreted by platelets, macrophages and fibroblasts and stimulates KC

proliferation by activating the EGF receptor (EGFR) that is located in the basal layer of the epithelium (Rheinwald and Green, 1977, Nanney et al., 1986). Interestingly, administration of EGF to wounds was shown to shorten healing times in patients with ulcers (Mohan, 2007) further supporting its involvement in wound healing.

In addition to the growth factors mentioned above, BMPs have also been proposed to have a role in wound healing. Specifically, Bone morphogenic protein 6 (Bmp6) has been suggested that it acts as an inhibitor of KC proliferation in order to promote the differentiation of KC from the basal to the suprabasal levels (McDonnell et al., 2001). It is also important in epithelial stem cell maintenance in the hair follicle as well as epithelial differentiation (Rendl et al., 2008a). BMP6 has been found to be up regulated in human skin ulcers, probably due to inhibition of KC proliferation (Lyons et al., 1989). It comes as no surprise that overexpression of this cytokine in mice has shown to severely delay reepithelialisation *in vivo* (Kaiser et al., 1998). As BMP6 enables differentiation but inhibits proliferation this suggests that a spatial and temporal regulation of this cytokine is necessary for re-establishing the wounded epidermis.

Studies have also provided evidence that cytokines such as ILs and CCs are important for wound repair. In a recent study, the macrophage response was studied in normal and diabetic mice wounds. It was found that there was a delay in macrophage response in diabetic wounds mainly due to decreased levels of Chemokine ligand 2 (CCL2) (Wood et al., 2014). In the same experiment, when Ccl2 was applied to diabetic wounds it restored the macrophage response thus demonstrating the importance of this cytokine for an inflammatory response.

Interleukin 6 (IL6) has been the centre of many studies involving wound healing (Turksen et al., 1992, Gallucci et al., 2001, Lin et al., 2003, McFarland-Mancini et al.,

2010) and has been proved to be an essential cytokine during the wound healing process. In an experiment using an *in vivo* assay, IL6 knockout mice had a significantly slower reepithelialisation than wild type (Lin et al., 2003, McFarland-Mancini et al., 2010). It has also been shown that addition of IL6 to wound beds can restore abnormal wound healing in IL6 deficient mice (Gallucci et al., 2001) displaying the importance of this cytokine for normal wound closure. Furthermore, studies involving the cytokine Interleukin 22 (IL22) have shown that IL22 Receptor (IL22R) knockout mice display a significant delay in wound closure (Kolumam et al., 2017). Another study showed that addition of IL22 significantly increased wound closure in diabetic mice (Avitabile et al., 2015) demonstrating its importance in wound repair.

Table 3.1.1. Summary of section 3.1.6.

Growth factor/cytokine	Importance in wound healing	References
PDGF-BB	Stimulates cell growth and proliferation.	(Heldin and Westermark, 1999)
	FDA approved for the treatment of diabetic foot ulcers.	(Nagai and Embil, 2002)
	Decreased levels in diabetic mice in comparison to the wild type.	(Beer et al., 1997)
Fgf7	Up regulated in the dermis on the wound edge.	(Werner et al., 1992)
EGF	Stimulates KC proliferation.	(Rheinwald and Green, 1977)
	Shortens healing times in patients with ulcers.	(Mohan, 2007)
BMP6	Inhibits KC proliferation and aids KC differentiation.	(McDonnell et al., 2001)
	Important in epithelial stem cell maintenance.	(Rendl et al., 2008b)
	Up regulated in human skin ulcers.	(Lyons et al., 1989)
	Overexpression severly delays reepithelialisation in mice.	(Kaiser et al., 1998)
Ccl2	Restores macrophage response in diabetic mice.	(Wood et al., 2014)
IL6	IL6 knockout mice have slower reepithelialisation.	(Lin et al., 2003, McFarland-Mancini et al., 2010)
	Can restore wound healing in IL6 deficient mice.	(Gallucci et al., 2001)
IL22	ILR22 knockout mice have a delay in wound closure.	(Kolumam et al., 2017)
	Increases healing times in diabetic mice.	(Avitabile et al., 2015)

3.1.8. Current strategies to advance our understanding in wound healing

Genetically modified mice have given us great insights into the cytokines and growth factors involved in the wound healing process, but we still need to elucidate the role of several cytokines in human wound healing as these two organisms have different characteristics and healing mechanisms. Mice heal by contraction of the wound bed while humans heal by reepithelialisation. Even though human and murine skin have the same layer of cells in their dermis and epidermis, they differ in the thickness with human skin being thicker than murine skin. In addition, murine skin is covered in hair follicles whereas human skin has hair follicles on specific sites with the addition of interfollicular dermis and epidermis which are the regions that do not contain any hair follicles (Zomer and Trentin, 2018). Also, sweat glands, which are present in human skin have been shown to play a role in immune response. This is however absent from mouse skin (Wong et al., 2011), which further highlights the differences between the two organisms.

Ex vivo punch biopsies have been used to study the effect of wound healing in human tissue (Stojadinovic and Tomic-Canic, 2013). Although these biopsies are giving us great insights to the wound healing process of humans, they are not readily available thus scientists have sought alternative methods to study wound healing. Several studies have described the use of 2D cell culture models to study reepithelialisation of the KC population in a more controlled environment using scratch assays *in vitro* (Liang et al., 2007, Walter et al., 2010). Primary KC are seeded *in vitro* in order to study migration using the scratch technique with the aid of cytokines and growth factors. This monoculture offers a convenient platform to study the reepithelialisation process *in vitro*.

The presence of growth factors *in vitro* migration assays as well as *in vivo* experiments has been shown to be vital during the wound healing process. PDGF is one of the first growth factors to be FDA approved for the use in diabetic foot ulcers. PDGF-BB has been tested for its efficacy in promoting wound closure in rat KC in an *in vitro* scratch assay and this has also been translated *in vivo* human studies (Nagai and Embil, 2002). Becaplermin is a PDGF-BB commercially available gel that has been branded as Regranex (Smith & Nephew). After several clinical trials on its efficacy over the years it was concluded that Regranex significantly increases healing rates and decreases time to complete healing (Papanas and Maltezos, 2007). However, recently, malignancies distant from the site of application have been reported and patients with prior malignancies were warned not to use the product. Therefore, even with promising recent advances research is still required to identify safe alternative solutions to treat chronic wounds.

3.2. Specific aims in Chapter 3

The use of growth factors seems promising in the treatment of chronic wounds. In the previous chapter I demonstrated that human DPFi, PFi and RFi maintain distinct behavioural and expression characteristics *in vitro* at an early passage. Given these results and the understanding that fibroblasts are a key player in wound healing, in this chapter I assess how fibroblast subtypes in human skin differentially affect KC migration and wound closure *in vitro*.

The first aim of this chapter was to identify if DPFi, PFi and RFi can have a paracrine effect on KC *in vitro*. After identifying that this was the case, I sought to narrow down the source of this effect, and see which cytokines released from fibroblasts are sufficient for wound closure. These results could provide possible therapeutic targets to accelerate wound closure that could potentially be used as a treatment to chronic wounds.

3.3. Materials and Methods

3.3.1. Human skin biopsies

For all the *in vitro* experiment, human skin biopsies were taken from the occipital scalp of patients (unless otherwise stated) undergoing surgical proceedings after receiving informed consent, and using IC-REC approved consent forms. Tissue is held under ICHTB HTA license 12275, and used in the ICHTB approved project R15055.

Table 3.3.1 provides full information on the patients used in this chapter. Biopsies used in Chapter 3 are from different patients than biopsies used in chapter 2, apart from P2D that has been used in both chapters.

Table 3.3.1. Human skin biopsies in Chapter 2.

Patient	Gender	Age	Site of isolation	Matched cell populations available
P2D	Male	64	Occipital scalp	DPFi, PFi, RFi
P3A	Male	49	Occipital scalp	DPFi, PFi, RFi
P3B	Male	34	Occipital scalp	KC
P3C	Male	48	Occipital scalp	KC

For the *ex vivo* experiment (3.3.12.), human abdominal skin with adipose tissue was purchased from Caltag Medsystems LTD.

3.3.2. Isolation and cell culture of fibroblasts and KC

Isolation and cell culture of fibroblasts and KC was commenced as described in Chapter 2 methods in sections 2.3.2. and 2.3.3. respectively.

3.3.3. Conditioned media collection

DPFi, PFi and RFi cells were seeded at a density of 6000 cells per cm^2 using Dulbecco's minimal essential medium (dMEM; Gibco Life Technologies) supplemented with 10% Fetal Bovine Serum (FBS; Gibco Life Technologies). After 24 hours, the cells were washed two times with Phosphate Buffered Saline (PBS; Gibco life technologies) and Epilife (Gibco Life Technologies) supplemented with Epilife defined growth supplement (EDGS; Gibco Life Technologies), which is the KC growth media used in my experiments, was added to the cultures. Conditioned media (CM) was collected 2 days after the addition of Epilife with EDGS. 2 days were chosen, as fibroblasts were found to undergo stress after 3 days in KC growth media (data not shown). The media was then filtered through a 0.22 µm pore sized filter to remove cell debris and aliquoted and stored at -20º C until used. Conditioned media was collected from DPFi, PFi and RFi from two patients aged 50 and 65 years old.

3.3.4. KC wound healing assays using fibroblast conditioned media

6 well plates were prepared by coating them using the coating matrix kit (Gibco Life Technologies) as described in section 2.3.3. Two different methods were used for the wound healing assay. The first method used was using 2-well inserts (Ibidi) that stick to the surface of the well and have a defined cell-free gap (approximately 500µm) in

the middle in order to study KC migration, while the second method was done by 'wounding' the cells using a p200 pipette.

In both methods, KC were seeded at a density of 6000 cells per cm^2 using Epilife supplemented with EDGS. When they reached confluency, in the first method, the Ibidi inserts were removed using sterile forceps, while in the second method, a p200 pipette tip was used to scratch the middle of the well to create a 'wound' in the cells (Figure 3.3.1.). The cells were then washed two times with PBS. Conditioned media obtained from DPFi, PFi and RFi as well as a control with just Epilife supplemented with EDGS was used. Photos were taken at 10 timepoints, from time 0 to 9, using a phase contrast microscope at x10 magnification for the Ibidi method and x5 magnification for the p200 method. The experiment was repeated three times obtaining photos of each condition in triplicate. Images were then analysed using the Image J software (refer to section 3.3.6.).

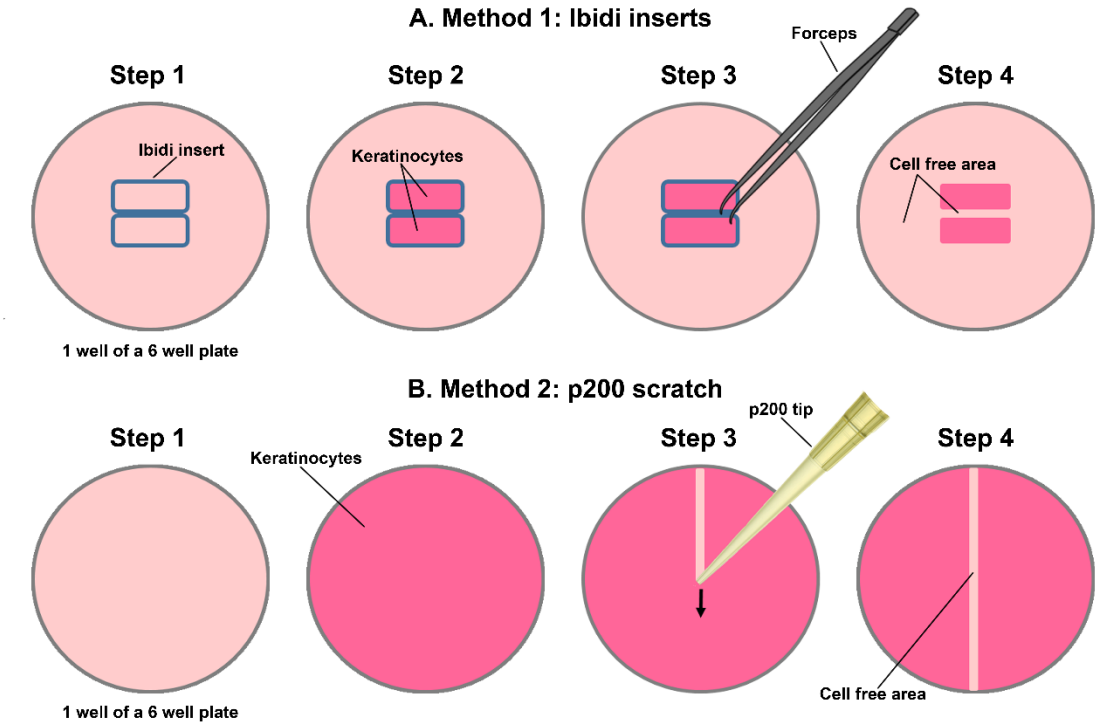


Figure 3.3.1. Two methods of performing a KC wound healing assay.

The first step of method 1, involved adhering the ibidi inserts in the surface of the well of a 6 well plate. Then, KC cells were seeded in the inner area of the insert as well as the rest of the plate. When the cells were confluent, the insert was removed with sterile forceps. Then, a cell free area of approximately 500 µm was left in the middle of the two KC cell fronts. (B) The second method was also performed in a 6 well plate. The KCs were seeded in the well, and when they reached confluency, a p200 pipette tip was used to scratch through the layer of KCs. A cell free area was left in the middle of the well.

3.3.5. Mitomycin C treated KC scratch assay using fibroblast conditioned media

The experiment was performed using the second method (p200 wounding) as explained in section 4.2.4. In this experiment, Mitomycin C (MITC; Sigma) was used on the KC to inhibit cell proliferation. Normal KC cultures were used as a control. Conditioned media and epilife with EDGS were used in the MITC treated KC as well

as the control. All conditions were done in triplicate. Photos were taken at 10 timepoints 1 hour apart, from time 0 to 9, using a phase contrast microscope at x5 magnification. Images were then analysed using the Image J software (see section 3.2.6.).

3.3.6. Scratch assay analysis

The 9 hour measurement was used to provide information about migration and velocity. Ten images were taken, at equal time intervals (1 hour), between the starting and end point. Optimally, the wound was not closed by the last timepoint, as the migration stops when the gap reaches confluency. In order to quantify the characteristics of the cell migration, the images were analysed with the image processing software Image J.

The images were loaded onto the software, and the scale was set for the correct magnification of the images. Then for each timepoint, the gap was measured and calculated in μm^2. The difference in μm^2 of the distance covered by the KC, was calculated by subtracting the total wounded area of each timepoint from the first to ensure consistency between results.

The cell front velocity of each wound was also calculated as follows:

-The cell free area was calculated in μm^2, and then the % of the cell free area was calculated by dividing the total area by the cell free area and multiplying with 100.

-The cell free area was then subtracted from 100 to get the cell covered area in %. Then, I subtracted the percentage at each time point to get %/h, and then I divided by 100 to get μm/h.

-This was multiplied by the total area of the image to get μm^2/h, which was then divided by the length/width of image and divided by 2 cell fronts.

The difference in μm^2 of the distance covered by the KC was analysed using a two-way Anova and plotted in line graphs as shown in the results.

3.3.7. Human cytokine antibody array

RayBio® C-Series human cytokine antibody array C1000 (RayBiotech) was used to analyse the conditioned media obtained from DPFi, PFi and RFi. The protocol and the reagents used were the ones provided by the kit supplier. All the solutions were prepared according to the manufacturer's instructions. The kit was removed from -20º C storage and the components were allowed to equilibrate to room temperature.

The antibody arrays were carefully removed from the plastic packaging and each membrane was placed (printed side up) into a well of the incubation tray provided. One membrane was used per conditioned media analysed. 2 ml of blocking buffer was pipetted into each well and incubated for 30 minutes at room temperature. The blocking buffer was then aspirated from each well. 1 ml of conditioned media was placed into each well and incubated overnight at 4°C on a rocking plate. The next day, the conditioned media was aspirated from each well. 2 ml of 1X Wash Buffer I was added into each well and incubate for 5 minutes at room temperature. This was repeated two more times for a total of 3 washes using fresh buffer and aspirating out

the buffer completely each time. Then, 2 ml of 1X Wash Buffer II was added into each well and incubated for 5 minutes at room temperature. This was repeated one more time for a total of 2 washes using fresh buffer and aspirating out the buffer completely each time. 1 ml of the pre-prepared Biotinylated Antibody Cocktail was into each well and incubated overnight at 4°C. The next day, 2 ml of 1X HRP-Streptavidin was added into each well and incubated overnight at 4°C. HRP-Streptavidin was aspirated from each well. The membranes were then washed with 2 ml of 1X Wash Buffer I and incubated for 5 minutes at room temperature. This was repeated two more times for a total of 3 washes using fresh buffer and aspirating out the buffer completely each time. Then, 2 ml of 1X Wash Buffer II was added into each well and incubate for 5 minutes at room temperature. This was repeated one more time for a total of 2 washes using fresh buffer and aspirating out the buffer completely each time.

The membranes were transferred, printed side up, onto a sheet of tissue paper lying on a flat surface. Excess wash buffer was removed by blotting the membrane edges with another piece of paper. The membranes were transferred, printed side up, onto a plastic sheet that was provided, lying on a flat surface. Into a single clean tube, equal volumes (1:1) of Detection Buffer C and Detection Buffer D were added. This was mixed well with a pipette. A total of 500 µl was measured to be enough for 1 membrane. The Detection Buffer mixture was gently pipetted onto each membrane and incubate for 2 minutes at room temperature. Exposure should ideally start within 5 minutes after finishing the last step and completed within 10-15 minutes as chemiluminescence signals will fade over time. Another plastic sheet was placed on top of the membranes by starting at one end and gently rolling the flexible plastic sheet across the surface to the opposite end to smooth out any air bubbles. The membranes

were ‘sandwiched’ between the two plastic sheets. The sandwiched membranes were transferred to the chemiluminescence imaging system to expose for 1 minute.

3.3.8. Human cytokine array analysis

The protein analyser plugin for Image J was used to analyse the cytokine array antibody membranes. Following installation of the plugin (instructions on download and setup can be found here: http://image.bio.methods.free.fr/ImageJ/?Protein-Array-Analyzer-for-ImageJ.html), the images were loaded individually onto the software and the analysis began using the "Array Analysis Menu" followed by the "Array Analysis" function. This action proposed a method of background subtraction and build a graphical interface for the dot matrix analysis. The visualisation was then optimised by activating some options available from the graphical interface. In short, three dots were selected forming angle (top-left, top-right and low-left) to set the interface of the membrane. Once the mask was set and recognised the membrane, a grid formed, and the matrix was measured automatically as a table of values.

Once the arrays were individually analysed using the "Array Analysis" tools, the "Group Pattern" menu then allows to obtain a global view of a set of arrays. The parent folder was set that was containing the analysed arrays. Then this folder was selected containing the array analyses by the "Masterize from Analysis Repertories" function. This function looks for result tables coming from the "Array Analysis" functions, in the parent folder. The tool explores any sub-levels, and builds a master image, or pattern, associated to a master table presenting all the results. The program exhibits two default master representations:

1. The default master pattern presents the arrays as they came from the analysis, with the visualization scaled between zero and the maximum values encountered in each array.

2. The initial normalized pattern presents a normalization between zero and the maximum value found in the master. This representation gives the most natural aspect of the modelled pattern compared to the initial images.

The masters were then normalised using the internal references provided by the manufacturer on the membrane as positive and negative controls, by using the "Group Pattern Menu" and "Set Internal Control and References". Each value was normalized following this formula:

Dot Value norm = (Dot Value - mean(Controls))/mean(References).

Once the normalised values were obtained, the following three correlations were made: DPFi vs PFi, DPFi vs RFi and PFi vs RFi by calculating the fold change (log2) and the p-value (log10) by using t-test with unequal variance. The cut off values were below p-value 0.05 and fold change ranging from -2 to 2.

3.3.9. Optimisation of cytokine concentrations and cytokine scratch assay

From the results obtained using the cytokine array, the following four recombinant human cytokines were chosen to assess their effect on KC migration; AXL receptor tyrosine kinase (AXL; R&D systems), Chemokine ligand 19 (CCL19; Biolegend), Bone morphogenic protein 6 (BMP6; Biolegend) and Interleukin 6 (IL6; Gibco, life technologies). The specific activity of each cytokine was specified as a range by the

supplier and three concentrations at the top, bottom and middle of this range were tested to obtain the concentration that yields the fastest wound gap closure (Figure 3.3.10.).

The cytokine scratch assay was performed with the p200 method, using the optimised cytokine concentrations as explained above. The images were analysed as explained in section 3.2.6.

Recombinant human PDGF-BB (Biolegend) was also purchased to compare its effect on KC reepithelialisation. This cytokine has been optimised by Biolegend in mouse fibroblasts in culture before and its maximum effect was recorded to be 5ng/ml, therefore this concentration was used for my experiments.

3.3.10. Microarray to determine the effect of AXL and DPFi CM on KC gene expression

3 wells of a 6 well plate were prepared by coating them using the coating matrix kit (Gibco Life Technologies) as described in section 2.3.3. KC were seeded at a density of 6000 cells per cm^2 using Epilife supplemented with EDGS. When they reached confluency, a p200 pipette tip was used to scratch the well in 4 different regions (in a hashtag pattern), to create a 'wound' in the cells. The cells were then washed two times with PBS. Conditioned media obtained from DPFi, AXL, and control with just Epilife supplemented with EDGS were used. Two biological replicates were used in this experiments with the patients aged between 35-55 years old.

After 6 hours, RNA was collected using the RNeasy Plus Micro Kit (Qiagen). Once the RNA was collected, and the concentration and quality of the samples was determined

using the nanodrop. The quality of the samples was in the acceptable range of A260/280 1.7-2.1. Then the samples were taken to a genomics facility (UK Bioinformatics LTD) where they were analysed by Mr David Chambers using GeneChip™ Human Genome U133 Plus 2.0 Array (Affymetrix).

In the genomics facility, the quality and quantity of the samples was retested using the Bio analyser. Then, they synthesized first-strand complementary DNA (cDNA) which was then converted to double-stranded cDNA, which acted as a template for *in vitro* transcription. This reaction used DNA polymerase and RNase H to degrade the RNA and synthesize second-strand cDNA. They then synthesized labelled complementary RNA (cRNA). After that, they purified the labelled cRNA removing enzymes, salts, inorganic phosphates, and unincorporated nucleotides in order to prepare the labelled cRNA for fragmentation. The purified cRNA was then fragmented by divalent cations and elevated temperature. The cRNA was then transferred for hybridization and scanning onto the GeneChip™ Human Genome U133 Plus 2.0 Array.

3.3.11. Microarray computational analysis

Raw data from the microarray were analysed using the commercial software package Genespring GX 14.9 (Agilent Technologies Inc.). The intensity values of the samples were normalised to be between 20-100%. Parametric tests, with the p-value set at 0.05 were performed to determine differential expression. Entities were chosen on a fold change cut off of >=2. A one way Anova test was performed on the same list of genes which generated 6 lists were genes were either up regulated or down regulated in AXL, DPFi CM and Epilife. These lists of genes were then uploaded into Ingenuity

Pathway Analysis software (IPA; Quiagen) to generate potential pathways that could be activated/inhibited by AXL, DPFi and Epilife.

3.3.12. Human *ex vivo* wound model

Human abdominal skin with adipose tissue was obtained with informed consent from a 45 year old female patient. Subcutaneous fat was removed then a 2 mm diameter partial thickness wound was made followed by an 8 mm outer wound, removing the epidermis and papillary dermis (Figure 3.3.2.). Using a 6 well plate, the punch within a punch wounds were cultured onto 2 non-woven gauze and a 0.45 μm nylon membrane (Millipore). 1.5 ml of William's E media (Life Technologies) supplemented with 1% P/S, 2 mM L-Glutamine (Gibco), 10 μg/ml Insulin (Sigma) and 10ng/ml Hydrocortisone (Sigma) were added onto the non-woven gauze in the well. In order to test the effect of the different cytokines in wound closure, 6 conditions were tested simultaneously, with 4 replicates of each condition. 5μl of AXL, CCL19, PDGF-BB, IL6, CCL19&AXL and Epilife supplemented with EDGS were added topically onto the wound. Media was changed daily with excess media being removed from the well and replaced with 1 ml fresh media. Topical application was also added daily as it was absorbed into the wound bed.

Images were taken every 24 hours with a stereo microscope until wound closure. The images were then analysed using Image J. Two-way ANOVA was used to analyse the difference in mm and comparisons were made at individual time points using the same test in Graphpad Prism 6.0.

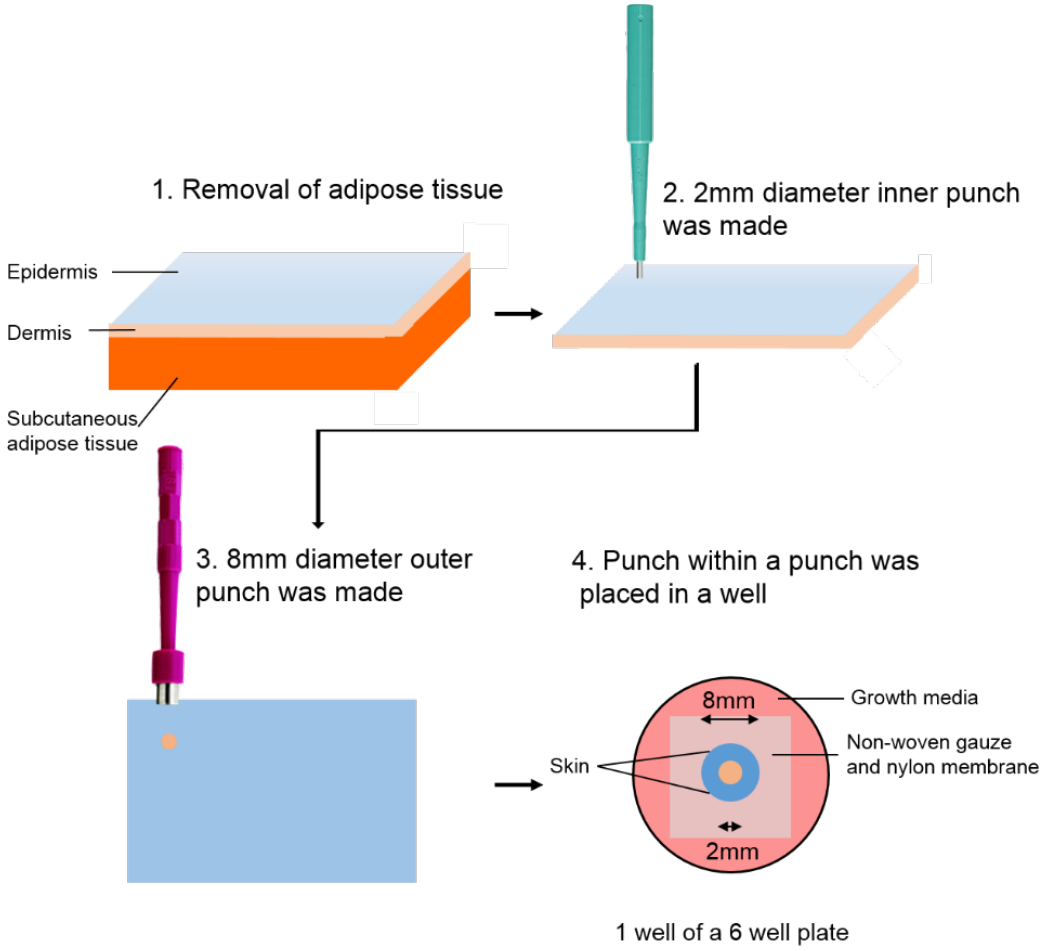


Figure 3.3.2. Schematic of experimental procedure to prepare skin for the human *ex vivo* wound assay.

(1) Human abdominal skin was processed and adipose tissue was removed. (2) A 2mm inner punch was made. (3) Then an 8mm outer punch was made. (4) The tissue was transferred in a well of a 6 well plate on non-woven gauze with a nylon membrane.

3.3.13. Statistical analysis of data

The data collected in this chapter, were analysed using Graphpad prism 6 and statistical analysis of each experiment is outlined in the corresponding method or figure legend. Number of biological replicates (N) and number of technical replicates (n) are also indicated in the figure legends.

3.4. Results

3.4.1. Scratch assay shows faster wound closure in KC with DPFi CM

Wound dressings containing growth factors have been previously used as a medical treatment for chronic wounds (Nagai and Embil, 2002). In an attempt to understand how the growth factors released by the dermal fibroblasts (DPFi, PFi and RFi) might affect the KC migration in culture, CM was collected from all three fibroblast populations from two patients, as described in method 3.3.3.

In an effort to mimic wound healing *in vitro*, in my first experiment, I used Ibidi inserts which when removed leave a defined cell free gap of approximately 500 μm between two KC cell fronts (Figure 3.4.1.). Conditioned media that was collected from DPFi, PFi and RFi as well as normal KC Epilife media, was added to the cells after the Ibidi inserts were removed. Figure 3.4.1. shows the wound closure over a period of 9 hours, with the four different media combinations. Analysis of the Ibidi experiment images, revealed that DPFi CM was promoting faster 'wound' closure than the other three conditions (Figure 3.4.2A), however this observation was not significant. The distance covered over 10 hours by KC when in DPFi CM was on average 916040 μm^2, while in RFi CM, PFi CM and Epilife media the KC covered a distance of 864594 μm^2, 752343 μm^2 and 831538 μm^2 respectively. The same trend was observed when the cell front velocity was calculated and the DPFi CM appeared to promote the fastest wound closure with a mean velocity of 25 μm/h.

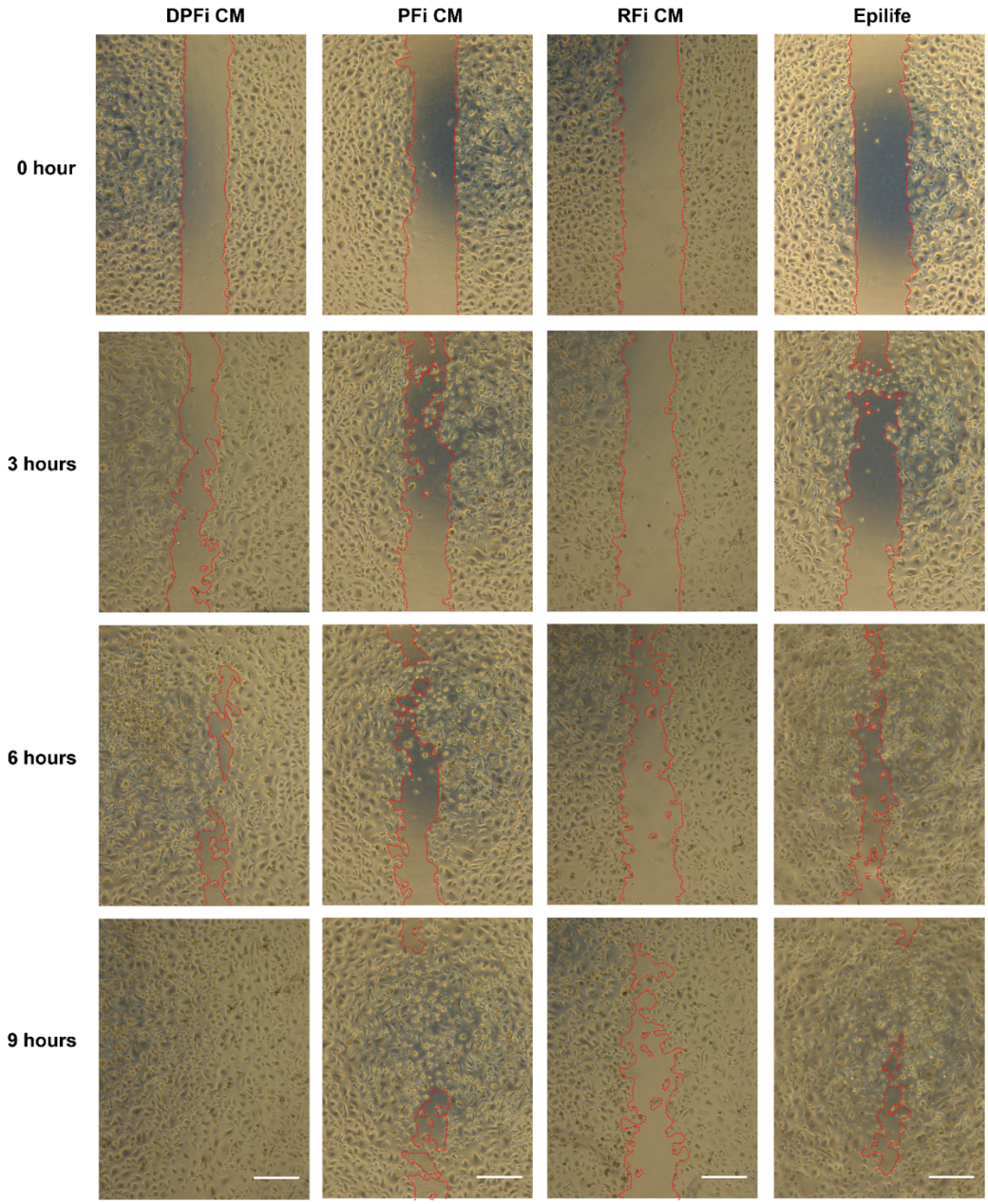
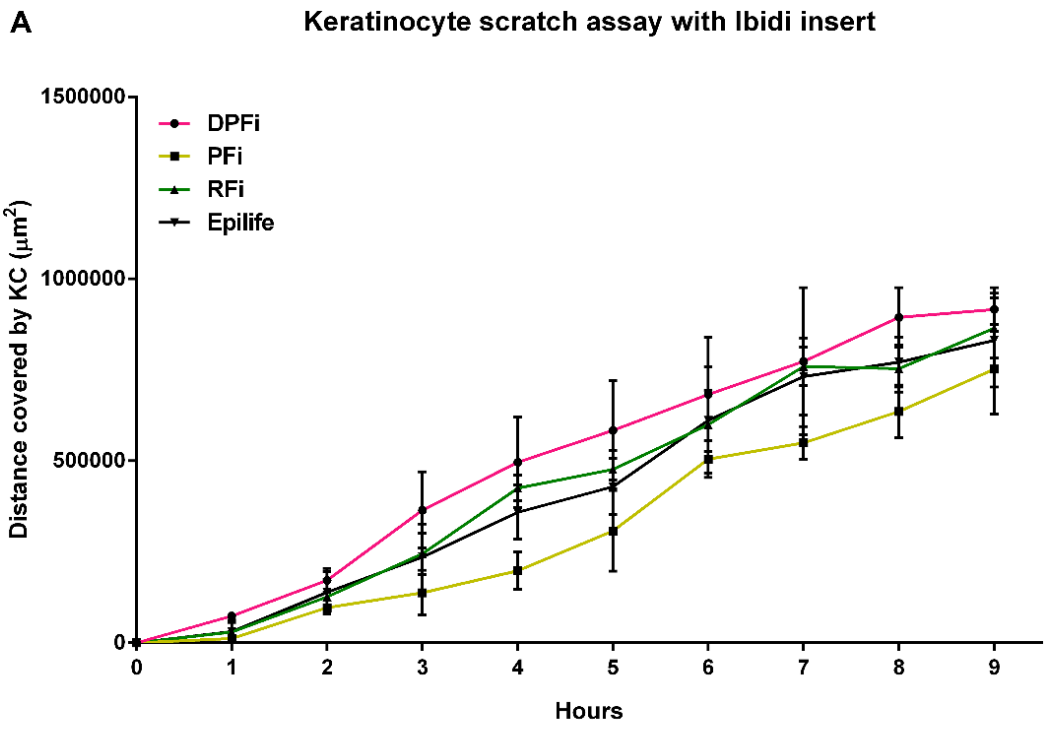


Figure 3.4.1. Ibidi insert wound healing assay.

The images above show the KC cells after the Ibidi inserts were removed. The cells were cultured for 9 hours in four different conditions; DPFi CM, PFi CM, RFi CM and Epilife media. The red dotted line separates the cell area from the cell free area. This figure shows a representative result from N=1 CM and N=1 KC. N=2 (P2D and P3A) and n=3 of the CM were used in this experiment with N=1 (P3B) KC. Scale bars are 200 μm.

A


Keratinocyte scratch assay with Ibidi insert
DPFi
PFi
RFi
Epilife
Distance covered by KC (µm²)
1500000
1000000
500000
0
0
1
2
3
4
5
6
7
8
9
Hours

B

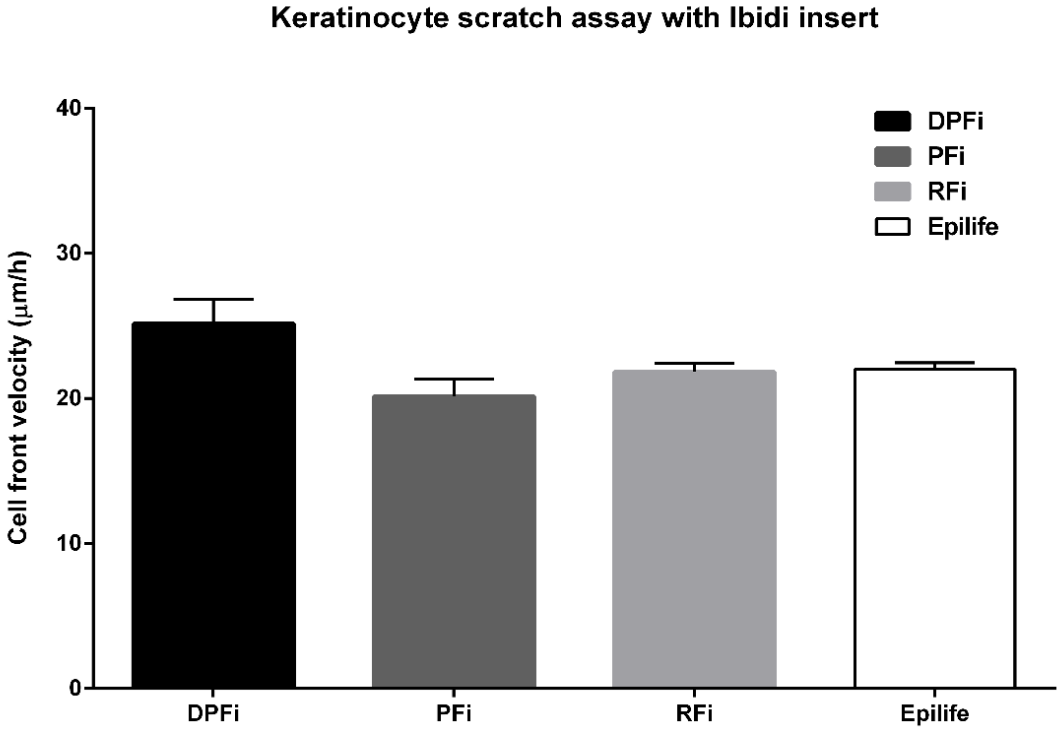

Keratinocyte scratch assay with Ibidi insert
DPFi
PFi
RFi
Epilife
Cell front velocity (µm/h)
40
30
20
10
0
DPFi
PFi
RFi
Epilife

Figure 3.4.2. KC scratch assay using the Ibidi inserts.

(A) The graph shows the distance covered by the KC in μm^2 when incubated DPFi CM (pink), PFi CM (gold), RFi CM (green) and Epilife media (black). (B) The bar chart shows the cell front velocity in μm/h after the KC were cultured for 10 hours in four different conditions; DPFi CM, PFi CM, RFi CM and Epilife media. This figure shows a representative result from N=1 CM and N=1 KC. N=2 (P2D and P3A) and n=3 of the CM were used in this experiment with N=1 (P3B) KC. Results were analysed using two-way Anova and the error bars represent standard error. Significance is displayed in the graph ($P \leq 0.05$ = *, $P \leq 0.01$ = **, $P \leq 0.001$ =***, $P \leq 0.0001$ =****).

Although these results were not significant, they were nevertheless intriguing as exactly the same trend was observed using CM from both patients (Appendix Figure A.2.). The results above raised the question of whether the ibidi inserts were appropriate for studying 'wound' healing *in vitro* as the cells were not physically wounded in the process of removing the insert. Therefore, I moved to another technique known as the scratch assay, that mimics a wounding environment, as the cells are physically wounded with a p200 pipette tip (Figure 3.4.3.). A schematic of the 'wound' closure is shown in figure 3.4.4. to clearly visualise how the 'wound' closed. As with the ibidi experiment, images were taken from time 0 to 9 hours later after the scratch and analysed using image J.

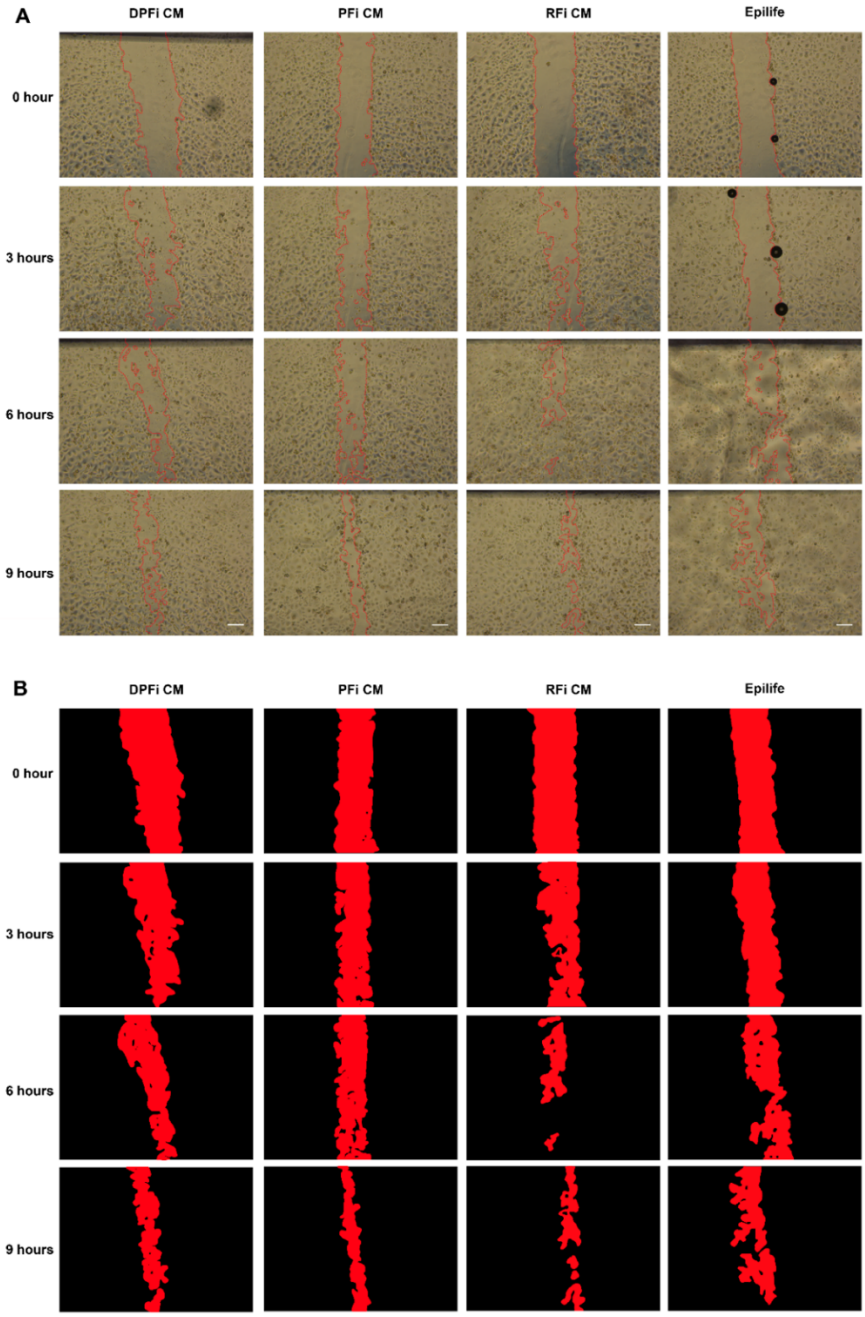


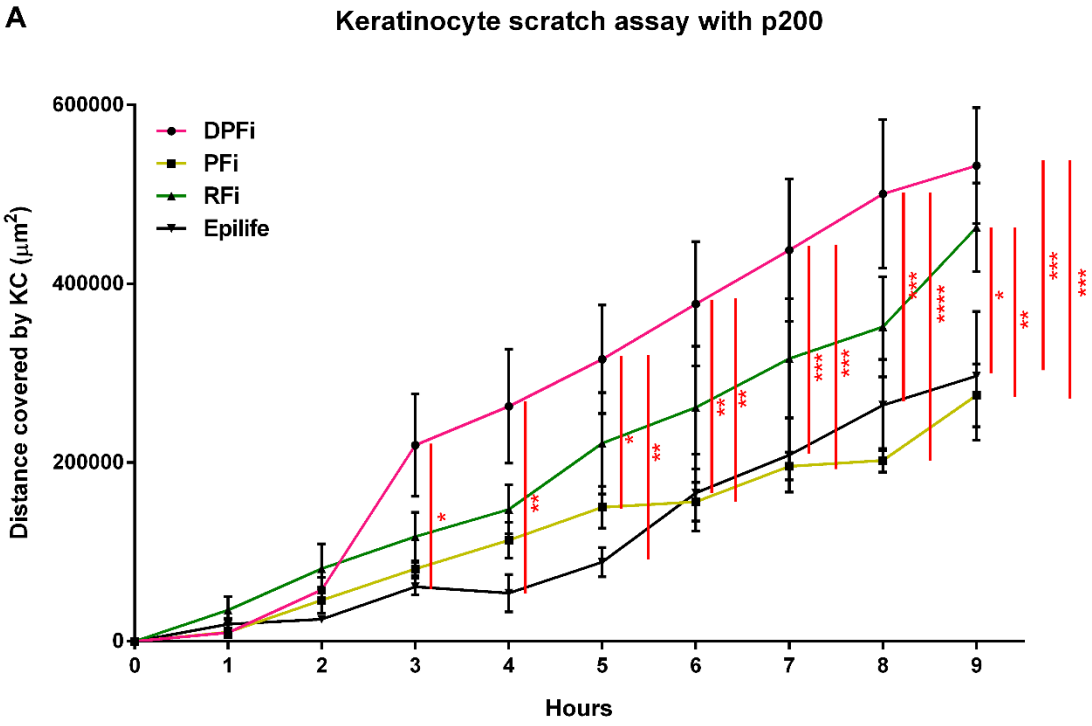
Figure 3.4.3. Scratch assay using a p200 pipette tip.

(A) KC cells were scratched with a p200 pipette tip and were cultured for 9 hours in four different conditions; DPFi CM, PFi CM, RFi CM and Epilife media. The red dotted line separates the cell area from the cell free area. Scale bars are 200 μm. (B) Schematic of (A). The red area illustrates the cell free area over the period of 9 hours. This figure shows a representative result from N=1 CM and N=1 KC. N=2 (P2D and P3A) and n=3 of the CM were used in this experiment with N=1 (P3B) KC.

The physical wounding of the KC, resulted in significant differences between the four media conditions. An interesting finding was that the RFi CM was able to significantly promote KC migration at the last time point, in comparison to Epilife. This supports my initial hypothesis that RFi release something which promotes wound healing. Remarkably, DPFi which are perhaps not involved in physiological healing can still accelerate healing over and above the RFi, PFi and Epilife control medium. In Figure 3.4.4A, it can be observed that from the 3rd hour, there is a significant increase in the distance covered by the KC when cultured with DPFi CM (219577 μm^2) when compared to Epilife media (61285 μm^2). The differences become more apparent with increasing time points. At the last timepoint, the KC migration when cultured with DPFi CM was 532153 μm^2 which was significantly higher than the PFi CM (275314 μm^2) and Epilife media (297101 μm^2). This intriguing result that the DPFi CM has the capacity to accelerate wound closure will be assessed later on in the chapter. In this experiment I used two biological repeats and three technical repeats for each patient and observed the same results throughout.

Further analysis of the scratch assay images, showed that the mean cell front velocity of the KC incubated with DPFi CM was 12 μm/h which was significantly faster than the PFi CM which had a mean cell front velocity of 4 μm/h. The RFi CM and Epilife media cell front velocities were 8 μm/h and 7 μm/h respectively. Altogether, these results highlight that the DPFi CM is able to promote faster KC migration in a stress environment, *in vitro*.

A


Keratinocyte scratch assay with p200
DPFi
PFi
RFi
Epilife
Distance covered by KC (µm²)
600000
400000
200000
0
0
1
2
3
4
5
6
7
8
9
Hours

B

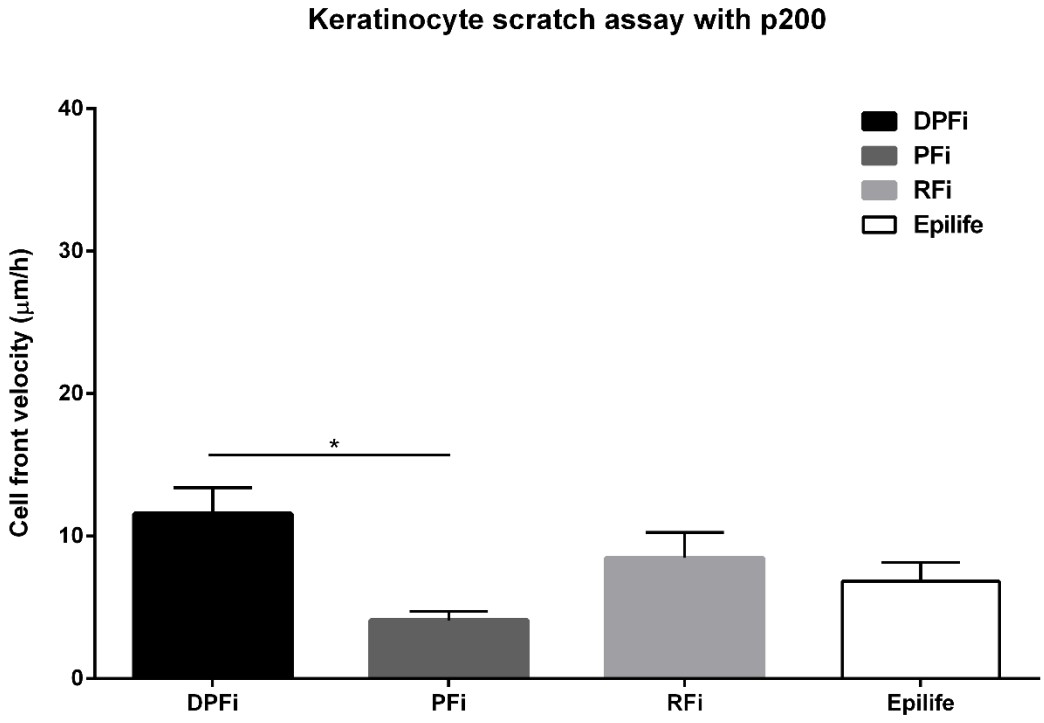

Keratinocyte scratch assay with p200
DPFi
PFi
RFi
Epilife
Cell front velocity (µm/h)
40
30
20
10
0
*
DPFi
PFi
RFi
Epilife

Figure 3.4.4. KC scratch assay analysis of the p200 experiment.

(A) The graph shows the distance covered by the KC in μm^2 when incubated DPFi CM (pink), PFi CM (gold), RFi CM (green) and Epilife media (black). (B) The bar chart shows the cell front velocity in μm/h after the KC were cultured for 10 hours in four different conditions; DPFi CM, PFi CM, RFi CM and Epilife media. This figure shows a representative result from N=1 CM and N=1 KC. N=2 (P2D and P3A) and n=3 of the CM were used in this experiment with N=1 (P3B) KC. Results were analysed using two-way Anova and the error bars represent standard error. Significance is displayed in the graph ($P \leq 0.05$ = *, $P \leq 0.01$ = **, $P \leq 0.001$ =***, $P \leq 0.0001$ =****).

3.4.2. Mitomycin C treatment of KC reveals faster 'wound' closure

KC use migration and proliferation in order to promote reepithelialisation after a wound. Therefore, I wanted to study these processes *in vitro*, in an effort to understand how the DPFi CM is able to promote faster wound closure.

To investigate the growth potential of the KC population *in vitro*, I propagated parallel cultures of KCs incubated with DPFi CM, PFi CM, RFi CM and Epilife media (Figure 3.4.5.). 4000 cells cm^{-2} were seeded in 6 well plates (total of 36000 cells per well) and cultured for 7 days in the aforementioned media. On the 7^{th} day the cells were trypsinised, counted and analysed to observe if there were differences in the rate of growth of the KC cultured in the four different media conditions. As expected, there was an increase in the number of cells from day 0 to day 7 in the culture of the DPFi CM and Epilife, that started from 4000 cells cm^{-2} and went to 6000 cells cm^{-2} and 10000 cells cm^{-2} in each culture respectively. After 7 days, Epilife media had promoted significantly more KC proliferation in comparison to the conditioned media obtained from DPFi, PFi and RFi.

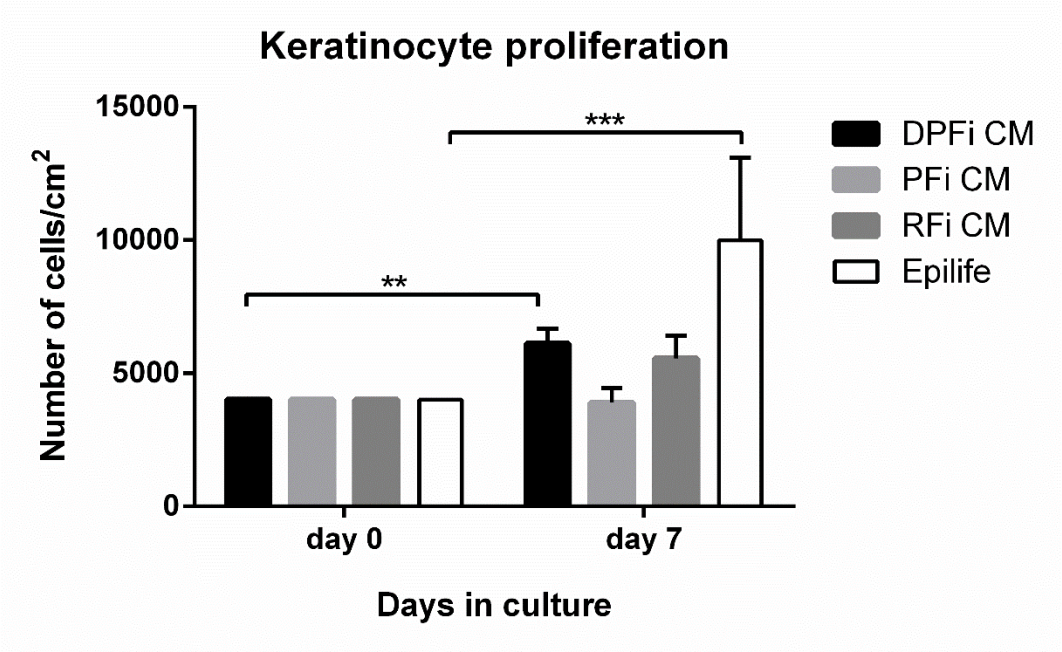


Figure 3.4.5. KC proliferation assay.

The bar chart shows the number of KC cells/cm^2 seeded at day 0 and the number of counted cells at day 7 of culturing them with DPFi CM, PFi CM, RFi CM and Epilife media. This figure shows a representative result from N=1 CM and N=1 KC. N=2 (P2D and P3A) and n=3 of the CM were used in this experiment with N=1 (P3B) KC. Results were analysed using two-way Anova and the error bars represent standard error. Significance is displayed in the graph ($P \leq 0.05$ = *, $P \leq 0.01$ = **, $P \leq 0.001$ =***, $P \leq 0.0001$ =****).

The above analysis, gave an insight to the growth rate of the KCs under different media conditions. To interrogate the impact of cell migration in the KCs, I inhibited cell division by using Mitomycin C (MITC). Then, the cells were scratched using a p200 and DPFi CM, PFi CM, RFi CM and Epilife media were added to the cells. Controls were also used, where the cells have not been treated with MITC. Remarkably, I observed that the MITC treated KC cells were migrating faster than the control group in all the 4 conditions (Figure 3.4.6.). In the case of the DPFi CM, RFi CM and Epilife media, the KC covered a significantly larger distance when they were treated with MITC than with the control (Figure 3.4.6A,C,D). When the cell front velocity of the MITC treated KC was analysed, it was found that the cells that were incubated with DPFi CM were migrating significantly faster with a mean velocity of 8 μm/h than the MITC treated KC that were incubated with PFi CM (2 μm/h) and RFi CM (1 μm/h; Figure 3.4.7.). This is different than what I expected to see as MITC blocks the proliferation of the cells, however it suggests that blocking the proliferation aids with the migration of the KC. Further experiments should be conducted in the future to identify the efficiency of MITC on the KC.

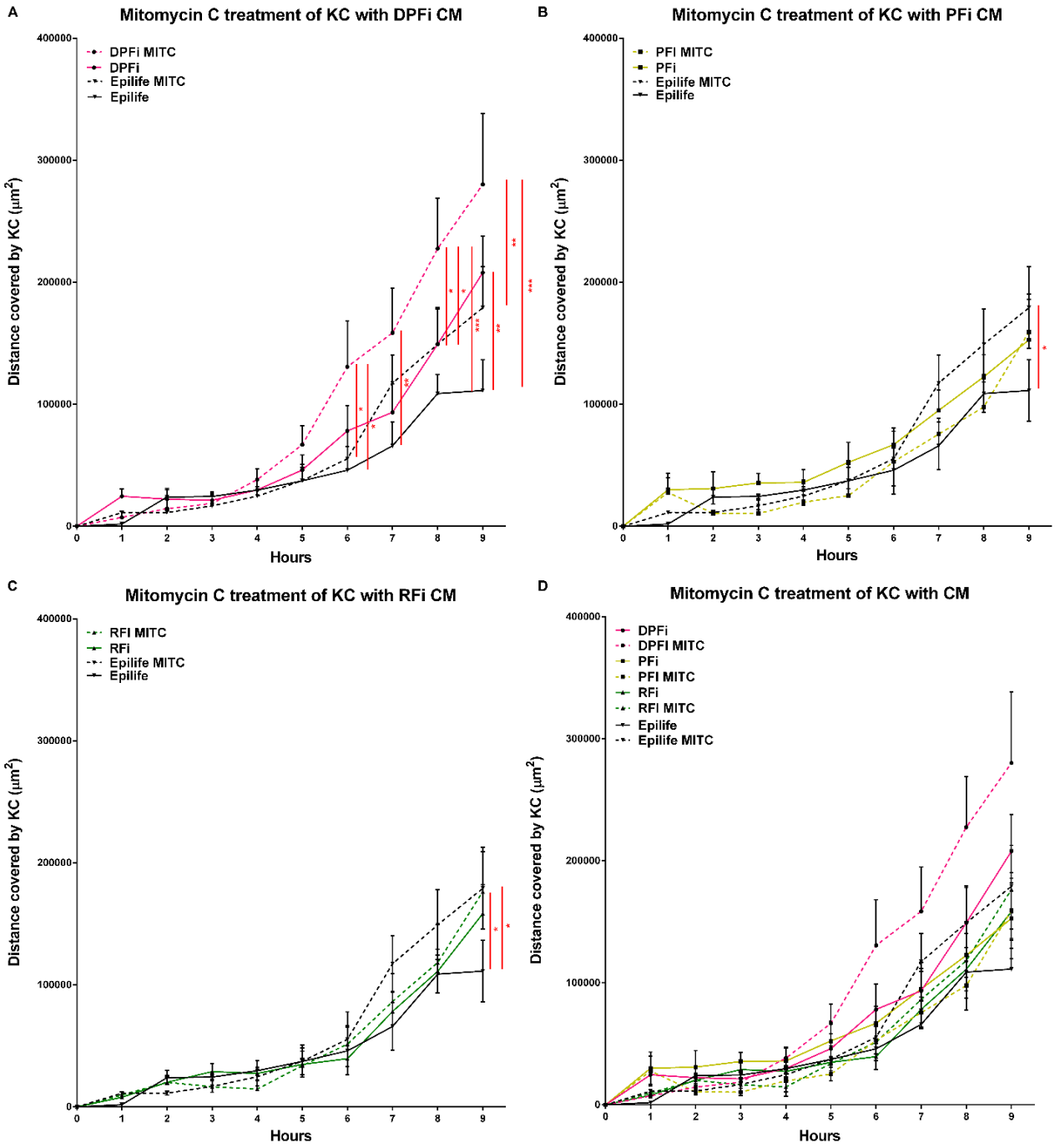

A
Mitomycin C treatment of KC with DPFi CM
DPFi MITC
DPFi
Epilife MITC
Epilife
Distance covered by KC (µm²)
Hours
B
Mitomycin C treatment of KC with PFi CM
PFI MITC
PFi
Epilife MITC
Epilife
Distance covered by KC (µm²)
Hours
C
Mitomycin C treatment of KC with RFi CM
RFI MITC
RFi
Epilife MITC
Epilife
Distance covered by KC (µm²)
Hours
D
Mitomycin C treatment of KC with CM
DPFi
DPFI MITC
PFi
PFI MITC
RFi
RFI MITC
Epilife
Epilife MITC
Distance covered by KC (µm²)
Hours

Figure 3.4.6. Distance covered by KC cells treated with MITC.

(A) The graph shows the distance covered in μm^2 by the control KC (solid line) and MITC treated KC (dotted line) when incubated with DPFi CM (pink) and Epilife media (black) over a period of 9 hours. (B) The graph shows the distance covered in μm^2 by the control KC (solid line) and MITC treated KC (dotted line) when incubated with PFi CM (gold) and Epilife media (black) over a period of 9 hours. (C) The graph shows the distance covered in μm^2 by the control KC (solid line) and MITC treated KC (dotted line) when incubated with RFi CM (green) and Epilife media (black) over a period of 9 hours. (D) The graph shows the summary of the other graphs in A-C without the significance. This figure shows a representative result from N=1 CM and N=1 KC. N=2 (P2D and P3A) and n=3 of the CM were used in this experiment with N=1 (P3B) KC. Results were analysed using two-way Anova and the error bars represent standard error. Significance is displayed in graphs A-C ($P \leq 0.05$ = *, $P \leq 0.01$ = **, $P \leq 0.001$ =***, $P \leq 0.0001$ =****).

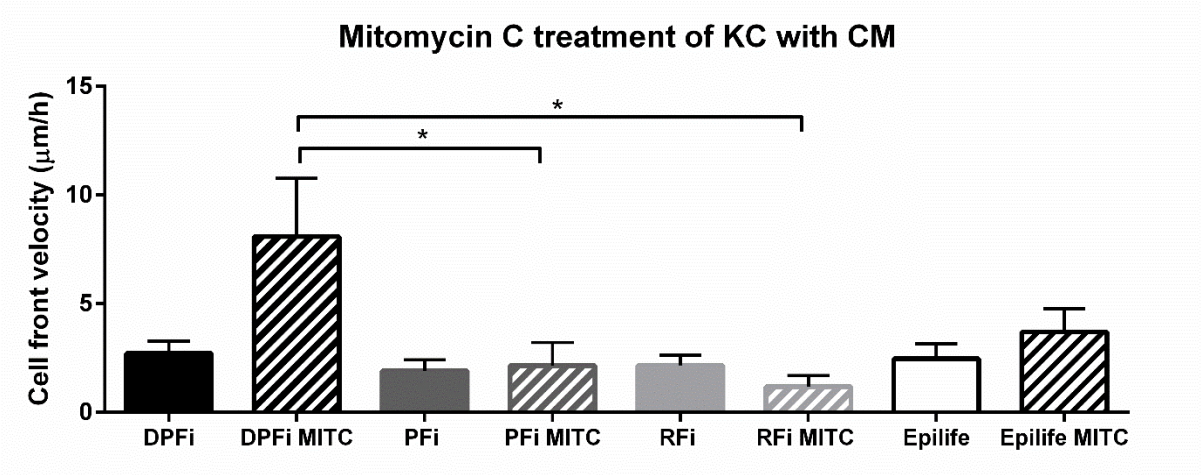


Figure 3.4.7. Cell front velocity of KC cells treated with MITC.

(A) The bar chart shows the cell front velocity in μm/h of the control KC (solid block) and MITC treated KC (dotted line block) when incubated with DPFi CM, PFi CM, RFi CM and Epilife media. This figure shows a representative result from N=1 CM and N=1 KC. N=1 (P2D) and n=3 CM were used in this experiment with N=1 (P3B) KC. Results were analysed using two-way Anova and the error bars represent standard error. Significance is displayed in the graph ($P \leq 0.05$ = *, $P \leq 0.01$ = **, $P \leq 0.001$ =***, $P \leq 0.0001$ =****).

3.4.3. Cytokine array reveals CCL19, AXL and BMP6 to be significantly expressed in the DPFi compared to PFi or RFi

Thus far, my findings seem to suggest that addition of DPFi CM to the KC culture, promotes significantly faster 'wound' closure *in vitro* when compared to the controls. This suggests that KC are responding to a growth factor or cytokine cocktail specifically released by the DPFi population. Next, I wanted to investigate the mechanism by which the DPFi CM affects the KC population. I therefore performed a human cytokine antibody array to compare the cytokines present in the conditioned media obtained from DPFi, PFi and RFi. The cytokine array had 120 proteins which were tested with the different conditioned media. The results were analysed using Image J and normalised against the controls to obtain the array shown in Figure 3.4.8. Using Image J software, I was able to obtain the intensity of each dot in the array and using the corresponding values three correlations were made: DPFi CM vs PFi CM, DPFi CM vs RFi CM and PFi CM vs RFi CM. Following that, the fold change and the p-value of each correlation was calculated and the cut off values were set to be below 0.05 for the p-value and ranging from -0.5 to 0.5 for log of the fold change.

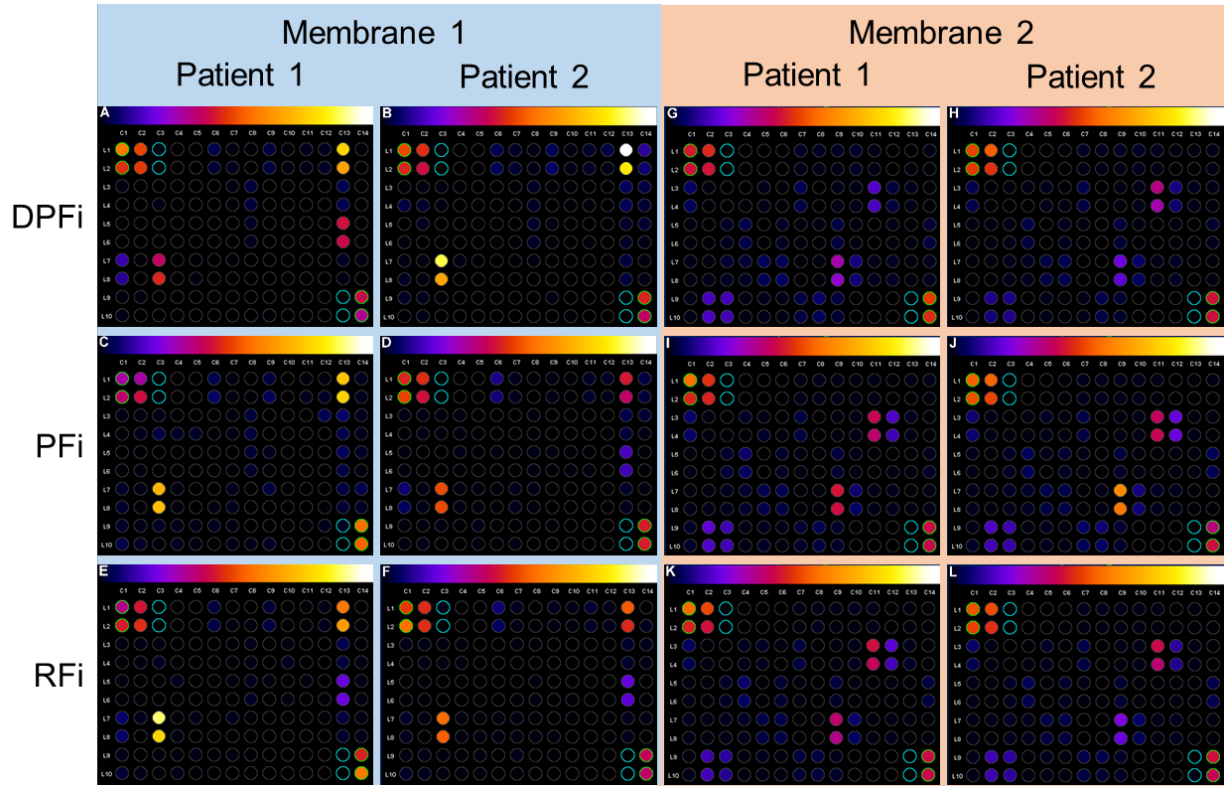


Figure 3.4.8. Normalised human cytokine antibody arrays.

(A) Membrane 1 of the cytokine antibody array with DPFi CM from patient 1. (B) Membrane 1 of the cytokine antibody array with DPFi CM from patient 2. (C) Membrane 1 of the cytokine antibody array with PFi CM from patient 1. (D) Membrane 1 of the cytokine antibody array with PFi CM from patient 2. (E) Membrane 1 of the cytokine antibody array with RFi CM from patient 1. (F) Membrane 1 of the cytokine antibody array with RFi CM from patient 2. (G) Membrane 2 of the cytokine antibody array with DPFi CM from patient 1. (H) Membrane 2 of the cytokine antibody array with DPFi CM from patient 2. (I) Membrane 2 of the cytokine antibody array with PFi CM from patient 1. (J) Membrane 2 of the cytokine antibody array with PFi CM from patient 2. (K) Membrane 2 of the cytokine antibody array with RFi CM from patient 1. (L) Membrane 2 of the cytokine antibody array with RFi CM from patient 2. Patient 1 is P2D and Patient 2 is P3A. Black/blue spots indicate low/no expression whereas yellow/white spots indicate high expression.

Interestingly, DPFi CM vs PFi CM identified 2 cytokines significantly released from DPFi; AXL and BMP6. CCL19 did not pass the fold change cut off, however it was identified in the DPFi vs RFi to be significantly released in the DPFi CM, therefore I decided to choose it for further analysis. In total, 8 proteins were significantly released in the the DPFi in DPFi CM vs RFi CM, including CCL19 and AXL. Thus the cytokines AXL, BMP6 and CCL19 were chosen to be tested in the 'wound' assay to investigate their impact on the KC population.

Many studies have also reported IL6 protein to be a key cytokine in the wound healing process (Turksen et al., 1992, Gallucci et al., 2001, Lin et al., 2003). In my cytokine array, IL6 was found to be significantly released in the RFi CM when compared to the PFi CM with a fold change of 1.9 (Figure 3.4.9.). This suggests that IL6 may be the cytokine enabling RFi CM to promote faster wound closure than PFi CM. Because of its reported involvement in wound healing, IL6 was chosen as a control cytokine for the next experiments.

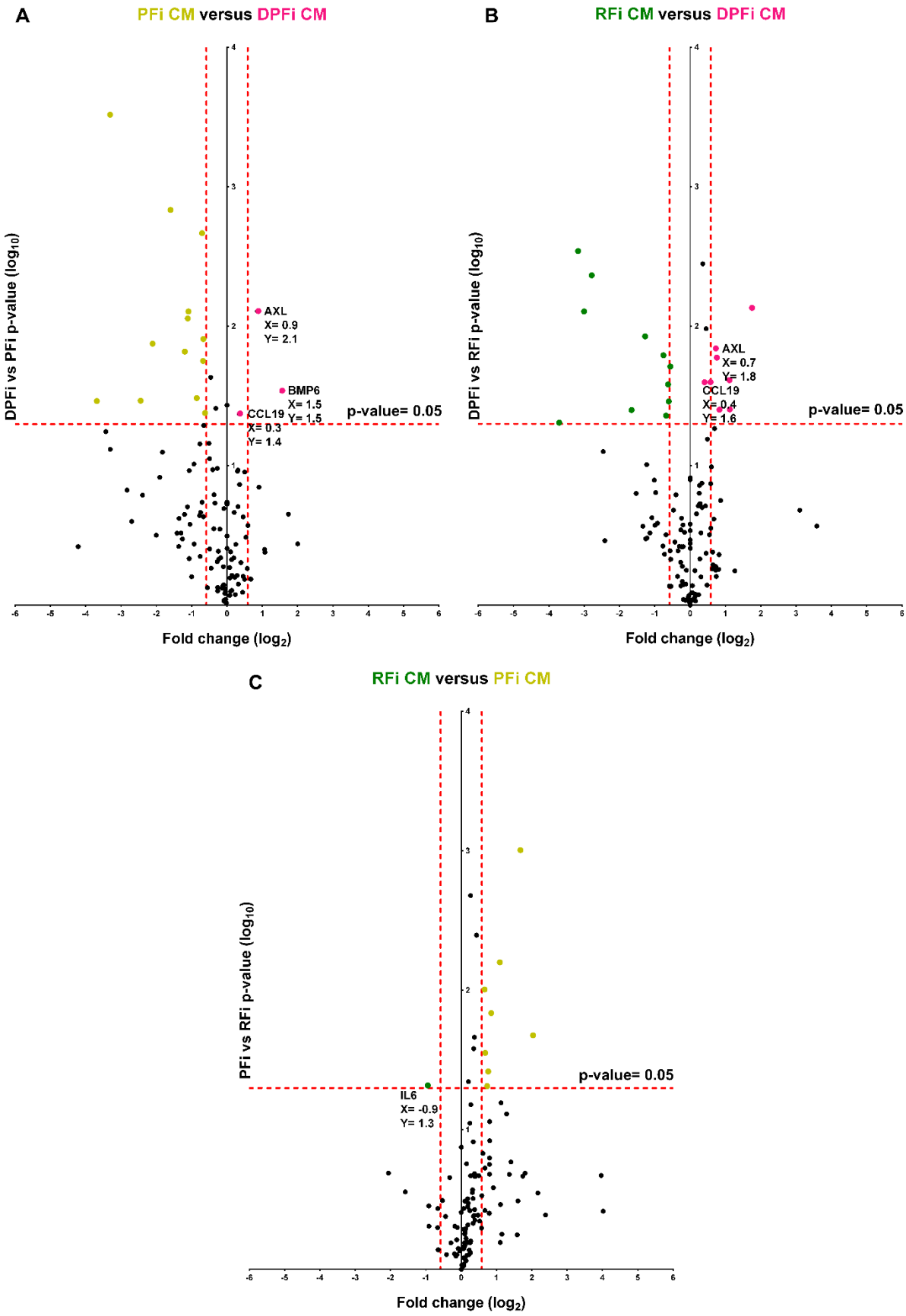

A
PFi CM versus DPFi CM
DPFi vs PFi p-value (log10)
Fold change (log2)
AXL
X= 0.9
Y= 2.1
BMP6
X= 1.5
Y= 1.5
CCL19
X= 0.3
Y= 1.4
p-value= 0.05
B
RFi CM versus DPFi CM
DPFi vs RFi p-value (log10)
Fold change (log2)
AXL
X= 0.7
Y= 1.8
CCL19
X= 0.4
Y= 1.6
p-value= 0.05
C
RFi CM versus PFi CM
PFi vs RFi p-value (log10)
Fold change (log2)
IL6
X= -0.9
Y= 1.3
p-value= 0.05

Figure 3.4.9. Correlation analysis between DPFi, PFi and RFi CM.

The volcano plots shows the fold change (log2) on the X axis and the p-value (log10) on the Y axis. The red dotted lines show the cut off values which for the p-value is 0.05 and for the fold change is ranging from -2 to 2. The black dots represent the cytokines that were not found to be significant in (A) PFi CM versus DPFi CM, (B) RFi CM versus DPFi CM and (C) RFi CM versus PFi CM. The pink dots in (A) and (B) represent the cytokines that appear to be significant in the DPFi CM, The green dots in (B) and (C) represent the cytokines that appears to be significant in the RFi CM and the yellow dots in (A) and (C) represent the cytokines that are significant in the PFi CM.

3.4.4. Scratch assay with overexpressed cytokines *in vitro*

Given that the biological activity of each cytokine varies in different populations, the cytokine concentrations had to be optimised before the effect on the KC population was tested. A range in which the CCL19, AXL, BMP6 and IL6 are biologically active was provided by the supplier. I performed scratch assays using three concentrations and analysed cell front velocity. My analysis reveals that the concentration in which the KC have the highest cell front velocity was 0.5 ng/mL for CCL19, 2 µg/mL for AXL, 0.03 µg/mL for BMP6 and 0.01 ng/mL for IL6. Going forward, the aforementioned concentrations were used for each cytokine (Figure 3.4.10.).

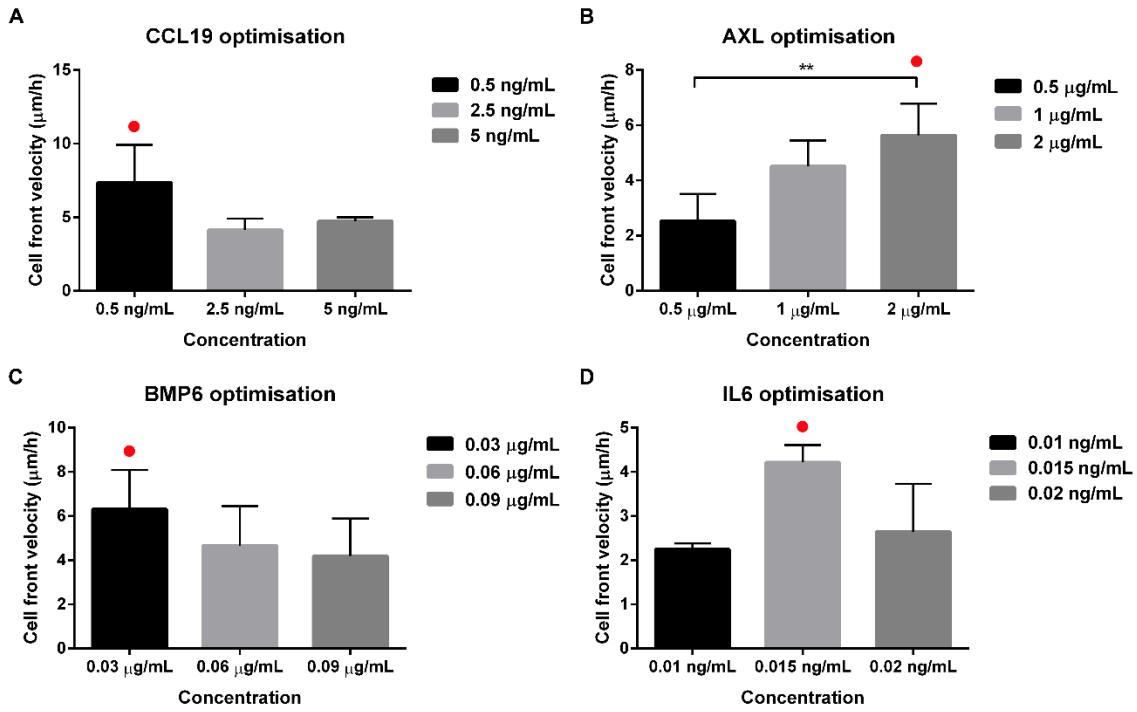


Figure 3.4.10. Cytokine optimisation.

(A) Human recombinant CCL19 was tested at three different concentrations 0.5 ng/mL, 2.5 ng/mL and 5 ng/mL. (B) Human recombinant AXL was tested at three different concentrations 0.5 µg/mL, 1 µg/mL and 2 µg/mL. (C) Human recombinant BMP6 was tested at three different concentrations 0.03 µg/mL, 0.06 µg/mL and 0.09 µg/mL. (C) Human recombinant IL6 was tested at three different concentrations 0.01 ng/mL, 0.015 ng/mL and 0.02 ng/mL. The red dot indicates the concentration selected for further experiments. n=3 of KC from P3B were used in this experiment. Results were analysed using two-way Anova and the error bars represent standard error. Significance is displayed in the graph ($P \leq 0.05$ = *, $P \leq 0.01$ = **, $P \leq 0.001$ =***, $P \leq 0.0001$ =****).

When the optimal concentration for each cytokine was established, I moved on to test each cytokine individually in a scratch assay assessing wound closure at several timepoints, and to observe if there were differences in KC migration when cultured with the four different cytokines; CCL19, AXL, BMP6 and IL6. DPFi CM, PFi CM, RFi CM and Epilife media were used as controls in this experiment (Figure 3.4.11A). By 6 hours, the distance covered by the KCs was significantly increased in the presence of CCL19 to 173659 μm^2 in contrast to Epilife which covered only 49580 μm^2 in the same period of time. The differences become clearer on the last timepoint, where CCL19, BMP6 and AXL significantly increased KC migration to 370248 μm^2, 344961 μm^2 and 302826 μm_2 respectively when compared to Epilife (111842 μm^2). When the cell front velocity was calculated, CCL19, AXL and BMP6 appeared to promote an insignificant but nevertheless faster migration of KC in comparison to the DPFi CM (Figure 3.4.11B). These results, suggest that the cytokines CCL19, AXL and BMP6 play a key role in KC reepithelialisation, *in vitro*.

What was interesting was that IL6 appeared to promote a similar KC migration effect to the RFi CM, which could suggest that the accelerated migration of the KC with RFi CM is part due to IL6, although further experiments should be carried out in the future to determine that. Furthermore, CCL19, BMP6 and AXL which are cytokines released by the DPFi, promoted migration over and above levels promoted by DPFi. This is a very intriguing result as that could mean that combinations of cytokines released by DPFi could be directly used for the promotion of KC migration. Thus, my next experiment was to test combinations of cytokines that are significantly released by DPFi and observe the effect they have on KC migration.

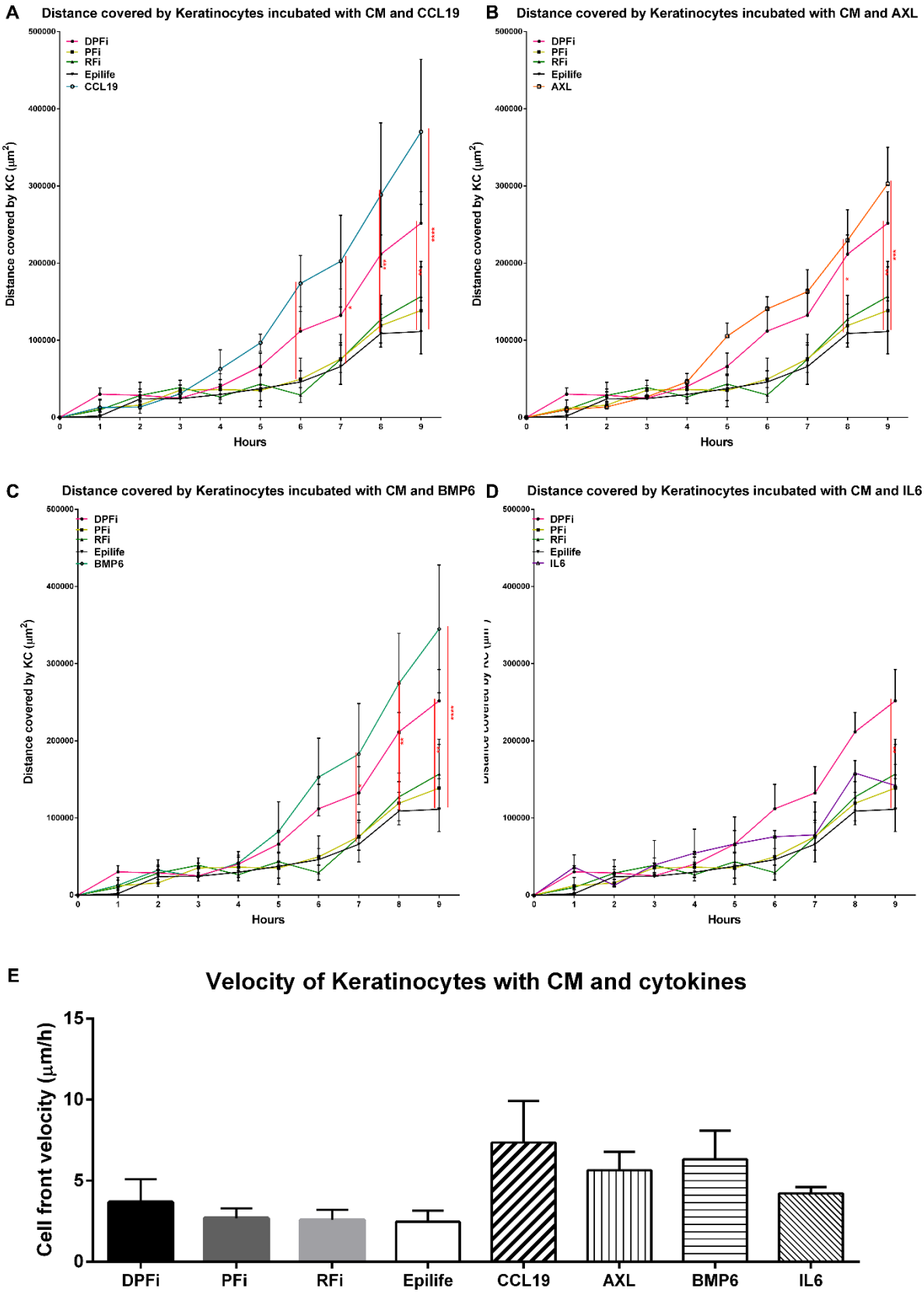

A
Distance covered by Keratinocytes incubated with CM and CCL19
DPFi
PFi
RFi
Epilife
CCL19
Distance covered by KC (µm²)
Hours
B
Distance covered by Keratinocytes incubated with CM and AXL
DPFi
PFi
RFi
Epilife
AXL
Distance covered by KC (µm²)
Hours
C
Distance covered by Keratinocytes incubated with CM and BMP6
DPFi
PFi
RFi
Epilife
BMP6
Distance covered by KC (µm²)
Hours
D
Distance covered by Keratinocytes incubated with CM and IL6
DPFi
PFi
RFi
Epilife
IL6
Hours
E
Velocity of Keratinocytes with CM and cytokines
Cell front velocity (µm/h)
DPFi
PFi
RFi
Epilife
CCL19
AXL
BMP6
IL6

Figure 3.4.11. Cytokine overexpression.

The graphs show the distance covered by the KC in μm^2 over a 9 hour period. DPFi CM is shown in pink, PFi CM in gold, RFi CM in green, Epilife in black, (A) CCL19 in light blue, (B) AXL in orange, (C) BMP6 in cyan and (D) IL6 in purple. Significance in A-D was calculated against Epilife. (E) The bar chart shows the cell front velocity of KC in μm/h with the addition of conditioned media from DPFi, PFi and RFi as well as the human recombinant cytokines CCL19, AXL, BMP6 and IL6. Epilife is also shown in the bar chart as a control. This figure shows a representative result from N=1 CM and N=1 KC. N=2 (P2D and P3A) and n=3 CM were used in this experiment with N=1 (P3B) KC. Results were analysed using two-way Anova and the error bars represent standard error. Significance is displayed in the graph ($P \leq 0.05$ = *, $P \leq 0.01$ = **, $P \leq 0.001$ =***, $P \leq 0.0001$ =****).

3.4.5. Scratch assay with combinations of overexpressed cytokines *in vitro*

Secreted proteins play an important role in maintaining homeostasis in an organism. This complex system always includes a cascade of events that result in an effect on the target cell(s). In the previous section, I found that the individual addition of CCL19, AXL and BMP6 cytokines has a significant effect in the distance covered by the KC across a scratch wound when compared to the control. At this point, I wanted to investigate the impact of overexpressing a combination of these cytokines and study the response of the KC population.

To address this question, I performed scratch assays with the individual addition of CCL19, AXL and BMP6 as well as four combinations of these cytokines. The combinations were as follows: CCL19 with AXL, CCL19 with BMP6, AXL with BMP6 and a combination of all three. When CCL19 and AXL were added together there was a significant increase in the mean cell front velocity of the cells which was 10.6 μm/h whereas individual CCL19 and AXL had a mean cell front velocity of 6.6 μm/h and 6.8 μm/h respectively (Figure 3.4.12A). No significant changes where observed in the other combinations stated above (Figure 3.4.12B-D).

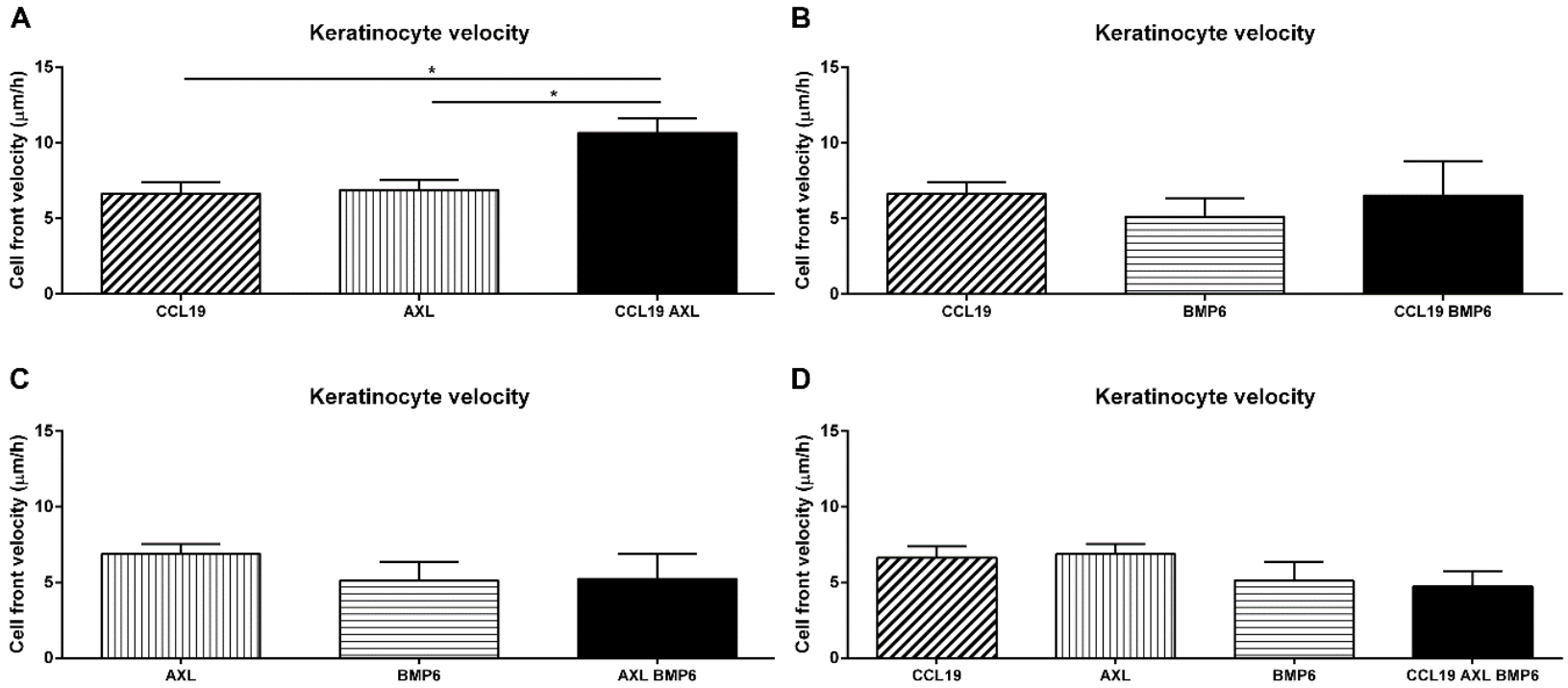

A
Keratinocyte velocity
Cell front velocity (µm/h)
15
10
5
0
*
*
CCL19
AXL
CCL19 AXL
B
Keratinocyte velocity
Cell front velocity (µm/h)
15
10
5
0
CCL19
BMP6
CCL19 BMP6
C
Keratinocyte velocity
Cell front velocity (µm/h)
15
10
5
0
AXL
BMP6
AXL BMP6
D
Keratinocyte velocity
Cell front velocity (µm/h)
15
10
5
0
CCL19
AXL
BMP6
CCL19 AXL BMP6

Figure 3.4.12. Cell front velocity with overexpression of cytokine combinations.

(A) The bar chart illustrates the following cytokine addition on KC velocity: CCL19, AXL and CCL19 plus AXL. (B) The bar chart illustrates the following cytokine addition on KC velocity: CCL19, BMP6 and CCL19 plus BMP6. (C) The bar chart illustrates the following cytokine addition on KC velocity: AXL, BMP6 and AXL plus BMP6. (D) The bar chart illustrates the following cytokine addition on KC velocity: CCL19, AXL, BMP6 and CCL19 plus AXL plus BMP6. N=1 (P3B) and n=3 were used in this experiment. Results were analysed using two-way Anova and the error bars represent standard error. Significance is displayed in the graph ($P \leq 0.05$ = *, $P \leq 0.01$ = **, $P \leq 0.001$ =***, $P \leq 0.0001$ =****).

3.4.6. Scratch assay with PDGF-BB

As mentioned earlier in the introduction, PDGF-BB is the only FDA approved cytokine for chronic wound healing. This has been now marked unsafe by the British government therefore alternative solutions should be found for chronic wounds. In an attempt to compare AXL with the commercialised PDGF-BB, I performed an *in vitro* wound healing assay. The scratch assay performed as usual but this time it was analysed with a live imaging system called Livecyte (Figure 3.4.13). From about 12 hours onwards there is a significant promotion of KC migration in the presence of AXL in comparison to DPFi CM and PDGF-BB. Therefore, in the *in vitro* study, AXL was able to promote KC migration at the same and higher levels than PDGF-BB. 6 replicates of each condition were used for this experiment, but caution must be kept with these results as the wound healing assay was only performed using one biological replicate.

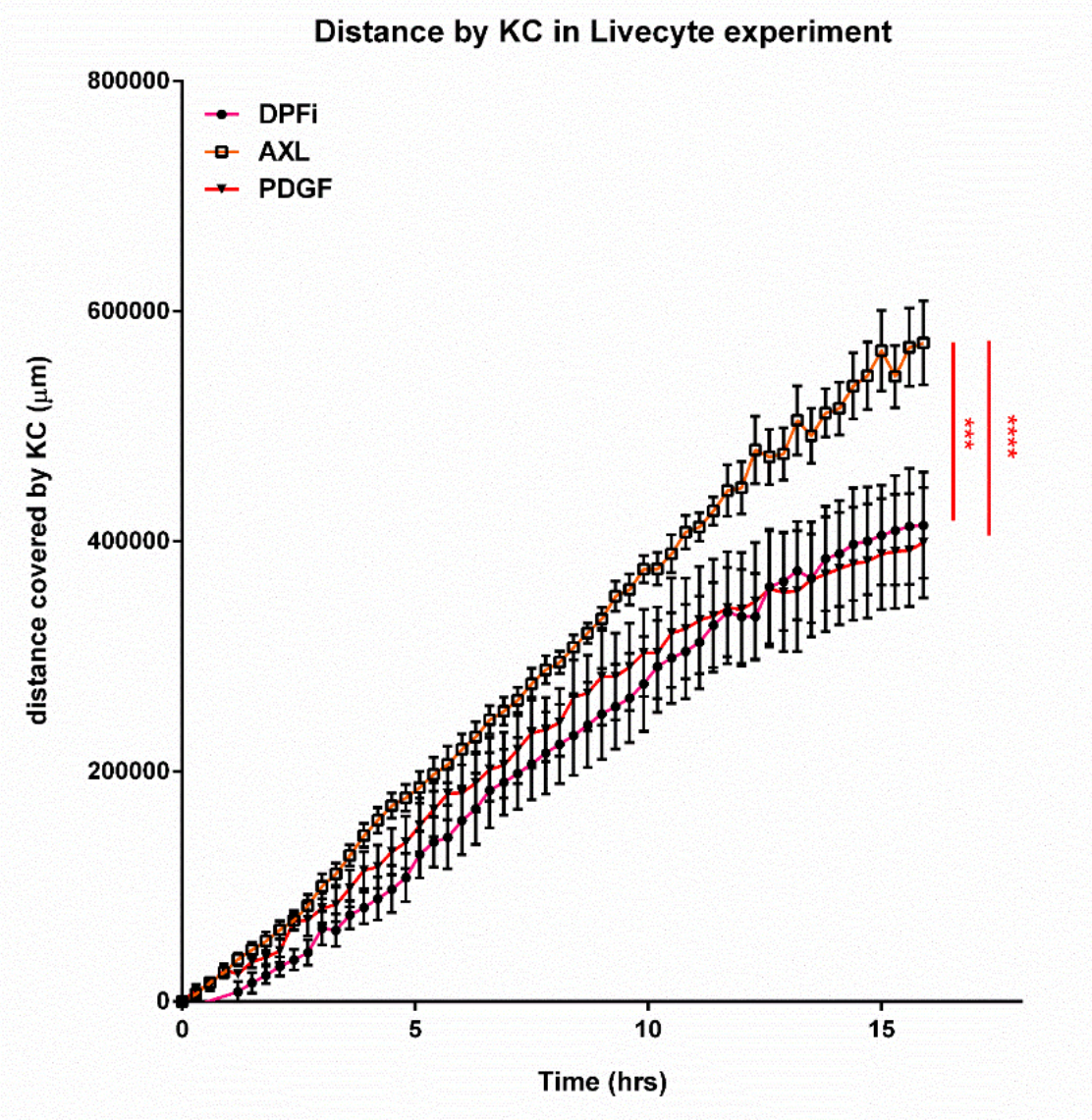


Figure 3.4.13. Scratch assay using Livecyte by Phasefocus.

The graph shows the area in μm^2 covered by the KC when DPFi CM (pink), AXL (orange) and PDGF-BB (red) are incubated with the KC. N=1 (P3C) and n=6 were used in this experiment. Results were analysed using two-way Anova and the error bars represent standard error. Significance is displayed in the graph ($P \leq 0.05$ = *, $P \leq 0.01$ = **, $P \leq 0.001$ =***, $P \leq 0.0001$ =****).

3.4.7. *Ex vivo* wound healing assay

Given the ability of AXL and CCL19 to promote KC migration both individually and in combination, I also wanted to see whether they would modulate wound healing in whole skin. In the *ex vivo* wound assay a 2 mm diameter partial thickness wound was made followed by an 8 mm outer wound (Figure 3.3.14A), removing the epidermis and papillary dermis. 5µl of AXL, CCL19, PDGF-BB, IL6, CCL19&AXL and Epilife supplemented with EDGS were added topically onto the wound. Images were taken every 24 hours with a stereo microscope until wound closure. The images were then analysed using Image J. Two-way ANOVA was used to analyse the difference in mm in all 6 replicates and comparisons were made at individual time points using the same test in Graphpad Prism 6.0.

The results show that in an *ex vivo* human skin wound, AXL is able to promote reepithelialisation significantly faster than Epilife and IL6 from the 3rd day onwards (Figure 3.4.14B). Also, the commercially available cytokine PDGF-BB and CCL19 were able to promote reepithelialisation significantly faster than Epilife and IL6 from the 4th day onwards. The cocktail of CCL19 and AXL appeared to affect wound closure less than CCL19 and AXL on their own, with no significant differences between this cocktail with the control. This experiment showed that the cytokine CCL19 are able to promote reepithelialisation at the same efficacy as the commercially available PDGF-BB but AXL is able to promote faster reepithelialisation than PDGF-BB and CCL19.

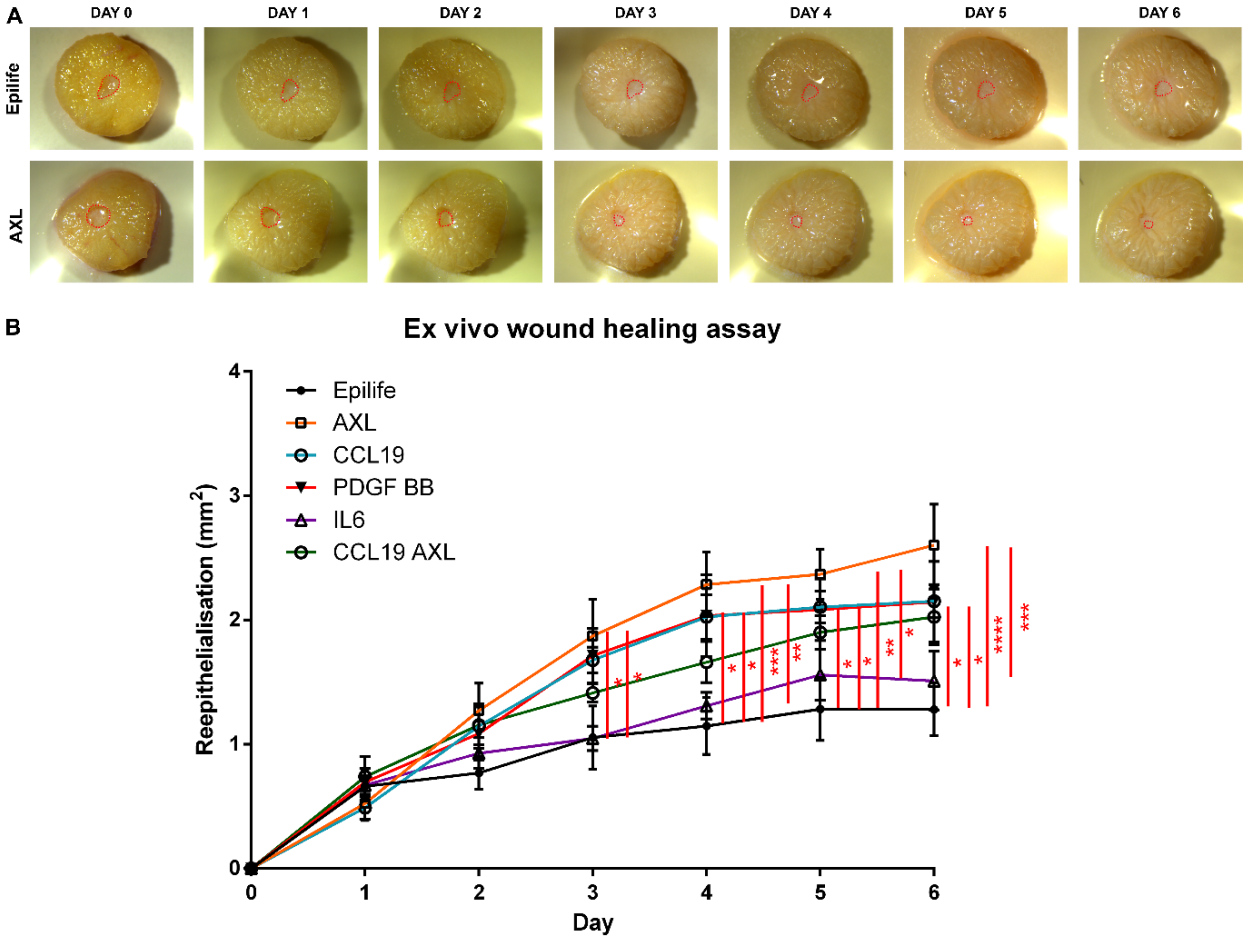


Figure 3.4.14. *Ex vivo* wound healing assay.

(A) Representative images of the *ex vivo* assay from day 0 to day 6 in Epilife and AXL. The red dotted line indicates the edge of the epithelium. N=1 and n=6 were used. (B) The graph shows the area in mm^2 covered by the KC when Epilife media (black), AXL (orange), CCL19 (light blue), PDGF-BB (red), IL6 (purple) and CCL19 AXL (green) were applied topically to the wound. Results were analysed using two-way Anova and the error bars represent standard error. Significance is displayed in the graph ($P \leq 0.05$ = *, $P \leq 0.01$ = **, $P \leq 0.001$ =***, $P \leq 0.0001$ =****).

3.4.8. Microarray reveals unique gene expression in response to AXL

CCL19 has been correlated with wound healing before. A study in 2004, showed that CCL19 was up regulated in mice oral wounds and proposed the use of CCL19 as a therapeutic to healing oral wounds (McGrory et al., 2004). To the best of my knowledge, AXL has not been involved in any studies accelerating wound closure. Literature research did not provide any information on how AXL could be influencing the cells to close the wound. In an attempt to understand how AXL regulates this acceleration of KC, I decided to perform a microarray where I compare AXL, DPFi CM and Epilife. In short, the KC were seeded to confluence and after scratching them with a p200, they were incubated in AXL, DPFi CM and Epilife for 6 hours. This time point was chosen as in the previous experiments, I started to see an acceleration of the KC after 4 hours, but I also wanted to collect RNA before the wound closed, therefore a median hour seemed appropriate. Then I extracted RNA, and sent the samples to a microarray facility at Kings College London where they generated biotin labelled cRNA for hybridization onto the 4133 Plus 2.0 Human Genechip. Data was provided in the format of a CEL file.

Raw data from the microarray analysis was analysed using Genespring GX 14.0. Analysis was done using 2 biological replicates with 3 conditions; KC in AXL, DPFi CM and Epilife. There were 54675 entities present on the Genechip used by the microarray facility. Entities were filtered based on their signal intensity values and only genes that passed the percentile threshold of 20% were analysed further (total of 48612 genes). Parametric tests were used with the p-value at 0.05 and the fold change at >=2 to determine significant differential expression two fold higher or lower across all conditions. The resulting list contained 2577 genes all of which passed the significance

threshold (Table A.1.). The PCA plot with the filtered list covers a total of 94.5% of all the variance of the significant genes present in the filtered data list with AXL and DPFi clustered more closely together than Epilife which means that they share less variance than Epilife (Figure 3.4.15A). Specifically, variance between Epilife media and both DPFi CM and AXL was on the 1st principle component rather than the 2nd while variance between DPFi CM and AXL was on the 2nd principle component. Normalised intensity values appeared to be similar in AXL and DPFi CM and most differences were identified between these two conditions and Epilife (Figure 3.4.15B).

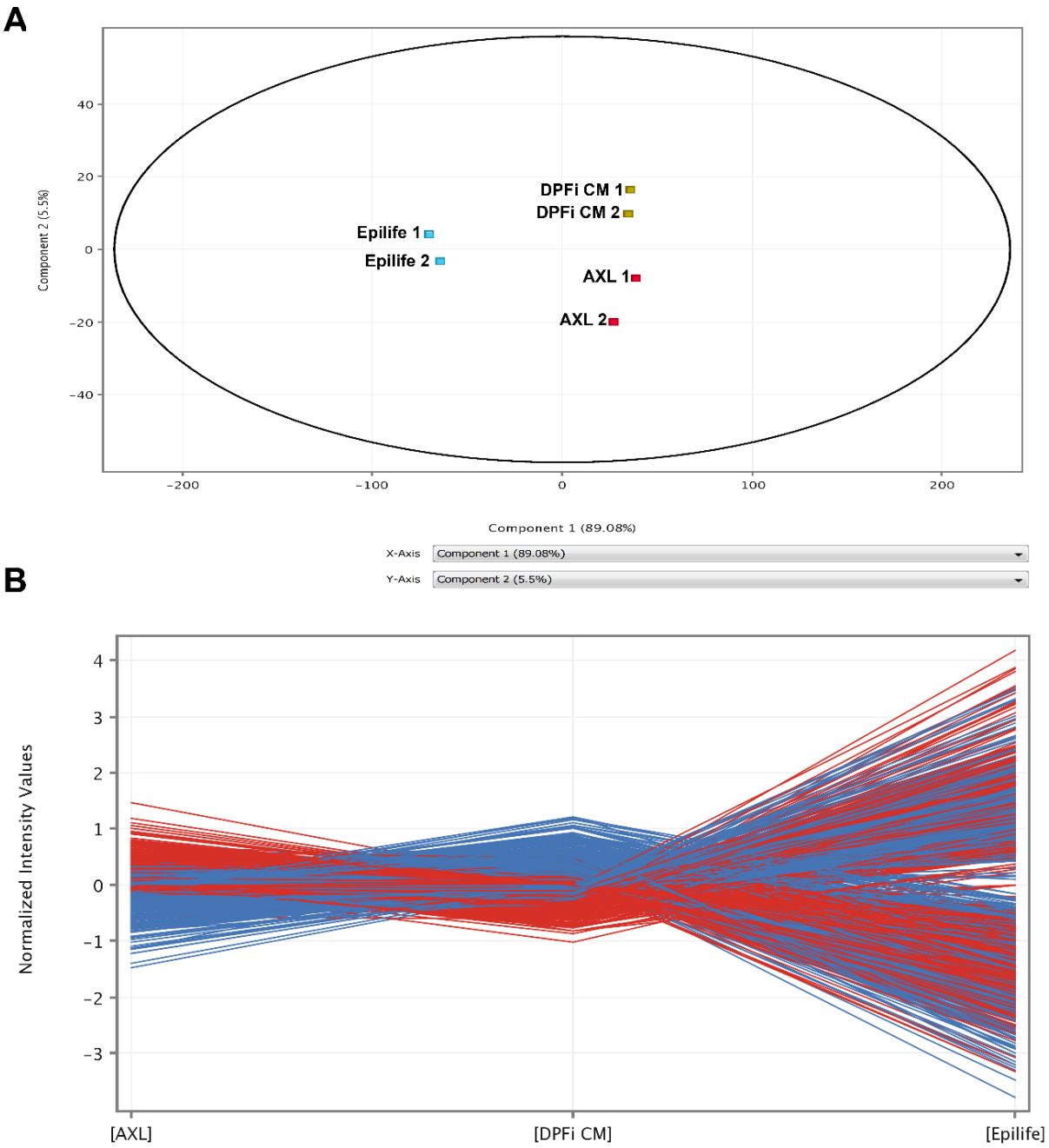


Figure 3.4.15. PCA plot and normalised signal intensity.

(A) The X-axis shows component 1 to be at 89.08% and the Y-axis shows component 2 to be at 5.5%. 3 conditions are shown on the plot with 2 patients; 1 (P3B) and 2 (P3C). Epilife is shown in light blue, DPFi CM in yellow and AXL in red. (B) Normalised intensity values of 2577 genes in response to AXL, DPFi CM and Epilife. High expression is shown in red and low expression is shown in blue.

To understand how AXL regulates KC reepithelialisation, a one way anova was used to generate 3 lists where all the conditions were compared in parallel; AXL vs DPFi, AXL vs Epilife and DPFi vs Epilife. Volcano plots were generated using the software, showing up regulated and down regulated genes in each comparison (Figure 3.4.16A-C). My main question in this experiment was how does DPFi CM and AXL regulate the KC to promote reepithelialisation? With that in mind, I wanted to look at all the genes that are up regulated or down regulated when treating KC with either DPFi CM or AXL.

The top Venn diagram in Figure 3.4.16D compares all up regulated genes between all the conditions. There are 11 genes significantly up regulated in AXL vs DPFi CM which can be seen on the heat map in Figure 3.4.17A. The bottom Venn diagram in Figure 3.4.16D compares all the down regulated genes between all conditions. 21 of those genes are significantly down regulated in AXL in comparison to the DPFi CM (Figure 3.4.17B).

There are 1507 genes up regulated in DPFi CM vs Epilife (Figure 3.4.16D), 1222 of which are also up regulated by AXL vs Epilife. Of these, 2 are also up regulated in AXL vs DPFi CM. However, 4 genes were not identified as differentially expressed in DPFi vs Epilife but were identified as up regulated in both AXL vs DPFi CM and AXL vs Epilife. 5 genes were only identified as up regulated in AXL vs DPFi CM and not in any other comparison.

In addition, there are 730 genes down regulated in DPFi CM vs Epilife (Figure 3.4.16D), 570 of which are also down regulated by AXL vs Epilife. 4 of these genes are also down regulated in AXL vs DPFi CM. Though, 5 genes were not identified as differentially expressed in DPFi vs Epilife but were identified as down regulated in both

AXL vs DPFi CM and AXL vs Epilife. 12 genes were only identified as down regulated in AXL vs DPFi CM and not in any other comparison.

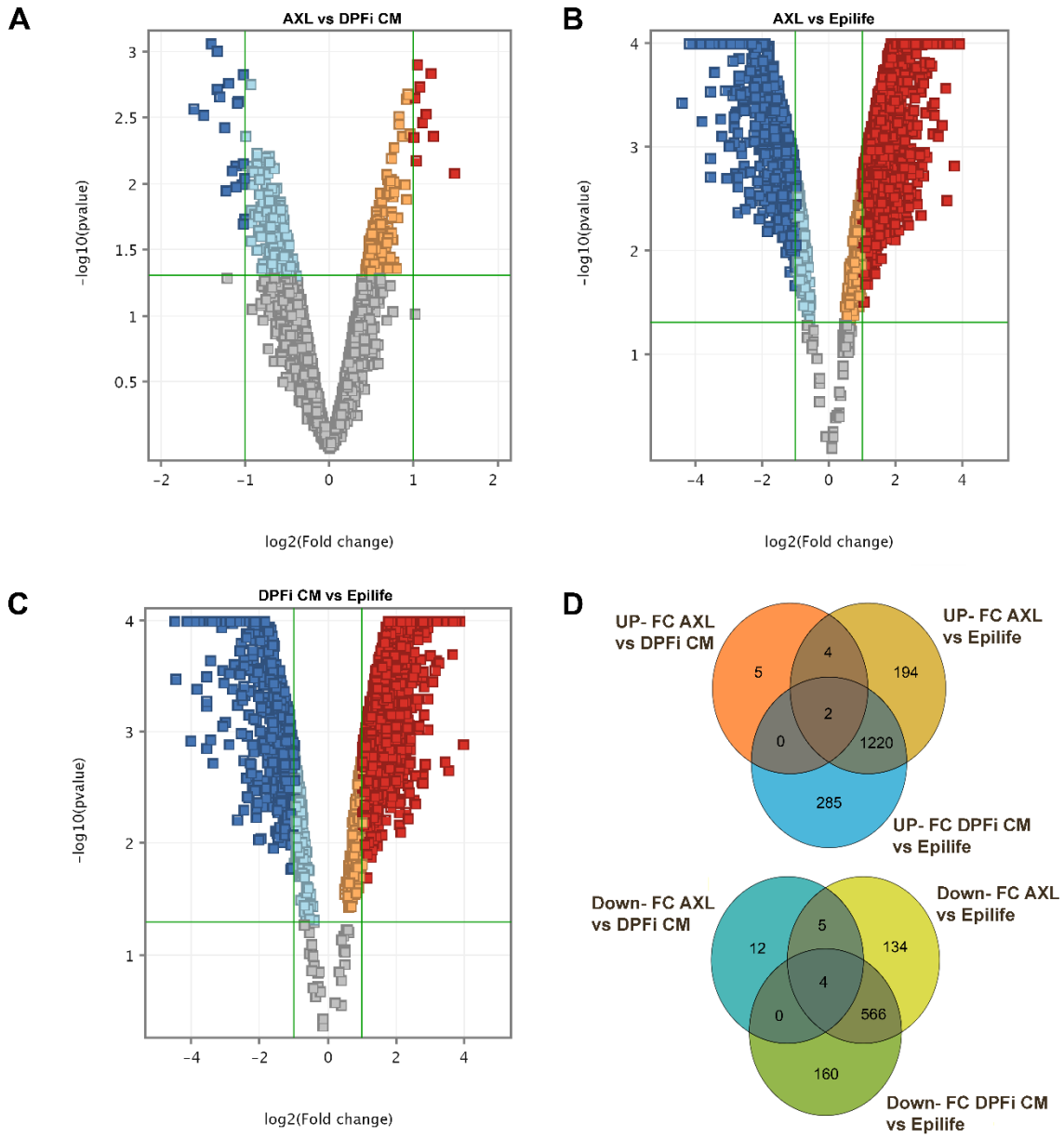
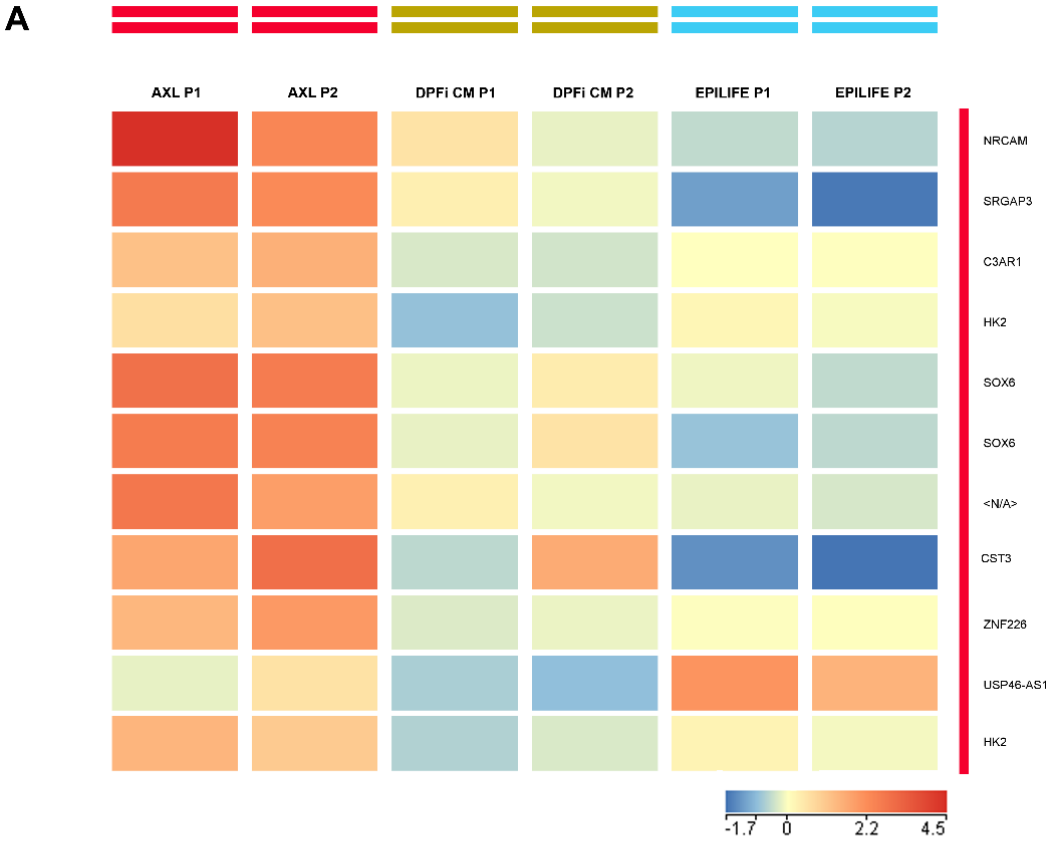


Figure 3.4.16. Volcano plots and Venn diagrams to compare up regulated and down regulated genes.

(A) The volcano plot shows AXL vs DPFi CM with AXL shown in red and DPFi CM shown in blue. (B) The volcano plot shows AXL vs Epilife with AXL shown in red and Epilife shown in blue. (C) The volcano plot shows DPFi CM vs Epilife with DPFi CM shown in red and Epilife shown in blue. (D) Venn diagrams compare all up regulated and down regulated conditions between them.


A
AXL P1
AXL P2
DPFi CM P1
DPFi CM P2
EPILIFE P1
EPILIFE P2
NRCAM
SRGAP3
C3AR1
HK2
SOX6
SOX6
<N/A>
CST3
ZNF226
USP46-AS1
HK2
-1.7
0
2.2
4.5

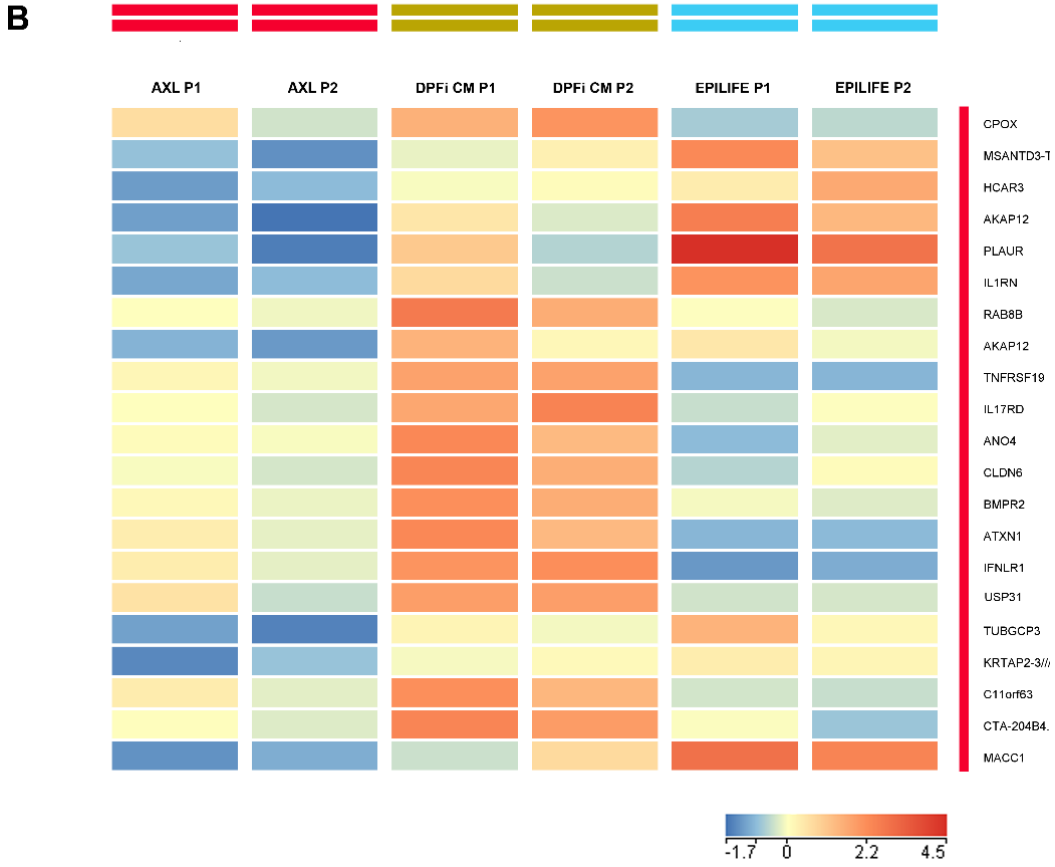

B
AXL P1
AXL P2
DPFi CM P1
DPFi CM P2
EPILIFE P1
EPILIFE P2
CPOX
MSANTD3-T
HCAR3
AKAP12
PLAUR
IL1RN
RAB8B
AKAP12
TNFRSF19
IL17RD
ANO4
CLDN6
BMPR2
ATXN1
IFNLR1
USP31
TUBGCP3
KRTAP2-3///
C11orf63
CTA-204B4.
MACC1
-1.7
0
2.2
4.5

Figure 3.4.17. Up regulated and down regulated genes in AXL.

(A) Heat map shows 11 genes identified which were up regulated in AXL vs DPFi CM. (B) Heat map shows 21 genes that are down regulated in AXL vs DPFi CM.

The heat map helps visualise how different genes are expressed in AXL vs DPFi CM. Even though certain genes are up regulated in AXL in comparison to the DPFi, some of them are still expressed in DPFi and Epilife. So as to elucidate which genes are uniquely expressed when AXL is present, 4 way Venn diagrams (Figure 3.4.18) were made to clearly visualise the distribution of the genes in the different comparisons. Three 4 way Venn diagrams were made each focusing on one condition at a time thereby identifying unique genes up regulated and down regulated in the selected condition; 6 entities in DPFi CM (Figure 3.4.18A), 15 entities in AXL (Figure 3.4.18B) and 1792 entities in Epilife (Figure 3.4.18C). As shown in Figure 3.3.18B, I was able to narrow down the list of genes to those specifically controlled by AXL. 6 genes were uniquely up regulated by AXL and 9 were down regulated. Table 3.4.1. shows the list of 15 transcripts that are up regulated and down regulated only in AXL two of which are repeated and one of which I could not determine the ID giving a total of 12 genes. All genes with fold change >2 or <-2 are considered statistically significant.

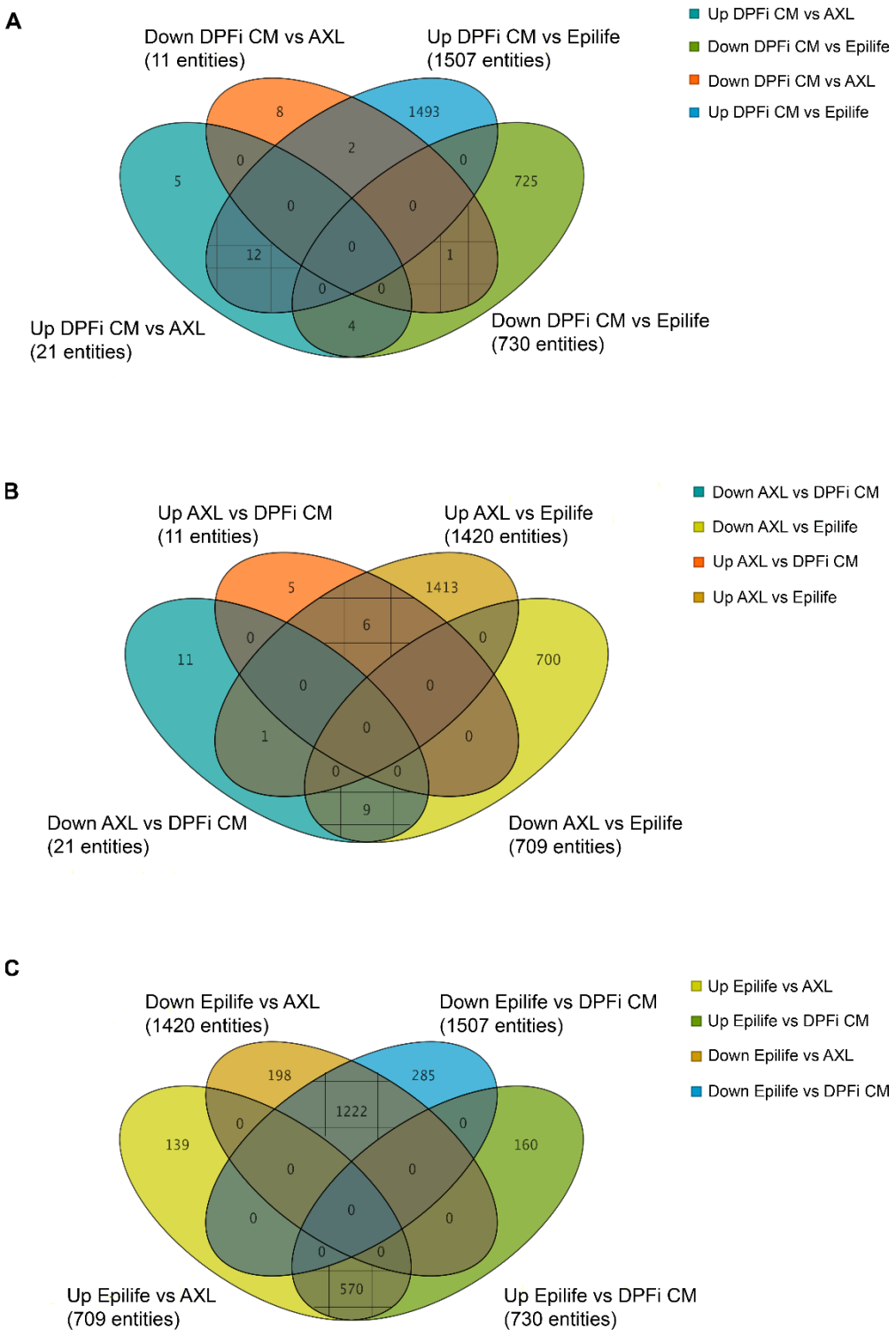


Figure 3.4.18. Four-way Venn diagrams.

Venn diagrams comparing up regulated and down regulated gene entities uniquely regulated by either (A) DPFi CM, (B) AXL or (C) Epilife. Hashed sections reveal genes uniquely regulated by DPFi CM (A), AXL (B) or Epilife (C).

Table 3.4.1. Up regulated and down regulated genes specific for AXL.

Probe set ID	Gene Symbol	FC AXL vs DPFi CM	FC AXL vs Epilife	FC DPFi CM vs Epilife
204105_s_at	NRCAM	2.78	4.55	1.64
209794_at	SRGAP3	2.10	8.17	3.88
227497_at	SOX6	2.30	3.03	1.32
227498_at	SOX6	2.15	3.98	1.85
227943_at	----	2.00	2.51	1.25
230343_at	CST3	2.01	8.71	4.33
205122_at	MSANTD3-TMEFF1///TMEFF1	-2.17	-4.32	-1.99
205220_at	HCAR3	-2.12	-3.17	-1.49
210517_s_at	AKAP12	-2.80	-6.07	-2.16
211924_s_at	PLAUR	-2.32	-9.57	-4.13
216243_s_at	IL1RN	-2.03	-4.30	-2.12
227529_s_at	AKAP12	-3.05	-2.37	1.29
1554086_at	TUBGCP3	-2.66	-3.60	-1.35
1555673_at	KRTAP2-3///KRTAP2-4	-2.22	-2.48	-1.12
1566764_at	MACC1	-2.35	-6.61	-2.82

3.4.9. Potential pathways activated by AXL

The microarray gave me a valuable insight as to what genes are activated when KC are incubated with AXL and DPFi CM. In an attempt to identify what pathways are activated by AXL and DPFi CM, I used IPA software to generate potential signaling pathways that are activated or inhibited in the KC inputting in the list of genes differentially regulated across all conditions (2577 genes) (Figure 3.4.19.). Using IPA I identified more than 100 pathways related to the significant genes in the microarray analysis. The higher the number of significant genes involved in a pathway the more probable that a pathway becomes activated or inactivated. Based on the z-score and trend I chose the top 4 pathways that seem to be related to my gene list. It appears that the acute phase response signaling is inhibited in KC by both AXL and DPFi CM in comparison to Epilife. Gαq, HGF and AMPK signaling are activated in KC with AXL

and DPFi CM in comparison to Epilife. Further data analysis using this software could provide more insight on the pathways related to the faster reepithelialisation of KC as well as master regulators of the process. This work is currently ongoing.

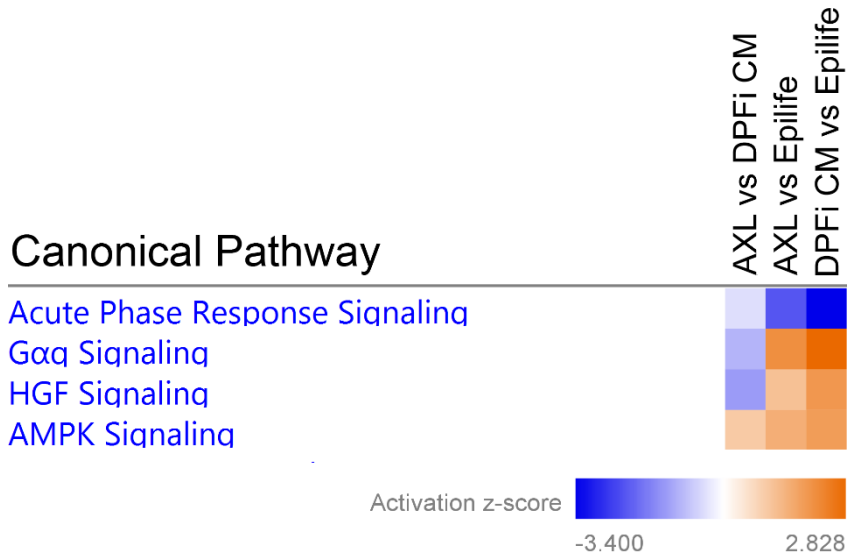


Figure 3.4.19. Pathways activated/inhibited by AXL and DPFi CM.

The heat maps shows the top 4 pathways activated/inhibited by AXL and DPFi CM in KC. The pathways are sorted with z-score with the highest shown in orange and the lowest shown in blue.

3.5. Discussion

3.5.1. Ibidi versus scratch assay: Which method best mimics the wounding effect?

Chronic wounds are a huge burden on patients and society (Gottrup et al., 2010, Guest et al., 2015). Test systems mimicking these conditions have been developed by scientists in order to find therapies. Genetically modified animal models are often used to investigate chronic wounds and have given great insights over the years (McFarland-Mancini et al., 2010, Kolumam et al., 2017). The drawback to the animal models is that their physiology is very different to that of the human body. The mechanism by which wound closure occurs in mice is mainly by contraction rather than by reepithelialisation, while in human skin wounds close by reepithelialisation. Therefore, human *ex vivo* and *in vitro* models need to be used in order to assess the efficacy of potential therapeutic targets.

The scratch assay technique has been used widely by many researches as a controlled environment to investigate wound healing before moving on to the *ex vivo* test system (Kioka et al., 2010, Huang et al., 2017). Over the years, investigators have raised issues over the reproducibility of the results, as the wounding varies from the pressure applied in each cell culture well. The ibidi insert is a new alternative method to study wound healing *in vitro* and it is supported that it is able to give reproducible results. Although it retains the same wound area in each experiment, when the ibidi inserts are used, the cell is not physically damaged as in an injury, so perhaps it is not an accurate model to study re-epithelisation in a monoculture.

In the experiments performed in this chapter to study wound closure, both the ibidi insert and the scratch assay method were used initially. When the CM from the three fibroblast populations were added to the 'wounded' KC, there was the same trend observed in both experiments; the DPFi CM was the fastest, followed by RFi CM and finally by the PFi CM and the control, however significant differences were only observed when the scratch assay was used, and not with ibidi inserts (Figure 3.5.1). In the scratch assay experiment, when the KC were physically wounded using a p200 pippete, the DPFi CM was able to promote reepithelialisation significantly faster than the control, PFi CM and RFi CM. This supports the notion that the wounding of KC perhaps activates a signalling response, and makes the cells more responsive to the DPFi CM. Thus, I concluded that the scratch assay technique is a more suitable method to study wound healing in a monoculture system.

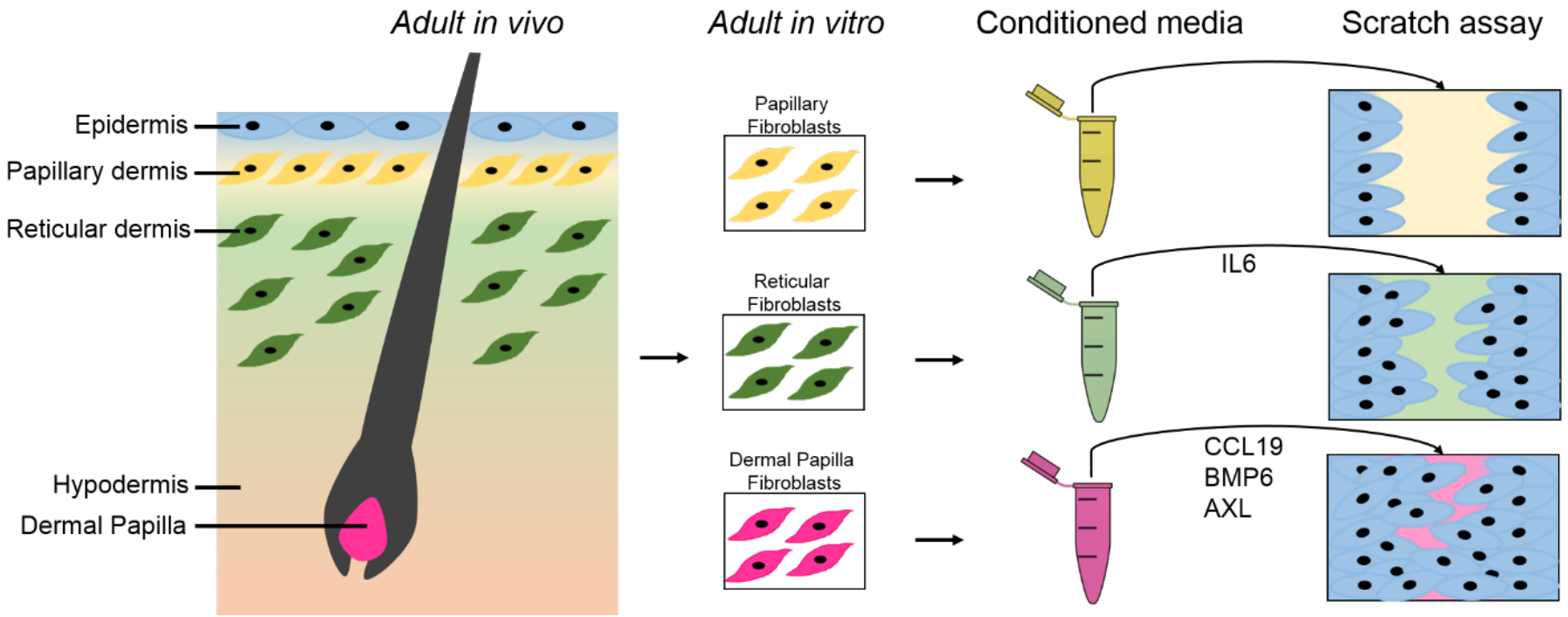

Adult in vivo
Adult in vitro
Conditioned media
Scratch assay
Epidermis
Papillary dermis
Reticular dermis
Hypodermis
Dermal Papilla
Papillary Fibroblasts
Reticular Fibroblasts
Dermal Papilla Fibroblasts
IL6
CCL19
BMP6
AXL

Figure 3.5.1. Chapter 3 methods and outcomes.

Three fibroblast subpopulations were isolated from a single occipital scalp biopsy; the PFi of the papillary dermis, the RFi of the reticular dermis and the DPFi of the dermal papilla. These populations were cultured and grown *in vitro* and conditioned media was collected from all of them. In turn, this conditioned media that contained all the cytokines and growth factors released by the fibroblasts was used on the KC of the epidermis in a controlled wound experiment *in vitro*. The DPFi conditioned media that contained CCL19, BMP6 and AXL amongst other cytokines, appeared to promote the fastest reepithelialisation.

3.5.2. DPFi CM promotes KC migration in a paracrine manner

Epithelial-mesenchymal interactions are vital to maintain skin homeostasis. In a wounded environment, it has been shown that the fibroblasts in the dermis play an important role during epitheliasation. Specifically, it has been previously shown in mice, that RFi are the first population to migrate into the wound and repopulate the dermis (Driskell et al., 2013). From this observation, I hypothesized that the RFi communicate with the KC to promote reepithelialisation of the epidermis. In an attempt to study that, the main objective of this chapter was to test if the fibroblasts isolated from human dermis release factors in culture which are able to promote KC migration. Once the technique for 'wounding' the KC was established, the next step was to use CM collected from DPFi, PFi and RFi and test whether they promoted wound closure.

My results showed that all three populations are able to promote migration of KC, with the RFi CM speeding up KC migration significantly in comparison to Epilife which supports my initial hypothesis. Surprisingly, DPFi CM significantly speeds up the process in comparison to the PFi CM and the control and also appear to promote faster migration of the KC than the RFi CM, although this was not a significant result. These results were compelling as in a normal wound there are no hair follicles to promote faster reepithelialisation. On the other hand, the RFi are present in a wounded site and the result that the CM collected from this population speeded up KC migration can be explained as a physiological response to wounding. This perhaps suggests that we could harness the property of DPFi CM to accelerate wound healing.

The accelerated proliferation of KC was only apparent after incubation with the DPFi CM. This suggests that the CM contains signals that are acting in a paracrine manner

and are altering the behaviour of the cell which in the control experiment are not present. At this point, it was safe to conclude that a growth factor or a cocktail of growth factors released from DPFi are promoting faster wound closure *in vitro*. Perhaps introducing cytokines released by DPFi could promote faster reepithelialisation and provide a solution for chronic wounds.

3.5.3. MITC induces enhanced migration

A recent study demonstrated the importance of cellular dynamics using live mice imaging (Park et al., 2017). This work highlights the existence of migratory and proliferative zones in a wound healing epidermis as well as the rate of migration and differentiation of the basal KC. I wanted to study the effect on wound closure when proliferation is inhibited, as in the paper above it was demonstrated that wound closure was not impaired by the inhibition of proliferation (Park et al., 2017). To translate their finding on a human *in vitro* system, MITC was used on the KC to inhibit cell division and study the migration of the cells. I found that treatment with MITC promoted faster wound closure in all the CM as well as the control although this finding was only significant in the DPFi CM and Epilife. This is an interesting finding, as it demonstrates that in an injured environment, inhibiting cell division promotes faster wound closure. Perhaps, as shown in the paper by Parker et al (Park et al., 2017) in live mice, when the differentiation zone is no longer present in human cells *in vitro*, the migratory zone increases in size and more cells are involved in the reepithelialisation. Even though this means that the affected area is larger, it's important to understand how cellular processes occur in a wounded environment.

3.5.4. IL6- an important cytokine for reepithelialisation

To interrogate the source of the impact that the CM was having on the KC, I performed a cytokine array to detect what cytokines were producing this effect. I was specifically questioning the DPFi as they appeared to promote a significant response in the KC migration. Three cytokines were significantly present in the DPFi CM; CCL19 and AXL compared to the PFi and RFi CM and BMP6 compared to the PFi CM. In the cytokine array, IL6 was detected to be present in the RFi CM culture compared to the PFi CM. Due to the fact that IL6 has been implicated to have a major role in promoting wound healing (Lin et al., 2003), and that the RFi CM promoted faster KC migration than the control, this factor was chosen to test its effects in comparison to the three novel cytokines detected in the DPFi CM.

When IL6 was tested using the scratch assay, it had a very similar effect on KC migration as RFi CM. This suggests that the accelerated wound healing response with RFi CM is part due to IL6. RFi were reported to be the first population to repopulate the dermal wound (Driskell et al., 2013). This finding along with my finding of IL6, could suggest that the RFi are migrating into the dermal wound bed and are releasing IL6 in order to recruit the KC and repopulate the wound bed (Figure 3.5.2.).

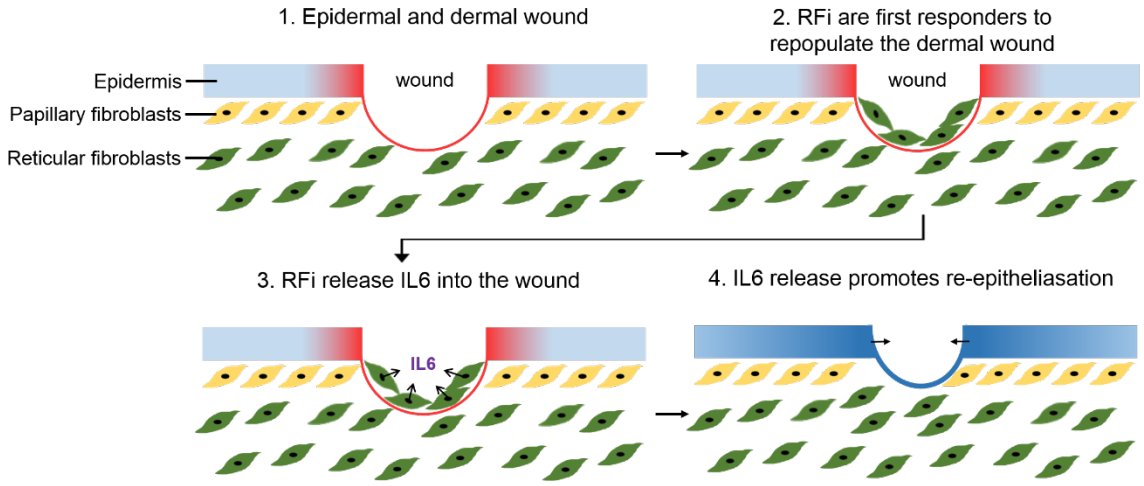


Figure 3.5.2. Proposed mechanism of IL6 in wound healing.

(1) In a wound, (2) the RFi were found to be the first responders and repopulate the dermal wound. (3) My proposed mechanism of wound healing is that as soon as the RFi repopulate the dermal wound, they release IL6 (4) to recruit the KC and promote reepithelialisation.

3.5.5. A novel cytokine in wound healing: AXL

CCL19, BMP6 and AXL released by DPFi all resulted in an accelerated wound healing response in the scratch assay experiments. BMP6 has been previously studied for its role in epithelial differentiation (McDonnell et al., 2001, Rendl et al., 2008a). There have also been a few studies recently involving CCL19 in wound healing. A study in 2004, showed the up regulation of CCL19 in mice oral wounds and proposed the use of this cytokine as a therapeutic to healing oral wounds (McGrory et al., 2004). Following that, another group has demonstrated the importance of CCL19 in remodelling mitral valves after injury by using human mitral valve interstitial cells (Wang et al., 2015). In addition, significantly higher expression of CCL19 is found in wild type mice wounds at day 5 after wounding in comparison to diabetic wounds (Finley et al., 2016). After extensive research, to my knowledge, there hasn't been a connection previously made between AXL and cutaneous wound healing. Therefore

this seems an intriguing cytokine to study as a novel therapeutic to promote wound closure.

Similarly to the *in vitro* experiments, the *ex vivo* wound healing assay demonstrated that my findings from the scratch assay could be translated into the 3D model. It is important to note, that the *ex vivo* skin model does not have immune cell attraction capability, therefore immune cell recruitment could not be tested with this model. In the punch within a punch assay, AXL was shown to significantly promote acceleration of reepithelialisation over and above CCL19, CCL19&AXL and PDGF-BB. Therefore, AXL is an attractive candidate for substituting the current treatment of chronic wounds.

3.5.6. AXL and regulation of reepithelialisation

AXL is a tyrosine kinase receptor protein in the TAM receptor tyrosine kinase family. The full structure of AXL is 894 amino acids (aa) long (Figure 3.5.3); it is a 140kDa glycoprotein with the gene located on chromosome 19q13.2 encoding 20 exons. Exons 1-10 encode the extracellular domain, which includes a signal peptide (aa 1-37), two immunoglobulin (Ig) domains (aa 37-124 for domain 1, aa 141-212 for domain 2), and two fibronectin type III (FNIII) domains (aa 224-322 for domain 1, aa 325-428 for domain 2) and is approximately 60-80 kDa (Figure 3.5.4A) (O'Bryan et al., 1991).

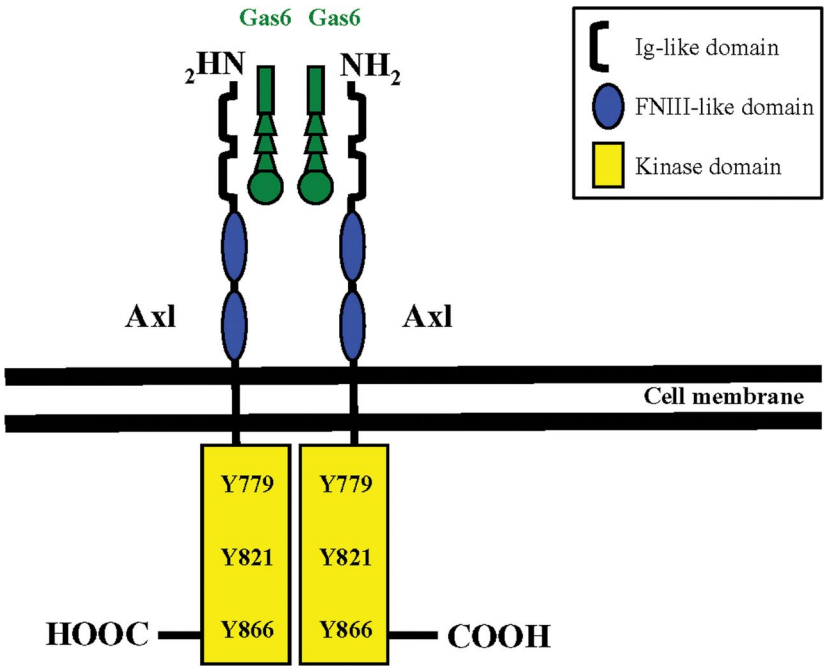


Figure 3.5.3. AXL receptor structure.

The extracellular domain of Axl has two Ig and two FN type III domains. Gas6 forms a complex with the extracellular region of AXL and activates the receptor (Korshunov, 2012).

Initially, it was confusing as to why a transmembrane protein was on the cytokine array. Researching AXL, I found that exon 11 of AXL which encodes the extracellular region (aa438-451) is subject to proteolytic cleavage along with exons 1-10 meaning the whole extracellular region of AXL (aa1-451) can be soluble (O'Bryan et al., 1995). Thus, in the cytokine array, I detected the extracellular region of AXL also known as soluble AXL. In my experiments I have used the soluble AXL (aa 33-440; Figure 3.5.4B) which in human plasma is known to bind the AXL ligand GAS6 and prevent it from activating the AXL receptor (Ekman et al., 2010). The extracellular region of AXL is also known to undergo homophilic binding to activate the receptor, therefore, another reason for the effect elicited by the soluble form of AXL may be as a result of binding through the extracellular region of AXL thus phosphorylating AXL (Korshunov, 2012).

A

```
  1 mawrcprmgr vplawclalc gwacmaprgt qaeespfvgn pgnitgargl tgtlrcqlqv
 61 qgeppevhwl rdgqilelad stqtqvplge deqddwivvs qlritslqls dtgqyqclvf
121 lghqtfvsqp gyvgleglpy fleepedrtv aantpfnlsc qaqgppepvd llwlqdavpl
181 atapghgpqr slhvpglnkt ssfsceahna kgvttsrtat itvlpqqprn lhlvsrqpte
241 levawtpgls giyplthctl qavlsddgmg iqagepdppe epltsqasvp phqlrlgslh
301 phtpyhirva ctssqgpssw thwlpvetpe gvplgppkni satrngsqaf vhwqeprapl
361 qgtllgyrla yqgqdtpevl mdiglrqevt lelqgdgsvs nltvcvaayt aagdgpwslp
421 vpleawrpvk epstpafswp wwyvllgavv aaacvlilal flvhrrkket rygevfeptv
481 ergelvvryr vrksysrrtt eatlnslgis eelkeklrdv mvdrhkvalg ktlgegefga
541 vmegqlnqdd silkvavktm kiaictrsel edflseavcm kefdhpnvmr ligvcfqgse
601 resfpapvvi lpfmkhgdlh sfllysrlgd qpvylptqml vkfmadiasg meylstkrfi
661 hrdlaarncm lnenmsvcva dfglskkiyn gdyyrqgria kmpvkwiaie sladrvytsk
721 sdvwsfgvtm weiatrgqtp ypgvenseiy dylrqgnrlk qpadcldgly almsrcweln
781 pqdrpsftel redlentlka lppaqepdei lyvnmdeggg ypeppgaagg adpptqpdpk
841 dscscltaae vhpagryvlc psttpspaqp adrgspaapg qedga
```

B

```
                              aa33   eespfvgn pgnitgargl tgtlrcqlqv
 61 qgeppevhwl rdgqilelad stqtqvplge deqddwivvs qlritslqls dtgqyqclvf
121 lghqtfvsqp gyvgleglpy fleepedrtv aantpfnlsc qaqgppepvd llwlqdavpl
181 atapghgpqr slhvpglnkt ssfsceahna kgvttsrtat itvlpqqprn lhlvsrqpte
241 levawtpgls giyplthctl qavlsddgmg iqagepdppe epltsqasvp phqlrlgslh
301 phtpyhirva ctssqgpssw thwlpvetpe gvplgppkni satrngsqaf vhwqeprapl
361 qgtllgyrla yqgqdtpevl mdiglrqevt lelqgdgsvs nltvcvaayt aagdgpwslp
421 vpleawrpvk epstpafswp   aa440
```

Figure 3.5.4. Amino acid sequence of Human AXL.

(A) Amino Acid sequence of human AXL, with peptide used in experiments underlined in black (aa33-440). (B) aa33-440 of AXL used in experiments. Ig domains are underlined in black, while and FNIII domains are underlined in grey.

To the best of my knowledge, there are no reports indicating a role for AXL or the soluble version of AXL in wound healing. In an attempt to understand how this soluble version of AXL is promoting faster reepithelialisation, using the list of genes I generated from the microarray analysis, I generated potential pathways that are regulated by AXL and DPFi CM in the KC during wound closure. The top pathway that appeared to be inhibited by AXL and DPFi CM was the acute phase response signaling. This pathway is responsible for promoting an inflammatory response that serves as protection to pathogens in response to injury. Inflammation is the first phase of wound healing and it has been suggested that inhibition of inflammation could lead

to faster and scarless wound closure. If DPFi CM and AXL are able to inhibit the inflammatory response during wound healing this could explain the faster reepithelialisation observed in my experiments. Further testing should be done to determine whether the *ex vivo* wounds are able to have decreased scarring when AXL is applied topically in comparison to the control.

3.5.7. AXL receptor could be stimulated by EGFR activation

Another explanation as to why AXL enhances KC reepithelialisation, lies in a recent study that focused on the effect on AXL receptor, when activating EGFR by EGF (Vouri et al., 2016). This paper, elegantly showed that in human glioblastoma cells AXL heterodimerizes with EGFR and activation of both receptors is stimulated by the addition of EGF. Methods section 2.3.3. clearly outlines the ingredients of EDGS which is the supplement added in Epilife, which has been used in all of my experiments in Chapter 3 as the KC growth media. EGF is one of the growth factors present, which further supports that EGF could be activating EGFR on KC and transactivating AXL at the same time. Perhaps, addition of sAXL further enhances this activation, thus observing the faster KC reepithelialisation as seen in this chapter. Further experiments should be carried out to identify if AXL is activated or inhibited and whether EGF could play a role in this process in human KC.

3.5.8. AXL: An attractive alternative to PDGF-BB in chronic wound healing

PDGF-BB is amongst the cytokines that have been FDA approved for its use in chronic wounds. Recently, malignancies have been reported and patients with prior malignancies were warned not to use the product. Therefore, alternative solutions need to be found to treat such wounds. In my experiments, I sought to compare the efficacy of PDGF-BB on the *ex vivo* model and compare its wound healing rate to AXL.

My results showed that AXL is able to promote faster reepithelialisation than PDGF-BB. Therefore, with further testing AXL could be an alternative to PDGF-BB in chronic wound healing.

3.5.9. Concluding remarks

In summary, in this chapter I demonstrated the importance of the mesenchymal-epithelial interactions in KC migration *in vitro*. CM obtained from DPFi promoted significantly faster KC migration in the scratch assay to cover the wound. The cytokine assay revealed three cytokines to be significantly more expressed in DPFi CM; CCL19, AXL and BMP6. These cytokines were found to promote significantly faster migration of KC from the control. Testing using an *ex vivo* system showed AXL to significantly promote reepithelialisation over and above CCL19 and PDGF-BB. The microarray analysis revealed unique genes up regulated and down regulated in AXL. Further testing of these genes could lead to AXL being a potential therapeutic solution to chronic wounds.

Chapter 4. Final discussions and future directions

4.1. General Discussion

4.1.1. Fibroblast heterogeneity and anatomic diversity

Fibroblasts are the most abundant cell type in the skin dermis and are defined by their ability to deposit ECM. They have key roles in skin and hair morphogenesis as well as wound healing but there is still a lot that needs to be elucidated about their mechanisms of action. For years this population of cells was largely unconsidered and assumed to have a supporting role. Recent research displayed the importance of this population of cells and with every new piece of evidence we understand a bit more about their function. The word fibroblast covers a broad population of cells that are dissimilar between them. Different body sites such as heart and tendons, differ in their in their fibroblast orientation, expression and ECM deposition (Doane and Birk, 1991). This becomes even more evident as this class of cells is highly heterogeneous even within a single body site; such as the skin dermis.

In this thesis, I have demonstrated that three human skin fibroblast populations, the DPFi, PFi and RFi which arise from a common developmental origin, maintain their distinct identities even when cultured in an *in vitro* environment where their environmental cues are no longer present. In addition, they deposit a unique combination of ECM proteins which further highlights their differences in culture. Focusing on the DPFi, my experiments demonstrated that occipital scalp DPFI do not differentiate with the same potential as frontal scalp DPFi. Frontal scalp is neural crest derived while occipital scalp is mesoderm derived, and so it might be a greater challenge for frontal DPFi to differentiate into osteoblasts compared to occipital scalp as they arise from a different lineage. These differences in expression as well as

differentiation potential, highlight how diverse the fibroblast population is within a single location as well as on different body sites. Perhaps the nomenclature fibroblast is not reflecting the existence of different subpopulations but if we are to begin to understand how they are involved in different processes, we should treat them as separate entities.

4.1.2. How plastic are dermal fibroblast subpopulations?

In chapter 2, one of the main questions that I asked was how diverse dermal subpopulations are in culture. *In vivo*, dermal fibroblasts are responsible for the bulk of the ECM that supports the tissue. Therefore, I pondered if in culture, these subpopulations were able to deposit unique ECMs as they do *in vivo*. To answer this question, I used mass spectroscopy to identify what proteins are present in the ECM deposited by DPFi, PFi and RFi *in vitro*. The results showed that these dermal subpopulations deposit different amounts of ECM proteins as well as unique matrices to one another. Following this, I wondered if the ECM is able to guide the identity of cell. For instance, if PFi were seeded on a DPFi matrix, would they still behave as PFi or would they adopt characteristics of the DPFi? In an attempt to answer this question I prepared ECM deposited by DPFi and seeded PFi and RFi in order to study their behavior *in vitro*. Due to a lot of optimization that needed to be done for this experiment, I wasn't able to carry it into completion but it would be something that I would like to study in the future.

4.1.3. DPFi and RFi: a potential source of myofibroblasts?

Myofibroblasts have been reported to be present during tissue injuries. It has long been reported that myofibroblasts are a differentiated form of dermal fibroblasts (Li

and Wang, 2011), although the specific source is still unknown. This 'activated' form of dermal fibroblasts is known to express α-SMA (Rockey et al., 2013). Several studies have investigated the mechanism by which the dermal fibroblasts differentiate into myofibroblasts and have reported that the most important stimulus is mechanical tension (Hinz, 2010).

In a normal environment *in vivo*, fibroblasts sit on a soft ECM. In a monolayer culture, flasks and plates are used to culture and expand them. The surface of the culture plates is stiffer than *in vivo* and thus it is natural that the cells could be phenotypically different. In a wounded area, the ECM is stiffer and perhaps an *in vitro* culture resembles more a wounded fibroblast phenotype than a normal phenotype. This observation could explain why a big percentage of the DPFi and RFi express α-SMA in culture, whereas *in vivo* only myofibroblasts are α-SMA positive. At this point, I have to acknowledge that *in vivo* dermal sheath cells are also α-SMA positive therefore perhaps the DPFi are de differentiating in culture into dermal sheath cells. Regardless, the notion that DPFi could be a source of myofibroblasts supports the idea that the stiff environment switches on a wounding response. Having said that, the PFi did not appear to express α-SMA in culture which made me postulate if certain fibroblast populations were more likely to express this gene. Could DPFi and RFi be the source of the myofibroblasts?

4.1.4. AXL: A novel therapeutic for wound closure

The epidermis is the body's first line of defense against external pathogens. In the case of a full thickness wound, it is vital for the cells in the dermis and epidermis to repair the wound in order to prevent exposure to intruding organisms. The proliferative KC in the basal layer of the epidermis need a surface to migrate onto as well as

instructive signals on what to do. The fibroblasts in the dermis contribute to wound healing by depositing ECM in the dermis. This ECM promotes KC migration as well as release signals to guide KC differentiation. It has been shown that the RFi in the lower dermis are the first contributors in dermal wound repopulation (Driskell et al., 2013). In my experiments, in chapter 3, I have found IL6 to be significantly released by the RFi *in vitro* in comparison to the PFi of the upper dermis. As discussed in chapter 3, several studies have shown that IL6 is a key cytokine in wound healing. This finding, along with the observation that RFi are the first to populate the dermal wound (Driskell et al., 2013), could mean that IL6 is released by RFi to promote re epithelialization of the wound.

That being said, a third population of cells the DPFi that arise from the same developmental progenitor as the PFi and RFi were found to release cytokines that promote even faster migration than RFi *in vitro*. One of the cytokines identified, and a novel one in the field, is AXL. To the best of my knowledge AXL has not been implicated with wound healing before. As no information could be found in the literature on the mechanism of action of AXL on KC, microarray analysis was used to determine what genes are activated/inhibited in the KC in response to AXL. Using this list of genes, I used the IPA software to help me determine how these genes are correlated between them. IPA gave me a list of all the pathways related to the genes up regulated/down regulated in AXL and DPFi CM. The top pathway in this list was the acute phase response signaling pathway that is responsible for the inflammatory reposnse in injury. This pathway was in fact inhibited by AXL and DPFi CM that led me to hypothesize that the absence of inflammation in my experiments led to faster reepithelialisation.

Further testing of this cytokine, using an *ex vivo* model, provided me with more information on the potential of the cytokine to be used as a treatment in wound closure. In this experiments, AXL appeared to be promoting significantly faster reepithelialisation than the control, at a similar rate as the commercialized cytokine for wound healing PDGF-BB. These results are very promising, as AXL could potentially be used as a therapeutic to chronic wounds.

4.2. Future directions

There are several aspects of this thesis that could be further researched:

4.2.1. Plasticity of DPFi, PFi and RFi in culture

With regards to the work on the plasticity of human dermal subpopulations in culture, it would be interesting to optimise the experiment and study whether the ECM is able to guide the identity of cell or if the cell is not plastic and cannot be altered by its environment. If the cells are plastic and are able to interchange their identities based on their environment, it would be a major breakthrough in the hair regeneration field.

4.2.2. Livecyte: alternative to current scratch assay method

Livecyte is a live imaging system designed by Phasefocus that enables quantitative cell analysis. My current scratch assay method involved manually imaging the wound every hour, and analysing the results in Image J. This alternative method, is able to track individual cells and give you morphological and dynamic data on the behaviour of the cell. I had the opportunity to try this system towards the end of my PhD and the results matched my scratch assay and *ex vivo* experiment. Going forward, this system would be ideal for analysing scratch assays as it gives more information out of a single experiment and is less time consuming.

4.2.3. *Ex vivo* wound healing assay

One of the natural next steps of the wound healing study, was to test if AXL is able to promote reepithelialisation at the same rate in an *ex vivo* model. This could take us a step further at utilizing this cytokine as a potential therapeutic to chronic wounds. I

managed to perform this experiment on one biopsy and the results are shown in Figure 3.4.14. For this experiment to be completed, a second biopsy is required to test if the result can be duplicated.

4.2.4. Mode of action of AXL

Moving forward, I would like to test if AXL is activated or inhibited in my experiments by using R428, a known AXL inhibitor. If AXL is activated in this instance, I would like to test if AXL is further enhanced when EGF activates EGFR. Complementing this, further analysis of the microarray results could give me great insights on the pathways that could potentially be involved after the addition of AXL in the KC scratch assay. Analysis and validation of the genes identified in this study would take us a step forward in answering how AXL is promoting faster reepithelialisation. In addition, I would like to evaluate if the genes expressed in KC in culture after incubation with AXL also get expressed at the leading edge of the punch within a punch wound following incubation with AXL.

4.2.5. Is AXL necessary?

Going forward, it would be interesting to identify whether AXL is necessary in DPFi CM to drive reepithelialisation. If AXL was removed from the CM, using an antibody specific to AXL to remove it, would reepithelialisation still occur at the same rate as when AXL was present? This study would help identify if AXL is the driving force of KC reepithelialisation in the DPFi CM. I have shown that AXL is sufficient to drive reepithelialisation but this experiment would uncover if it also necessary.

References

ALEXANDER, C. M., KASZA, I., YEN, C. L., REEDER, S. B., HERNANDO, D., GALLO, R. L., JAHODA, C. A., HORSLEY, V. & MACDOUGALD, O. A. 2015. Dermal white adipose tissue: a new component of the thermogenic response. *J Lipid Res,* 56**,** 2061-9.

ALONSO, L. & FUCHS, E. 2006. The hair cycle. *J Cell Sci,* 119**,** 391-3.

ANDL, T., REDDY, S. T., GADDAPARA, T. & MILLAR, S. E. 2002. WNT Signals Are Required for the Initiation of Hair Follicle Development. *Developmental Cell,* 2**,** 643-653.

ASHCROFT, G. S., HORAN, M. A. & FERGUSON, M. W. 1997. The effects of ageing on wound healing: immunolocalisation of growth factors and their receptors in a murine incisional model. *J Anat,* 190 (Pt 3)**,** 351-65.

AVITABILE, S., ODORISIO, T., MADONNA, S., EYERICH, S., GUERRA, L., EYERICH, K., ZAMBRUNO, G., CAVANI, A. & CIANFARANI, F. 2015. Interleukin-22 Promotes Wound Repair in Diabetes by Improving Keratinocyte Pro-Healing Functions. *J Invest Dermatol,* 135**,** 2862-2870.

AZZARONE, B. & MACIEIRA-COELHO, A. 1982. Heterogeneity of the kinetics of proliferation within human skin fibroblastic cell populations. *J Cell Sci,* 57**,** 177-187.

BEER, H. D., LONGAKER, M. T. & WERNER, S. 1997. Reduced expression of PDGF and PDGF receptors during impaired wound healing. *J Invest Dermatol,* 109**,** 132-8.

BOUTET, E., LIEBERHERR, D., TOGNOLLI, M., SCHNEIDER, M., BANSAL, P., BRIDGE, A. J., POUX, S., BOUGUELERET, L. & XENARIOS, I. 2016. UniProtKB/Swiss-Prot, the Manually Annotated Section of the UniProt KnowledgeBase: How to Use the Entry View. *Methods Mol Biol,* 1374**,** 23-54.

BRANT, J. O., LOPEZ, M. C., BAKER, H. V., BARBAZUK, W. B. & MADEN, M. 2015. A Comparative Analysis of Gene Expression Profiles during Skin Regeneration in Mus and Acomys. *PLoS One,* 10**,** e0142931.

CASTOR, C. W., PRINCE, R. K. & DORSTEWITZ, E. L. 1962. Characteristics of human "fibroblasts" cultivated in vitro from different anatomical sites. *Lab Invest,* 11**,** 703-13.

CHANG, C.-H., JIANG, T.-X., LIN, C.-M., BURRUS, L. W., CHUONG, C.-M. & WIDELITZ, R. 2004. Distinct Wnt members regulate the hierarchical morphogenesis of skin regions (spinal tract) and individual feathers. *Mechanisms of development,* 121**,** 157-171.

CHANG, H. Y., CHI, J. T., DUDOIT, S., BONDRE, C., VAN DE RIJN, M., BOTSTEIN, D. & BROWN, P. O. 2002. Diversity, topographic differentiation, and positional memory in human fibroblasts. *Proceedings of the National Academy of Sciences of the United States of America,* 99**,** 12877-12882.

CHEN, D., JARRELL, A., GUO, C., LANG, R. & ATIT, R. 2012. Dermal beta-catenin activity in response to epidermal Wnt ligands is required for fibroblast proliferation and hair follicle initiation. *Development (Cambridge, England),* 139**,** 1522-1533.

COLLINS, C. A., KRETZSCHMAR, K. & WATT, F. M. 2011. Reprogramming adult dermis to a neonatal state through epidermal activation of beta-catenin. *Development,* 138**,** 5189-99.

DHOUAILLY, D. 1973. Dermo-epidermal interactions between birds and mammals: differentiation of cutaneous appendages. *J Embryol Exp Morphol,* 30**,** 587-603.

DHOUAILLY, D. & SENGEL, P. 1972. Morphogenesis of feather and hair, studied by means of heterospecific associations of dermis and epidermis between chicken and mice. *Comptes rendus hebdomadaires des seances de l'Academie des sciences. Serie D: Sciences naturelles,* 275**,** 479-482.

DOANE, K. J. & BIRK, D. E. 1991. Fibroblasts retain their tissue phenotype when grown in three-dimensional collagen gels. *Exp Cell Res,* 195**,** 432-42.

DRISKELL, R. R., GIANGRECO, A., JENSEN, K. B., MULDER, K. W. & WATT, F. M. 2009. Sox2-positive dermal papilla cells specify hair follicle type in mammalian epidermis. *Development (Cambridge, England),* 136**,** 2815-2823.

DRISKELL, R. R., JAHODA, C. A. B., CHUONG, C.-M., WATT, F. M. & HORSLEY, V. 2014. Defining dermal adipose tissue. *Experimental dermatology,* 23**,** 629-631.

DRISKELL, R. R., LICHTENBERGER, B. M., HOSTE, E., KRETZSCHMAR, K., SIMONS, B. D., CHARALAMBOUS, M., FERRON, S. R., HERAULT, Y., PAVLOVIC, G., FERGUSON-SMITH, A. C. & WATT, F. M. 2013. Distinct fibroblast lineages determine dermal architecture in skin development and repair. *Nature,* 504**,** 277-281.

DRISKELL, R. R. & WATT, F. M. 2015. Understanding fibroblast heterogeneity in the skin. *Trends in cell biology,* 25**,** 92-99.

EKMAN, C., STENHOFF, J. & DAHLBACK, B. 2010. Gas6 is complexed to the soluble tyrosine kinase receptor Axl in human blood. *J Thromb Haemost,* 8**,** 838-44.

ENSHELL-SEIJFFERS, D., LINDON, C. & MORGAN, B. A. 2008. The serine protease Corin is a novel modifier of the Agouti pathway. *Development,* 135**,** 217-25.

EVANS, A. R. & PINZUR, M. S. 2005. Health-related quality of life of patients with diabetes and foot ulcers. *Foot Ankle Int,* 26**,** 32-7.

FINLEY, P. J., DECLUE, C. E., SELL, S. A., DEBARTOLO, J. M. & SHORNICK, L. P. 2016. Diabetic Wounds Exhibit Decreased Ym1 and Arginase Expression with Increased Expression of IL-17 and IL-20. *Adv Wound Care (New Rochelle),* 5**,** 486-494.

FRANCO-BARRAZA, J., BEACHAM, D. A., AMATANGELO, M. D. & CUKIERMAN, E. 2016. Preparation of Extracellular Matrices Produced by Cultured and Primary Fibroblasts. *Curr Protoc Cell Biol,* 71**,** 10 9 1-10 9 34.

GABBIANI, G., RYAN, G. B. & MAJNE, G. 1971. Presence of modified fibroblasts in granulation tissue and their possible role in wound contraction. *Experientia,* 27**,** 549-50.

GALLUCCI, R. M., SUGAWARA, T., YUCESOY, B., BERRYANN, K., SIMEONOVA, P. P., MATHESON, J. M. & LUSTER, M. I. 2001. Interleukin-6 treatment augments cutaneous wound healing in immunosuppressed mice. *J Interferon Cytokine Res,* 21**,** 603-9.

GHETTI, M., TOPOUZI, H., THEOCHARIDIS, G., PAPA, V., WILLIAMS, G., BONDIOLI, E., CENACCHI, G., CONNELLY, J. T. & HIGGINS, C. A. 2017. Sub-Populations of Dermal Skin Fibroblasts Secrete Distinct Extracellular Matrix: Implications for Using Skin Substitutes in the Clinic. *Br J Dermatol*.

GONZALES, K. A. U. & FUCHS, E. 2017. Skin and Its Regenerative Powers: An Alliance between Stem Cells and Their Niche. *Dev Cell,* 43**,** 387-401.

GOTTRUP, F., APELQVIST, J., PRICE, P. & EUROPEAN WOUND MANAGEMENT ASSOCIATION PATIENT OUTCOME, G. 2010. Outcomes in controlled and comparative studies on non-healing wounds: recommendations to improve the quality of evidence in wound management. *J Wound Care,* 19**,** 237-68.

GRECO, V., CHEN, T., RENDL, M., SCHOBER, M., PASOLLI, H. A., STOKES, N., DELA CRUZ-RACELIS, J. & FUCHS, E. 2009. A two-step mechanism for stem cell activation during hair regeneration. *Cell stem cell,* 4**,** 155-169.

GUEST, J. F., AYOUB, N., MCILWRAITH, T., UCHEGBU, I., GERRISH, A., WEIDLICH, D., VOWDEN, K. & VOWDEN, P. 2015. Health economic burden that wounds impose on the National Health Service in the UK. *BMJ Open,* 5.

GUO, S. & DIPIETRO, L. A. 2010. Factors affecting wound healing. *J Dent Res,* 89**,** 219-29.

GUO, X., HUTCHEON, A. E., MELOTTI, S. A., ZIESKE, J. D., TRINKAUS-RANDALL, V. & RUBERTI, J. W. 2007. Morphologic characterization of organized extracellular matrix deposition by ascorbic acid-stimulated human corneal fibroblasts. *Invest Ophthalmol Vis Sci,* 48**,** 4050-60.

GURTNER, G. C., WERNER, S., BARRANDON, Y. & LONGAKER, M. T. 2008. Wound repair and regeneration. *Nature,* 453**,** 314-21.

HANDJISKI, B. K., EICHMULLER, S., HOFMANN, U., CZARNETZKI, B. M. & PAUS, R. 1994. Alkaline phosphatase activity and localization during the murine hair cycle. *Br J Dermatol,* 131**,** 303-10.

HARPER, R. A. & GROVE, G. 1979. Human skin fibroblasts derived from papillary and reticular dermis: differences in growth potential in vitro. *Science (New York, N.Y.),* 204**,** 526-7.

HASEBE, Y., HASEGAWA, S., DATE, Y., NAKATA, S., YAGAMI, A., IWATA, Y., SUGIURA, K. & AKAMATSU, H. 2017. Localization of collagen type 5 in the papillary dermis and its role in maintaining stem cell functions. *J Dermatol Sci*.

HE, J., DONG, J., WANG, T., XU, H., DAI, C., MA, S. & ZHU, L. 2011. Bone morphogenetic protein receptor IB as a marker for enrichment of osteogenic precursor-like cells in human dermis. *Archives of Dermatological Research,* 303**,** 581-590.

HELDIN, C. H. & WESTERMARK, B. 1999. Mechanism of action and in vivo role of platelet-derived growth factor. *Physiol Rev,* 79**,** 1283-316.

HIGGINS, C. A., CHEN, J. C., CERISE, J. E., JAHODA, C. A. & CHRISTIANO, A. M. 2013. Microenvironmental reprogramming by three-dimensional culture enables dermal papilla cells to induce de novo human hair-follicle growth. *Proc Natl Acad Sci U S A,* 110**,** 19679-88.

HIGGINS, C. A., RICHARDSON, G. D., FERDINANDO, D., WESTGATE, G. E. & JAHODA, C. A. 2010. Modelling the hair follicle dermal papilla using spheroid cell cultures. *Exp Dermatol,* 19**,** 546-8.

HIGGINS, C. A., WESTGATE, G. E. & JAHODA, C. A. 2009. From telogen to exogen: mechanisms underlying formation and subsequent loss of the hair club fiber. *J Invest Dermatol,* 129**,** 2100-8.

HINZ, B. 2010. The myofibroblast: paradigm for a mechanically active cell. *J Biomech,* 43**,** 146-55.

HSU, Y. C., LI, L. & FUCHS, E. 2014. Emerging interactions between skin stem cells and their niches. *Nat Med,* 20**,** 847-56.

HU, M. S. & LONGAKER, M. T. 2016. Dipeptidyl Peptidase-4, Wound Healing, Scarring, and Fibrosis. *Plastic and reconstructive surgery,* 138**,** 1026-1031.

HUANG, H., ZHANG, Q., LIU, J., HAO, H., JIANG, C. & HAN, W. 2017. Granulocyte-Colony Stimulating Factor (G-CSF) Accelerates Wound Healing in Hemorrhagic Shock Rats by Enhancing Angiogenesis and Attenuating Apoptosis. *Med Sci Monit,* 23**,** 2644-2653.

HUH, S. H., NARHI, K., LINDFORS, P. H., HAARA, O., YANG, L., ORNITZ, D. M. & MIKKOLA, M. L. 2013. Fgf20 governs formation of primary and secondary dermal condensations in developing hair follicles. *Genes Dev,* 27**,** 450-8.

JACOBSON, C. M. 1966. A comparative study of the mechanisms by which X-irradiation and genetic mutation cause loss of vibrissae in embryo mice. *Journal of embryology and experimental morphology,* 16**,** 369-379.

JAHODA, C. A., HORNE, K. A., MAUGER, A., BARD, S. & SENGEL, P. 1992. Cellular and extracellular involvement in the regeneration of the rat lower vibrissa follicle. *Development,* 114**,** 887-97.

JAHODA, C. A. & REYNOLDS, A. J. 2001. Hair follicle dermal sheath cells: unsung participants in wound healing. *Lancet,* 358**,** 1445-8.

JAHODA, C. A., REYNOLDS, A. J., CHAPONNIER, C., FORESTER, J. C. & GABBIANI, G. 1991. Smooth muscle alpha-actin is a marker for hair follicle dermis in vivo and in vitro. *Journal of cell science,* 99 (Pt 3)**,** 627-636.

JAHODA, C. A., REYNOLDS, A. J. & OLIVER, R. F. 1993. Induction of hair growth in ear wounds by cultured dermal papilla cells. *The Journal of investigative dermatology,* 101**,** 584-590.

JAHODA, C. A. B., HORNE, K. A. & OLIVER, R. F. 1984. Induction of hair growth by implantation of cultured dermal papilla cells. *Nature,* 311**,** 560-562.

JAHODA, C. A. B. & REYNOLDS, A. J. 1993. Dermal-Epidermal Interactions-Follicle Derived Cell Populations in the Study of Hair-Growth Mechanisms. *J Investig Dermatol,* 101**,** 33S-38S.

JAHODA, C. A. B., WHITEHOUSE, J., REYNOLDS, A. J. & HOLE, N. 2003. Hair follicle dermal cells differentiate into adipogenic and osteogenic lineages. *Experimental dermatology,* 12**,** 849-859.

JANSON, D., SAINTIGNY, G., MAHE, C. & EL GHALBZOURI, A. 2013. Papillary fibroblasts differentiate into reticular fibroblasts after prolonged in vitro culture. *Experimental dermatology,* 22**,** 48-53.

JANSON, D. G., SAINTIGNY, G., VAN ADRICHEM, A., MAHE, C. & EL GHALBZOURI, A. 2012. Different Gene Expression Patterns in Human Papillary and Reticular Fibroblasts. *J Invest Dermatol,* 132**,** 2565-2572.

JIANG, B., LI, Y., LIANG, P., LIU, Y., HUANG, X., TONG, Z., ZHANG, P., HUANG, X., LIU, Y. & LIU, Z. 2015. Nucleolin enhances the proliferation and migration of heat-denatured human dermal fibroblasts. *Wound repair and regeneration : official publication of the Wound Healing Society [and] the European Tissue Repair Society,* 23**,** 807-818.

JIMENEZ, F., GARDE, C., POBLET, E., JIMENO, B., ORTIZ, J., MARTINEZ, M. L., GUTIERREZ-RIVERA, A., PEREZ-LOPEZ, V., ETXANIZ, U., NAVEDA, C., HIGUERA, J. L., EGUES, N., ESCARIO, E. & IZETA, A. 2012. A pilot clinical study of hair grafting in chronic leg ulcers. *Wound Repair Regen,* 20**,** 806-14.

JIMENEZ, F., POBLET, E. & IZETA, A. 2015. Reflections on how wound healing-promoting effects of the hair follicle can be translated into clinical practice. *Exp Dermatol,* 24**,** 91-4.

JOOST, S., ZEISEL, A., JACOB, T., SUN, X., LA MANNO, G., LÖNNERBERG, P., LINNARSSON, S. & KASPER, M. 2017. Single-Cell Transcriptomics Reveals that Differentiation and Spatial Signatures Shape Epidermal and Hair Follicle Heterogeneity. *Cell Systems,* 3**,** 221-237.e9.

KAISER, S., SCHIRMACHER, P., PHILIPP, A., PROTSCHKA, M., MOLL, I., NICOL, K. & BLESSING, M. 1998. Induction of bone morphogenetic protein-6 in skin wounds.

Delayed reepitheliazation and scar formation in BMP-6 overexpressing transgenic mice. *J Invest Dermatol,* 111**,** 1145-52.

KIOKA, N., ITO, T., YAMASHITA, H., UEKAWA, N., UMEMOTO, T., MOTOYOSHI, S., IMAI, H., TAKAHASHI, K., WATANABE, H., YAMADA, M. & UEDA, K. 2010. Crucial role of vinexin for keratinocyte migration in vitro and epidermal wound healing in vivo. *Exp Cell Res,* 316**,** 1728-38.

KOLUMAM, G., WU, X., LEE, W. P., HACKNEY, J. A., ZAVALA-SOLORIO, J., GANDHAM, V., DANILENKO, D. M., ARORA, P., WANG, X. & OUYANG, W. 2017. IL-22R Ligands IL-20, IL-22, and IL-24 Promote Wound Healing in Diabetic db/db Mice. *PLoS One,* 12**,** e0170639.

KORSHUNOV, V. A. 2012. Axl-dependent signalling: a clinical update. *Clin Sci (Lond),* 122**,** 361-8.

LAURENS, N., KOOLWIJK, P. & DE MAAT, M. P. 2006. Fibrin structure and wound healing. *J Thromb Haemost,* 4**,** 932-9.

LEE, D. Y. & CHO, K. H. 2005. The effects of epidermal keratinocytes and dermal fibroblasts on the formation of cutaneous basement membrane in three-dimensional culture systems. *Arch Dermatol Res,* 296**,** 296-302.

LEIROS, G. J., KUSINSKY, A. G., DRAGO, H., BOSSI, S., STURLA, F., CASTELLANOS, M. L., STELLA, I. Y. & BALANA, M. E. 2014. Dermal papilla cells improve the wound healing process and generate hair bud-like structures in grafted skin substitutes using hair follicle stem cells. *Stem Cells Transl Med,* 3**,** 1209-19.

LI, B. & WANG, J. H. 2011. Fibroblasts and myofibroblasts in wound healing: force generation and measurement. *J Tissue Viability,* 20**,** 108-20.

LI, Y.-H., ZHANG, K., YE, J.-X., LIAN, X.-H. & YANG, T. 2011. Wnt10b promotes growth of hair follicles via a canonical Wnt signalling pathway. *Clinical and experimental dermatology,* 36**,** 534-540.

LIANG, C. C., PARK, A. Y. & GUAN, J. L. 2007. In vitro scratch assay: a convenient and inexpensive method for analysis of cell migration in vitro. *Nat Protoc,* 2**,** 329-33.

LIN, Z. Q., KONDO, T., ISHIDA, Y., TAKAYASU, T. & MUKAIDA, N. 2003. Essential involvement of IL-6 in the skin wound-healing process as evidenced by delayed wound healing in IL-6-deficient mice. *J Leukoc Biol,* 73**,** 713-21.

LYONS, K. M., PELTON, R. W. & HOGAN, B. L. 1989. Patterns of expression of murine Vgr-1 and BMP-2a RNA suggest that transforming growth factor-beta-like genes coordinately regulate aspects of embryonic development. *Genes Dev,* 3**,** 1657-68.

MCDONNELL, M. A., LAW, B. K., SERRA, R. & MOSES, H. L. 2001. Antagonistic effects of TGFbeta1 and BMP-6 on skin keratinocyte differentiation. *Exp Cell Res,* 263**,** 265-73.

MCFARLAND-MANCINI, M. M., FUNK, H. M., PALUCH, A. M., ZHOU, M., GIRIDHAR, P. V., MERCER, C. A., KOZMA, S. C. & DREW, A. F. 2010. Differences in wound healing in mice with deficiency of IL-6 versus IL-6 receptor. *J Immunol,* 184**,** 7219-28.

MCGRORY, K., FLAITZ, C. M. & KLEIN, J. R. 2004. Chemokine changes during oral wound healing. *Biochem Biophys Res Commun,* 324**,** 317-20.

MESSENGER, A. G., ELLIOTT, K., WESTGATE, G. E. & GIBSON, W. T. 1991. Distribution of extracellular matrix molecules in human hair follicles. *Ann N Y Acad Sci,* 642**,** 253-62.

MILLAR, S. 2002. Molecular mechanisms regulating hair follicle development. *Journal of Investigative Dermatology***,** 216-225.

MINE, S., NO, F. & PAGEON, H. 2008. Aging alters functionally human dermal papillary fibroblasts but not reticular fibroblasts: a new view of skin morphogenesis and aging. *PLoS One,* 3**,** e4066.

MOHAN, V. K. 2007. Recombinant human epidermal growth factor (REGEN-D 150): effect on healing of diabetic foot ulcers. *Diabetes Res Clin Pract,* 78**,** 405-11.

NAGAI, M. K. & EMBIL, J. M. 2002. Becaplermin: recombinant platelet derived growth factor, a new treatment for healing diabetic foot ulcers. *Expert Opin Biol Ther,* 2**,** 211-8.

NANNEY, L. B., STOSCHECK, C. M., MAGID, M. & KING, L. E., JR. 1986. Altered [125I]epidermal growth factor binding and receptor distribution in psoriasis. *J Invest Dermatol,* 86**,** 260-5.

O'BRYAN, J. P., FRIDELL, Y. W., KOSKI, R., VARNUM, B. & LIU, E. T. 1995. The transforming receptor tyrosine kinase, Axl, is post-translationally regulated by proteolytic cleavage. *J Biol Chem,* 270**,** 551-7.

O'BRYAN, J. P., FRYE, R. A., COGSWELL, P. C., NEUBAUER, A., KITCH, B., PROKOP, C., ESPINOSA, R., 3RD, LE BEAU, M. M., EARP, H. S. & LIU, E. T. 1991. axl, a transforming gene isolated from primary human myeloid leukemia cells, encodes a novel receptor tyrosine kinase. *Mol Cell Biol,* 11**,** 5016-31.

PABLOS, J. L., EVERETT, E. T., LEROY, E. C. & NORRIS, J. S. 1998. Thrombospondin 1 is expressed by mesenchymal cells in mouse post-natal skin and hair follicle development. *Histochem J,* 30**,** 461-5.

PAPANAS, N. & MALTEZOS, E. 2007. Growth factors in the treatment of diabetic foot ulcers: new technologies, any promises? *Int J Low Extrem Wounds,* 6**,** 37-53.

PARK, S., GONZALEZ, D. G., GUIRAO, B., BOUCHER, J. D., COCKBURN, K., MARSH, E. D., MESA, K. R., BROWN, S., ROMPOLAS, P., HABERMAN, A. M., BELLAICHE, Y. & GRECO, V. 2017. Tissue-scale coordination of cellular behaviour promotes epidermal wound repair in live mice. *Nat Cell Biol,* 19**,** 155-163.

PEARTON, D. J., YANG, Y. & DHOUAILLY, D. 2005. Transdifferentiation of corneal epithelium into epidermis occurs by means of a multistep process triggered by dermal developmental signals. *Proceedings of the National Academy of Sciences of the United States of America,* 102**,** 3714-3719.

PFLIEGER, D., CHABANE, S., GAILLARD, O., BERNARD, B. A., DUCOROY, P., ROSSIER, J. & VINH, J. 2006. Comparative proteomic analysis of extracellular matrix proteins secreted by two types of skin fibroblasts. *Proteomics,* 6**,** 5868-5879.

PHILIPPEOS, C., TELERMAN, S., OULES, B., PISCO, A. O., SHAW, T. J., ELGUETA, R., LOMBARDI, G., DRISKELL, R. R., SOLDIN, M., LYNCH, M. D. & WATT, F. M. 2018. Spatial and single-cell transcriptional profiling identifies functionally distinct human dermal fibroblast subpopulations. *J Invest Dermatol*.

PLIKUS, M. V. 2012. New activators and inhibitors in the hair cycle clock: targeting stem cells' state of competence. *The Journal of investigative dermatology.*

PLIKUS, M. V., BAKER, R. E., CHEN, C.-C., FARE, C., DE LA CRUZ, D., ANDL, T., MAINI, P. K., MILLAR, S. E., WIDELITZ, R. & CHUONG, C.-M. 2011. Self-organizing and stochastic behaviors during the regeneration of hair stem cells. *Science (New York, N.Y.),* 332**,** 586-589.

PLIKUS, M. V., GUERRERO-JUAREZ, C. F., ITO, M., LI, Y. R., DEDHIA, P. H., ZHENG, Y., SHAO, M., GAY, D. L., RAMOS, R., HSI, T. C., OH, J. W., WANG, X., RAMIREZ, A., KONOPELSKI, S. E., ELZEIN, A., WANG, A., SUPAPANNACHART, R. J., LEE, H. L., LIM, C. H., NACE, A., GUO, A., TREFFEISEN, E., ANDL, T., RAMIREZ, R. N., MURAD, R., OFFERMANNS, S., METZGER, D., CHAMBON, P., WIDGEROW, A. D., TUAN, T. L., MORTAZAVI, A., GUPTA, R. K., HAMILTON, B. A., MILLAR, S. E., SEALE, P., PEAR, W. S., LAZAR, M. A. & COTSARELIS, G. 2017. Regeneration of fat cells from myofibroblasts during wound healing. *Science,* 355**,** 748-752.

PRICE, V. H. 2003. Androgenetic alopecia in women. *J Investig Dermatol Symp Proc,* 8**,** 24-7.

RAHMANI, W., ABBASI, S., HAGNER, A., RAHARJO, E., KUMAR, R., HOTTA, A., MAGNESS, S., METZGER, D. & BIERNASKIE, J. 2014. Hair follicle dermal stem cells regenerate the dermal sheath, repopulate the dermal papilla, and modulate hair type. *Dev Cell,* 31**,** 543-58.

REDD, M. J., COOPER, L., WOOD, W., STRAMER, B. & MARTIN, P. 2004. Wound healing and inflammation: embryos reveal the way to perfect repair. *Philos Trans R Soc Lond B Biol Sci,* 359**,** 777-84.

RENDL, M., POLAK, L. & FUCHS, E. 2008a. BMP signaling in dermal papilla cells is required for their hair follicle-inductive properties. *Genes and Development,* 22**,** 543-557.

RENDL, M., POLAK, L. & FUCHS, E. 2008b. BMP signaling in dermal papilla cells is required for their hair follicle-inductive properties. *Genes Dev,* 22**,** 543-57.

REYNOLDS, A. J., LAWRENCE, C., CSERHALMI-FRIEDMAN, P. B., CHRISTIANO, A. M. & JAHODA, C. A. 1999. Trans-gender induction of hair follicles. *Nature,* 402**,** 33-4.

REZZA, A., WANG, Z., SENNETT, R., QIAO, W., WANG, D., HEITMAN, N., MOK, K. W., CLAVEL, C., YI, R., ZANDSTRA, P., MA'AYAN, A. & RENDL, M. 2016. Signaling Networks among Stem Cell Precursors, Transit-Amplifying Progenitors, and their Niche in Developing Hair Follicles. *Cell reports,* 14**,** 3001-3018.

RHEINWALD, J. G. & GREEN, H. 1975. Seria cultivation of strains of human epidemal keratinocytes: the formation keratinizin colonies from single cell is. *Cell,* 6**,** 331-343.

RHEINWALD, J. G. & GREEN, H. 1977. Epidermal growth factor and the multiplication of cultured human epidermal keratinocytes. *Nature,* 265**,** 421-4.

RICHARDSON, G. D., ARNOTT, E. C., WHITEHOUSE, C. J., LAWRENCE, C. M., HOLE, N. & JAHODA, C. A. B. 2005. Cultured cells from the adult human hair follicle dermis can be directed toward adipogenic and osteogenic differentiation. *The Journal of investigative dermatology.*

RINKEVICH, Y., WALMSLEY, G. G., HU, M. S., MAAN, Z. N., NEWMAN, A. M., DRUKKER, M., JANUSZYK, M., KRAMPITZ, G. W., GURTNER, G. C., LORENZ, H. P., WEISSMAN, I. L. & LONGAKER, M. T. 2015. Identification and isolation of a dermal lineage with intrinsic fibrogenic potential. *Science,* 348.

RINN, J. L., BONDRE, C., GLADSTONE, H. B., BROWN, P. O. & CHANG, H. Y. 2006. Anatomic demarcation by positional variation in fibroblast gene expression programs. *PLoS genetics,* 2**,** e119.

ROCKEY, D. C., WEYMOUTH, N. & SHI, Z. 2013. Smooth muscle alpha actin (Acta2) and myofibroblast function during hepatic wound healing. *PLoS One,* 8**,** e77166.

ROMPOLAS, P., DESCHENE, E. R., ZITO, G., GONZALEZ, D. G., SAOTOME, I., HABERMAN, A. M. & GRECO, V. 2012. Live imaging of stem cell and progeny behaviour in physiological hair-follicle regeneration. *Nature,* 487**,** 496-499.

SCHAFER, I. A., PANDY, M., FERGUSON, R. & DAVIS, B. R. 1985a. Comparative observation of fibroblasts derived from the papillary and reticular dermis of infants and adults: growth kinetics, packing density at confluence and surface morphology. *Mech Ageing Dev,* 31**,** 275-93.

SCHAFER, I. A., PANDY, M., FERGUSON, R. & DAVIS, B. R. 1985b. Comparative observation of fibroblasts derived from the papillary and reticular dermis of infants and adults: Growth kinetics, packing density at confluence and surface morphology. *Mechanisms of Ageing and Development,* 31**,** 275-293.

SCHONHERR, E., BEAVAN, L. A., HAUSSER, H., KRESSE, H. & CULP, L. A. 1993. Differences in decorin expression by papillary and reticular fibroblasts in vivo and in vitro. *Biochem J,* 290 (Pt 3)**,** 893-9.

SCHULTZ, G. S. & WYSOCKI, A. 2009. Interactions between extracellular matrix and growth factors in wound healing. *Wound Repair Regen,* 17**,** 153-62.

SEIFERT, A. W., KIAMA, S. G., SEIFERT, M. G., GOHEEN, J. R., PALMER, T. M. & MADEN, M. 2012. Skin shedding and tissue regeneration in African spiny mice (Acomys). *Nature,* 489**,** 561-5.

SENNETT, R., WANG, Z., REZZA, A., GRISANTI, L., ROITERSHTEIN, N., SICCHIO, C., MOK, K. W., HEITMAN, N. J., CLAVEL, C., MA'AYAN, A. & RENDL, M. 2015. An Integrated Transcriptome Atlas of Embryonic Hair Follicle Progenitors, Their Niche, and the Developing Skin. *Developmental cell,* 34**,** 577-591.

SHAW, T. J. & MARTIN, P. 2009. Wound repair at a glance. *J Cell Sci,* 122**,** 3209-13.

SOMA, T., TAJIMA, M. & KISHIMOTO, J. 2005. Hair cycle-specific expression of versican in human hair follicles. *J Dermatol Sci,* 39**,** 147-54.

SORRELL, J. M., BABER, M. A. & CAPLAN, A. I. 2004. Site-matched papillary and reticular human dermal fibroblasts differ in their release of specific growth factors/cytokines and in their interaction with keratinocytes. *Journal of cellular physiology,* 200**,** 134-145.

SORRELL, J. M., BABER, M. A. & CAPLAN, A. I. 2007. Clonal characterization of fibroblasts in the superficial layer of the adult human dermis. *Cell Tissue Res,* 327**,** 499-510.

SORRELL, J. M., BABER, M. A. & CAPLAN, A. I. 2008. Human dermal fibroblast subpopulations; differential interactions with vascular endothelial cells in coculture: nonsoluble factors in the extracellular matrix influence interactions. *Wound Repair Regen,* 16**,** 300-9.

SORRELL, J. M. & CAPLAN, A. I. 2004. Fibroblast heterogeneity: more than skin deep. *J Cell Sci,* 117**,** 667-75.

SRIRAM, G., BIGLIARDI, P. L. & BIGLIARDI-QI, M. 2015. Fibroblast heterogeneity and its implications for engineering organotypic skin models in vitro. *European journal of cell biology,* 94**,** 483-512.

STÅHL, P. L., SALMÉN, F., VICKOVIC, S., LUNDMARK, A., NAVARRO, J. F., MAGNUSSON, J., GIACOMELLO, S., ASP, M., WESTHOLM, J. O., HUSS, M., MOLLBRINK, A., LINNARSSON, S., CODELUPPI, S., BORG, Å., PONTÉN, F., COSTEA, P. I., SAHLÉN, P., MULDER, J., BERGMANN, O., LUNDEBERG, J. & FRISÉN, J. 2016. Visualization and analysis of gene expression in tissue sections by spatial transcriptomics. *Science,* 353**,** 78-82.

STOJADINOVIC, O. & TOMIC-CANIC, M. 2013. Human ex vivo wound healing model. *Methods Mol Biol,* 1037**,** 255-64.

TAJRISHI, M. M., TUTEJA, R. & TUTEJA, N. 2011. Nucleolin: The most abundant multifunctional phosphoprotein of nucleolus. *Communicative & integrative biology,* 4**,** 267-275.

THEOCHARIDIS, G., DRYMOUSSI, Z., KAO, A. P., BARBER, A. H., LEE, D. A., BRAUN, K. M. & CONNELLY, J. T. 2016. Type VI Collagen Regulates Dermal Matrix Assembly and Fibroblast Motility. *The Journal of investigative dermatology,* 136**,** 74-83.

THULABANDU, V., CHEN, D. & ATIT, R. P. 2017. Dermal fibroblast in cutaneous development and healing. *Wiley Interdiscip Rev Dev Biol*.

TOBIN, D. J. 2017. Introduction to skin aging. *J Tissue Viability,* 26**,** 37-46.

TOPOUZI, H. & HIGGINS, C. A. 2016. Changing faces: Can a new identity stop balding? *Experimental dermatology*.

TOPOUZI, H., LOGAN, N. J., WILLIAMS, G. & HIGGINS, C. A. 2017. Methods for the isolation and 3D culture of dermal papilla cells from human hair follicles. *Exp Dermatol,* 26**,** 491-496.

TRACY, L. E., MINASIAN, R. A. & CATERSON, E. J. 2016. Extracellular Matrix and Dermal Fibroblast Function in the Healing Wound. *Advances in wound care,* 5**,** 119-136.

TURKSEN, K., KUPPER, T., DEGENSTEIN, L., WILLIAMS, I. & FUCHS, E. 1992. Interleukin 6: insights to its function in skin by overexpression in transgenic mice. *Proc Natl Acad Sci U S A,* 89**,** 5068-72.

VAN AMERONGEN, R. & NUSSE, R. 2009. Towards an integrated view of Wnt signaling in development. *Development (Cambridge, England),* 136**,** 3205-14.

VOURI, M., CROUCHER, D. R., KENNEDY, S. P., AN, Q., PILKINGTON, G. J. & HAFIZI, S. 2016. Axl-EGFR receptor tyrosine kinase hetero-interaction provides EGFR with access to pro-invasive signalling in cancer cells. *Oncogenesis,* 5**,** e266.

WALTER, M. N., WRIGHT, K. T., FULLER, H. R., MACNEIL, S. & JOHNSON, W. E. 2010. Mesenchymal stem cell-conditioned medium accelerates skin wound healing: an in vitro study of fibroblast and keratinocyte scratch assays. *Exp Cell Res,* 316**,** 1271-81.

WANG, T., HE, J., ZHANG, Y., SHI, W., DONG, J., PEI, M. & ZHU, L. 2016. A Selective Cell Population From Dermis Strengthens Bone Regeneration. *Stem cells translational medicine*.

WANG, X., WANG, L., MIAO, L., ZHAO, R., WU, Y. & KONG, X. 2015. CC-chemokine receptor 7 and its ligand CCL19 promote mitral valve interstitial cell migration and repair. *J Biomed Res,* 29**,** 456-64.

WATT, F. M. & COLLINS, C. A. 2008. Role of beta-catenin in epidermal stem cell expansion, lineage selection, and cancer. *Cold Spring Harb Symp Quant Biol,* 73**,** 503-12.

WERNER, S. & GROSE, R. 2003. Regulation of Wound Healing by Growth Factors and Cytokines. *Physiol Rev,* 83**,** 835-870.

WERNER, S., KRIEG, T. & SMOLA, H. 2007a. Keratinocyte – Fibroblast Interactions in Wound Healing. 127**,** 998-1008.

WERNER, S., KRIEG, T. & SMOLA, H. 2007b. Keratinocyte-fibroblast interactions in wound healing. *J Invest Dermatol,* 127**,** 998-1008.

WERNER, S., PETERS, K. G., LONGAKER, M. T., FULLER-PACE, F., BANDA, M. J. & WILLIAMS, L. T. 1992. Large induction of keratinocyte growth factor expression in the dermis during wound healing. *Proc Natl Acad Sci U S A,* 89**,** 6896-900.

WERNER, S. & SMOLA, H. 2001. Paracrine regulation of keratinocyte proliferation and differentiation. *Trends Cell Biol,* 11**,** 143-6.

WONG, V. W., SORKIN, M., GLOTZBACH, J. P., LONGAKER, M. T. & GURTNER, G. C. 2011. Surgical approaches to create murine models of human wound healing. *J Biomed Biotechnol,* 2011**,** 969618.

WOOD, S., JAYARAMAN, V., HUELSMANN, E. J., BONISH, B., BURGAD, D., SIVARAMAKRISHNAN, G., QIN, S., DIPIETRO, L. A., ZLOZA, A., ZHANG, C. & SHAFIKHANI, S. H. 2014. Pro-inflammatory chemokine CCL2 (MCP-1) promotes healing in diabetic wounds by restoring the macrophage response. *PLoS One,* 9**,** e91574.

XUE, M. & JACKSON, C. J. 2015. Extracellular Matrix Reorganization During Wound Healing and Its Impact on Abnormal Scarring. *Adv Wound Care (New Rochelle),* 4**,** 119-136.

YAMAGUCHI, Y., ITAMI, S., TARUTANI, M., HOSOKAWA, K., MIURA, H. & YOSHIKAWA, K. 1999. Regulation of keratin 9 in nonpalmoplantar keratinocytes by palmoplantar fibroblasts through epithelial-mesenchymal interactions. *J Invest Dermatol,* 112**,** 483-8.

YANG, H., ADAM, R. C., GE, Y., HUA, Z. L. & FUCHS, E. 2017. Epithelial-Mesenchymal Micro-niches Govern Stem Cell Lineage Choices. *Cell,* 169**,** 483-496.e13.

ZOMER, H. D. & TRENTIN, A. G. 2018. Skin wound healing in humans and mice: Challenges in translational research. *J Dermatol Sci,* 90**,** 3-12.

ZUK, P. A., ZHU, M., MIZUNO, H., HUANG, J., FUTRELL, J. W., KATZ, A. J., BENHAIM, P., LORENZ, H. P. & HEDRICK, M. H. 2001. Multilineage cells from human adipose tissue: implications for cell-based therapies. *Tissue Eng,* 7**,** 211-28.

Appendix

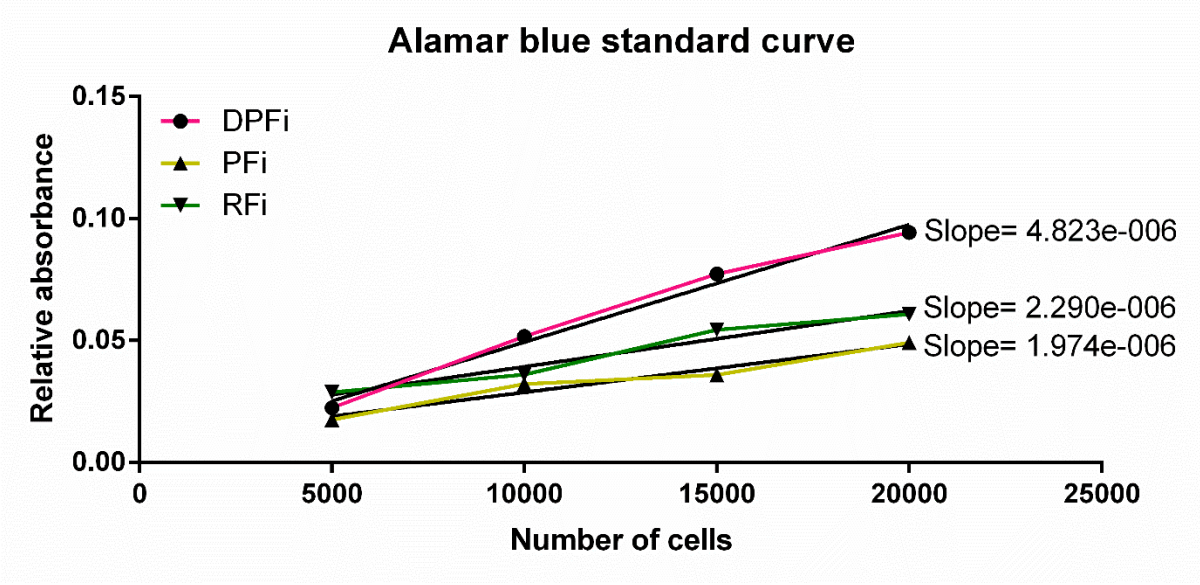


Figure A.1. Alamar blue standard curve graph.

The graph shows the relative absorbance of 5000, 10000, 15000 and 20000 DPFi, PFi and RFi cells. The linear regression was calculated for each population and the slope of the line is shown on the graph. Using this slope, the relative absorbance of the cells was normalised as demonstrated in figure 2.4.5.

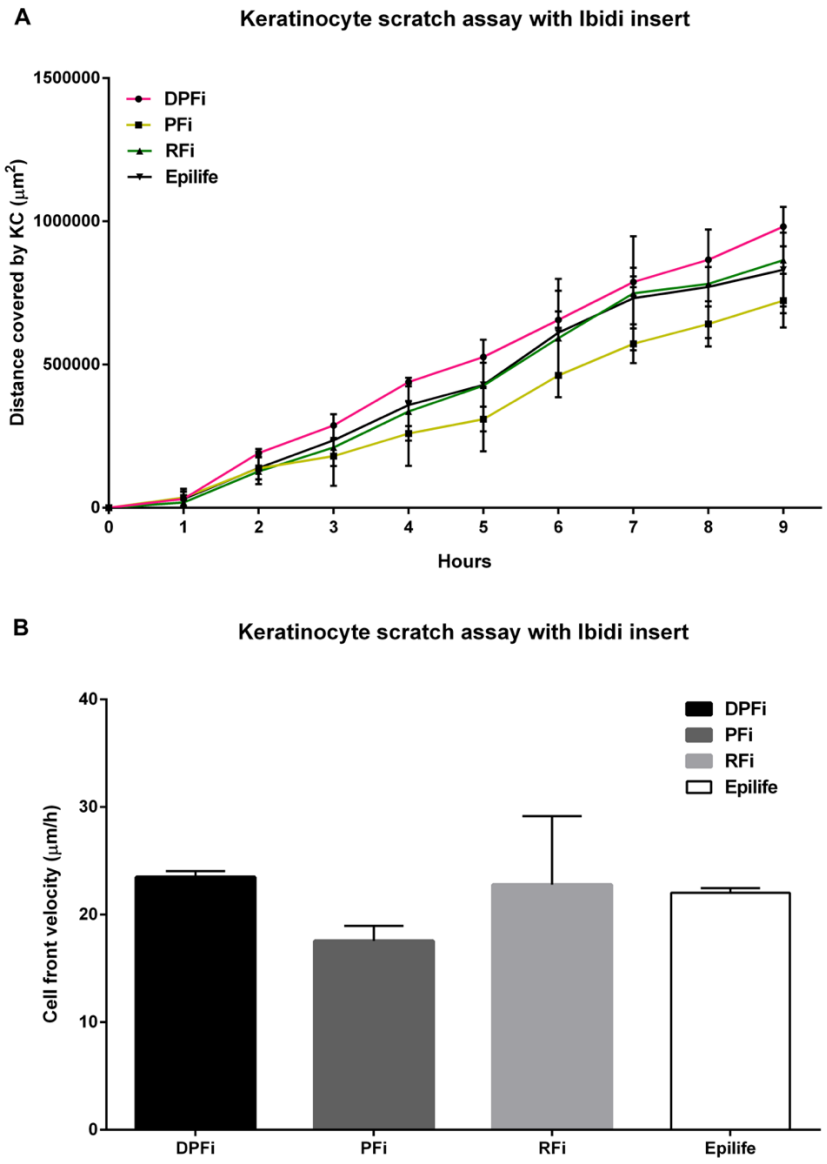


Figure A.2. Analysis of the KC wound healing assay of the second patient using the Ibidi inserts. (A) The graph shows the distance covered by the KC in µm^2 when incubated DPFi CM (pink), PFi CM (gold), RFi CM (green) and Epilife media (black). (B) The bar chart shows the cell front velocity in µm/h after the KC were cultured for 10 hours in four different conditions; DPFi CM, PFi CM, RFi CM and Epilife media. This figure shows a representative result from N=1 CM and N=1 KC. N=2 (P2D and P3A) and n=3 of the CM were used in this experiment with N=1 (P3B) KC. Results were analysed using two-way Anova and the error bars represent standard error. Significance is displayed in the graph ($P \leq 0.05$ = *, $P \leq 0.01$ = **, $P \leq 0.001$ =***, $P \leq 0.0001$ =****).

Table A.1. Fold change of 2577 genes in the KC differentially regulated across all conditions.

Probe Set ID	Gene Symbol	FC AXL vs DPFi CM	FC AXL vs Epilife	FC DPFi CM vs Epilife
AFFX-HUMISGF3A/M97935_MA_at	STAT1	1.10	-2.03	-2.24
1405_i_at	CCL5	-1.00	-4.04	-4.03
200659_s_at	PHB	1.42	2.02	1.42
200676_s_at	UBE2L3	-1.02	2.61	2.65
200685_at	SRSF11	-1.02	2.97	3.02
200730_s_at	PTP4A1	-1.46	-2.71	-1.86
200768_s_at	MAT2A	1.05	3.29	3.13
200811_at	CIRBP	1.13	-1.88	-2.13
200813_s_at	PAFAH1B1	1.06	2.06	1.94
200816_s_at	PAFAH1B1	1.09	2.56	2.35
200855_at	NCOR1	-1.11	2.09	2.32
200856_x_at	NCOR1	-1.22	2.49	3.04
200880_at	DNAJA1	1.25	2.11	1.69
200898_s_at	MGEA5	1.15	-3.85	-4.41
200912_s_at	EIF4A2	1.01	-2.26	-2.28
201008_s_at	LOC101060503///TXNIP	1.13	-4.69	-5.31
201009_s_at	LOC101060503///TXNIP	1.20	-5.61	-6.71
201010_s_at	LOC101060503///TXNIP	1.36	-3.79	-5.15
201080_at	PIP4K2B	1.13	2.35	2.08
201129_at	SRSF7	1.22	-1.83	-2.23
201158_at	NMT1	1.36	2.67	1.96
201159_s_at	NMT1	1.26	3.02	2.40
201169_s_at	BHLHE40	-1.09	-2.26	-2.07
201170_s_at	BHLHE40	-1.36	-2.29	-1.69
201182_s_at	CHD4	-1.24	1.90	2.36
201208_s_at	TNFAIP1	-1.02	-2.02	-1.98
201213_at	PPP1R7	1.01	2.59	2.57
201230_s_at	ARIH2	1.12	2.25	2.01
201324_at	EMP1	-1.35	-2.02	-1.50
201325_s_at	EMP1	-1.74	-2.62	-1.51
201337_s_at	VAMP3	-1.17	-2.19	-1.87
201355_s_at	BAZ2A	-1.06	1.95	2.07
201383_s_at	NBR1	1.24	-2.26	-2.80
201423_s_at	CUL4A	-1.02	2.11	2.15
201424_s_at	CUL4A	-1.42	1.94	2.75
201448_at	TIA1	-1.33	2.11	2.80
201449_at	TIA1	-1.17	2.31	2.71
201471_s_at	SQSTM1	1.01	-2.33	-2.36
201556_s_at	VAMP2	-1.31	-3.90	-2.98
201557_at	VAMP2	-1.05	-2.89	-2.77

201744_s_at	LUM	-1.09	-8.75	-8.06
201748_s_at	SAFB	1.09	3.06	2.81
201772_at	AZIN1	-1.30	-2.43	-1.87
201824_at	RNF14	-1.33	-2.23	-1.67
201846_s_at	RYBP	-1.09	-2.11	-1.94
201904_s_at	CTDSPL	-1.01	2.07	2.09
201906_s_at	CTDSPL	1.16	3.17	2.73
201928_at	PKP4	-1.18	1.95	2.29
201959_s_at	MYCBP2	1.02	3.68	3.60
201960_s_at	MYCBP2	1.10	3.59	3.25
201962_s_at	RNF41	-1.24	1.89	2.34
202014_at	PPP1R15A	-1.29	-3.36	-2.60
202050_s_at	ZMYM4	-1.19	1.93	2.30
202051_s_at	ZMYM4	-1.24	2.06	2.55
202057_at	KPNA1	-1.07	3.61	3.87
202098_s_at	PRMT2	1.29	3.72	2.89
202111_at	SLC4A2	-1.02	2.09	2.13
202126_at	PRPF4B	-1.10	1.98	2.19
202129_s_at	RIOK3	-1.01	-2.03	-2.01
202134_s_at	WWTR1	-1.11	-2.18	-1.95
202137_s_at	ZMYND11	-1.58	1.55	2.46
202172_at	VEZF1	-1.07	2.14	2.28
202206_at	ARL4C	-1.71	2.48	4.24
202207_at	ARL4C	-1.52	2.30	3.50
202208_s_at	ARL4C	-1.31	2.43	3.18
202220_at	KIAA0907	-1.25	4.85	6.07
202256_at	CD2BP2	1.40	2.23	1.59
202294_at	STAG1	-1.11	1.91	2.11
202319_at	SENP6	-1.34	2.35	3.16
202342_s_at	TRIM2	-1.24	2.06	2.56
202349_at	TOR1A	-1.02	2.02	2.07
202353_s_at	PSMD12	-1.18	2.16	2.55
202357_s_at	CFB	-1.02	-3.21	-3.16
202360_at	MAML1	-1.23	1.66	2.04
202379_s_at	NKTR	1.50	2.15	1.44
202380_s_at	NKTR	1.11	3.31	2.98
202388_at	RGS2	1.81	-1.64	-2.97
202390_s_at	HTT	1.24	2.92	2.36
202396_at	TCERG1	-1.14	1.76	2.01
202426_s_at	RXRA	1.30	-2.51	-3.25
202449_s_at	RXRA	1.11	2.58	2.32
202451_at	GTF2H1	1.07	4.11	3.86
202454_s_at	ERBB3	-1.33	1.92	2.55
202469_s_at	CPSF6	1.01	2.54	2.51

202478_at	TRIB2	-1.11	4.89	5.45
202498_s_at	SLC2A3	-1.91	-4.83	-2.53
202499_s_at	SLC2A3	-1.47	-3.81	-2.59
202510_s_at	TNFAIP2	-1.71	-5.01	-2.93
202525_at	PRSS8	-1.20	-2.68	-2.23
202558_s_at	HSPA13	-1.29	-2.82	-2.19
202611_s_at	MED14	-1.74	1.59	2.76
202630_at	APPBP2	-1.12	2.83	3.17
202642_s_at	TRRAP	-1.29	2.45	3.17
202647_s_at	NRAS	-1.44	-3.09	-2.15
202662_s_at	ITPR2	-1.18	1.73	2.04
202672_s_at	ATF3	-1.51	-3.56	-2.35
202679_at	NPC1	-1.10	-2.45	-2.23
202684_s_at	RNMT	1.19	-2.36	-2.81
202694_at	STK17A	1.17	5.89	5.03
202708_s_at	HIST2H2BE	1.12	-2.45	-2.73
202715_at	CAD	1.25	2.71	2.17
202743_at	PIK3R3	1.32	3.98	3.01
202748_at	GBP2	1.70	-3.08	-5.23
202755_s_at	GPC1	1.23	-2.13	-2.63
202762_at	ROCK2	-1.13	3.20	3.62
202772_at	HMGCL	1.34	-1.77	-2.37
202790_at	CLDN7	-1.15	-2.66	-2.31
202792_s_at	PPP6R2	1.18	2.34	1.98
202800_at	SLC1A3	1.15	2.98	2.60
202815_s_at	HEXIM1	-1.02	4.29	4.38
202857_at	CNPY2	1.27	2.16	1.70
202866_at	DNAJB12	1.02	3.64	3.59
202891_at	NIT1	1.22	-1.85	-2.25
202897_at	SIRPA	-1.10	1.84	2.02
202931_x_at	BIN1	-1.01	2.19	2.21
202951_at	STK38	-1.13	3.60	4.06
202955_s_at	ARFGEF1	-1.34	1.91	2.56
202973_x_at	FAM13A	1.45	3.23	2.22
202996_at	POLD4	1.15	-2.02	-2.33
203018_s_at	SSX2IP	1.14	2.45	2.15
203019_x_at	SSX2IP	1.12	2.54	2.27
203043_at	ZBED1	-1.09	1.88	2.05
203063_at	PPM1F	-1.05	3.48	3.67
203127_s_at	SPTLC2	-1.08	-2.24	-2.08
203150_at	RABEPK	1.41	2.30	1.63
203187_at	DOCK1	-1.07	2.00	2.14
203188_at	B3GNT1	-1.13	2.60	2.95
203196_at	ABCC4	-1.11	2.24	2.49

203222_s_at	TLE1	-1.12	2.16	2.42
203234_at	UPP1	1.05	-4.28	-4.51
203242_s_at	PDLIM5	-1.47	-3.18	-2.16
203339_at	SLC25A12	1.11	3.48	3.12
203340_s_at	SLC25A12	1.30	2.86	2.20
203344_s_at	RBBP8	1.54	2.56	1.66
203387_s_at	TBC1D4	-1.09	2.77	3.02
203438_at	STC2	1.69	3.91	2.32
203482_at	FAM178A	1.21	2.86	2.37
203486_s_at	ARMC8	-1.17	1.71	2.01
203487_s_at	ARMC8	-1.01	3.86	3.89
203518_at	LYST	-1.22	4.51	5.51
203525_s_at	APC	-1.21	1.86	2.25
203527_s_at	APC	-1.62	2.63	4.26
203579_s_at	SLC7A6	1.10	2.52	2.30
203580_s_at	SLC7A6	-1.33	3.71	4.93
203611_at	TERF2	-1.15	1.82	2.10
203636_at	MID1	-1.07	2.92	3.11
203638_s_at	FGFR2	1.11	3.00	2.71
203639_s_at	FGFR2	1.18	2.94	2.49
203648_at	TATDN2	1.16	2.02	1.74
203651_at	ZFYVE16	-1.06	2.06	2.17
203678_at	FAN1	1.62	3.00	1.85
203688_at	PKD2	-1.10	2.58	2.82
203723_at	ITPKB	-1.06	2.45	2.60
203736_s_at	PPFIBP1	-1.54	-2.06	-1.34
203753_at	TCF4	1.27	3.28	2.58
203775_at	SLC25A13	-1.06	2.19	2.33
203791_at	DMXL1	-1.23	2.01	2.48
203804_s_at	LUC7L3	-1.15	2.81	3.23
203825_at	BRD3	1.09	4.16	3.81
203848_at	AKAP8	1.17	2.79	2.39
203906_at	IQSEC1	1.12	3.49	3.11
203918_at	PCDH1	-1.26	-2.42	-1.92
203941_at	INTS9	1.22	2.19	1.80
203947_at	CSTF3	1.25	6.00	4.82
203950_s_at	CLCN6	-1.25	1.76	2.20
203958_s_at	ZBTB40	1.05	2.20	2.09
203959_s_at	ZBTB40	1.21	3.56	2.96
203966_s_at	PPM1A	-1.32	1.77	2.33
203970_s_at	PEX3	1.06	2.35	2.22
204014_at	DUSP4	-1.21	3.51	4.24
204029_at	CELSR2	-1.32	1.60	2.12
204036_at	LPAR1	1.01	3.14	3.09

204037_at	LPAR1	1.19	3.26	2.74
204042_at	WASF3	-1.14	2.07	2.37
204066_s_at	AGAP1	1.04	3.70	3.55
204068_at	STK3	-1.36	1.87	2.55
204069_at	MEIS1	1.05	2.41	2.30
204103_at	CCL4	1.17	-1.93	-2.27
204105_s_at	NRCAM	2.78	4.55	1.64
204107_at	NFYA	1.21	-2.22	-2.68
204109_s_at	NFYA	1.13	-2.65	-2.99
204156_at	SIK3	-1.25	2.65	3.31
204172_at	CPOX	-2.02	1.52	3.07
204174_at	ALOX5AP	1.24	-1.88	-2.33
204202_at	IQCE	-1.06	6.06	6.42
204224_s_at	GCH1	-1.57	-2.34	-1.49
204241_at	ACOX3	-1.02	2.04	2.08
204249_s_at	LMO2	1.07	-2.60	-2.78
204260_at	CHGB	1.20	-1.75	-2.09
204263_s_at	CPT2	1.54	-1.48	-2.29
204264_at	CPT2	1.27	-1.60	-2.03
204307_at	TECPR2	1.29	3.81	2.95
204336_s_at	RGS19	-1.03	2.24	2.31
204358_s_at	FLRT2///LOC100506718	1.11	2.55	2.30
204359_at	FLRT2///LOC100506718	-1.02	6.04	6.19
204366_s_at	GTF3C2	1.29	2.43	1.89
204373_s_at	CEP350	-1.20	2.61	3.12
204376_at	VPRBP	1.06	4.48	4.24
204377_s_at	VPRBP	1.24	2.99	2.41
204401_at	KCNN4	1.34	-1.62	-2.17
204442_x_at	LTBP4	1.14	-1.87	-2.14
204478_s_at	RABIF	-1.19	1.72	2.05
204491_at	PDE4D	1.35	-2.04	-2.75
204494_s_at	C15orf39	-1.14	-2.14	-1.87
204497_at	ADCY9	1.00	5.02	4.99
204514_at	DPH2	1.50	2.09	1.39
204573_at	CROT	-1.10	2.27	2.50
204602_at	DKK1	-1.17	2.29	2.68
204646_at	DPYD	-1.46	1.81	2.64
204650_s_at	APBB3	1.37	-1.85	-2.55
204662_at	CCP110	-1.26	1.77	2.22
204665_at	SIKE1	1.06	-1.94	-2.05
204686_at	IRS1	1.04	3.53	3.40
204740_at	CNKSR1	1.19	-2.46	-2.92
204783_at	MLF1	-1.90	-3.51	-1.85

204789_at	FMNL1	-1.09	-3.19	-2.94
204791_at	NR2C1	-1.00	2.25	2.25
204805_s_at	H1FX	-1.33	-3.54	-2.65
204807_at	TMEM5	1.47	4.00	2.73
204808_s_at	TMEM5	1.34	2.39	1.78
204821_at	BTN3A3	1.11	2.25	2.03
204853_at	ORC2	-1.05	2.56	2.70
204902_s_at	ATG4B	1.41	2.52	1.79
204935_at	PTPN2	1.05	-2.04	-2.13
204937_s_at	ZNF274	1.30	-2.37	-3.09
204956_at	MTAP	-1.27	2.38	3.02
204967_at	SHROOM2	1.11	3.92	3.52
204981_at	SLC22A18	1.22	-1.98	-2.42
204982_at	GIT2	-1.00	-4.32	-4.30
205015_s_at	TGFA	-1.21	-2.14	-1.77
205070_at	ING3	1.01	2.36	2.35
205073_at	CYP2J2	1.14	2.26	1.99
205074_at	SLC22A5	-1.27	2.72	3.45
205092_x_at	ZBTB1	-1.66	8.76	14.50
205109_s_at	ARHGEF4	1.70	2.66	1.56
205122_at	MSANTD3-TMEFF1///TMEFF1	-2.17	-4.32	-1.99
205123_s_at	MSANTD3-TMEFF1///TMEFF1	-1.29	-2.08	-1.62
205134_s_at	NUFIP1	1.06	2.24	2.11
205138_s_at	UST	-1.02	-2.41	-2.38
205171_at	PTPN4	1.04	2.33	2.23
205193_at	MAFF	-1.14	-2.53	-2.21
205214_at	STK17B	-1.63	-2.90	-1.78
205220_at	HCAR3	-2.12	-3.17	-1.49
205231_s_at	EPM2A	-1.03	2.84	2.93
205330_at	MN1	-1.08	2.41	2.61
205346_at	ST3GAL2	1.36	-1.62	-2.21
205356_at	USP13	1.11	3.09	2.79
205380_at	PDZK1	-1.44	2.07	2.97
205386_s_at	MDM2	-1.15	-2.64	-2.29
205397_x_at	SMAD3	1.07	-2.63	-2.80
205398_s_at	SMAD3	1.17	-2.32	-2.71
205416_s_at	ATXN3	-1.34	-2.26	-1.68
205421_at	SLC22A3	-1.28	1.80	2.30
205442_at	MFAP3L	-1.13	4.47	5.06
205448_s_at	MAP3K12	-1.13	2.11	2.38
205449_at	SAC3D1	1.17	2.68	2.29
205451_at	FOXO4	1.03	2.21	2.15
205457_at	C6orf106	-1.20	-2.07	-1.72
205476_at	CCL20	-1.08	-15.55	-14.42

205498_at	GHR	1.13	2.35	2.09
205591_at	OLFM1	1.10	-6.25	-6.89
205595_at	DSG3	1.05	-2.23	-2.33
205676_at	CYP27B1	-1.44	2.21	3.18
205677_s_at	DLEU1	1.26	3.90	3.10
205681_at	BCL2A1	1.15	-10.33	-11.85
205702_at	PHTF1	-1.01	2.54	2.58
205705_at	ANKRD26	-1.86	1.96	3.64
205706_s_at	ANKRD26	1.12	2.60	2.31
205709_s_at	CDS1	-1.40	1.93	2.70
205730_s_at	ABLIM3	-1.01	2.00	2.02
205761_s_at	DUS4L	1.24	-2.37	-2.94
205762_s_at	DUS4L	1.31	-1.54	-2.02
205805_s_at	ROR1	1.28	2.95	2.30
205816_at	ITGB8	1.00	-3.17	-3.18
205858_at	NGFR	1.28	-9.34	-11.93
205891_at	ADORA2B	-1.00	2.77	2.77
205933_at	SETBP1	-1.36	3.49	4.77
206061_s_at	DICER1	-1.16	1.95	2.27
206081_at	SLC24A1	1.19	-2.10	-2.50
206095_s_at	LOC100996657///SRSF10	-1.01	2.27	2.29
206114_at	EPHA4	1.33	2.48	1.86
206172_at	IL13RA2	1.03	-21.43	-22.01
206173_x_at	GABPB1	1.02	-2.94	-3.00
206186_at	MPP3	1.05	2.17	2.07
206191_at	ENTPD3	-1.08	2.14	2.31
206196_s_at	RUNDC3A	1.31	-2.68	-3.52
206237_s_at	NRG1	1.34	3.47	2.59
206238_s_at	YAF2	-1.26	1.72	2.17
206239_s_at	SPINK1	-1.17	-2.42	-2.08
206376_at	SLC6A15	1.27	2.44	1.93
206411_s_at	ABL2	-1.05	-5.89	-5.61
206437_at	S1PR4	1.31	-1.61	-2.11
206460_at	AJAP1	1.04	2.53	2.44
206482_at	PTK6	1.08	-2.06	-2.22
206527_at	ABAT	-1.12	-2.04	-1.82
206552_s_at	TAC1	1.00	-2.87	-2.88
206618_at	IL18R1	-1.47	3.13	4.60
206665_s_at	BCL2L1	1.25	-1.72	-2.16
206752_s_at	DFFB	-1.16	3.91	4.53
206769_at	TMSB4Y	1.23	-1.75	-2.14
206853_s_at	MAP3K7	-1.15	3.13	3.61
206858_s_at	HOXC6	-1.20	2.18	2.61
206874_s_at	SLK	-1.10	3.88	4.27

206877_at	MXD1	1.13	-1.92	-2.18
206912_at	FOXE1	1.24	3.16	2.54
206958_s_at	UPF3A	1.03	2.41	2.34
207082_at	CSF1	-1.21	-2.77	-2.30
207296_at	ZNF343	1.02	-2.34	-2.39
207318_s_at	CDK13	-1.07	1.95	2.09
207321_s_at	ABCB9	1.68	2.52	1.50
207345_at	FST	-1.12	2.50	2.79
207366_at	KCNS1	-1.09	3.63	3.96
207416_s_at	NFATC3	-1.22	1.80	2.19
207480_s_at	MEIS2	1.15	2.78	2.42
207559_s_at	ZMYM3	-1.04	3.20	3.33
207564_x_at	OGT	-1.33	2.34	3.11
207766_at	CDKL1	-1.07	2.14	2.29
207821_s_at	PTK2	-1.50	2.10	3.15
207839_s_at	TMEM8B	1.47	-1.54	-2.25
207871_s_at	ST7///ST7-OT3	1.43	3.67	2.57
207920_x_at	ZFX	1.07	2.01	1.88
207956_x_at	PDS5B	-1.46	2.25	3.29
207993_s_at	CHP1	1.04	-4.24	-4.39
208055_s_at	HERC4	-1.02	3.41	3.49
208081_s_at	ZNF442	1.51	-5.80	-8.73
208153_s_at	FAT2	1.10	3.18	2.89
208228_s_at	FGFR2	1.17	2.83	2.41
208230_s_at	NRG1	1.27	2.59	2.03
208231_at	NRG1	1.04	2.96	2.84
208252_s_at	CHST3	-1.02	-2.14	-2.11
208445_s_at	BAZ1B	1.02	2.30	2.26
208546_x_at	HIST1H2BH	1.12	-2.46	-2.75
208580_x_at	HIST1H4A	1.11	-2.36	-2.62
208583_x_at	HIST1H2AG	1.17	-1.93	-2.25
208615_s_at	PTP4A2	-1.46	1.56	2.27
208707_at	EIF5	-1.05	4.61	4.82
208760_at	UBE2I	1.24	5.06	4.08
208769_at	EIF4EBP2	-1.54	1.51	2.33
208776_at	PSMD11	-1.19	2.95	3.51
208820_at	PTK2	-1.31	1.56	2.04
208835_s_at	LUC7L3	1.08	3.36	3.11
208866_at	CSNK1A1	-1.16	1.77	2.05
208886_at	H1F0	-1.37	-4.05	-2.96
208914_at	GGA2	1.01	2.97	2.94
208933_s_at	LGALS8	1.05	2.01	1.91
208940_at	SEPHS1	1.34	5.39	4.01
208957_at	ERP44	1.43	-2.03	-2.91

209015_s_at	DNAJB6	-1.46	2.72	3.98
209027_s_at	ABI1	-1.29	-2.34	-1.82
209037_s_at	EHD1	-1.03	-2.88	-2.79
209083_at	CORO1A	1.06	-2.36	-2.51
209090_s_at	SH3GLB1	-1.21	2.18	2.63
209105_at	NCOA1	-1.33	2.20	2.93
209106_at	NCOA1	1.00	2.04	2.03
209119_x_at	NR2F2	1.05	2.17	2.07
209153_s_at	TCF3	1.03	4.27	4.12
209175_at	SEC23IP	-1.19	1.89	2.25
209176_at	SEC23IP	-1.04	5.80	6.05
209198_s_at	SYT11	-1.40	1.80	2.53
209209_s_at	FERMT2	-1.53	-2.16	-1.41
209236_at	SLC23A2	-1.15	1.74	2.01
209240_at	OGT	-1.32	5.04	6.63
209246_at	ABCF2	1.21	2.73	2.26
209271_at	BPTF	1.08	4.84	4.50
209281_s_at	ATP2B1	-1.22	3.29	4.02
209285_s_at	FAM208A	-1.10	7.75	8.50
209289_at	NFIB	1.21	2.29	1.89
209290_s_at	NFIB	1.19	2.03	1.71
209291_at	ID4	1.19	-4.39	-5.21
209294_x_at	TNFRSF10B	1.18	-1.88	-2.22
209297_at	ITSN1	-1.30	2.36	3.06
209298_s_at	ITSN1	-1.31	2.74	3.60
209304_x_at	GADD45B	1.06	-2.02	-2.13
209318_x_at	PLAGL1	-1.27	3.81	4.84
209348_s_at	MAF	-1.43	1.89	2.71
209349_at	RAD50	1.21	2.34	1.93
209380_s_at	ABCC5	1.26	5.92	4.70
209385_s_at	PROSC	-1.27	1.72	2.18
209387_s_at	TM4SF1	-1.47	-4.12	-2.81
209390_at	TSC1	-1.02	2.38	2.44
209398_at	HIST1H1C	1.34	-1.81	-2.41
209400_at	SLC12A4	-1.24	-2.00	-1.61
209441_at	RHOBTB2	1.26	2.11	1.67
209447_at	SYNE1	-1.40	2.06	2.88
209467_s_at	MKNK1	1.08	2.46	2.28
209473_at	ENTPD1	1.27	3.34	2.63
209497_s_at	RBM4B	-1.33	1.87	2.49
209508_x_at	CFLAR	-1.01	-2.66	-2.63
209593_s_at	TOR1B	1.04	2.20	2.12
209627_s_at	OSBPL3	-1.25	2.83	3.55
209630_s_at	FBXW2	-1.08	2.15	2.31

209647_s_at	SOCS5	-1.43	2.22	3.17
209648_x_at	SOCS5	-1.37	2.39	3.27
209667_at	CES2	1.54	-1.62	-2.50
209668_x_at	CES2	1.43	-1.56	-2.24
209725_at	UTP20	1.22	2.75	2.26
209736_at	SOX13	-1.16	-2.47	-2.13
209744_x_at	ITCH	-1.09	-2.09	-1.91
209780_at	PHTF2	-1.22	2.19	2.67
209794_at	SRGAP3	2.10	8.17	3.88
209799_at	PRKAA1	1.05	-2.47	-2.58
209805_at	PMS2///PMS2CL	1.48	-1.75	-2.59
209815_at	PTCH1	-1.13	2.30	2.60
209821_at	IL33	1.46	-10.34	-15.05
209845_at	MKRN1	-1.48	-3.49	-2.35
209849_s_at	RAD51C	1.10	2.67	2.42
209876_at	GIT2	-1.04	3.78	3.94
209884_s_at	SLC4A7	-1.41	1.56	2.19
209890_at	TSPAN5	-1.15	1.82	2.09
209902_at	ATR	1.51	2.34	1.55
209906_at	C3AR1	2.06	1.51	-1.36
209925_at	OCLN	-1.24	-2.82	-2.28
209939_x_at	CFLAR	-1.41	-3.48	-2.47
209967_s_at	CREM	1.11	3.27	2.96
209969_s_at	STAT1	1.03	-2.91	-3.00
209989_at	ZNF268	1.20	-1.72	-2.06
210035_s_at	RPL5///SNORA66///SNORD21	-1.08	2.06	2.22
210047_at	SLC11A2	1.02	2.73	2.68
210048_at	NAPG	1.07	-1.93	-2.06
210095_s_at	IGFBP3	1.38	-3.39	-4.69
210117_at	SPAG1	-1.70	1.87	3.20
210144_at	TBC1D22A	1.19	2.59	2.18
210164_at	GZMB	1.52	-6.80	-10.36
210200_at	WWP2	1.13	-4.65	-5.23
210201_x_at	BIN1	-1.01	2.21	2.22
210205_at	B3GALT4	-1.55	-2.62	-1.68
210233_at	IL1RAP	1.22	-3.96	-4.84
210285_x_at	WTAP	1.20	-1.84	-2.20
210320_s_at	DDX52	-1.44	1.48	2.13
210335_at	RASSF9	1.10	3.16	2.86
210347_s_at	BCL11A	-1.00	3.62	3.63
210357_s_at	SMOX	1.09	-1.84	-2.00
210365_at	LOC100506403///RUNX1	-1.21	2.19	2.66
210389_x_at	TUBD1	1.20	5.31	4.43
210405_x_at	TNFRSF10B	1.21	-1.78	-2.15

210462_at	BLZF1	-1.13	-4.95	-4.37
210473_s_at	GPR125	1.22	3.01	2.47
210510_s_at	NRP1	1.20	-3.40	-4.07
210517_s_at	AKAP12	-2.80	-6.07	-2.16
210544_s_at	ALDH3A2	1.06	2.01	1.90
210555_s_at	NFATC3	1.06	2.13	2.02
210563_x_at	CFLAR	-1.18	-3.26	-2.75
210564_x_at	CFLAR	-1.20	-3.32	-2.76
210608_s_at	FUT2	-1.66	-2.55	-1.54
210631_at	NF1	-1.05	-4.40	-4.17
210636_at	PPARD	-1.19	-6.51	-5.45
210664_s_at	TFPI	-1.08	-2.86	-2.64
210699_at		1.04	2.08	2.00
210710_at	AGGF1	1.03	-2.28	-2.36
210787_s_at	CAMKK2	-1.27	-2.08	-1.64
210845_s_at	PLAUR	-1.90	-7.39	-3.89
210916_s_at	CD44	-1.22	-2.14	-1.76
211078_s_at	STK3	-1.38	-2.58	-1.87
211222_s_at	HAP1	1.04	-2.58	-2.69
211257_x_at	ZNF638	1.12	2.90	2.60
211313_s_at	BAZ1B	1.12	2.06	1.85
211316_x_at	CFLAR	1.05	-2.52	-2.65
211484_s_at	DSCAM	1.31	3.25	2.48
211506_s_at	IL8	1.09	-4.39	-4.77
211554_s_at	APAF1	-1.37	-3.95	-2.88
211672_s_at	ARPC4	-1.08	-2.09	-1.94
211704_s_at	SPIN2A///SPIN2B	1.39	-1.65	-2.31
211732_x_at	HNMT	1.34	-1.58	-2.11
211740_at	ICA1	1.13	-10.47	-11.85
211760_s_at	VAMP4	-1.27	-2.59	-2.05
211774_s_at	MMACHC	1.37	2.22	1.62
211862_x_at	CFLAR	-1.01	-2.31	-2.28
211865_s_at	FZR1	1.01	-2.54	-2.56
211883_x_at	CEACAM1	1.07	-1.97	-2.11
211924_s_at	PLAUR	-2.32	-9.57	-4.13
212028_at	RBM25	1.40	3.63	2.59
212030_at	RBM25	1.17	2.39	2.05
212034_s_at	EXOC7	1.24	2.46	1.98
212095_s_at	MTUS1	1.35	2.05	1.52
212118_at	TRIM27	1.16	4.19	3.61
212131_at	LSM14A	1.00	2.31	2.30
212138_at	PDS5A	-1.42	2.41	3.43
212140_at	PDS5A	-1.24	2.49	3.09
212143_s_at	IGFBP3	1.33	-2.24	-2.99

212173_at	AK2	1.50	2.20	1.47
212234_at	ASXL1	1.08	2.71	2.50
212237_at	ASXL1	1.30	2.69	2.07
212248_at	MTDH	-1.06	3.03	3.22
212254_s_at	DST	1.09	2.62	2.40
212260_at	GIGYF2	-1.04	2.18	2.26
212261_at	GIGYF2	1.07	2.01	1.87
212263_at	QKI	-1.69	1.55	2.62
212268_at	SERPINB1	-1.12	-2.36	-2.10
212288_at	FNBP1	1.00	4.25	4.25
212309_at	CLASP2	-1.31	1.73	2.26
212323_s_at	VPS13D	1.02	2.21	2.18
212330_at	TFDP1	-1.25	1.81	2.25
212343_at	YIPF6	1.09	2.87	2.62
212354_at	SULF1	1.38	2.38	1.73
212355_at	KHNYN	1.19	-1.80	-2.15
212356_at	KHNYN	-1.16	2.28	2.64
212374_at	FEM1B	-1.10	-2.03	-1.85
212375_at	EP400	-1.03	2.05	2.10
212382_at	TCF4	-1.20	2.23	2.68
212387_at	TCF4	1.32	3.47	2.62
212388_at	USP24	-1.03	2.37	2.44
212429_s_at	GTF3C2	1.31	2.43	1.86
212435_at	TRIM33	-1.31	2.24	2.95
212439_at	IP6K1	-1.00	2.13	2.14
212471_at	AVL9	-1.06	-2.22	-2.10
212482_at	RMND5A	-1.15	1.74	2.00
212498_at	Mar-06	-1.02	2.09	2.15
212513_s_at	USP33	-1.09	1.94	2.11
212517_at	ATRN	1.11	2.64	2.38
212526_at	SPG20	-1.41	1.63	2.30
212547_at	BRD3	-1.06	3.08	3.27
212598_at	WDFY3	-1.38	2.35	3.25
212611_at	DTX4	-1.06	2.28	2.41
212614_at	ARID5B	1.01	2.00	1.98
212616_at	CHD9	-1.34	2.22	2.97
212621_at	TMEM194A	-1.10	2.45	2.70
212635_at	TNPO1	-1.26	1.82	2.31
212655_at	ZCCHC14	-1.19	4.09	4.86
212657_s_at	IL1RN	-1.46	-2.19	-1.50
212659_s_at	IL1RN	-1.26	-2.86	-2.26
212660_at	PHF15	1.08	4.20	3.88
212668_at	SMURF1	-1.03	-2.51	-2.44
212676_at	NF1	-1.32	1.58	2.08

212678_at	NF1	-1.46	2.39	3.48
212689_s_at	KDM3A	1.07	-2.09	-2.23
212693_at	MDN1	1.25	2.65	2.13
212701_at	TLN2	1.44	4.14	2.88
212704_at	ZCCHC11	-1.23	2.32	2.86
212708_at	MSL1	-1.01	1.98	2.00
212714_at	LARP4	-1.09	2.46	2.67
212715_s_at	MICAL3	1.04	2.53	2.44
212718_at	PAPOLA	-1.33	1.57	2.09
212720_at	PAPOLA	-1.55	2.27	3.53
212727_at	DLG3	-1.30	1.55	2.02
212730_at	SYNM	-1.08	2.03	2.18
212757_s_at	CAMK2G	-1.06	2.06	2.18
212760_at	UBR2	-1.17	4.65	5.46
212771_at	FAM171A1	-1.14	2.23	2.55
212774_at	ZBTB18	-1.33	1.71	2.27
212779_at	KIAA1109	-1.32	1.93	2.54
212780_at	SOS1	-1.15	3.70	4.26
212786_at	CLEC16A	1.12	2.42	2.17
212796_s_at	TBC1D2B	-1.25	4.31	5.40
212799_at	STX6	-1.38	1.46	2.01
212805_at	PRUNE2	1.37	2.66	1.94
212810_s_at	SLC1A4	-1.06	2.78	2.95
212820_at	DMXL2	-1.13	2.33	2.64
212834_at	DDX52	1.14	7.57	6.62
212875_s_at	C2CD2	1.03	5.47	5.32
212877_at	KLC1	1.00	-2.10	-2.11
212878_s_at	KLC1	1.24	-1.82	-2.25
212880_at	WDR7	1.22	3.16	2.60
212888_at	DICER1	-1.09	1.96	2.14
212927_at	SMC5	-1.32	1.74	2.30
212930_at	ATP2B1	-1.30	1.98	2.56
212944_at	SLC5A3	-1.29	2.57	3.31
212972_x_at	APBB2	-1.16	2.04	2.37
212974_at	DENND3	-1.29	-3.04	-2.36
212991_at	FBXO9	1.29	2.46	1.91
213020_at	GOSR1	-1.26	2.58	3.26
213029_at	NFIB	1.22	3.42	2.81
213035_at	ANKRD28	-1.11	2.98	3.29
213038_at	RNF19B	-1.23	-2.04	-1.66
213051_at	ZC3HAV1	-1.16	2.18	2.54
213058_at	TTC28	1.05	3.26	3.09
213063_at	ZC3H14	1.19	4.43	3.72
213064_at	ZC3H14	1.06	2.55	2.40

213065_at	ZFC3H1	-1.07	2.16	2.31
213116_at	NEK3	1.10	-2.10	-2.31
213164_at	SLC5A3	1.04	2.98	2.87
213165_at	CEP350	1.03	2.31	2.23
213195_at	LYRM9	1.46	-2.21	-3.22
213199_at	C2CD3	1.09	2.71	2.49
213221_s_at	SIK2	-1.10	2.77	3.05
213230_at	CDR2L	-1.25	4.16	5.20
213233_s_at	KLHL9	1.14	-1.80	-2.06
213234_at	KIAA1467	-1.21	1.68	2.03
213238_at	ATP10D	-1.09	2.88	3.14
213239_at	PIBF1	1.04	2.12	2.04
213243_at	VPS13B	-1.18	3.22	3.79
213250_at	CCDC85B	1.29	-1.60	-2.05
213252_at	SH3PXD2A	-1.28	2.24	2.87
213262_at	SACS	-1.18	3.15	3.72
213266_at	RP11-355D13.4	1.20	3.02	2.51
213269_at	ZNF248	1.23	4.56	3.72
213273_at	TENM4	-1.07	2.32	2.49
213288_at	MBOAT2	-1.50	2.22	3.33
213295_at	CYLD	1.02	2.24	2.19
213306_at	MPDZ	-1.06	2.48	2.62
213329_at	SRGAP2///SRGAP2D	1.20	3.28	2.74
213331_s_at	NEK1	1.02	2.44	2.39
213336_at	BAZ1B	1.02	2.04	1.99
213361_at	TDRD7	-1.25	1.82	2.29
213383_at	SBF1	1.31	2.19	1.67
213385_at	CHN2	1.12	3.47	3.11
213387_at	ATAD2B	-1.49	2.05	3.04
213403_at		1.07	7.44	6.96
213424_at	KIAA0895	-1.48	2.46	3.63
213425_at	WNT5A	-1.32	3.58	4.73
213448_at		1.35	2.26	1.67
213449_at	POP1	1.20	2.81	2.35
213483_at	PPWD1	1.09	2.50	2.28
213500_at		1.14	2.21	1.94
213509_x_at	CES2	1.41	-1.51	-2.14
213538_at	SON	-1.33	-2.23	-1.68
213554_s_at	CDV3	1.37	-2.38	-3.26
213555_at	RWDD2A	1.20	-2.06	-2.48
213560_at	GADD45B	-1.04	-2.02	-1.94
213570_at	EIF4E2	-1.04	-3.33	-3.22
213573_at	KPNB1	-1.11	1.86	2.06
213578_at	BMPR1A	-1.44	1.98	2.85

213615_at	LPCAT3	1.44	3.12	2.17
213624_at	SMPDL3A	-1.38	2.10	2.90
213635_s_at	SAFB	1.20	2.91	2.43
213637_at	DDX52	-1.28	5.57	7.16
213647_at	DNA2	-1.76	1.33	2.34
213654_at	TAF5L	-1.04	2.11	2.19
213659_at	ZNF75D	1.04	3.83	3.69
213664_at	SLC1A1	-1.16	2.15	2.49
213667_at	LOC100862671///SRCAP	1.01	-2.97	-2.98
213677_s_at	PMS1	1.41	5.04	3.57
213700_s_at	PKM	1.03	-2.17	-2.25
213701_at	C12orf29	-1.13	1.92	2.16
213705_at	GGCX	-1.00	3.01	3.02
213721_at	SOX2	1.27	-1.59	-2.03
213750_at	RSL1D1	1.15	3.90	3.40
213759_at	ARL4C	-1.21	1.98	2.39
213775_x_at	ZNF638///ZNF638-IT1	1.13	2.43	2.15
213785_at	IPO9	1.05	3.44	3.27
213805_at	ABHD5	-1.23	2.39	2.93
213822_s_at	UBE3B	1.05	-2.03	-2.13
213823_at	HOXA11	1.21	-1.82	-2.20
213832_at	KCND3	-1.34	3.44	4.60
213889_at	PIGL	-1.24	-3.09	-2.50
213891_s_at	TCF4	-1.01	4.98	5.01
213906_at	MYBL1	-1.16	4.62	5.37
213959_s_at	RPGRIP1L	1.04	5.45	5.26
213971_s_at	SUZ12///SUZ12P1	-1.15	1.92	2.20
213984_at	PDS5A	-1.11	-4.01	-3.61
213998_s_at	DDX17	-1.07	-2.45	-2.30
214036_at	EFNA5	1.01	3.00	2.97
214073_at	CTTN	-1.35	-2.54	-1.89
214076_at	GFOD2	1.21	-1.71	-2.06
214083_at	PPP2R5C	1.06	-3.26	-3.46
214088_s_at	FUT3	-1.31	-2.46	-1.87
214102_at		-1.01	2.12	2.14
214108_at	MAX	-1.19	-2.04	-1.72
214124_x_at	FGFR1OP	-1.11	2.85	3.15
214126_at		-1.23	2.45	3.03
214127_s_at	SRRT	-1.42	1.55	2.19
214160_at		-1.14	-2.49	-2.18
214168_s_at	TJP1	-1.06	-2.35	-2.22
214169_at	SUN1	-1.22	-3.35	-2.75
214290_s_at	HIST2H2AA3///HIST2H2AA4	1.13	-1.90	-2.15
214299_at	TOP3A	1.11	2.78	2.51

214309_s_at		-1.30	2.68	3.48
214358_at	ACACA	1.02	-2.65	-2.70
214390_s_at	BCAT1	1.01	-2.29	-2.32
214439_x_at	BIN1	-1.02	1.97	2.00
214469_at	HIST1H2AB///HIST1H2AE	1.04	-3.03	-3.16
214486_x_at	CFLAR	1.04	-2.20	-2.29
214542_x_at	HIST1H3F	1.03	-2.25	-2.32
214583_at	DDI2///RSC1A1	1.00	-3.21	-3.21
214659_x_at	YLPM1	1.11	2.18	1.96
214699_x_at	WIPI2	-1.11	3.30	3.67
214704_at	TCF25	-1.17	-2.96	-2.53
214748_at	N4BP2L2	1.21	3.14	2.59
214790_at	SENP6	1.02	-5.72	-5.85
214792_x_at	VAMP2	-1.02	-3.42	-3.34
214808_at	LOC100996615	-1.08	2.44	2.64
214823_at	ZNF204P	1.08	2.42	2.24
214881_s_at	UBTF	1.26	-2.13	-2.68
214891_at	FBXO21	1.17	2.07	1.77
214919_s_at	ANKHD1///ANKHD1-EIF4EBP3///EIF4EBP3	1.44	3.22	2.24
214923_at	ATP6V1D	-1.41	1.54	2.17
214925_s_at	SPTAN1	1.15	-3.31	-3.81
214959_s_at	API5	1.06	-1.97	-2.08
214960_at	API5	-1.02	-2.36	-2.32
214962_s_at	NUP160	-1.18	-2.34	-1.98
214963_at	NUP160	1.14	-2.40	-2.74
214998_at	AAK1	-1.02	-3.12	-3.05
215016_x_at	DST	1.09	2.79	2.56
215030_at	GRSF1	-1.16	4.39	5.07
215034_s_at	TM4SF1	-1.19	-4.12	-3.47
215046_at	KANSL1L	-1.14	3.03	3.44
215066_at	PTPRF	1.04	-2.25	-2.34
215068_s_at	FBXL18	-1.29	1.60	2.06
215078_at	LOC100129518///SOD2	1.01	-11.76	-11.89
215082_at	ELOVL5	1.11	-1.83	-2.03
215100_at	ADTRP	1.04	-2.23	-2.32
215149_at		-1.18	2.79	3.30
215223_s_at	LOC100129518///SOD2	1.02	-2.50	-2.55
215233_at	JMJD6	1.22	2.04	1.67
215254_at	RCAN1	1.17	-2.57	-3.01
215260_s_at	TCF3	-1.12	3.40	3.82
215359_x_at	LOC101060181///ZNF44	1.00	-2.12	-2.12
215458_s_at	SMURF1	-1.05	-2.51	-2.39
215491_at	MYCL1	-1.26	-3.29	-2.61
215495_s_at	SAMD4A	-1.35	-2.15	-1.59

215543_s_at	LARGE	-1.27	1.87	2.38
215561_s_at	IL1R1	-1.20	-2.35	-1.95
215617_at	SPATS2L	-1.33	2.78	3.69
215629_s_at	DLEU2///DLEU2L	-1.63	-2.62	-1.61
215716_s_at	ATP2B1	-1.10	1.86	2.04
215725_at	DGCR11	1.18	-1.82	-2.14
215731_s_at	MPHOSPH9	1.45	4.56	3.15
215779_s_at	HIST1H2BC	1.01	-2.00	-2.03
215977_x_at	GK	-1.02	-2.02	-1.99
215991_s_at	EMC1	-1.63	1.41	2.29
215993_at	OTTHUMG00000163875	1.40	-11.76	-16.51
216020_at	IFIH1	-1.16	-3.14	-2.71
216202_s_at	SPTLC2	-1.23	-2.29	-1.86
216221_s_at	PUM2	-1.21	2.19	2.64
216236_s_at	SLC2A14///SLC2A3	-1.64	-4.53	-2.76
216243_s_at	IL1RN	-2.03	-4.30	-2.12
216260_at	DICER1	1.11	-2.02	-2.25
216262_s_at	TGIF2	-1.02	2.38	2.43
216279_at	ZNF460	-1.07	-2.08	-1.93
216303_s_at	MTMR1	-1.25	-4.63	-3.70
216399_s_at	SCAPER	-1.07	2.29	2.44
216479_at	RPL21	-1.04	-2.07	-1.99
216804_s_at	PDLIM5	-1.36	-3.15	-2.31
216843_x_at	PMS2P1	1.34	-1.50	-2.01
217047_s_at	FAM13A	1.21	3.25	2.68
217094_s_at	ITCH	1.02	-2.01	-2.05
217122_s_at	SLC35E2///SLC35E2B	1.05	2.04	1.95
217167_x_at	GK	-1.10	-2.20	-2.00
217173_s_at	LDLR	1.07	-1.97	-2.11
217403_s_at	ZNF227	1.17	2.58	2.21
217445_s_at	GART	1.18	2.50	2.11
217529_at	ORAI2	-1.21	3.39	4.08
217579_x_at		-1.07	-2.60	-2.44
217612_at	TIMM50	1.04	2.42	2.33
217627_at	ZNF573	1.51	2.95	1.96
217657_at		-1.14	13.65	15.62
217682_at	OTTHUMG00000178148///RP11-473I1.9	-1.21	-2.70	-2.22
217785_s_at	YKT6	1.09	-3.29	-3.57
217796_s_at	NPLOC4	1.08	2.42	2.23
217828_at	SLTM	-1.10	3.44	3.78
217842_at	C7orf55-LUC7L2///LUC7L2	1.03	2.48	2.40
217853_at	TNS3	1.34	2.81	2.09
217865_at	RNF130	-1.07	2.15	2.30
217879_at	CDC27	-1.23	1.79	2.21

217880_at	CDC27	-1.20	2.06	2.46
217904_s_at	BACE1	1.31	2.29	1.75
217905_at	MCMBP	1.12	5.03	4.47
217924_at	C6orf106	-1.37	1.67	2.29
217928_s_at	PPP6R3	-1.08	2.81	3.03
217930_s_at	TOLLIP	1.29	-1.72	-2.21
217935_s_at	UQCC	1.21	3.22	2.67
217986_s_at	BAZ1A	-1.33	1.89	2.52
218019_s_at	PDXK	1.08	2.90	2.70
218040_at	PRPF38B	-1.16	3.15	3.66
218093_s_at	ANKRD10	-1.55	2.46	3.81
218125_s_at	CCDC25	1.29	2.16	1.67
218129_s_at	NFYB	1.16	-2.14	-2.48
218138_at	MKKS	1.23	5.29	4.32
218139_s_at	AP5M1	-1.23	2.17	2.66
218158_s_at	APPL1	-1.41	1.48	2.08
218173_s_at	WHSC1L1	-1.12	6.63	7.40
218249_at	ZDHHC6	1.06	2.29	2.16
218259_at	MKL2	-1.13	2.09	2.37
218268_at	TBC1D15	-1.12	1.85	2.07
218279_s_at		1.12	-1.92	-2.15
218280_x_at	HIST2H2AA3///HIST2H2AA4	1.15	-1.95	-2.24
218304_s_at	OSBPL11	-1.26	1.83	2.31
218326_s_at	LGR4	-1.16	2.21	2.56
218404_at	SNX10	-1.25	-2.06	-1.64
218421_at	CERK	-1.33	3.09	4.11
218452_at	SMARCAL1	1.31	2.17	1.67
218490_s_at	ZNF302	1.36	2.71	1.99
218498_s_at	ERO1L	-1.16	-2.20	-1.89
218515_at	PAXBP1	1.14	2.96	2.60
218546_at	C1orf115	1.04	-3.03	-3.15
218566_s_at	CHORDC1	-1.10	6.67	7.32
218614_at	KIAA1551	-1.31	-3.44	-2.63
218632_at	HECTD3	1.05	2.04	1.94
218686_s_at	RHBDF1	1.07	-2.11	-2.27
218724_s_at	TGIF2	1.16	2.68	2.31
218744_s_at	PACSIN3	-1.02	2.01	2.04
218754_at	NOL9	1.03	2.17	2.11
218764_at	PRKCH	-1.13	1.89	2.14
218783_at	INTS7	-1.06	7.37	7.83
218823_s_at	KCTD9	-1.62	-2.01	-1.24
218842_at	RPAP3	1.03	2.81	2.72
218901_at	PLSCR4	-1.79	1.49	2.67
218915_at	NF2	1.03	2.02	1.97

218923_at	CTBS	-1.35	-2.64	-1.96
218924_s_at	CTBS	-1.12	-2.01	-1.80
218927_s_at	CHST12	-1.11	2.01	2.23
218973_at	EFTUD1	-1.03	2.20	2.26
218984_at	PUS7	-1.01	2.88	2.91
219002_at	FASTKD1	1.32	3.09	2.34
219006_at	NDUFAF4	1.30	2.23	1.71
219012_s_at	C11orf30	-1.19	1.84	2.19
219062_s_at	ZCCHC2	-1.35	1.68	2.27
219083_at	SHQ1	1.12	2.58	2.31
219094_at	ARMC8	1.08	-2.58	-2.78
219120_at	C2orf44	1.13	2.53	2.23
219130_at	TRMT13	1.29	3.00	2.32
219142_at	RASL11B	1.48	4.05	2.74
219153_s_at	THSD4	1.36	-2.12	-2.87
219161_s_at	CKLF///CKLF-CMTM1	-1.46	1.61	2.34
219165_at	PDLIM2	1.07	-2.66	-2.85
219166_at	DNAAF2	-1.00	2.26	2.28
219247_s_at	ZDHHC14	1.10	3.82	3.49
219253_at	TMEM185B	1.15	-1.76	-2.03
219256_s_at	SH3TC1	-1.03	-2.23	-2.17
219289_at	HEATR3	1.29	4.08	3.16
219292_at	THAP1	-1.29	1.56	2.01
219298_at	ECHDC3	1.22	-1.98	-2.41
219307_at	PDSS2	1.04	2.03	1.95
219328_at	DDX31	1.29	2.20	1.70
219377_at	GAREM	1.15	2.31	2.01
219434_at	TREM1	1.14	-2.36	-2.67
219440_at	RAI2	1.03	-2.37	-2.43
219441_s_at	LRRK1	1.06	2.48	2.35
219453_at	KLHL36	-1.18	-2.23	-1.89
219464_at	CA14	1.16	-2.06	-2.39
219481_at	TTC13	-1.07	2.21	2.37
219494_at	RAD54B	1.01	2.23	2.22
219495_s_at	ZNF180	-1.20	1.79	2.14
219506_at	C1orf54	-1.31	-2.87	-2.19
219515_at	PRDM10	-1.25	4.12	5.15
219520_s_at	WWC3	-1.15	4.76	5.49
219528_s_at	BCL11B	-1.45	6.55	9.47
219542_at	NEK11	1.65	4.76	2.87
219567_s_at	EXO5	-1.02	2.81	2.86
219572_at	CADPS2	-1.12	2.17	2.42
219581_at	TSEN2	1.33	3.72	2.79
219586_at	WDR59	1.26	-2.11	-2.66

219610_at	ARHGEF28	-1.18	3.87	4.55
219630_at	PDZK1IP1	-1.01	-2.86	-2.84
219638_at	FBXO22	1.01	-2.64	-2.67
219657_s_at	KLF3	-1.22	-2.94	-2.41
219679_s_at	WAC	1.08	2.28	2.11
219681_s_at	RAB11FIP1	-1.70	-4.35	-2.56
219683_at	FZD3	-1.11	3.47	3.87
219716_at	APOL6	1.12	-2.59	-2.91
219731_at	ENTPD1-AS1	1.32	3.25	2.47
219754_at	RBM41	-1.03	3.33	3.44
219770_at	GTDC1	1.08	2.54	2.35
219774_at	CCDC93	-1.21	-2.18	-1.80
219809_at	WDR55	-1.01	3.22	3.27
219817_at	MAPKAPK5-AS1	1.03	-2.02	-2.07
219821_s_at	GFOD1	-1.03	2.48	2.54
219822_at	MTRF1	1.23	3.81	3.11
219832_s_at	HOXC13	1.21	2.36	1.96
219856_at	C1orf116	-1.06	-2.69	-2.54
219875_s_at	DESI2	-1.04	-3.68	-3.53
219901_at	FGD6	-1.01	-2.40	-2.38
219904_at	ZSCAN5A	1.21	3.88	3.20
219917_at	ZCCHC4	1.05	2.70	2.58
219931_s_at	KLHL12	1.24	-1.73	-2.15
219951_s_at	DZANK1	-1.17	3.16	3.70
219982_s_at	SERF1A///SERF1B	-1.05	2.39	2.51
219987_at	ERVMER34-1	1.28	3.92	3.06
220007_at	METTL8	1.05	2.77	2.63
220044_x_at	LUC7L3	1.08	3.16	2.93
220047_at	SIRT4	-1.39	1.50	2.09
220052_s_at	TINF2	-1.00	-4.53	-4.51
220085_at	HELLS	-1.28	2.29	2.93
220088_at	C5AR1	1.93	2.91	1.51
220097_s_at	TMEM104	1.14	2.06	1.81
220099_s_at	C7orf55-LUC7L2///LUC7L2	-1.42	1.84	2.61
220102_at	FOXL2	-1.28	3.08	3.95
220123_at	SLC35F5	-1.23	-6.79	-5.50
220128_s_at	NIPAL2	-1.13	2.12	2.41
220138_at	HAND1	-1.02	-2.66	-2.62
220141_at	C11orf63	-1.50	3.93	5.90
220143_x_at	LUC7L	1.10	2.14	1.95
220173_at	CCDC176	-1.05	2.73	2.87
220195_at	MBD5	-1.45	2.74	3.97
220233_at	FBXO17	1.05	2.39	2.27
220242_x_at	ZNF701	-1.15	-2.41	-2.10

220251_at	DIEXF	1.02	3.81	3.74
220274_at	IQCA1	-1.25	3.80	4.74
220275_at	CUZD1	1.08	2.47	2.29
220289_s_at	AIM1L	1.13	-2.17	-2.45
220297_at	BTBD7	1.26	2.79	2.20
220305_at	MAVS	1.26	2.96	2.36
220326_s_at	ARHGEF40	-1.50	1.64	2.45
220355_s_at	PBRM1	-1.10	1.97	2.18
220372_at	DNAJC28	-1.06	2.67	2.82
220402_at	TP53AIP1	1.15	3.35	2.91
220459_at	MCM3AP-AS1	1.07	3.20	3.00
220475_at	SLC28A3	-1.02	-3.57	-3.50
220633_s_at	HP1BP3	1.27	-1.59	-2.01
220638_s_at	CBLC	1.24	-2.18	-2.71
220664_at	SPRR2C	1.05	-3.95	-4.13
220713_at	DENND6B	1.50	-1.44	-2.16
220738_s_at	RPS6KA6	-1.01	3.08	3.12
220740_s_at	SLC12A6	1.08	-3.81	-4.10
220742_s_at	NGLY1	1.20	2.85	2.37
220751_s_at	FAXDC2	-1.10	-3.90	-3.55
220770_s_at	C5orf54	-1.03	3.74	3.85
220926_s_at	EDEM3	-1.19	1.93	2.29
220938_s_at	GMEB1	-1.12	-2.03	-1.80
220943_s_at	NDUFAF7	1.04	2.23	2.14
220953_s_at	MTMR12	-1.04	-2.84	-2.72
220955_x_at	RAB23	-1.59	1.49	2.37
220992_s_at	TRMT1L	1.14	3.20	2.80
220997_s_at	DIAPH3	-1.28	-2.83	-2.21
221006_s_at	SNX27	-1.58	1.93	3.04
221015_s_at	CDADC1	1.16	2.92	2.51
221016_s_at	TCF7L1	1.05	2.31	2.19
221028_s_at	GFOD2	1.09	2.35	2.16
221029_s_at	WNT5B	-1.23	3.98	4.91
221047_s_at	MARK1	-1.05	2.00	2.11
221103_s_at	WDR52	1.54	2.11	1.37
221215_s_at	RIPK4	-1.11	1.90	2.11
221218_s_at	TPK1	1.07	2.63	2.46
221221_s_at	KLHL3	1.49	2.46	1.66
221222_s_at	C1orf56	1.24	3.02	2.43
221272_s_at	C1orf21	-1.03	2.48	2.57
221326_s_at	TUBD1	-1.00	3.03	3.04
221477_s_at	LOC100129518///SOD2	-1.18	-2.53	-2.14
221524_s_at	RRAGD	1.06	-10.33	-10.98
221527_s_at	PARD3	-1.13	3.72	4.20

221538_s_at	PLXNA1	1.24	2.79	2.25
221552_at	ABHD6	-1.03	4.91	5.03
221556_at	CDC14B	-1.23	1.87	2.31
221560_at	MARK4	-1.18	1.98	2.34
221564_at	PRMT2	1.08	2.08	1.93
221569_at	AHI1	1.21	5.14	4.25
221575_at	SCLY	-1.13	2.04	2.31
221582_at	HIST3H2A	1.10	-2.26	-2.49
221588_x_at	ALDH6A1	-1.28	-2.74	-2.13
221589_s_at	ALDH6A1	-1.21	-2.23	-1.84
221601_s_at	FAIM3	1.32	-2.61	-3.45
221602_s_at	FAIM3	1.07	-2.08	-2.22
221673_s_at	CSNK1G1	1.08	-2.16	-2.34
221679_s_at	ABHD6	1.19	2.17	1.82
221692_s_at	MRPL34	1.20	2.55	2.13
221752_at	SSH1	-1.20	2.31	2.78
221825_at	ANGEL2	-1.09	6.67	7.27
221833_at	LOC100507577///LONP2	1.46	2.39	1.64
221864_at	ORAI3	1.24	-1.73	-2.14
221873_at	ZNF143	-1.08	1.89	2.05
221880_s_at	FAM174B	-1.34	2.30	3.07
221904_at	FAM131A	-1.51	-4.10	-2.72
221927_s_at	ABHD11	1.39	-1.73	-2.41
221962_s_at	UBE2H	-1.36	-3.42	-2.51
221965_at	OTTHUMG00000168850	1.28	3.73	2.91
221985_at	KLHL24	-1.71	1.68	2.88
221988_at	SMIM7	-1.01	2.58	2.59
222032_s_at	USP7	1.06	2.21	2.08
222048_at	CRYBB2P1	1.13	2.27	2.01
222085_at	FAM174B	-1.34	2.39	3.20
222088_s_at	SLC2A14///SLC2A3	-1.37	-4.09	-2.99
222099_s_at	LSM14A	-1.04	2.28	2.38
222146_s_at	TCF4	1.34	2.85	2.13
222156_x_at	CCPG1///DYX1C1-CCPG1	-1.46	1.43	2.09
222177_s_at	SCAND2P	1.21	2.52	2.08
222183_x_at	AC005943.5	1.11	2.60	2.34
222250_s_at	INTS7	1.47	2.09	1.42
222270_at	SMEK2	1.22	-3.36	-4.11
222305_at	HK2	2.34	1.32	-1.77
222309_at		-1.32	-4.80	-3.64
222316_at		1.18	-2.71	-3.19
222333_at	ALS2CL	1.44	-1.80	-2.58
222343_at	BCL2L11	-1.07	-3.13	-2.93
222350_at		-1.21	-5.71	-4.70

32099_at	SAFB2	1.02	2.64	2.59
35776_at	ITSN1	1.02	2.50	2.44
36499_at	CELSR2	-1.58	1.71	2.69
36552_at	C2CD3	-1.07	3.26	3.49
36564_at	RNF19B	-1.21	-2.23	-1.85
37028_at	PPP1R15A	-1.18	-3.01	-2.55
37384_at	PPM1F	1.19	3.52	2.96
37433_at	PIAS2	-1.11	3.74	4.16
37943_at	ZFYVE26	1.14	2.67	2.33
38241_at	BTN3A3	1.17	2.06	1.76
38766_at	LOC100862671///SRCAP	1.03	-2.70	-2.79
41644_at	SASH1	1.15	2.63	2.29
45288_at	ABHD6	-1.10	4.57	5.03
47069_at	PRR5	1.14	3.49	3.07
47773_at	FBXO42	1.04	2.12	2.04
48030_i_at	FAXDC2	-1.20	-3.59	-2.99
48031_r_at	FAXDC2	-1.46	-4.79	-3.28
50376_at	ZNF444	1.29	2.04	1.59
51158_at	FAM174B	-1.40	2.82	3.94
55065_at	MARK4	-1.07	2.43	2.60
58780_s_at	ARHGEF40	-1.43	1.43	2.05
63009_at	SHQ1	1.26	2.57	2.04
65472_at	C2orf68	1.02	3.91	3.84
74694_s_at	RABEP2	1.19	2.04	1.71
222434_at	ENAH	-1.20	1.83	2.20
222450_at	PMEPA1	-1.03	2.51	2.59
222471_s_at	KCMF1	-1.07	2.29	2.45
222480_at	UBE2Q1	1.10	3.49	3.18
222483_at	EFHD2	1.14	-2.09	-2.40
222490_at	POLR3E	1.11	4.30	3.86
222526_at	GATAD2A	1.17	3.08	2.62
222531_s_at	AP5M1	-1.18	2.17	2.55
222559_s_at	RPRD1A	-1.08	3.41	3.67
222566_at	SUV420H1	-1.14	5.45	6.23
222585_x_at	KRCC1	1.21	2.12	1.75
222586_s_at	OSBPL11	-1.48	1.59	2.35
222618_at	SMU1	-1.00	2.13	2.13
222624_s_at	ZNF639	-1.08	2.06	2.23
222627_at	VPS54	-1.37	1.48	2.04
222629_at	REV1	1.16	2.65	2.28
222647_at	SLC35C1	1.02	2.17	2.13
222663_at	RIOK2	1.07	3.40	3.17
222664_at	KCTD15	1.16	3.32	2.87
222668_at	KCTD15	-1.30	5.16	6.69

222691_at	SLC35B3	1.03	2.92	2.83
222694_at	MGC2752	1.02	3.15	3.09
222704_at	POLR1A	1.51	2.16	1.43
222709_at	ATG7	-1.11	2.27	2.51
222710_at	AMIGO3///GMPPB	1.26	2.26	1.79
222720_x_at	C1orf27	1.39	2.09	1.50
222743_s_at	C11orf71	1.08	-1.91	-2.06
222748_s_at	TXNL4B	1.21	-1.67	-2.02
222749_at	SUFU	-1.04	2.21	2.30
222759_at	SUV420H1	-1.02	-3.74	-3.67
222761_at	BIVM	-1.25	1.85	2.31
222763_s_at	SFT2D3///WDR33	-1.26	-2.21	-1.75
222767_s_at	C12orf49	-1.11	-2.19	-1.97
222790_s_at	RSBN1	-1.23	1.86	2.30
222805_at	MANEA	-1.21	1.95	2.35
222806_s_at	C11orf30	1.04	2.29	2.21
222807_at	C11orf30	-1.12	1.81	2.03
222809_x_at	CCDC85C	-1.08	1.89	2.04
222815_at	RLIM	1.16	-2.59	-3.01
222819_at	CTPS2	-1.04	2.06	2.14
222820_at	TNRC6C	1.08	2.31	2.14
222846_at	RAB8B	-2.38	1.08	2.56
222875_at	DHX33	1.08	2.02	1.87
222883_at	SELRC1	1.31	2.70	2.05
222884_at	ZNF346	1.26	2.36	1.87
222891_s_at	BCL11A	-1.10	3.09	3.40
222893_s_at	RPAP2	1.09	2.79	2.57
222895_s_at	BCL11B	-1.34	3.52	4.73
222924_at	SLMAP	-1.31	1.57	2.06
222932_at	EHF	-1.36	-2.44	-1.79
222941_at	USP46	1.21	3.24	2.68
222946_s_at	AUNIP	1.15	3.43	2.98
223007_s_at	TMEM245	-1.06	2.94	3.13
223008_s_at	TMEM245	-1.17	3.40	3.97
223028_s_at	SNX9	-1.14	-2.02	-1.76
223059_s_at	FAM107B	-1.82	-2.03	-1.11
223092_at	ANKH	-1.02	2.12	2.16
223093_at	ANKH	-1.26	2.19	2.77
223104_at	JAGN1	1.23	2.09	1.70
223119_s_at	USP47	1.52	3.00	1.97
223162_s_at	KIAA1147	-1.58	2.76	4.36
223182_s_at	AGPAT3	1.02	2.42	2.38
223194_s_at	SLC22A23	1.27	4.21	3.30
223199_at	MKNK2	-1.34	-2.28	-1.70

223213_s_at	ZHX1	1.02	2.11	2.06
223228_at	LDOC1L	-1.17	2.01	2.34
223241_at	SNX8	1.26	-2.96	-3.74
223295_s_at	LUC7L	1.07	2.66	2.49
223300_s_at	CCDC82	-1.03	2.41	2.49
223314_at	TSPAN14	-1.29	1.82	2.35
223345_at	HDAC8	1.14	2.16	1.90
223347_at	MUM1	1.37	4.08	2.97
223348_x_at	MUM1	-1.01	2.09	2.10
223351_at	C17orf80	1.23	2.89	2.36
223378_at	GLIS2	-1.39	1.45	2.02
223385_at	CYP2S1	-1.30	-2.42	-1.86
223388_s_at	ZFYVE1	1.16	-2.27	-2.65
223400_s_at	PBRM1	-1.41	1.85	2.60
223404_s_at	TRMT1L	-1.26	2.12	2.68
223408_s_at	OTTHUMG00000177963	1.00	4.95	4.94
223409_at	OTTHUMG00000177963	1.13	5.65	5.02
223413_s_at	LYAR	1.26	2.04	1.62
223432_at	OSBP2	-1.11	-2.67	-2.40
223437_at	PPARA	-1.09	3.80	4.15
223438_s_at	PPARA	-1.01	4.00	4.02
223455_at	TCHP	1.09	2.05	1.88
223459_s_at	C1orf56	1.27	2.12	1.66
223467_at	RASD1	-1.04	-2.37	-2.29
223476_s_at	C12orf65	1.13	2.59	2.29
223484_at	C15orf48	1.09	-7.90	-8.64
223495_at	CCDC8	-1.06	2.89	3.08
223497_at	FAM135A	-1.14	4.97	5.67
223511_at	SPRTN	-1.27	2.36	3.00
223551_at	PKIB	-1.63	-4.00	-2.45
223555_at	GON4L	1.26	-1.87	-2.36
223594_at	TMEM117	1.15	2.33	2.03
223596_at	SLC12A6	-1.08	-4.82	-4.45
223651_x_at	CDC23	-1.56	-3.80	-2.43
223683_at	ZMYND15	1.15	-1.81	-2.09
223707_at	RPL27A///SNORA3	1.25	7.15	5.73
223712_at	PCBD2	-1.40	2.12	2.97
223735_at	ARL6	-1.53	1.93	2.97
223758_s_at	GTF2H2	1.14	-1.95	-2.22
223776_x_at	TINF2	1.12	-3.20	-3.57
223780_s_at	MED13	-1.04	-2.13	-2.05
223846_at	AZI2	-1.06	-2.16	-2.03
223849_s_at	MOV10	1.31	-1.64	-2.14
223882_at	FAM172A	1.05	-2.78	-2.93

223959_at	DNAL1	-1.01	2.48	2.50
223997_at	FNIP1	-1.31	-3.03	-2.31
224014_at	ZNF160	1.05	-2.24	-2.34
224064_s_at	DHDDS	1.04	-2.01	-2.09
224065_at	HIPK2	-1.05	-2.73	-2.61
224076_s_at	WHSC1L1	-1.08	3.37	3.65
224215_s_at	DLL1	-1.25	3.07	3.85
224318_s_at	KANSL3	1.10	2.14	1.95
224352_s_at	CFL2	-1.61	3.16	5.10
224443_at	LINC00467	1.69	-2.08	-3.52
224454_at	ETNK1	-1.33	-3.13	-2.36
224470_at	SEC22C	-1.21	2.05	2.48
224471_s_at	BTRC	-1.15	2.45	2.82
224484_s_at	BRMS1L	-1.07	2.28	2.44
224500_s_at	MON1A	1.26	2.38	1.88
224558_s_at	MALAT1	1.11	2.02	1.82
224562_at	WASF2	1.08	-1.97	-2.12
224565_at	MIR612///NEAT1	1.23	-1.94	-2.38
224566_at	MIR612///NEAT1	1.26	-2.14	-2.70
224618_at	PTBP3	-1.52	-2.06	-1.35
224635_s_at	BIRC6	-1.19	2.07	2.46
224657_at	ERRFI1	-1.41	-2.18	-1.55
224672_x_at	MESDC2	1.04	2.16	2.08
224682_at	ANKIB1	-1.26	1.67	2.10
224688_at	TMEM248	1.09	2.87	2.64
224701_at	PARP14	-1.14	1.76	2.01
224704_at	TNRC6A	1.01	2.94	2.92
224707_at	CYSTM1	-1.08	-2.21	-2.05
224711_at	YY1	-1.14	4.42	5.04
224718_at	YY1	-1.10	3.85	4.22
224728_at	ATPAF1	-1.49	4.05	6.04
224736_at	CCAR1	1.06	2.10	1.98
224737_x_at	CCAR1	-1.05	2.14	2.24
224797_at	ARRDC3	1.08	-10.11	-10.97
224809_x_at	TINF2	1.03	-3.61	-3.73
224822_at	DLC1	-1.05	2.06	2.16
224826_at	GPCPD1	1.10	-3.66	-4.04
224835_at	GPCPD1	1.34	-2.85	-3.81
224849_at	TTC17	1.10	4.48	4.08
224851_at	CDK6	-1.15	2.23	2.57
224852_at	TTC17	-1.09	2.59	2.82
224865_at	FAR1	-1.18	2.83	3.34
224882_at	ACSS1	1.04	2.03	1.96
224895_at	YAP1	-1.25	2.07	2.59

224900_at	ANKFY1	-1.03	2.13	2.19
224908_s_at	TTL	-1.04	1.98	2.07
224964_s_at	GNG2	1.04	-4.67	-4.88
224977_at	C6orf89	1.11	3.32	3.00
224988_at	C6orf89	1.05	-2.25	-2.36
224999_at	EGFR	-1.03	1.99	2.05
225015_s_at	STK40	-1.27	-2.48	-1.95
225022_at	GOPC	1.01	3.41	3.37
225031_at	CHD6	-1.13	2.98	3.36
225045_at	CCDC88A	-1.21	3.46	4.17
225046_at	LOC389831	-1.06	2.72	2.88
225072_at	ZCCHC3	-1.12	-3.66	-3.27
225076_s_at	ZNFX1	1.26	-1.68	-2.13
225085_at	USP40	1.35	2.05	1.52
225108_at	AGPS	-1.09	1.93	2.11
225109_at	OGFOD1	-1.05	2.32	2.44
225123_at	SESN3	1.05	2.72	2.59
225137_at	NFATC3	-1.05	2.02	2.13
225139_at	NFATC3	1.10	2.42	2.20
225142_at	JHDM1D	-1.68	-3.60	-2.14
225144_at	BMPR2	-1.70	2.23	3.79
225145_at	NCOA5	-1.14	3.13	3.56
225157_at	MLXIP	-1.17	2.71	3.16
225164_s_at	EIF2AK4	-1.11	2.04	2.25
225170_at	WDR5	-1.05	2.12	2.23
225171_at	ARHGAP18	-1.15	-2.36	-2.05
225173_at	ARHGAP18	-1.15	-2.05	-1.77
225177_at	RAB11FIP1	-1.39	1.93	2.67
225191_at	CIRBP	1.07	-2.27	-2.43
225197_at	OTTHUMG00000178149	-1.01	-2.56	-2.53
225217_s_at	BRPF3	1.02	2.78	2.73
225219_at	SMAD5	-1.14	2.52	2.87
225223_at	SMAD5	-1.13	1.93	2.19
225251_at	RAB24	1.68	-1.57	-2.64
225266_at	ZNF652	-1.25	2.51	3.14
225283_at	ARRDC4	-1.24	-3.79	-3.06
225290_at	ETNK1	-1.48	1.84	2.73
225313_at	FAM217B	-1.07	3.09	3.30
225318_at		-1.17	1.75	2.06
225336_at	SCAF11	-1.06	2.49	2.65
225341_at	MTERFD3	-1.06	4.10	4.33
225343_at	TMED8	-1.26	1.65	2.08
225346_at	MTERFD3	1.23	3.46	2.81
225348_at	LOC100996657///SRSF10	-1.01	2.42	2.45

225387_at	TSPAN5	-1.28	1.76	2.26
225388_at	TSPAN5	-1.46	2.26	3.29
225396_at	RBBP4	1.37	3.08	2.25
225432_s_at	CSRP2BP	1.37	3.72	2.71
225444_at	UBN2	-1.36	1.87	2.54
225445_at	UBN2	-1.06	2.80	2.95
225446_at	BRWD1	-1.42	-4.10	-2.88
225468_at	PATL1	-1.81	1.32	2.40
225473_at	SOGA1	1.01	4.21	4.18
225486_at	ARID2	-1.07	4.63	4.95
225490_at	ARID2	1.25	2.31	1.85
225497_at	ATE1	-1.26	2.14	2.69
225499_at	RALGAPA2	-1.10	3.36	3.68
225502_at	DOCK8	1.15	2.68	2.32
225509_at	SAP30L	-1.16	7.32	8.47
225534_at	SMIM19	1.43	-1.59	-2.27
225543_at	GTF3C4	-1.14	3.69	4.21
225545_at	EEF2K///LOC101060570	1.15	2.26	1.96
225546_at	EEF2K	-1.01	3.17	3.20
225554_s_at	ANAPC7	1.44	2.34	1.62
225558_at	GIT2	-1.01	9.92	10.03
225560_at	POMT2	1.26	2.46	1.95
225563_at	PAN3	-1.27	1.71	2.17
225569_at	CTA-204B4.6///OTTHUMG00000172354	-1.23	1.98	2.43
225579_at	PQLC3	1.11	-1.93	-2.13
225594_at	CREBZF	1.15	2.60	2.26
225601_at	HMGB3	-1.09	6.19	6.77
225623_at	KIAA1737	-1.11	2.18	2.41
225658_at	SPOPL	-1.50	1.40	2.09
225666_at	TMTC4	-1.39	3.31	4.60
225711_at	ARL6IP6	-1.34	1.68	2.24
225716_at	BRI3BP	-1.11	2.74	3.02
225729_at	C6orf89	1.33	2.98	2.24
225733_at	B3GALT6	1.12	2.41	2.15
225738_at	RAPGEF1	-1.14	1.83	2.08
225747_at	COQ10A	1.00	2.14	2.13
225752_at	NIPA1	-1.52	1.38	2.09
225755_at	KLHDC8B	-1.34	1.75	2.35
225805_at	HNRNPU	1.13	2.28	2.02
225811_at	C11orf58	-1.07	1.90	2.04
225813_at	RC3H2	-1.12	2.21	2.48
225842_at	PHLDA1	-1.13	2.52	2.86
225845_at	ZBTB44	-1.26	2.66	3.36
225855_at	EPB41L5	-1.51	-7.12	-4.73

225856_at	CLOCK	-1.19	2.17	2.58
225881_at	SLC35B4	-1.09	2.80	3.05
225882_at	SLC35B4	1.20	4.35	3.61
225884_s_at	GZF1	1.31	-1.81	-2.37
225890_at	MGME1	1.50	2.62	1.74
225917_at		-1.25	1.65	2.07
225921_at	NIN	-1.04	2.70	2.81
225930_at	NKIRAS1	-1.11	2.57	2.86
225935_at	CUX1	-1.32	2.79	3.68
225945_at	ZNF655	1.06	2.97	2.79
225953_at	RPRD1A	-1.32	2.42	3.19
225970_at	DDHD1	-1.34	1.93	2.59
225971_at	DDHD1	-1.18	4.54	5.37
225978_at	RIMKLB	1.02	-2.76	-2.81
225985_at	PRKAA1	-1.13	3.26	3.69
225988_at	HERC4	-1.19	2.28	2.72
225989_at	HERC4	-1.03	3.80	3.92
225990_at	BOC	1.27	5.00	3.94
226012_at	ANKRD11	1.15	2.85	2.47
226021_at	RDH10	-1.12	2.15	2.41
226034_at	DUSP4	-1.42	2.54	3.60
226038_at	LONRF1	-1.19	-2.05	-1.73
226040_at	LOC100996615	-1.09	3.33	3.64
226044_at	TDP1	-1.13	2.32	2.63
226045_at	FRS2	-1.13	2.32	2.63
226065_at	PRICKLE1	-1.04	6.92	7.19
226077_at	RNF145	-1.09	2.00	2.19
226089_at	RABL3	1.03	-2.03	-2.10
226105_at	C1GALT1	-1.24	1.91	2.38
226116_at	DFFA	1.11	2.30	2.08
226117_at	TIFA	-1.23	2.07	2.55
226118_at	CENPO	1.21	3.93	3.23
226139_at	CCDC149	1.18	2.25	1.90
226148_at	ZBTB44	-1.03	2.93	3.02
226150_at	PPAPDC1B	1.10	-2.05	-2.25
226152_at	TTC7B	-1.30	1.81	2.36
226157_at	TFDP2	1.02	5.15	5.07
226161_at	SLC30A6	-1.01	2.03	2.05
226169_at	SBF2	-1.25	1.94	2.42
226170_at	EYA3	-1.03	2.66	2.74
226179_at	SLC25A37	-1.05	5.01	5.28
226180_at	WDR36	1.05	3.75	3.57
226183_at	GSK3B	-1.25	1.90	2.38
226185_at	CDS1	-1.13	2.21	2.49

226187_at	CDS1	-1.15	1.76	2.04
226224_at	FOXK2	1.06	6.12	5.80
226230_at	SMEK2	1.01	5.07	5.01
226234_at	GDF11	-1.05	3.32	3.48
226235_at	LINC00667	1.10	-1.84	-2.04
226263_at	SNRNP48	-1.00	2.05	2.06
226272_at	RCAN3	-1.55	1.48	2.29
226291_at	ALS2	1.06	3.64	3.43
226295_at	ITFG2///LOC100507424	1.46	-1.39	-2.03
226306_at	C6orf1	1.11	-2.19	-2.42
226316_at	RBM26	-1.19	4.07	4.85
226317_at	PPP4R2	-1.19	1.68	2.00
226322_at	TMTC1	1.26	4.35	3.46
226350_at	CHML	1.20	3.42	2.85
226354_at	LACTB	-1.11	1.93	2.14
226359_at	GTPBP1	1.26	-1.66	-2.09
226360_at	ZNRF3	1.05	2.35	2.23
226361_at	TMEM42	1.29	-1.84	-2.37
226366_at	SHPRH	-1.37	1.76	2.40
226367_at	KDM5A	-1.02	2.29	2.33
226368_at	CHST11	-1.56	2.54	3.96
226372_at	CHST11	-1.18	2.16	2.56
226377_at	NFIC	-1.12	2.66	2.98
226390_at	STARD4	-1.25	-2.48	-1.98
226416_at	ERI1	-1.08	2.82	3.03
226426_at	ADNP	-1.16	4.17	4.84
226431_at	FAM117B	-1.10	3.56	3.92
226432_at	ETNK1	-1.60	1.34	2.15
226450_at	INSR	-1.10	3.86	4.25
226463_at	ATP6V1C1	-1.11	4.84	5.37
226473_at	CBX2	1.08	3.08	2.85
226485_at	VSIG10	-1.18	2.66	3.14
226487_at	FAM222A	1.27	2.29	1.80
226491_x_at	PTBP1	1.08	2.02	1.87
226495_at	MAVS	1.17	2.65	2.27
226500_at	ZBTB47	1.06	2.09	1.97
226510_at	HEATR5A	-1.34	1.89	2.53
226532_at		-1.18	1.94	2.30
226561_at	AGFG1	-1.34	3.56	4.77
226568_at	FAM102B	-1.88	1.65	3.10
226576_at	ARHGAP26	-1.45	2.87	4.17
226583_at	C12orf76	-1.02	-2.25	-2.21
226590_at	ZNF618	-1.06	4.24	4.50
226592_at	ZNF618	-1.31	4.38	5.73

226602_s_at	BCR	-1.06	2.65	2.80
226604_at	TMTC3	-1.04	3.28	3.43
226615_at	XPR1	-1.26	2.21	2.80
226628_at	THOC2	-1.28	2.41	3.08
226641_at	ANKRD44	-1.41	1.85	2.59
226644_at	MIB2	1.02	-2.05	-2.09
226649_at	PANK1	-1.22	4.78	5.85
226652_at	USP3	1.03	3.86	3.74
226660_at	RPS6KB1	-1.29	1.82	2.35
226663_at	ANKRD10-IT1	1.24	2.01	1.62
226684_at	ATG2B	1.06	2.80	2.65
226685_at	SNTB2	-1.19	2.61	3.11
226687_at	PRPF40A	1.46	5.02	3.43
226688_at	TCAIM	-1.36	6.07	8.27
226722_at	FAM20C	-1.19	2.70	3.22
226734_at	EIF4E2	-1.32	2.74	3.62
226754_at	ZNF251	-1.29	1.75	2.26
226770_at	MAGI3	-1.46	1.56	2.28
226773_at	PPM1K	-1.26	3.42	4.30
226775_at	ENY2	1.16	2.53	2.17
226787_at	ZNF18	1.53	-1.49	-2.28
226793_at	LINC00294	-1.08	2.77	2.99
226794_at	STXBP5	-1.21	3.74	4.53
226800_at	EFCAB7	1.33	5.61	4.22
226821_at		1.03	5.44	5.27
226828_s_at	HEYL	-1.44	-2.08	-1.44
226833_at	CYB5D1	1.43	2.66	1.86
226848_at		1.49	4.78	3.21
226849_at	DENND1A	-1.19	2.14	2.53
226853_at	BMP2K	-1.73	1.77	3.06
226862_at	MBD1	1.16	-3.14	-3.64
226868_at	GXYLT1	1.10	3.40	3.10
226872_at	RFX2	1.21	2.66	2.19
226874_at	KLHL8	1.18	2.18	1.85
226895_at	NFIC	1.21	2.13	1.76
226905_at	FAM101B	-1.55	1.62	2.51
226912_at	ZDHHC23	1.04	2.52	2.44
226947_at	GUSBP1///GUSBP4///LOC100996497	1.76	2.48	1.41
226948_at	RHBDD1	1.13	-2.17	-2.44
226955_at	AFAP1L1	-1.01	2.54	2.56
226964_at	TTBK2	-1.39	2.30	3.20
226969_at	MTR	1.36	6.99	5.15
226978_at	PPARA	-1.57	2.61	4.08
226986_at	WIPI2	1.00	3.23	3.22

226987_at	RBM15B	-1.05	5.64	5.90
226993_at	TRIP12	-1.09	3.69	4.03
227001_at	NIPAL2	1.33	2.05	1.55
227011_at	ZNF672	1.17	-1.78	-2.08
227025_at	PPHLN1	-1.09	3.18	3.46
227026_at	MPHOSPH8	1.05	2.67	2.54
227031_at	SNX13	-1.25	1.83	2.29
227032_at	PLXNA2	-1.22	3.91	4.75
227040_at	NHLRC3	-1.35	2.58	3.49
227067_x_at	NOTCH2///NOTCH2NL	1.17	-3.28	-3.83
227069_at	CUX1	-1.11	3.26	3.61
227077_at	ZNF286A///ZNF286B	1.04	2.12	2.05
227099_s_at	C11orf96	1.23	-2.56	-3.16
227103_s_at	ECE2	1.44	2.69	1.87
227107_at		-1.06	2.05	2.18
227109_at	CYP2R1	1.16	2.36	2.04
227128_s_at	TACSTD2	-1.55	-2.10	-1.35
227142_at	PLEKHG5	1.15	-1.90	-2.20
227155_at	LMO4	1.00	2.59	2.58
227169_at	DNAJC18	-1.02	2.24	2.29
227175_at	MCL1	1.02	-2.20	-2.24
227177_at	CORO2A	-1.19	2.31	2.74
227179_at	STAU2	-1.19	1.89	2.25
227201_at	LOC643837	1.02	2.29	2.24
227204_at	PARD6G	-1.16	2.01	2.33
227246_at	PLRG1	-1.04	3.00	3.11
227247_at	PLEKHA8	-1.34	1.63	2.18
227256_at	USP31	-1.17	3.56	4.16
227270_at	FAM200B	1.01	2.41	2.38
227277_at	MTDH	-1.44	2.91	4.19
227280_s_at	CCNYL1	-1.21	1.69	2.04
227288_at	SREK1IP1	-1.29	2.35	3.04
227293_at		1.19	2.99	2.51
227312_at	SNTB2	-1.38	1.91	2.65
227331_at	ZNF740	1.01	2.07	2.04
227335_at	DIDO1	-1.00	11.58	11.62
227337_at	ANKRD37	1.28	-3.01	-3.85
227341_at	BEND7	-1.81	2.91	5.26
227350_at	HELLS	-1.63	1.85	3.02
227368_at		-1.02	-4.82	-4.72
227375_at	ANKRD13C	-1.18	1.83	2.16
227376_at	GLI3	1.02	2.74	2.69
227385_at	PPAPDC2	1.14	-1.96	-2.23
227407_at	TAPT1	-1.01	2.20	2.23

227408_s_at	SNX25	-1.35	1.58	2.12
227422_at	STRN	-1.41	1.60	2.25
227426_at	SOS1	-1.11	11.30	12.51
227449_at	EPHA4	1.41	14.92	10.56
227467_at	RDH10	-1.06	2.52	2.69
227472_at	DDA1	1.03	2.39	2.32
227476_at	LPGAT1	-1.11	2.38	2.63
227478_at	SETBP1	-1.37	5.16	7.06
227485_at	DDX26B	-1.17	2.23	2.59
227486_at	NT5E	1.06	-2.05	-2.17
227491_at	ELOVL6	1.39	2.80	2.02
227492_at	OCLN	-1.74	-4.99	-2.87
227497_at	SOX6	2.30	3.03	1.32
227498_at	SOX6	2.15	3.98	1.85
227499_at	FZD3	-1.23	3.25	4.00
227502_at	OTTHUMG00000157537	-1.19	2.24	2.67
227525_at	GLCCI1	-1.77	2.55	4.51
227529_s_at	AKAP12	-3.05	-2.37	1.29
227533_at		-1.68	1.52	2.56
227543_at	RNASEH2C	1.23	2.16	1.76
227547_at	OTTHUMG00000177126	1.11	2.21	2.00
227559_at	NDUFAF4	1.01	9.14	9.02
227579_at	FER	-1.36	1.57	2.13
227594_at	ZMYM6	1.26	4.04	3.20
227595_at	ZMYM6	1.26	2.75	2.18
227604_at	TMEM185B	1.30	4.47	3.42
227611_at	TARSL2	-1.30	1.75	2.27
227618_at		-1.23	2.80	3.45
227622_at	PCF11	1.13	-4.02	-4.53
227623_at	CACNA2D1	-1.51	1.45	2.19
227630_at	PPP2R5E	-1.08	2.94	3.17
227633_at	RHEB	-1.07	2.03	2.18
227645_at	PIK3R5	-1.06	-2.27	-2.15
227649_s_at	SRGAP2///SRGAP2D	1.06	-2.61	-2.78
227657_at	RNF150	1.05	-3.64	-3.81
227665_at		-1.44	2.39	3.43
227677_at	JAK3	-1.13	-2.72	-2.40
227680_at	ZNF326	-1.12	2.00	2.25
227685_at	TMF1	-1.35	1.83	2.48
227689_at	ZNF227	1.35	2.60	1.93
227699_at	L3HYPDH	1.22	2.07	1.70
227713_at	KATNAL1	-1.41	1.61	2.27
227718_at	PURB	-1.05	-4.27	-4.08
227757_at	CUL4A	1.04	-2.74	-2.85

227770_at	COG8	1.47	2.89	1.97
227787_s_at	MED30	-1.69	-2.09	-1.24
227790_at	UBE3D	1.39	7.43	5.33
227807_at	PARP9	1.09	-2.07	-2.26
227812_at	TNFRSF19	-2.03	1.96	3.97
227815_at	VPS33A	1.04	2.52	2.42
227820_at	TBC1D25	1.05	2.46	2.34
227822_at	ZNF605	1.25	7.62	6.11
227839_at	MBD5	1.15	5.41	4.71
227854_at		-1.03	3.41	3.52
227855_at	ARHGEF40	-1.11	1.83	2.03
227866_at	LOC100505519///TIAM2	-1.46	3.43	4.99
227876_at	ARHGAP39	-1.17	2.47	2.89
227904_at	AZI2	-1.10	-2.61	-2.38
227905_s_at	AZI2	-1.00	-2.02	-2.01
227908_at	TBC1D24	-1.02	5.37	5.50
227917_at	LOC100506990	-1.19	1.90	2.25
227920_at	BEND3	1.18	2.53	2.15
227925_at	ST3GAL4-AS1	-1.33	2.57	3.42
227936_at	TMEM68	-1.09	-2.03	-1.87
227943_at		2.00	2.51	1.25
227944_at	PTPN3	1.12	2.26	2.02
227950_at	UBE2H	-1.32	-3.09	-2.34
227955_s_at	EFNA5	-1.04	2.90	3.03
227959_at		1.03	2.39	2.33
227967_at	TUBGCP5	1.38	2.22	1.61
227980_at	ZNF322	-1.05	2.67	2.80
227985_at	LOC100506098	-1.11	-9.20	-8.26
227988_s_at	VPS13A	1.13	2.66	2.35
227995_at	LOC100509635	1.18	2.05	1.73
227997_at	IL17RD	-2.52	1.05	2.63
228002_at	GTPBP4///IDI2	1.36	2.22	1.64
228006_at	PTEN	1.11	7.27	6.54
228016_s_at		1.19	-1.72	-2.04
228020_at	PTCD3	1.50	4.43	2.95
228026_at	SIKE1	-1.51	1.66	2.50
228032_s_at	DENND1B	-1.36	1.70	2.32
228039_at	DDX46	-1.25	2.24	2.79
228044_at	SERP2	-1.59	1.99	3.17
228045_at		1.09	3.20	2.94
228054_at	TMEM44	1.06	5.70	5.38
228063_s_at	NAP1L5	1.34	-2.29	-3.07
228066_at	C17orf96	1.20	2.25	1.86
228070_at	PPP2R5E	-1.29	3.11	4.00

228081_at	CCNG2	-1.07	2.72	2.92
228095_at	PHF14	1.39	3.77	2.72
228103_s_at	AC007362.3	-1.42	-2.19	-1.54
228110_x_at		1.37	-2.11	-2.89
228115_at	GAREM	-1.17	3.09	3.62
228149_at	C7orf60	1.07	2.11	1.98
228153_at	RNF144B	-1.24	1.81	2.25
228156_at		-1.49	2.66	3.96
228172_at	OTTHUMG00000175795	1.66	4.23	2.54
228177_at	CREBBP	1.15	4.12	3.57
228181_at	SLC30A1	1.11	-3.56	-3.94
228190_at	ATG4C	1.04	2.84	2.75
228234_at	TICAM2///TMED7-TICAM2	-1.02	2.12	2.17
228239_at	LOC101060027///SMIM11	1.22	2.05	1.69
228259_s_at	EPB41L4A-AS1	1.51	2.93	1.94
228274_at	SDSL	1.13	-5.09	-5.73
228277_at	FBXL19	1.00	2.81	2.81
228280_at	ZC3HAV1L	-1.56	2.41	3.77
228282_at	MFSD8	-1.14	2.41	2.74
228310_at	ENAH	-1.02	4.79	4.89
228318_s_at	CRIPAK	1.12	2.44	2.17
228321_s_at	NAA30	-1.31	-2.75	-2.09
228341_at	NUDT16	1.10	2.32	2.12
228346_at	ZNF844	1.00	-5.78	-5.79
228356_at	ANKRD11	1.51	-1.64	-2.48
228359_at	UBASH3B	-1.22	-2.26	-1.85
228380_at	SENP2	-1.06	9.88	10.51
228390_at	RAB30	1.08	3.16	2.93
228395_at	GNL3	1.73	5.02	2.89
228400_at	SHROOM3	-1.36	2.07	2.81
228416_at	ACVR2A	-1.11	2.35	2.60
228420_at	PDCD2	1.34	2.58	1.93
228423_at	MAP9	1.24	3.52	2.83
228432_at	RAB3IP	-1.46	-4.76	-3.26
228433_at	NFYA	1.36	3.60	2.65
228449_at	MORC2-AS1	1.01	3.60	3.57
228465_at		1.62	-3.14	-5.08
228466_at	GABPB2	1.19	2.24	1.88
228476_at	KIAA1407	1.67	2.37	1.42
228479_at	SOAT1	-1.25	4.19	5.24
228482_at	CDRT4///TVP23C-CDRT4	-1.16	1.99	2.31
228512_at	PTCD3	1.12	3.15	2.80
228515_at	LOC90784///POLR1A	1.88	5.52	2.94
228519_x_at	CIRBP	1.43	-1.48	-2.12

228523_at	NANOS1	1.36	3.40	2.50
228526_at	NANOS1	1.38	2.27	1.64
228535_at	RAD1	-1.03	3.80	3.92
228551_at	DENND5B	1.30	5.66	4.35
228568_at	GCOM1///MYZAP	-1.71	-3.30	-1.93
228570_at	BTBD11	1.45	-2.98	-4.30
228574_at	TMTC2	-1.20	1.90	2.28
228605_at	UBXN2A	-1.67	2.65	4.42
228627_at	TLK2	-1.30	4.91	6.36
228639_at		-1.03	3.00	3.09
228661_s_at	LOC100506029///LOC100506051	1.46	3.28	2.24
228671_at	TMEM201	1.30	3.43	2.63
228686_at	FLJ33630	-1.09	1.98	2.16
228694_at		-1.10	2.97	3.26
228696_at	SLC45A3	-1.08	2.27	2.46
228702_at	FLJ43663	1.26	-6.86	-8.66
228711_at	ZNF37A	1.13	2.83	2.51
228716_at	THRB	-1.24	2.60	3.23
228722_at	PRMT2	-1.41	2.39	3.36
228734_at	UBE2V2	-1.19	2.07	2.48
228736_at	HELQ	1.38	4.77	3.45
228742_at		-1.15	-4.02	-3.50
228751_at	CLK4	-1.02	1.97	2.01
228760_at	SRSF8	-1.05	3.60	3.78
228762_at	LFNG	1.12	2.27	2.02
228763_at	MDP1///NEDD8-MDP1	1.19	-1.78	-2.12
228764_s_at	MDP1///NEDD8-MDP1	1.25	-2.20	-2.75
228765_at	GTF2IRD2	1.15	-2.10	-2.41
228776_at	GJC1	-1.20	2.62	3.16
228777_at	KBTBD3	-1.28	2.11	2.71
228778_at	MCPH1	1.29	-1.59	-2.05
228786_at	PTCHD3P1	-1.10	3.25	3.58
228789_at	MTMR6	-1.37	1.47	2.02
228797_at	NLN	1.31	4.47	3.40
228809_at	CXorf40A///CXorf40B	1.31	4.34	3.32
228810_at	CCNYL1	-1.26	-2.07	-1.65
228817_at	ALG9	-1.11	2.95	3.27
228841_at	LYRM7	1.25	2.10	1.68
228843_at	ARL10	-1.07	4.58	4.88
228861_at	CDS2	-1.33	1.84	2.43
228865_at	C1orf116	1.05	-2.07	-2.18
228891_at	SEMA4D	1.33	3.87	2.90
228902_at	NUP214	1.51	2.29	1.52
228905_at	PCM1	1.09	2.69	2.47

228914_at		-1.38	2.96	4.09
228920_at	ZNF260	1.10	2.71	2.46
228932_at		-1.03	2.99	3.09
228948_at	EPHA4	1.60	8.38	5.25
228955_at	LRP8	1.26	2.23	1.76
228963_at		-1.11	1.96	2.17
228965_s_at	PANK2	-1.03	-3.86	-3.74
228966_at	PANK2	-1.73	-6.33	-3.66
228967_at	EIF1	1.09	5.43	5.01
228980_at	RAD51L3-RFFL///RFFL	-1.40	-2.01	-1.44
228987_at	FAM49B	1.11	11.45	10.31
228991_at	CDK13	-1.19	1.73	2.06
228998_at	TNRC6B	-1.05	3.41	3.59
228999_at	CHD2///LOC100507217	1.18	-3.13	-3.70
229005_at	MCTP2	1.08	2.29	2.12
229007_at	LOC283788	-1.06	1.97	2.08
229018_at	METTL25	-1.00	4.31	4.33
229021_at	MCTP2	1.38	6.58	4.77
229064_s_at	RCAN3	-1.47	-2.79	-1.90
229066_at		1.20	3.08	2.56
229070_at	ADTRP	-1.10	-2.23	-2.02
229072_at	RAB30	1.05	4.91	4.67
229075_at	SPATA5	-1.20	2.88	3.45
229131_at	EXD2	-1.28	2.64	3.38
229132_at	MINA	-1.04	2.86	2.99
229134_at	VANGL1	-1.21	5.14	6.23
229135_at	FASTKD2	1.47	2.18	1.49
229146_at	C7orf31	1.03	2.97	2.89
229155_at		1.37	2.64	1.93
229167_at	PURA	-1.14	2.21	2.53
229180_at	WWC1	1.39	2.73	1.96
229194_at	PCGF5	-1.43	-2.21	-1.54
229202_at		1.43	2.54	1.77
229221_at	CD44	-1.47	-2.37	-1.61
229232_at	LRRC57	-1.21	-2.14	-1.77
229240_at	ZDHHC21	-1.55	1.46	2.27
229267_at	ANAPC1///LOC730268	1.26	2.18	1.74
229287_at	PCNX	-1.00	3.31	3.31
229292_at	EPB41L5	-1.31	-2.00	-1.53
229295_at	IL17RA	1.23	4.10	3.34
229325_at	ZZZ3	-1.08	2.09	2.26
229333_at		1.23	6.00	4.88
229342_at	C17orf85	1.01	5.96	5.92
229359_at		1.16	3.44	2.97

229366_at		1.12	3.33	2.96
229370_at	LOC100996388	1.30	-1.87	-2.42
229382_at	FAM212B	1.11	3.17	2.87
229394_s_at	ARHGAP35	1.12	3.10	2.78
229397_s_at	ARHGAP35	1.15	2.74	2.37
229405_at	KIF7	1.10	2.52	2.29
229417_at		-1.05	3.35	3.53
229423_at	CHEK1	1.08	-2.38	-2.56
229428_at	TIMM23	-1.14	-2.16	-1.90
229484_at	PPM1J	1.26	-1.66	-2.10
229492_at	VANGL1	-1.37	2.70	3.68
229494_s_at	PHLDA2	-1.07	-2.50	-2.33
229511_at	SMARCE1	1.06	-3.08	-3.26
229513_at	STRBP	-1.20	2.96	3.54
229517_at	PTPDC1	-1.20	2.82	3.38
229519_at	FXR1	-1.22	-3.02	-2.48
229528_at	SBNO1	-1.05	3.90	4.10
229531_at		1.65	3.65	2.22
229532_at	ZNF502	1.18	-1.70	-2.00
229539_at	ABCB8	1.45	4.42	3.04
229564_at	RRP7A	1.32	2.82	2.14
229572_at	ATP6V0A2	1.28	11.76	9.18
229573_at	USP9X	-1.17	2.20	2.57
229577_at	AGPAT6	1.08	4.67	4.33
229587_at	UBA2	-1.09	2.07	2.26
229598_at	COBLL1	-1.47	2.51	3.68
229608_at	FAM212B	-1.25	1.66	2.08
229611_at	LMLN	1.44	3.83	2.65
229616_s_at	GRAMD2	1.29	-1.83	-2.37
229624_at	OPA3	1.29	2.19	1.70
229632_s_at	INTS10	1.47	2.68	1.82
229657_at	THRB	-1.29	2.37	3.06
229665_at	CSTF3	-1.20	-2.07	-1.72
229666_s_at	CSTF3	-1.03	-2.10	-2.03
229674_at	SERTAD4	-1.35	1.93	2.61
229676_at	MTPAP	1.07	-2.77	-2.96
229690_at	FAM109A	-1.10	2.13	2.34
229695_at		1.24	-4.70	-5.80
229704_at		-1.23	2.53	3.11
229710_at	LOC101060023	1.01	5.69	5.62
229741_at	MAVS	1.09	3.30	3.04
229744_at	SSFA2	-1.05	-3.90	-3.70
229764_at	LOC101060141///TPRG1	-1.03	-2.47	-2.39
229778_at	C12orf39	-1.12	-2.96	-2.64

229796_at	SIX4	-1.13	1.79	2.02
229832_x_at	SH3TC1	1.08	-2.37	-2.56
229845_at	MAPKAP1	-1.14	-2.44	-2.15
229849_at	WIPF3	1.14	2.61	2.29
229850_at	KDSR	-1.32	1.87	2.47
229852_at	NMNAT1	-1.02	2.41	2.47
229857_s_at	KANSL1-AS1	1.49	-1.96	-2.92
229868_s_at	GDF15	1.02	-2.83	-2.88
229894_s_at	RAB43	1.29	-3.54	-4.58
229896_at	AC083884.8	-1.23	2.17	2.67
229926_at	MIR3682	-1.06	2.61	2.77
229927_at	LEMD1	1.09	-4.33	-4.71
229939_at	ENDOV///LOC100507440	1.11	-1.97	-2.19
229958_at	CLN8	1.07	4.75	4.44
229969_at	SEC63	1.13	2.21	1.96
229986_at	LOC100287163///ZNF717	-1.24	-2.36	-1.90
230009_at	FAM118B	-1.13	2.38	2.70
230013_s_at	ARHGAP23	1.28	-1.75	-2.24
230029_x_at	UBR3	-1.09	2.13	2.32
230056_at	BPTF	-1.16	4.21	4.87
230069_at	SFXN1	-1.04	2.11	2.18
230082_at		-1.46	2.25	3.27
230098_at	PHF20L1	-1.10	6.24	6.85
230122_at	MLLT10	-1.46	1.76	2.58
230133_at	RC3H2	1.03	-3.91	-4.02
230134_s_at	RC3H2	-1.25	-3.50	-2.80
230150_at	BCAP29	-1.08	2.34	2.53
230154_at	WAC	1.07	2.29	2.13
230177_at	GTF2H2B	-1.19	3.05	3.62
230178_s_at	ELP2	1.24	2.91	2.34
230183_at	EXT1	-1.03	2.48	2.55
230185_at	THAP9	1.18	-2.89	-3.41
230192_at	TRIM13	-1.47	4.07	5.98
230206_at	DOCK5	-1.08	2.24	2.42
230207_s_at	DOCK5	-1.07	2.11	2.26
230210_at	SUN1	-1.14	-2.35	-2.06
230211_at	TRIP11	-1.15	2.27	2.62
230230_at	PTPN4	-1.06	4.36	4.61
230234_at	FXN	-1.03	2.23	2.29
230240_at		1.18	2.97	2.52
230241_at	TOR1AIP2	1.10	2.36	2.16
230263_s_at	DOCK5	-1.04	2.22	2.30
230266_at	RAB7B	1.57	3.73	2.38
230267_at	OTTHUMG00000179824	1.08	2.48	2.30

230275_at	ARSI	-1.13	1.99	2.25
230294_at	OTTHUMG00000032279	1.44	-1.73	-2.50
230307_at	SLC25A21-AS1	1.07	-2.86	-3.07
230321_at	TOR1AIP2	-1.08	2.65	2.85
230336_at		-1.71	3.34	5.70
230343_at		2.01	8.71	4.33
230346_x_at		1.16	-1.87	-2.17
230348_at	LATS2	1.16	-1.95	-2.28
230350_at		1.12	7.26	6.51
230369_at	GPR161	-1.49	8.48	12.66
230399_at		-1.07	2.14	2.29
230403_at	RFX3	-1.64	1.85	3.03
230407_at	SBNO1	-1.08	2.72	2.92
230434_at	PHOSPHO2	1.06	5.43	5.14
230444_at	PDE7A	-1.09	3.05	3.32
230454_at	ICA1L	-1.11	3.12	3.48
230469_at	RTKN2	-1.92	1.83	3.53
230492_s_at	GPCPD1	1.39	-3.80	-5.28
230511_at	CREM	-1.12	2.27	2.55
230518_at	MPZL2	1.05	-2.40	-2.51
230528_s_at	MGC2752	1.01	3.34	3.31
230535_s_at	ATP5E	1.16	3.24	2.79
230566_at	MORC2-AS1	1.18	4.34	3.67
230571_at		-1.18	2.37	2.79
230610_at		1.05	4.08	3.90
230613_at	GMEB1	-1.35	2.61	3.52
230618_s_at		-1.34	1.69	2.27
230667_at	FAM204A	-1.25	1.71	2.14
230676_s_at	TMEM19	-1.25	1.67	2.09
230684_at	GTPBP10	1.15	3.45	3.01
230687_at	SLC13A3	1.02	-2.00	-2.03
230689_at		-1.23	4.92	6.04
230697_at	BBS5	1.17	-2.65	-3.08
230710_at	MIR210HG	-1.28	-4.20	-3.28
230721_at	C16orf52///LOC101060634	-1.27	5.33	6.76
230762_at		1.29	-2.48	-3.21
230764_at		-1.12	-3.62	-3.24
230766_at	GART	1.13	3.60	3.20
230777_s_at	PRDM15	1.27	3.39	2.67
230778_at		-1.13	2.06	2.33
230787_at	OTTHUMG00000012496///RP11-126K1.6	1.49	-2.28	-3.40
230821_at	ZNF148	-1.48	3.42	5.08
230828_at		1.48	-1.82	-2.69
230831_at	FRMD5	-1.50	7.01	10.52

230888_at	WDR91	-1.35	1.53	2.07
230922_x_at	FUNDC2	1.10	2.18	1.98
230938_x_at	ATF5	1.26	-1.66	-2.09
230948_at	OTTHUMG00000183966	-1.24	3.67	4.55
230951_at	EPB41L5	-1.80	1.28	2.30
230967_s_at	USP7	1.23	2.40	1.95
230968_at	GS1-465N13.1	-1.58	4.84	7.64
230974_at	DDX19B	-1.18	1.79	2.11
230979_at		-1.66	2.51	4.18
231004_s_at		-1.16	-3.54	-3.06
231017_at	STK11	1.19	2.31	1.94
231019_x_at	C19orf26	-1.08	1.91	2.06
231022_at	OCLN	-1.97	-5.05	-2.56
231041_at	POLR1E	1.47	2.91	1.98
231055_at		-1.25	7.24	9.09
231062_at	DOCK9-AS2	1.15	-3.31	-3.81
231078_at	SLC25A37	-1.28	-3.91	-3.05
231086_at		1.11	5.62	5.07
231094_s_at	LOC100996643///MTHFD1L	1.05	-2.30	-2.42
231115_at	POLH	1.33	2.66	2.00
231171_at		1.61	2.20	1.37
231188_at	ZSCAN2	-1.15	3.23	3.71
231234_at	CTSC	1.39	3.51	2.54
231255_at	MPRIP	1.14	-2.01	-2.28
231331_at		1.01	7.21	7.13
231343_at		1.70	-1.50	-2.55
231370_at	PPM1A	-1.19	1.86	2.22
231399_at	RAB3IP	-1.07	1.87	2.00
231406_at	ORAI2	-1.00	3.43	3.44
231416_at	DHDH	1.05	-7.04	-7.39
231417_at		1.00	-2.21	-2.22
231540_at	LOC100130691	1.58	2.21	1.40
231576_at		-1.30	1.96	2.54
231585_at	VPS13A	1.04	2.14	2.06
231613_at	OTTHUMG00000037359///RP11-322F10.2	-1.31	1.62	2.12
231635_x_at	RNF31	1.41	-1.77	-2.49
231656_x_at	OSBPL10	1.40	-1.85	-2.59
231681_x_at	HIST3H2A	1.07	-2.01	-2.16
231689_at	TRPM7	-1.59	1.81	2.87
231716_at	RC3H2	-1.12	1.95	2.18
231776_at	EOMES	1.29	2.07	1.60
231810_at	BRI3BP	-1.07	2.55	2.72
231835_at	FAM213B	1.27	3.32	2.62
231851_at	RAVER2	-1.06	4.35	4.60

231864_at	ZNF33A	1.31	2.70	2.07
231869_at	KIAA1586	-1.30	2.69	3.48
231871_at	GPR180	-1.22	1.88	2.29
231878_at	PAGR1	1.23	3.39	2.76
231890_at		-1.09	2.80	3.04
231924_at	LINC00958	-1.06	2.31	2.44
231931_at	PRDM15	1.30	3.08	2.37
231944_at	ERO1LB	1.21	2.48	2.04
231954_at	DKFZP434I0714	1.16	-4.27	-4.97
231960_at	BRWD1	-1.34	2.72	3.66
231964_at	BICD1	-1.39	5.01	6.95
231967_at	PHF20L1	1.25	-3.85	-4.83
231970_at	GPATCH2L	-1.10	-2.73	-2.48
231984_at	MTAP	1.00	6.46	6.44
232004_at	HNRNPR	-1.24	1.79	2.23
232007_at	AGPAT5	1.14	4.01	3.51
232052_at	SETD5-AS1	1.03	-2.62	-2.69
232060_at	ROR1	-1.25	2.59	3.22
232067_at	FAXC	-1.01	4.19	4.25
232071_at	MRPL19	-1.21	1.65	2.00
232105_at	BLACAT1	1.15	-1.75	-2.02
232145_at	C2orf68	1.65	-1.21	-2.01
232147_at	SLX4	-1.03	2.90	2.99
232183_at	SERAC1	-1.48	3.05	4.51
232184_at	ALS2	-1.61	-4.65	-2.89
232216_at	YME1L1	-1.15	-3.04	-2.63
232229_at	SETX	-1.18	-4.60	-3.89
232244_at	KIAA1161	-1.14	2.61	2.98
232254_at		-1.20	2.46	2.96
232277_at	SLC28A3	-1.62	-9.84	-6.06
232360_at	EHF	-1.51	-2.21	-1.46
232493_at		-1.20	2.25	2.70
232533_at	METTL8	1.61	3.01	1.86
232579_at	LOC100134229	1.17	-5.10	-5.95
232589_at	LOC100506029	1.52	3.50	2.30
232593_at	NEURL3	1.16	-2.87	-3.34
232609_at	CRB3	-1.08	-2.09	-1.93
232613_at	PBRM1	-1.17	1.95	2.29
232860_x_at	RBM41	-1.05	2.20	2.30
232895_s_at		-1.10	-2.26	-2.06
232909_s_at	BPTF	-1.08	6.52	7.01
232961_at	SPATS2L	1.03	-2.14	-2.20
233003_at		1.01	-2.90	-2.93
233006_at	Sep-04	1.85	-1.24	-2.29

233023_at		1.19	-1.90	-2.28
233054_at	CNOT2	1.07	-3.51	-3.76
233069_at	PPP4R1L	1.01	-2.94	-2.96
233078_at	API5	1.19	2.83	2.38
233093_s_at	BIRC6	-1.16	1.83	2.12
233116_at	OTTHUMG00000175500///U82695.10	-1.23	4.40	5.40
233325_at	SLC35D2	-1.04	2.43	2.51
233339_s_at	ARID1B	1.16	-1.80	-2.10
233461_x_at	ZNF226	2.02	1.66	-1.22
233570_at		1.00	-2.26	-2.26
233587_s_at	SIPA1L2	-1.24	-2.01	-1.61
233675_s_at	TPTE2P6	1.04	-2.92	-3.04
233820_at	OTTHUMG00000176337	-1.75	4.49	7.86
234726_s_at	TMEM168	1.06	2.35	2.22
234733_s_at	FANCM	1.22	6.96	5.70
234936_s_at	CC2D2A	1.42	3.53	2.48
234982_at	UBR3	-1.17	2.19	2.56
234986_at	GCLM	-1.29	2.26	2.91
234998_at	RAB11A	-1.07	-2.27	-2.12
235007_at	BBS7	-1.18	2.52	2.97
235009_at	BOD1L1	1.03	2.24	2.18
235046_at	INPP4B	-1.66	2.69	4.47
235071_at	PPP3R1///WDR92	1.22	2.32	1.90
235086_at	THBS1	-1.02	3.26	3.32
235090_at	ZNF710	-1.29	-2.05	-1.59
235093_at	PEX13	-1.42	1.58	2.23
235094_at		-1.15	-2.97	-2.59
235107_at	PIAS2	1.05	6.18	5.88
235120_at	SEC22C	-1.31	2.02	2.66
235133_at	ZDHHC14	-1.57	1.35	2.12
235151_at	LOC283357	-1.42	3.86	5.50
235156_at	BRWD3	-1.25	2.18	2.72
235159_at		-1.09	2.38	2.59
235177_at	METTL21A	-1.02	3.30	3.38
235182_at	ISM1	1.42	7.18	5.04
235195_at	FBXW2	1.12	2.96	2.64
235215_at	ERCC4	-1.37	4.32	5.91
235224_s_at	CAND1	1.52	2.86	1.89
235227_at	STXBP5	-1.30	3.76	4.88
235253_at	RAD1	1.02	2.26	2.21
235255_at	ATP6V0A2	-1.01	2.72	2.75
235259_at	PACRGL	1.42	3.39	2.39
235299_at	SLC41A2	-1.78	2.66	4.73
235302_at	GPATCH2L	-1.63	2.96	4.84

235307_at	LMTK2	-1.08	-4.74	-4.40
235320_at	ARL6	-1.05	9.02	9.44
235333_at	B4GALT6	-1.21	1.80	2.18
235347_at	LRCH3	1.06	3.47	3.26
235373_at	LOC100506314	1.22	2.06	1.69
235386_at	OTTHUMG00000160053///RP11-774O3.3	-1.10	1.91	2.10
235387_at	GSTCD	-1.15	2.12	2.43
235392_at		1.04	2.75	2.66
235399_at	ERCC2	-1.06	2.13	2.26
235423_at	ORC2	1.03	3.36	3.26
235428_at	LOC100507316	1.34	-8.38	-11.21
235436_at	DDX31	1.32	4.65	3.54
235441_at		1.32	4.73	3.59
235459_at	RNF41	-1.04	4.49	4.66
235470_at	NAA38	-1.05	3.37	3.52
235479_at	CPEB2	-1.30	-3.17	-2.43
235484_at	PTAR1	-1.21	2.02	2.44
235497_at	LOC643837	-1.36	3.33	4.53
235505_s_at	LRPAP1	1.14	3.15	2.78
235508_at	PML	-1.04	-4.98	-4.81
235531_at		1.15	4.83	4.20
235553_at	GAPVD1	-1.15	3.24	3.71
235566_at	TMF1	-1.19	2.46	2.93
235577_at	ZNF652	-1.53	2.54	3.88
235579_at	SCAF11	1.00	-3.94	-3.94
235609_at	BRIP1	1.02	3.41	3.35
235610_at	ALKBH8	-1.01	2.87	2.88
235625_at	VPS41	-1.27	1.73	2.20
235644_at	CCDC138	1.11	4.68	4.22
235656_s_at		1.32	2.25	1.70
235659_at		-1.24	2.12	2.63
235667_at	USP46-AS1	2.04	-1.71	-3.48
235677_at	SRR	1.34	2.26	1.69
235683_at	SESN3	1.17	2.61	2.23
235684_s_at	SESN3	1.15	2.07	1.80
235711_at	PURB	-1.09	-2.21	-2.02
235725_at	SMAD4	-1.13	2.56	2.91
235737_at	TSLP	1.20	-2.11	-2.54
235745_at	ERN1	1.06	-2.74	-2.90
235761_at	CTA-445C9.15	-1.50	2.87	4.29
235768_at	SH3RF2	1.26	4.35	3.45
235782_at		-1.20	6.26	7.48
235787_at	CDC37L1	-1.54	2.89	4.46
235789_at	KDM4B///LOC100507022	1.18	-1.87	-2.20

235810_at	ZNF182	1.19	2.91	2.44
235825_at		1.64	-1.87	-3.07
235842_at		1.20	-1.75	-2.10
235846_at	FSBP///RAD54B	-1.23	-2.23	-1.82
235858_at	CREBBP	-1.14	2.44	2.78
235882_at	VPS53	-1.09	3.93	4.29
235893_at		1.14	2.68	2.34
235913_at	ZNF880	1.43	-3.45	-4.93
235918_x_at	CEP97	-1.53	2.03	3.11
235922_at		-1.04	-2.65	-2.54
235937_at	OCLN	-1.51	-2.68	-1.78
235957_at	GRIP1	-1.20	6.14	7.40
235980_at	PIK3CA	-1.63	2.32	3.78
235989_at		1.36	2.25	1.66
236004_at		1.07	3.41	3.18
236044_at	PPAPDC1A	-1.42	2.39	3.40
236066_at		1.06	2.02	1.91
236081_at	SNCA	1.18	3.77	3.18
236090_at		1.03	3.20	3.10
236104_at	HNRNPLL	-1.37	2.16	2.97
236105_at	ZBTB10	-1.40	1.61	2.26
236106_at		1.04	2.58	2.48
236117_at		1.07	-2.11	-2.25
236124_at	LOC153546	1.05	-3.05	-3.20
236179_at	CDH11	-1.54	2.66	4.11
236202_at		-1.08	1.99	2.15
236210_at		-1.05	3.27	3.43
236219_at	SLC35G1	-1.17	3.02	3.52
236261_at	OSBPL6	1.28	4.84	3.78
236268_at	SEC22C	-1.52	2.18	3.32
236313_at	CDKN2B	-1.07	1.96	2.09
236321_at	FAM200B	-1.41	3.30	4.67
236346_at		-1.24	1.62	2.02
236350_at		-1.02	3.70	3.79
236358_at		1.27	-2.26	-2.87
236380_at		-1.06	3.99	4.24
236384_at	C17orf85	1.04	6.62	6.37
236397_at		1.23	-2.66	-3.28
236420_s_at	ANO4	-2.05	1.48	3.02
236430_at	TMED6	1.58	2.98	1.89
236458_at		-1.36	4.07	5.52
236476_at		-1.33	2.23	2.96
236480_at	MIR210HG	-1.02	-2.84	-2.78
236489_at	GPR110	1.00	6.11	6.10

236507_at	ZDHHC3	1.00	2.31	2.31
236514_at	ACOT8	-1.01	-2.65	-2.63
236600_at	SPG20	-1.76	2.58	4.55
236619_at		-1.56	1.45	2.27
236665_at	CCDC18	1.11	2.19	1.97
236718_at	MYO10	-1.47	3.66	5.38
236723_at		-1.35	1.77	2.38
236791_at		-1.08	-3.84	-3.56
236834_at	SCFD2	1.20	2.01	1.68
236898_at		1.16	-3.24	-3.76
236905_at	OTTHUMG00000039470///RP5-1068B5.3	1.20	3.87	3.24
236922_at		-1.10	3.08	3.40
236935_at	PTPN4	-1.08	2.78	2.99
236982_at		1.14	-4.24	-4.83
236990_at	AC062029.1///OTTHUMG00000155049	1.43	-2.94	-4.19
237002_at	NCDN	1.60	2.34	1.47
237019_at		1.54	-1.41	-2.17
237081_at		-1.03	-2.01	-1.95
237097_at		-1.21	2.83	3.42
237143_at		-1.71	1.81	3.10
237166_at		1.31	-1.78	-2.32
237194_at		-1.49	2.05	3.07
237268_at	DSCAM	1.04	4.10	3.95
237299_at		-1.15	6.61	7.63
237309_at		-1.04	-5.33	-5.12
237419_at		1.06	3.68	3.47
237435_at		-1.01	4.50	4.53
237444_at	KIF13A	-1.19	2.11	2.50
237464_at	LOC101060589///SMG1	1.46	-5.17	-7.55
237465_at	USP53	-1.15	-11.91	-10.38
237470_at	DOCK7	-1.14	-2.38	-2.08
237593_at		-1.06	-4.75	-4.48
237654_at	PPP1R36	1.04	-2.03	-2.11
237706_at	STXBP4	-1.01	3.47	3.51
237810_at	CLDN6	-2.47	1.05	2.61
237842_at	MAP7D3	-1.29	10.47	13.54
237899_at	LOC100506374	-1.29	3.04	3.90
237916_at		1.15	-1.76	-2.01
237947_at		1.14	-2.62	-2.98
238015_at	C4orf46	-1.24	2.06	2.54
238031_at	OTTHUMG00000176862///RP11-347C12.10	1.38	-1.82	-2.51
238035_at	SP3	-1.32	3.07	4.05
238037_at	LMLN	1.20	3.63	3.03
238039_at	LOC728769	1.04	-2.63	-2.73

238043_at	ARID1B	1.29	2.19	1.70
238055_at	LOC100505549	-1.15	3.35	3.86
238057_at	USP45	-1.08	3.32	3.57
238067_at	TBC1D8B	-1.20	1.78	2.14
238076_at	GATAD2B	1.11	4.53	4.08
238098_at		1.55	-1.52	-2.36
238106_at		1.59	2.37	1.49
238115_at	DNAJC18	1.02	3.11	3.06
238129_s_at	FZD2	-1.19	3.39	4.02
238135_at	AGTRAP	-1.04	5.24	5.44
238164_at	USP6NL-IT1	1.03	-2.95	-3.04
238186_at		1.29	4.60	3.57
238228_at		1.07	-5.49	-5.89
238327_at	ODF3B	1.15	-2.30	-2.65
238333_s_at	PAOX	1.74	2.28	1.31
238389_s_at		1.23	-1.66	-2.04
238418_at	SLC35B4	1.04	3.04	2.92
238422_at	LBX2-AS1	1.29	-1.76	-2.28
238431_at		-1.09	2.19	2.39
238432_at	DLGAP1-AS1	1.29	-1.71	-2.20
238453_at	FGFBP3	1.15	-1.99	-2.28
238467_at	OTTHUMG00000178798///RP11-159D12.9	1.03	2.68	2.60
238470_at	SYS1	-1.05	2.47	2.59
238477_at	KIF1C	-1.39	3.55	4.92
238488_at	IPO11///LRRC70	1.38	-2.07	-2.86
238494_at	TRAF3IP1	-1.24	3.41	4.24
238507_at		-1.70	2.07	3.52
238509_at	CUL1	-1.24	-7.33	-5.90
238513_at	PRRG4	-1.75	1.52	2.66
238514_at	TMEM25	1.18	2.04	1.73
238516_at	BMPR2	-2.15	1.09	2.34
238520_at	TRERF1	1.09	6.43	5.90
238542_at	ULBP2	-1.37	-2.62	-1.92
238545_at	BRD7	1.20	2.92	2.43
238554_at	CYB5B	-1.05	2.95	3.09
238568_s_at	NPC1	1.12	2.59	2.31
238597_at	ANKRD13C	-1.32	4.57	6.05
238598_s_at		-1.15	4.26	4.88
238602_at	DIS3L2	-1.11	-3.69	-3.33
238615_at	ERLIN2	-1.09	-3.11	-2.85
238617_at	KIF26B	1.18	4.23	3.59
238624_at	NLK	-1.25	-3.42	-2.74
238631_at		1.90	2.20	1.16
238633_at	EPC1	-1.18	-3.65	-3.09

238637_at		1.14	4.44	3.90
238646_at		1.12	-4.04	-4.52
238652_at		-1.04	2.35	2.45
238653_at		-1.10	2.70	2.97
238656_at		1.10	3.05	2.78
238670_at	RAD18	1.22	3.77	3.08
238673_at	SAMD12	-1.03	5.25	5.43
238684_at	SETDB2	1.09	5.76	5.30
238692_at	BTBD11	1.29	-3.26	-4.20
238694_at	DGKE	1.29	2.85	2.21
238728_at		1.08	2.29	2.13
238753_at	NCS1	-1.14	1.76	2.00
238755_at	RASSF10	-1.26	5.58	7.03
238758_at		1.34	-3.05	-4.07
238802_at	TYSND1	-1.71	2.85	4.88
238803_at	HECTD2	1.13	-2.41	-2.72
238813_at	APEX2	-1.01	2.67	2.70
238818_at	KIAA1429	-1.03	2.72	2.79
238827_at	SH3RF2	1.24	2.08	1.68
238853_at	RAB3IP	-1.16	2.50	2.89
238887_at	LOC100630918	1.38	-1.72	-2.37
238888_at		-1.16	1.90	2.21
238890_at	BRWD1	-1.02	5.38	5.47
238893_at	LINC00936	1.12	-1.81	-2.02
238920_at		1.20	-2.52	-3.01
238923_at	SPOP	1.21	3.27	2.69
238927_at		1.41	-3.60	-5.09
238929_at	SRSF8	-1.05	3.89	4.08
238933_at	IRS1	1.26	3.62	2.86
239033_at		-1.25	3.68	4.59
239038_at	C1orf52	-1.15	3.26	3.75
239047_at	FAM122C	1.14	-3.90	-4.45
239056_at	SEC22C	-1.25	2.21	2.76
239069_s_at		-1.37	-2.07	-1.51
239081_at		1.14	-2.06	-2.35
239105_at		1.88	-1.09	-2.05
239122_at		1.01	-2.54	-2.56
239159_at	GOSR2	-1.16	-6.58	-5.67
239184_at		1.33	3.09	2.33
239187_at	DCAF16	1.09	-2.31	-2.51
239207_at	KDM5C	-1.33	1.74	2.31
239208_s_at	YBEY	1.10	2.22	2.03
239212_at	LTV1	1.02	-5.50	-5.63
239218_at	PDE1C	-1.26	2.16	2.72

239292_at		-1.42	2.10	2.98
239334_at		-1.19	-2.92	-2.44
239341_at		1.03	-2.53	-2.61
239355_at	GMCL1	-1.44	2.26	3.25
239375_at		-1.21	-4.81	-3.97
239391_at	FAM120AOS	-1.07	2.25	2.40
239410_at		2.20	1.45	-1.52
239423_at		-1.41	1.64	2.31
239425_at	DCUN1D5	-1.03	2.23	2.29
239431_at	TICAM2///TMED7-TICAM2	1.36	2.68	1.97
239486_at		-1.89	1.34	2.54
239538_at	ZRANB3	1.37	2.70	1.97
239577_at		-1.87	1.09	2.04
239578_at		-1.31	2.61	3.43
239581_at	ARL10	-1.39	2.84	3.93
239582_at	PML	1.17	3.09	2.63
239615_at	SLC22A5	1.13	-1.82	-2.05
239637_at	RAB18	1.09	3.17	2.90
239644_at		1.07	2.07	1.94
239652_at		-1.46	1.78	2.61
239700_at	ZNF710	1.23	-1.73	-2.13
239704_at	RNF144B	1.09	-1.99	-2.17
239710_at	FIGN	-1.15	2.78	3.19
239725_at	PGAP1	-1.20	1.73	2.08
239730_at	DGCR14///TSSK2	1.28	4.60	3.60
239760_at	OTTHUMG00000177839	1.26	2.18	1.73
239763_at	PRDM11	1.05	3.19	3.04
239790_s_at		1.26	3.06	2.43
239797_at		1.04	-2.47	-2.56
239834_at		1.09	2.86	2.63
239863_at	OTTHUMG00000176157///RP11-305E6.4	1.00	3.05	3.04
239866_at		-1.07	5.71	6.11
239899_at	RNF145	-1.04	4.07	4.23
239920_at	UBTF	1.30	-1.56	-2.02
239922_at	CCDC142	-1.14	2.23	2.54
239947_at		1.44	-1.60	-2.30
239982_at	OTTHUMG00000175864	1.45	-1.43	-2.09
240040_at	PSTK	1.49	5.45	3.66
240044_x_at	TNRC6B	-1.10	2.06	2.27
240050_s_at	PPM1K	-1.35	2.71	3.66
240063_at	GUSBP5	1.25	-4.57	-5.71
240066_at	AC000123.3	-1.14	2.95	3.38
240121_x_at		-1.04	2.51	2.61

240172_at	ERGIC2	1.12	2.93	2.62
240185_at	LOC100147773	1.20	-2.87	-3.43
240218_at	DSCAM	1.09	9.64	8.84
240282_at	WDR1	-1.16	-6.09	-5.28
240294_at	HIPK2	1.28	-1.65	-2.11
240379_at	PKP4	1.31	3.46	2.65
240382_at	OTTHUMG00000175897	1.11	-2.54	-2.83
240391_at	NDUFB2	1.04	2.23	2.15
240454_at		-1.38	-4.27	-3.10
240475_at	EGOT	-1.55	-6.69	-4.32
240663_at		1.25	-3.52	-4.39
240738_at		-1.44	-3.17	-2.20
240762_at		-1.22	1.69	2.06
240768_x_at		-1.39	-2.31	-1.67
240781_x_at	DCUN1D1	-1.47	1.80	2.64
240793_at	OTTHUMG00000180307///RP11-171I2.2	1.19	2.05	1.72
240796_at		1.18	-1.89	-2.22
240873_x_at	DAB2	1.03	-2.64	-2.73
240964_at		-1.02	-2.81	-2.76
240982_at	CARS	-1.33	-5.88	-4.40
240983_s_at	CARS	-1.23	-2.66	-2.16
241015_at		1.23	2.19	1.78
241027_at	OPA1	1.02	-2.63	-2.68
241252_at	ESCO2	-1.07	-2.00	-1.86
241355_at	HR	-1.18	2.75	3.24
241364_at	TMEM57	-1.45	2.29	3.31
241374_at	TMEM39A	1.41	2.34	1.66
241433_at	RCOR3	-1.16	-3.69	-3.17
241453_at	PTK2	-1.41	-5.08	-3.62
241482_at	EPHA1	-1.63	-3.97	-2.44
241689_at		-1.21	6.20	7.50
241708_at	DOCK1	1.06	-2.58	-2.74
241735_at	LOC100996477///RASSF8	-1.44	-2.11	-1.47
241746_at	CUL7	-1.15	-2.82	-2.44
241747_s_at	CUL7	-1.02	-2.13	-2.09
241776_at		1.18	2.31	1.96
241808_at	ZC2HC1A	-1.31	-2.22	-1.69
241809_at	FAM212B	1.01	2.15	2.13
241825_at	TYW5	-1.32	3.26	4.32
241840_at		1.29	3.25	2.51
241863_x_at		-1.74	1.15	2.00
241877_at		1.02	-2.88	-2.93
241881_at	TRIM58	-1.35	3.16	4.26
241933_at	QRSL1	1.08	4.19	3.90

241937_s_at	WDR4	1.26	2.86	2.27
241968_at	C4orf29	1.04	5.42	5.20
242045_at		-2.00	-2.59	-1.30
242049_s_at	NBAS	-1.36	1.50	2.04
242073_at		-1.14	-11.32	-9.92
242089_at		1.29	2.74	2.12
242157_at	CHD9	-1.39	1.45	2.02
242166_at		-1.20	-4.31	-3.59
242176_at	MEF2A	1.06	-4.79	-5.09
242201_at	PMS2P5	1.20	-2.18	-2.61
242210_at	ZNF24	-1.09	-2.14	-1.96
242220_at	SPTBN1	-1.23	2.59	3.18
242230_at	ATXN1	-2.05	1.91	3.93
242255_at	WDR37	-1.25	-3.91	-3.12
242258_at		1.07	2.83	2.66
242263_at	TMED5	1.09	3.28	3.00
242289_at		1.26	3.01	2.39
242291_at	EIF4ENIF1	1.08	2.09	1.93
242304_at	WIBG	-1.30	-2.46	-1.89
242389_at	LUC7L3	-1.17	4.13	4.83
242414_at	QPRT	1.04	3.16	3.02
242423_x_at		-1.18	1.86	2.19
242433_at	ZBTB11	1.03	-5.23	-5.38
242434_at		-1.04	2.69	2.81
242477_at	TTC39B	-1.56	-2.95	-1.90
242523_at		-1.31	-2.60	-1.99
242557_at	ZNRD1-AS1	1.23	3.18	2.58
242564_at		1.16	2.30	1.98
242584_at	FAM161A	-1.50	3.31	4.97
242590_at		1.40	3.13	2.24
242594_at	BOD1L1	1.24	-2.47	-3.06
242711_x_at	FANCM	1.14	2.26	1.98
242731_x_at		-1.23	4.20	5.15
242740_at		-1.48	-2.40	-1.62
242752_at	PPM1K	-1.15	3.01	3.47
242761_s_at	ZNF420	1.18	2.46	2.09
242812_at	HCG18	1.19	-2.61	-3.10
242834_at		-1.56	2.03	3.17
242847_at	C11orf30	-1.15	6.01	6.88
242963_at	SGMS2	-1.25	-2.16	-1.73
242979_at	IRS1	-1.21	4.43	5.36
242982_x_at	ITGB8	1.19	-2.60	-3.10
243000_at	CDK6	1.08	-3.96	-4.29
243024_at	ZNF394	1.08	2.00	1.85

243069_at		1.27	-3.19	-4.04
243084_at	CALD1	-1.25	-5.25	-4.21
243087_at	WDR63	1.66	2.78	1.68
243092_at	PAN3-AS1	1.22	-3.63	-4.45
243118_at	CEP57L1	-1.19	-2.26	-1.89
243176_at	ARL5A	-1.35	2.52	3.41
243220_at		-1.05	5.91	6.20
243299_at		-1.02	-6.16	-6.06
243310_at		-1.23	1.63	2.00
243367_at		1.70	2.64	1.55
243376_at	TANK	-1.17	-2.45	-2.10
243379_at		1.08	-2.10	-2.27
243405_at		-1.58	1.85	2.92
243417_at	ZADH2	1.28	2.98	2.32
243560_at		1.35	-1.71	-2.31
243570_at	SPCS2	-1.02	2.51	2.56
243582_at	SH3RF2	1.31	7.34	5.59
243605_at		-1.08	-5.85	-5.41
243631_at		1.01	-2.57	-2.61
243657_at		1.14	2.56	2.25
243661_at	ZNF273	-1.40	-3.04	-2.18
243704_at	GPATCH2	-1.25	2.06	2.57
243718_at		1.21	2.70	2.22
243733_at		-1.18	-2.55	-2.17
243740_at		-1.45	2.78	4.05
243749_s_at	LOC100507316	1.36	-3.47	-4.70
243782_at		-1.03	-2.55	-2.48
243796_at		1.07	-1.89	-2.02
243829_at	BRAF	-1.25	-10.17	-8.12
243835_at	ZDHHC21	-1.50	2.12	3.19
243837_x_at	AC018816.3///OTTHUMG00000155240	-1.08	2.97	3.20
243861_at	FNIP1	-1.06	-3.58	-3.39
243868_at	RFX3	-1.11	4.60	5.09
243904_at	STXBP5	-1.28	2.97	3.79
243907_at		-1.01	2.56	2.57
243948_at		-1.23	4.75	5.84
243973_at		1.23	-1.88	-2.31
243976_at		-1.23	2.60	3.21
243999_at	SLFN5	-1.25	-5.21	-4.17
244020_at		-1.27	-7.15	-5.65
244028_at	USP15	-1.14	2.24	2.55
244032_at		-1.10	3.51	3.85
244033_at	CEP128	-1.39	7.97	11.10
244070_at	SYNE1	-1.08	-2.70	-2.50

244075_at		1.39	-1.90	-2.65
244121_at	UBR3	-1.22	2.11	2.58
244241_x_at		-1.47	1.40	2.06
244246_at	MIPOL1	-1.12	3.13	3.49
244261_at	IFNLR1	-2.30	2.29	5.28
244308_at	OTTHUMG00000018106///RP11-38L15.3	-1.03	2.14	2.20
244324_at	C18orf54	-1.64	2.21	3.61
244354_at	STRN	-1.30	1.83	2.37
244362_at		1.20	-1.78	-2.14
244397_at		-1.06	-2.30	-2.16
244411_at	LOC100507316	1.36	-1.75	-2.38
244424_at	LOC439938	-1.31	-2.48	-1.89
244428_at	DNMT3A	1.02	-7.34	-7.47
244441_at		-2.17	1.22	2.65
244481_at	OTTHUMG00000175898	-1.30	-3.48	-2.67
244499_at	THAP2	1.09	-2.08	-2.27
244555_at		-1.01	-2.05	-2.02
244659_at	LOC100131015	1.06	-4.81	-5.07
244660_at	ELAVL1	-1.04	3.21	3.34
244661_at	SOAT1	-1.50	2.63	3.95
244734_at	MTHFSD	1.05	-2.92	-3.05
244787_at		1.09	2.64	2.42
244829_at	LINC00518	-1.12	-3.09	-2.77
244834_at	RSG1	1.21	3.06	2.53
244881_at	LMLN	1.20	3.59	2.98
1552314_a_at	EYA3	-1.03	-3.90	-3.78
1552330_at	CENPBD1	1.21	2.11	1.75
1552332_at	TRIOBP	1.04	-2.80	-2.91
1552334_at	TRIOBP	-1.22	-3.05	-2.50
1552423_at	ETV3	-1.07	-5.43	-5.08
1552473_at	GAMT	1.41	-1.52	-2.13
1552477_a_at	IRF6	-1.42	-2.54	-1.79
1552491_at	IDI2	1.39	2.21	1.60
1552502_s_at	RHBDL2	-1.61	2.09	3.36
1552519_at	ACVR1C	-1.67	-2.74	-1.64
1552573_s_at	MIPOL1	1.24	2.22	1.79
1552701_a_at	CARD16	1.12	-1.88	-2.10
1552792_at	SOCS4	-1.78	-2.09	-1.17
1552928_s_at	TAB3	-1.50	-2.04	-1.36
1552930_at	MMEL1	-1.01	1.99	2.01
1552931_a_at	PDE8A	-1.37	1.65	2.26
1552969_a_at	ZMYM6	-1.56	-2.54	-1.62
1553034_at	SDCCAG8	1.30	2.80	2.16
1553117_a_at	STK38	-1.49	3.56	5.30

1553140_at	PELO	1.03	3.11	3.02
1553158_at	CEP19	1.18	2.95	2.51
1553227_s_at	BRWD1	1.03	2.10	2.03
1553269_at	ZNF718	-1.09	3.30	3.60
1553299_at	DUSP5P1	-1.43	-6.80	-4.77
1553311_at	C20orf197	-1.43	1.45	2.07
1553313_s_at	SLC5A3	1.53	2.83	1.85
1553391_at	CXorf58	1.41	3.03	2.15
1553775_at	FLJ31715	1.60	-1.97	-3.15
1553852_at	VPS13B	1.00	-2.13	-2.13
1553960_at	SNX21	-1.79	1.21	2.17
1554007_at		-1.46	8.91	12.98
1554008_at	OSMR	-1.17	-12.58	-10.77
1554014_at	CHD2///LOC100507217	-1.60	-3.93	-2.46
1554015_a_at	CHD2///LOC100507217	-1.45	-3.63	-2.51
1554019_s_at	CEP57L1	-1.28	3.05	3.91
1554038_at	LARP1B	1.28	3.54	2.77
1554039_at	C14orf159	1.16	-2.29	-2.66
1554045_at	ZNF24	1.22	-3.39	-4.15
1554052_at	CNOT1	1.08	-2.58	-2.78
1554068_s_at	C12orf66	1.63	2.65	1.62
1554086_at	TUBGCP3	-2.66	-3.60	-1.35
1554095_at	RBM33	-1.42	-3.93	-2.77
1554096_a_at	RBM33	1.03	-2.96	-3.05
1554097_a_at	MIR31HG	-1.37	1.95	2.67
1554110_at	CDCP1	1.22	-18.54	-22.56
1554122_a_at	HSD17B12	1.59	-4.00	-6.35
1554141_s_at	WDR78	1.26	2.37	1.87
1554145_a_at	PPP1R21	-1.47	-7.20	-4.89
1554246_at	C1orf210	-1.92	-3.84	-2.00
1554249_a_at	ZNF638///ZNF638-IT1	-1.59	1.33	2.11
1554250_s_at	TRIM73	-1.36	2.10	2.87
1554264_at	CKAP2	-1.21	-3.18	-2.64
1554274_a_at	SSH1	-1.70	-4.36	-2.57
1554283_at	CCRN4L	-1.17	-2.22	-1.90
1554290_at	HERC3	-1.09	-2.30	-2.11
1554291_at	UHRF1BP1L	-1.10	-3.36	-3.06
1554293_at	TTBK2	-1.48	-3.27	-2.21
1554294_s_at	TTBK2	-1.67	-3.18	-1.90
1554295_x_at	TTBK2	-1.21	-2.48	-2.04
1554309_at	EIF4G3	-1.55	-8.00	-5.17
1554319_at	RPS6KA5	1.02	-5.24	-5.36
1554341_a_at	HELQ	-1.04	-2.96	-2.84
1554342_s_at	HELQ	1.07	-2.44	-2.61

1554354_at	SIAE	-1.01	-2.66	-2.63
1554355_a_at	SIAE	1.19	-11.72	-13.90
1554364_at	PPP2R5C	-1.56	-3.18	-2.04
1554415_at	TAF5L	1.23	-1.73	-2.13
1554470_s_at	ZBTB44	-1.06	4.54	4.80
1554472_a_at	PHF20L1	-1.02	-4.74	-4.64
1554520_at	LOC100996810///LOC283861	1.64	-3.41	-5.58
1554547_at	FAM13C	1.38	-2.34	-3.22
1554575_a_at	BPNT1	-1.05	2.49	2.62
1554586_a_at	RHOBTB2	1.34	2.42	1.81
1554594_at	ARHGAP27	-1.06	-4.49	-4.24
1554621_at	DGKE	1.06	-6.56	-6.95
1554623_x_at	DGKE	-1.26	-7.48	-5.93
1554728_at	SLC9A1	1.23	-2.51	-3.08
1554793_at	UBE3C	-1.03	-2.64	-2.57
1554794_a_at	UBE3C	-1.16	-3.05	-2.63
1554822_at	PHTF2	-1.22	-3.84	-3.15
1554849_at	TOR1A	-1.28	-14.25	-11.11
1554886_a_at	MLXIP	1.23	-2.60	-3.19
1554905_x_at	FRMD8	-1.35	-2.32	-1.72
1554906_a_at	MPHOSPH6	1.09	-4.02	-4.39
1554961_at	FGFR4	1.07	-1.92	-2.05
1554999_at	RASGEF1B	1.16	-5.18	-5.99
1555022_at	RGS12	-1.01	2.34	2.36
1555082_a_at	NEK11	1.15	2.80	2.44
1555108_at	SLC10A7	-1.31	-9.13	-6.98
1555137_a_at	FGD6	-1.01	-2.85	-2.82
1555225_at	C1orf43	1.02	-1.98	-2.03
1555259_at	ZAK	-1.09	-7.10	-6.52
1555279_at	ARMC8	-1.21	-2.71	-2.24
1555281_x_at	ARMC8	-1.13	-2.67	-2.37
1555292_at	STRIP2	-1.61	-5.94	-3.69
1555390_at	NOP9	-1.21	-2.01	-1.67
1555439_at	GTF3C3	-1.06	-2.03	-1.92
1555441_at	UBA6	-1.22	-5.83	-4.79
1555461_at		1.36	5.97	4.40
1555464_at	IFIH1	-1.16	-3.25	-2.81
1555486_a_at	PRR5L	-1.20	3.46	4.16
1555487_a_at	ACTR3B	1.61	3.54	2.20
1555673_at	KRTAP2-3///KRTAP2-4	-2.22	-2.48	-1.12
1555677_s_at	SMC1A	-1.15	2.05	2.35
1555766_a_at	GNG2	-1.20	-6.72	-5.60
1555787_at	C11orf63	-2.01	1.31	2.64
1555842_at	CYTH2	1.50	4.53	3.03

1555846_a_at		1.03	2.80	2.72
1555854_at	AKR1C1	1.14	3.04	2.66
1555894_s_at	MTSS1L	1.03	2.45	2.38
1555895_at	DNM2	1.27	2.07	1.63
1555897_at		1.34	2.88	2.15
1555929_s_at		-1.11	2.05	2.27
1556033_at	FLJ39739	-1.12	-2.25	-2.00
1556042_s_at	LOC338799	1.20	-1.72	-2.06
1556047_s_at	MAGEE1	-1.60	1.74	2.80
1556063_s_at	RPP30	-1.04	2.02	2.10
1556111_s_at		1.06	4.47	4.21
1556134_a_at	B3GNT5	-1.41	-3.58	-2.55
1556136_at	MYLK4	-1.01	2.22	2.25
1556162_at	IGSF3	-1.15	-3.11	-2.71
1556172_at		1.70	3.17	1.86
1556173_a_at		1.77	2.59	1.47
1556178_x_at	TAF8	-1.07	1.89	2.02
1556195_a_at	OTTHUMG00000175735	-1.02	-3.21	-3.14
1556228_a_at	VCPIP1	-1.29	1.73	2.23
1556301_at	LOC100287015	-1.08	-2.04	-1.89
1556321_a_at	MESDC1	-1.09	2.17	2.37
1556332_at		-1.42	3.49	4.95
1556341_s_at	MAPK12	1.10	-2.06	-2.26
1556389_at	CNPY3	1.27	4.41	3.48
1556393_at		1.13	3.07	2.71
1556558_s_at	ENTPD3-AS1	-1.10	1.84	2.03
1556582_at	PVR	1.22	2.99	2.44
1556613_s_at	DPY19L4	1.13	-3.04	-3.43
1556809_a_at	RAP2A	1.30	3.55	2.72
1556835_s_at	LOC100652770	-1.09	-2.52	-2.30
1556911_at	ALMS1-IT1///ALMS1-IT1	-1.39	-6.29	-4.54
1557055_s_at	LOC643837	1.26	-1.93	-2.44
1557067_s_at	LUC7L	1.04	2.63	2.53
1557100_s_at	HECTD1	-1.38	1.51	2.08
1557114_a_at	C19orf82	1.29	-1.67	-2.15
1557126_a_at	PLD1	-1.12	-2.95	-2.63
1557218_s_at	FANCB	-1.22	1.85	2.26
1557257_at	BCL10	-1.75	-6.41	-3.66
1557258_a_at	BCL10	1.09	-4.33	-4.73
1557265_at	CTD-2270P14.5	1.22	-4.57	-5.58
1557285_at		1.15	3.07	2.66
1557293_at	LINC00969	1.52	3.02	1.98
1557331_at	POLR1B	1.30	2.18	1.68
1557347_at	MCPH1	1.15	3.97	3.46

1557370_s_at	MYCBP2	1.14	3.54	3.10
1557531_a_at	C10orf55	-1.28	-4.66	-3.64
1557576_at	PAQR3	-1.33	2.01	2.69
1557616_at	ZNF496	1.06	-1.98	-2.09
1557636_a_at	C7orf57	-1.33	-11.10	-8.34
1557667_at		-1.14	3.95	4.51
1557684_at	ZNF286A	1.05	2.51	2.38
1557818_x_at	OTTHUMG00000016921///RP11-432M24.4	1.22	-1.72	-2.11
1557945_at	TCTE3	1.06	-1.90	-2.01
1557984_s_at	RPAP3	1.02	2.13	2.08
1558041_a_at	KIAA0895L	1.45	2.57	1.77
1558062_at	FBXO10	-1.13	-2.03	-1.80
1558117_s_at	USP31	-1.58	3.13	4.94
1558142_at	TNRC6B	-1.14	2.26	2.58
1558208_at		-1.12	-3.76	-3.35
1558215_s_at	UBTF	1.23	-1.94	-2.40
1564150_a_at	C12orf79	1.08	-2.24	-2.41
1558250_s_at	OTTHUMG00000169422	-1.04	3.93	4.10
1558290_a_at	MIR1204///PVT1	1.60	2.83	1.77
1558305_at	GIGYF2	-1.05	-3.27	-3.11
1558369_at	MPHOSPH9	1.20	3.60	3.01
1558522_at		1.04	3.35	3.21
1558703_at	SLC46A1	1.45	4.82	3.31
1558722_at	ZNF252P	1.22	2.09	1.71
1558740_s_at		1.08	2.05	1.91
1558754_at	ZNF763	-1.07	-2.68	-2.50
1558760_at		1.17	-1.95	-2.29
1558761_a_at	FAM120AOS	1.06	3.86	3.64
1558764_at	OTTHUMG00000172747///RP3-496C20.1	-1.11	2.83	3.16
1558765_a_at	OTTHUMG00000172747///RP3-496C20.1	-1.45	2.61	3.78
1558868_a_at	DSE	1.20	-2.65	-3.17
1558919_a_at	SEC23IP	1.52	2.30	1.51
1558930_at	LINC00460	1.12	-2.06	-2.31
1558967_s_at	HCG18	-1.19	-2.07	-1.74
1559006_at		1.32	5.97	4.51
1559007_s_at		1.44	5.03	3.50
1559009_at		1.18	-2.23	-2.64
1559026_at	PPP1R26-AS1	1.01	-1.98	-2.00
1559108_at	LOC100996816///VPS53	-1.48	1.40	2.07
1559201_a_at		-1.27	3.14	3.98
1559203_s_at	KRAS	1.00	-2.33	-2.34
1559266_s_at	SKIDA1	-1.65	1.89	3.10
1559382_at	SMIM7	1.38	-1.76	-2.42
1559393_at	ALDH1L2	1.31	-1.69	-2.21

1559467_at	OTTHUMG00000176726///RP11-81A1.6	1.09	-3.09	-3.37
1559477_s_at	MEIS1	1.04	2.15	2.07
1559485_at	ATG2B	-1.23	1.75	2.16
1559532_at	ARIH2OS	-1.04	-2.35	-2.27
1559585_at	DDX60L	-1.02	-3.34	-3.27
1559607_s_at	GBP6	-1.11	-2.25	-2.03
1559960_x_at	SYCE1L	1.66	-1.31	-2.17
1569867_at	EME2	1.20	3.07	2.57
1569868_s_at	EME2	1.23	2.24	1.82
1560048_at		1.02	2.99	2.93
1560071_a_at		1.03	3.45	3.36
1560089_at	LOC100289019	1.54	4.72	3.06
1560138_at	KIAA0226	-1.12	-4.76	-4.24
1560222_at		-1.63	2.67	4.34
1560434_x_at	CLTA	-1.83	1.16	2.12
1560553_at	TIAF1	1.16	-3.36	-3.90
1560579_s_at	LOC100506392	-1.12	2.18	2.44
1560622_at		-1.12	-3.21	-2.87
1560647_at	TSPYL1	-1.62	1.48	2.40
1560738_at		1.02	-14.97	-15.34
1560739_a_at		1.22	-14.46	-17.59
1561042_at	CTA-204B4.6///OTTHUMG00000172354	-2.52	1.21	3.07
1561301_at	MAGI1-IT1	-1.07	-2.15	-2.01
1561486_at	OTTHUMG00000176147///RP11-666N19.1	-1.40	1.66	2.31
1561595_x_at		1.29	-1.87	-2.42
1561834_a_at		-1.22	-2.09	-1.72
1561893_at		-1.45	1.50	2.17
1567107_s_at	TPM4	-1.15	-2.02	-1.77
1562098_at	OTTHUMG00000170194///RP11-135F9.4	1.13	3.00	2.66
1562323_at		-1.24	-2.26	-1.82
1562460_at	CNDP2	1.13	-2.55	-2.89
1562761_at	NMRK1	-1.15	-3.19	-2.76
1562966_at	KIAA1217	-1.15	2.32	2.67
1563404_at		-1.12	-2.00	-1.79
1564295_at	FLJ25917	-1.03	-2.03	-1.96
1564653_s_at	LEKR1	1.03	-3.10	-3.20
1564796_at	EMP1	-1.76	-2.49	-1.41
1565627_a_at		-1.08	2.97	3.19
1565628_at		-1.22	2.75	3.35
1566256_s_at	GPR180	-1.59	6.74	10.70
1566257_at	GPR180	-1.50	6.07	9.11
1566557_at	BAIAP2-AS1	1.12	3.47	3.11
1566603_s_at	RPUSD3	-1.16	2.86	3.32
1566764_at	MACC1	-2.35	-6.61	-2.82

1566980_at		1.15	-1.98	-2.27
1567032_s_at	ZNF160	-1.02	-2.46	-2.40
1568619_s_at	ITPRIPL2	-1.18	1.78	2.09
1568629_s_at	PIK3R2	1.17	2.35	2.02
1568665_at	RNF103	-1.05	-2.26	-2.16
1568699_at	IFT43	-1.26	-3.18	-2.52
1568777_at	EML5	-1.13	4.17	4.71
1568781_at		-1.08	2.77	2.99
1568805_at	NCOA7	-1.06	-7.77	-7.34
1568868_at	CYP27C1	-1.09	2.92	3.18
1568874_at	NCOA6	-1.36	-8.57	-6.30
1568913_at	NSUN3	1.31	-4.64	-6.06
1568997_at	POLR1E	1.66	5.99	3.60
1569076_a_at	ZNF836	-1.08	-4.85	-4.51
1569077_x_at	ZNF836	-1.39	-4.20	-3.03
1569086_at	LOC100287177	1.65	-1.24	-2.05
1569132_s_at	ARSK	-1.04	-2.01	-1.93
1569133_x_at	ARSK	1.27	-1.91	-2.42
1569149_at	PDLIM7	1.15	-4.82	-5.57
1569150_x_at	PDLIM7	1.27	-4.70	-5.96
1569191_at	ZNF826P	-1.20	-2.34	-1.95
1569380_a_at	HERPUD1	1.41	-2.28	-3.21
1569439_at		-1.64	7.62	12.47
1569659_at	LOC100506895	1.65	5.34	3.23
1569699_at	AK7	1.33	-1.81	-2.41
1569703_a_at		-1.16	-6.59	-5.66
1569714_at	ZFYVE20	1.01	-5.86	-5.94
1569827_at	ATG7	-1.11	-5.02	-4.54
1570038_at	ZNF595///ZNF718	-1.05	-2.00	-1.91
1570042_a_at	ADAM9	-1.12	-12.06	-10.76
1570061_at		1.09	2.16	1.97